

# **Expression and interactions of the ubiquitin receptor ZNF216**

By

**Joanna Strachan, BSc.**



**The University of  
Nottingham**

UNITED KINGDOM • CHINA • MALAYSIA

School of Biomedical Sciences

University of Nottingham Medical School

Queen's Medical Centre

Nottingham, U.K.

Thesis submitted to the University of Nottingham for the degree of

Doctor of Philosophy

**July 2012**

## Abstract

Muscle atrophy is a feature of many chronic diseases and contributes to both morbidity and mortality, emphasising the importance of understanding the molecular pathways involved. *Zinc finger protein 216 (ZNF216)* is an atrogene, a gene which is up-regulated during and directly mediates skeletal muscle atrophy, and encodes the ubiquitin (Ub) receptor protein ZNF216. Herein it is demonstrated that ZNF216 mRNA levels increase in the extensor digitorum longus (EDL) in a lipopolysaccharide (LPS)-infusion rat model of muscle atrophy, relative to saline control. However, combined administration of low level dexamethasone (Dex) with LPS, although sparing muscles from atrophy, did not blunt ZNF216 expression which parallels previous observations for the atrogenes muscle atrophy F-box protein (MAFbx) and muscle RING-finger 1 (MuRF1). ZNF216 expression levels were further elevated in biceps femoris muscle in rats dosed with the statin drug simvastatin (in which severe muscle damage and atrophy occurs), relative to control rats. The ZNF216 protein's Ub-binding ability and its reported association with the 26S proteasome indicates it may shuttle proteins targeted for degradation to the proteasome as part of the atrophy programme. We utilised immobilised recombinant ZNF216 protein and its Ub-binding Znf\_A20 domain alone to capture Ub-modified proteins from rat skeletal muscle that may represent ZNF216's substrates. Bound proteins specifically eluted by deubiquitination were identified *via* liquid chromatography tandem mass spectrometry (LC-MS/MS) and included adenylate kinase 1 (AK1) and actin, both previously proposed as substrates of MuRF1. However, ion scores for all candidates were below the accepted threshold of significance and immunoblotting failed to validate LC-MS/MS data. This approach also revealed an increase in a low molecular weight Ub-positive protein from EDL muscle after 24hrs of LPS infusion. Retrospective analysis revealed this Ub-positive protein was consistently captured in other experiments and confirmed by protein MS and immunoblotting to represent an unmodified and unanchored (i.e. not attached to a substrate) K48-linked Ub dimer. Subsequent capture of the Ub dimer using the Znf\_UBP domain of isopeptidase T (isoT), a Ub-binding domain selective for the free C-terminus of Ub, confirmed the dimer was unanchored and also revealed a ladder of longer endogenous unanchored poly-Ub chains. Optimised affinity capture conditions has afforded the first opportunity to purify longer free poly-Ub chains and perform the initial molecular analyses of endogenous unanchored poly-Ub purified from *in vivo* sources.

## **Acknowledgements**

Firstly, I must thank my supervisors, Dr Robert Layfield, Professor Sheila Gardiner and Professor Paul Greenhaff, who have each provided different and invaluable perspectives on my project. I must particularly thank Rob for all of his support, guidance and eternal optimism (and for a fairly constant supply of chocolate and/or pastries during the days and the late nights). Thanks to James Cavey, for this project existing in the first place and for his eternal guidance... even at times that I didn't know I needed it... Thanks to Barry Shaw and his seemingly ceaseless patience with lab-, grammar- and crossword-related queries over the years. And for the fancy coffee. Dan Foxler (oh Danny Boy), I must thank for letting me endlessly nag him about, well, everything and for all of his advice and encouragement... I must thank Alice Goode, not only for providing a digital radio for the lab and bringing a girl's influence into the lab, but for being such a good(e) friend; and I can't thank Alice, without also thanking Ryan Atkins, but more for his invaluable proof-reading (and less for the girl-influence). Idris Sidique, thanks for all the banana cake! Not sure I would've got through all of this without him, with his invaluable mixture of optimism and realism. Lynn Bedford, thanks not only for the mouse brains, but also for those long non-science chats.

I am also grateful to David Tooth, Matt Carlisle and Kevin Bailey for various mass spectrometry-related support and guidance, and to my collaborators Mark Searle, Tom Garner, Jed Long, Lucy Roach, Kleitos Sokratous and Neil Oldham.

I'd also like to thank various people past and present in or connected to the lab, or around the department; Katherine "It's Friday" Bridge, Mo Mee and Debby Channing (for providing a motherly influence!), Sarah Skirrow, Vicky James, Laura Bufton, Laura Lyons, Dave Carrier, James Dorrian and Tao Wright.

I can't forget my friends outside of the lab, that may not live close but have not only for shown (very believable) interest when I've practiced obscure biochemistry related presentations in their presence, but also for their loyalty and being like an extended family (in a nice way). Finally, I must thank my Dad, my (definitely-not-evil) stepmum Mary and my Nan. You have supported me throughout university, not only in making sure I didn't end up desolate but also in always being there throughout the highs and lows.

## **Table of contents**

|   |           |
|---|-----------|
| Abstract  | i         |
| Acknowledgements  | ii        |
| Table of contents   | iii       |
| Abbreviations   | xiv       |
| <b>CHAPTER 1</b>  | <b>1</b>  |
| <b>General Introduction</b>   | <b>1</b>  |
| 1.1. Introduction   | 2         |
| 1.2. Clinical importance of skeletal muscle atrophy   | 2         |
| 1.3. Models of skeletal muscle atrophy  | 4         |
| 1.4. Sensitivity to muscle atrophy is dependent on muscle type and species                    | 6         |
| 1.5. Understanding molecular mechanisms that instigate muscle wasting                         | 9         |
| 1.6. Atrogenes  | 13        |
| 1.7. Skeletal muscle atrophy up-regulates components of the ubiquitin proteasome system (UPS) | 14        |
| 1.8. The importance of the ubiquitin proteasome system (UPS) during normal cellular function  | 17        |
| 1.9. Components of UPS  | 19        |
| <i>1.9.1. Enzymes required for polyubiquitination</i>   | <i>19</i> |
| <i>1.9.1.1. MAFbx</i>   | <i>24</i> |
| <i>1.9.1.2. MuRF1</i>   | <i>27</i> |
| <i>1.9.1.3. 26S Proteasome</i>  | <i>29</i> |
| <i>1.9.1.4. Deubiquitinating enzymes</i>  | <i>32</i> |
|   | iii       |

|   |           |
|---|-----------|
| 1.9.1.5. Ubiquitin  | 34        |
| 1.9.1.5.1. Monoubiquitination                               | 35        |
| 1.9.1.5.2. Polyubiquitinated substrates                     | 38        |
| 1.9.1.5.3. Unanchored polyubiquitin                         | 42        |
| 1.9.1.5.4. Ubiquitin binding proteins                       | 43        |
| 1.9.1.5.5. Methods for purifying polyubiquitinated proteins | 45        |
| 1.10.    ZNF216   | 47        |
| 1.10.1. Structure of ZNF216                                 | 47        |
| 1.10.2. Biochemical function                                | 47        |
| 1.11. Aims  | 51        |
| <b>CHAPTER 2</b>  | <b>52</b> |
| <b>Materials and Methods</b>                                | <b>52</b> |
| 2.1. Experimental animals                                   | 53        |
| 2.1.1. Intravenous endotoxin and chemical reagents          | 53        |
| 2.1.2. Protocol   | 53        |
| 2.2. Protein-to-DNA ratio                                   | 53        |
| 2.2.1. Protein and DNA extraction                           | 53        |
| 2.2.1.1. Solutions  | 53        |
| 2.2.1.2. Protocol   | 54        |
| 2.2.2. Protein quantification: Lowry method                 | 55        |
| 2.2.2.1. Solutions  | 55        |
| 2.2.2.2. Protocol   | 55        |
| 2.2.3. DNA quantification                                   | 56        |
| 2.2.3.1. Solutions  | 56        |
| 2.2.3.2. Protocol   | 56        |

|   |    |
|---|----|
| 2.3. RNA extraction                                     | 56 |
| 2.3.1. Solutions  | 56 |
| 2.3.2. Protocol   | 57 |
| 2.4. cDNA synthesis                                     | 57 |
| 2.4.1. Solutions  | 57 |
| 2.4.2. Protocol   | 58 |
| 2.5. TaqMan analysis                                    | 58 |
| 2.5.1. Solutions  | 58 |
| 2.5.2. Protocol   | 59 |
| 2.6. DNA electrophoresis                                | 60 |
| 2.6.1. Solutions  | 60 |
| 2.6.2. Protocol   | 60 |
| 2.7. Plasmids   | 61 |
| 2.8. Cloning  | 61 |
| 2.8.1. PCR amplification                                | 61 |
| 2.8.1.1. Solutions                                      | 61 |
| 2.8.1.2. Protocol                                       | 62 |
| 2.8.2. Restriction digest and ligation                  | 62 |
| 2.8.2.1. Solutions                                      | 62 |
| 2.8.2.2. Protocol                                       | 63 |
| 2.9. Site-directed mutagenesis                          | 64 |
| 2.9.1. Solutions  | 64 |
| 2.9.2. Protocol   | 64 |
| 2.10. Transformation of <i>E. coli</i> with plasmid DNA | 65 |
| 2.10.1. Solutions                                       | 65 |

|   |    |
|---|----|
| 2.10.2. Protocol  | 65 |
| 2.11. Glycerol stocks of <i>E. coli</i>                                     | 66 |
| 2.11.1. Solutions   | 66 |
| 2.11.2. Protocol  | 66 |
| 2.12. GST-fusion protein overexpression                                     | 66 |
| 2.12.1. Solutions   | 66 |
| 2.12.2. Protocol  | 67 |
| 2.13. Sodium dodecyl sulphate polyacrylamide-gel electrophoresis (SDS PAGE) | 67 |
| 2.13.1. Solutions   | 67 |
| 2.13.2 Protocol   | 68 |
| 2.14. Two-dimensional gel electrophoresis (2DE)                             | 69 |
| 2.14.1. Solutions   | 69 |
| 2.14.2 Protocol   | 70 |
| 2.15. Western blotting  | 71 |
| 2.15.1. Solutions   | 71 |
| 2.15.2. Protocol  | 72 |
| 2.16. Thrombin cleavage   | 72 |
| 2.16.1. Solutions   | 72 |
| 2.16.2. Protocol  | 73 |
| 2.17. Coupling protein to Sepharose beads                                   | 73 |
| 2.17.1. Solutions   | 73 |
| 2.17.2. Protocol  | 74 |
| 2.18. Deubiquitination assay  | 75 |
| 2.18.1. Solutions   | 75 |

|   |    |
|---|----|
| 2.18.2. Protocol                        | 75 |
| 2.19. Ubiquitin–Sepharose binding assay | 75 |
| 2.19.1. Solutions                       | 75 |
| 2.19.2. Protocol                        | 76 |
| 2.20. Polyubiquitin chain-binding assay | 77 |
| 2.20.1. GST-tagged proteins             | 77 |
| 2.20.1.1. Solutions                     | 77 |
| 2.20.1.2. Protocol                      | 77 |
| 2.20.2. Thrombin cleaved proteins       | 78 |
| 2.20.2.1. Solutions                     | 78 |
| 2.20.2.2. Protocol                      | 78 |
| 2.21. MG132 treatment of U20S cells     | 79 |
| 2.21.1. Solutions                       | 79 |
| 2.22.2. Protocol                        | 79 |
| 2.22. Pulldown Assays                   | 79 |
| 2.22.1. Rat muscle                      | 79 |
| 2.22.1.1. Affinity chromatography       | 79 |
| 2.22.1.1.1. Solutions                   | 80 |
| 2.22.1.1.2. Protocol                    | 80 |
| 2.22.1.2. Deubiquitination              | 81 |
| 2.22.1.2.1. Solutions                   | 81 |
| 2.22.1.2.2. Protocol                    | 81 |
| 2.22.2. Mouse cortex                    | 82 |
| 2.22.2.1. Affinity chromatography       | 82 |
| 2.22.2.1.1. Solutions                   | 82 |
| 2.22.2.1.2. Protocol                    | 83 |
| 2.22.3. U20S cells                      | 83 |

|  |           |
|--|-----------|
| 2.22.2.1. <i>Affinity chromatography</i>   | 83        |
| 2.22.2.1.1. <i>Solutions</i>   | 83        |
| 2.22.2.1.2. <i>Protocol</i>  | 84        |
| 2.22.3. <i>Human muscle</i>  | 84        |
| 2.22.2.1. <i>Affinity chromatography</i>   | 84        |
| 2.22.2.1.1. <i>Solutions</i>   | 84        |
| 2.22.2.1.2. <i>Protocol</i>  | 85        |
| 2.23. <i>Trypsinolysis and mass spectrometry analysis</i>  | 85        |
| 2.23.1. <i>Solutions</i>   | 85        |
| 2.23.2. <i>Protocol</i>  | 86        |
| <b>CHAPTER 3</b>   | <b>87</b> |
| <b>Expression profiling of ZNF216 in different models of skeletal muscle atrophy</b>                               | <b>87</b> |
| 3.1. <i>Introduction</i>   | 88        |
| 3.2. <i>Primer and probe sets specifically target ZNF216, MAFbx, MuRF1, Fbxo25, AWP1 and HMBS mRNA sequences</i>   | 89        |
| 3.3. <i>Continuous infusion of LPS for 24h decreases the protein-to-DNA ratio of rat EDL muscle</i>                | 92        |
| 3.4. <i>Continuous infusion of LPS for 24h increases ZNF216 mRNA levels in rat EDL muscle</i>                      | 98        |
| 3.5. <i>Low dose Dex treatment fails to blunt increases in ZNF216 mRNA levels induced by LPS in rat EDL muscle</i> | 100       |
| 3.6. <i>Daily simvastatin treatment for 12 days increases ZNF216 mRNA levels in rat EDL muscle</i>                 | 102       |
| 3.7. <i>Discussion</i>   | 104       |

|   |            |
|---|------------|
| 3.7.1. <i>ZNF216 mRNA expression is upregulated in EDL muscle in an LPS-infusion model of sepsis</i>  | 104        |
| 3.7.2. <i>ZNF216 mRNA expression is induced to a lesser level than other atrogenes under LPS-induced atrophy and statin-induced myopathy conditions</i> | 105        |
| 3.7.3. <i>Fbxo25 may compete with MAFbx for binding to components of SCF-type E3s in rats</i>   | 107        |
| 3.7.4. <i>ZNF216 may be activated by the same pathways as atrogenes MAFbx and MuRF1</i>   | 108        |
| 3.7.5. <i>Statin-induced myopathy induces ZNF216 expression</i>   | 108        |
| 3.7.6. <i>Protein-to-DNA ratio may not be a sensitive indicator of skeletal muscle atrophy</i>  | 110        |
| <b>CHAPTER 4</b>  | <b>112</b> |
| <b>Functional characterisation of the ZNF216 protein</b>  | <b>112</b> |
| 4.1. Introduction   | 113        |
| 4.2. Recombinant GST-rZNF216 protein binds to ubiquitin-Sepharose   | 115        |
| 4.3. Recombinant GST-rZNF216 protein binds to K48- and K63-linked polyubiquitin chains  | 116        |
| 4.4. Recombinant GST-rZNF216 protein does not exhibit deubiquitinating activity   | 121        |
| 4.5. Using immobilised rZNF216 protein to purify <i>in vivo</i> ubiquitinated skeletal muscle proteins  | 125        |
| 4.5.1. <i>Profile of rat skeletal muscle proteins binding to wild type or C30/33A mutant rZNF216 are indistinguishable by SDS PAGE</i>                  | 128        |

|  |            |
|--|------------|
| 4.5.2. Two-dimensional gel electrophoresis (2DE) preferentially resolves lower molecular weight rZNF216-binding proteins   | 131        |
| 4.5.3. Spot pattern of ubiquitin-positive rZNF216-binding proteins resolved by 2DE is similar to that of unanchored polyubiquitin chains                               | 133        |
| 4.5.4. Optimising affinity capture by ZNF216 of ubiquitinated proteins using different buffers   | 135        |
| 4.5.5. Using on bead deubiquitination to identify ubiquitinated muscle proteins bound to FL rZNF216 and the Znf_A20 domain under optimised affinity capture conditions | 137        |
| 4.5.6. LC-MS/MS analyses of deubiquitinated FL rZNF216/Znf_A20 domain-binding proteins   | 142        |
| 4.6. Discussion  | 148        |
| 4.6.1. ZNF216 polyubiquitin binding and linkage specificity  | 148        |
| 4.6.2. ZNF216 as a shuttle protein for polyubiquitinated proteins  | 150        |
| 4.6.3. Znf_A20 and ZNF216-binding polyubiquitinated protein candidates revealed by LC-MS/MS  | 152        |
| 4.6.4. Limitations of the LC-MS/MS approach  | 154        |
| 4.6.5. Utilising the Znf_A20 domain of ZNF216 to bind polyubiquitinated proteins   | 155        |
| <b>CHAPTER 5</b>   | <b>157</b> |
| <b>Polyubiquitinated protein profiling and the purification of unanchored polyubiquitin chains</b>   | <b>157</b> |
| 5.1. Introduction  | 158        |
| 5.2 The Znf_A20 domain can be used to profile global ubiquitination changes in proteasome-knockout mouse brains  | 158        |

|  |     |
|--|-----|
| 5.3. The Znf_A20 domain can be used to profile global ubiquitination changes in cells following pharmacological proteasome inhibition    | 161 |
| 5.4. The Znf_A20 domain reveals subtle changes in the profile of ubiquitinated proteins in rat EDL muscle after 24 hours of LPS infusion | 162 |
| 5.5. Reassessment of the presumed diubiquitin band purified by the Znf_A20 domain  | 165 |
| 5.6. Unanchored polyubiquitin chains   | 169 |
| 5.6.1. <i>Physiological significance of unanchored polyubiquitin chains</i>  | 169 |
| 5.6.2. <i>PMF analysis confirms ubiquitin sequence in the presumed ubiquitin dimer purified using Znf_A20 domain</i>                     | 170 |
| 5.6.3. <i>The Znf_A20-purified ubiquitin dimer from skeletal muscle is K48-linked</i>  | 173 |
| 5.6.3.1 <i>Evidence from K48-polyubiquitin specific immunoblotting of the ubiquitin dimer</i>  | 173 |
| 5.6.3.2. <i>Mass spectrometry analysis confirms the K48 linkage within the ubiquitin dimer</i>   | 175 |
| 5.6.3.4. <i>The Znf_A20 domain shows no apparent ubiquitin linkage specificity in the gas phase</i>                                      | 178 |
| 5.6.4. <i>The Znf_A20 domain binds via the acidic D58 interaction surface on ubiquitin</i>   | 180 |
| 5.6.5. <i>Structural models of monoubiquitin and diubiquitin binding Znf_A20</i>   | 182 |
| 5.6.6. <i>Sparing of K48-Ub<sub>2</sub> from USP2-mediated deubiquitination</i>  | 185 |
| 5.6.7. <i>The Znf_UBP domain of isopeptidase T binds the free C-terminus of unanchored polyubiquitin</i>                                 | 187 |
| 5.6.8. <i>Specificity of the Znf_UBP domain for unanchored polyubiquitin</i>   | 189 |
| 5.6.9. <i>Skeletal muscle diubiquitin binds to the Znf_UBP domain</i>  | 192 |

|   |            |
|---|------------|
| 5.6.10. Existence of longer chains of unanchored polyubiquitin in the Znf_UBP domain-purified fractions | 194        |
| 5.6.11. Increase in unanchored polyubiquitin chains following MG132 treatment of cultured cells         | 196        |
| 5.6.12. Optimisation for purification of unanchored polyubiquitin chains                                | 196        |
| 5.7 Discussion  | 202        |
| 5.7.1. Evidence that the skeletal muscle ubiquitin dimer is an endogenous species                       | 202        |
| 5.7.2. Proposed biological roles of unanchored polyubiquitin  | 204        |
| 5.7.3. Biological role of shorter unanchored polyubiquitin  | 207        |
| 5.7.4. Characterisation of unanchored polyubiquitin chains purified via the Znf_UBP domain              | 208        |
| 5.7.5. Stability of unanchored polyubiquitin chains   | 209        |
| 5.7.6. Predominance of K48-linked unanchored polyubiquitin  | 210        |
| <b>CHAPTER 6</b>  | <b>212</b> |
| <b>General discussion</b>   | <b>212</b> |
| 6.1. Summary  | 213        |
| 6.2. The Znf_A20 domain does not bind monoubiquitin in pulldowns and shows no linkage specificity       | 214        |
| 6.3. Sparing of diubiquitin during USP2 deubiquitination  | 215        |
| 6.4. Possible novel roles of ZNF216 and unanchored polyubiquitin chains during skeletal muscle atrophy  | 216        |
| 6.5. Final conclusions and future work  | 218        |
| References  | 221        |

|             |     |
|-------------|-----|
| Appendix I  | 234 |
| Appendix II | 235 |

## Abbreviations

|                |  |
|----------------|--|
| 2DE            | Two-dimensional gel electrophoresis                |
| AAA            | ATPase associated with various cellular activities |
| AK1            | Adenylate kinase 1                                 |
| AWP1           | Protein associated with PRK1                       |
| Atg5           | Autophagy-related gene 5                           |
| AMP            | Adenosine monophosphate                            |
| ATP            | Adenosine triphosphate                             |
| cDNA           | Complementary DNA                                  |
| CARD           | Caspase activation and recruitment domains         |
| CD14           | Cluster of differentiation 14                      |
| CID            | Collision induced dissociation                     |
| CLP            | Cecal ligation and puncture                        |
| CNBr Seph 4B   | Cyanogen bromide activated Sepharose-4B            |
| C <sub>t</sub> | Cycle-threshold                                    |
| Cul1           | Cullin 1   |
| CYLD           | Cylindromatosis (turban tumor syndrome)            |
| Dex            | Dexamethasone                                      |
| DNA            | Deoxyribonucleic acid                              |
| DMSO           | Dimethyl sulphoxide                                |
| DTT            | Dithiothreitol                                     |
| DUB            | Deubiquitinating enzyme                            |
| ECD            | Electron-capture dissociation                      |
| EDL            | Extensor digitorum longus                          |

|                 |   |
|-----------------|---|
| ESI             | Electrospray ionisation                                     |
| Fbxo25          | F-box protein 25  |
| FL              | Full length   |
| FOXO            | Forkhead box, class O                                       |
| GAPDH           | Glyceraldehyde 3-phosphate-dehydrogenase                    |
| HAUSP           | Herpes simplex virus associated ubiquitin-specific protease |
| HECT            | Homologous to the E6-AP carboxyl terminus                   |
| HEK293          | Human embryonic kidney cell line 293                        |
| HIV             | Human immunodeficiency virus                                |
| HMBS            | Hydroxymethylbilane synthase                                |
| HRP             | Horseradish peroxidase                                      |
| HTLV-1          | Human T-cell leukemia virus type 1                          |
| IEF             | Isoelectric focussing                                       |
| IFN- $\gamma$ , | Interferon-gamma  |
| IGF1            | Insulin-like growth factor 1                                |
| IGF1-BP5        | Insulin-like growth factor 1-binding protein 5              |
| I $\kappa$ B    | Inhibitory proteins of $\kappa$ B family                    |
| IKK             | I $\kappa$ B kinase   |
| IL-1            | Interleukin-1   |
| IL-6            | Interleukin-6   |
| IRAK            | IL-1 receptor-associated kinase                             |
| IsoT            | Isopeptidase T  |
| IPG             | Immobilised pH gradient                                     |
| i.v.            | Intravenously   |

|           |  |
|-----------|--|
| JAMM      | Jab/MPN domain-associated metallopeptidase                 |
| Kd        | Dissociation constant                                      |
| KO        | Knock-out  |
| LCD       | Leucine-charged residue-rich                               |
| LC-MS/MS  | Liquid chromatography tandem mass spectrometry             |
| LPS       | Lipopolysaccharide   |
| LRRs      | Leucine-rich repeats                                       |
| MALDI-TOF | Matrix-assisted laser desorption/ionisation time-of-flight |
| MHC       | Myosin heavy chain   |
| MS        | Mass spectrometry  |
| MS/MS     | Tandem mass spectrometry                                   |
| MyBP-C    | Myosin-binding protein C                                   |
| MyLC1/2   | Myosin light chains 1/2                                    |
| MyHC      | Myosin heavy chain   |
| NLS       | Nuclear localisation signal                                |
| OTU       | Ovarian tumour   |
| Otu1      | Otubain 1  |
| p38 MAPK  | p38 mitogen-activated protein kinase                       |
| PCR       | Polymerase chain reaction                                  |
| mRNA      | Messenger RNA  |
| MAFbx     | Muscle atrophy F-box protein                               |
| MDM2      | Murine double minute 2                                     |
| MuRF1     | Muscle RING-finger 1                                       |
| MVB       | Multi-vesicular bodies                                     |

|                |  |
|----------------|--|
| MyD88          | Myeloid differentiation primary gene 88                        |
| NEM            | N-ethylmaleimide   |
| NEMO           | NF- $\kappa$ B essential modifier                              |
| NF- $\kappa$ B | Nuclear factor kappa-light-chain-enhancer of activated B cells |
| NIK            | NF- $\kappa$ B-inducing kinase                                 |
| NMR            | Nuclear magnetic resonance                                     |
| pI             | Protein iso-electric point                                     |
| <i>Psmc1</i>   | Proteasome 26S subunit ATPase 1 gene                           |
| PMF            | Peptide mass fingerprinting                                    |
| PI3K           | PI3-kinase   |
| RABEX5         | RAB5 guanine nucleotide exchange factor                        |
| RAD23          | Radiation sensitivity abnormal 23                              |
| RANK           | Receptor and activator of NF- $\kappa$ B                       |
| Rfu1           | Regulator of free ubiquitin chains 1                           |
| RHD            | Rel homology domain  |
| RIG-I          | Retinoid-inducible gene 1                                      |
| RING           | Really interesting new gene                                    |
| RIP1           | Receptor interacting protein 1                                 |
| RNA            | Ribonucleic acid   |
| RNAi           | RNA interference   |
| Rpn            | Regulatory particle non-ATPase                                 |
| RT-PCR         | Real time PCR  |
| SCF complex    | Skp1-Cul1-F-box protein complex                                |
| SDS PAGE       | Sodium dodecyl sulphate polyacrylamide gel electrophoresis     |

|              |  |
|--------------|--|
| Skp1         | S-phase kinase-associated protein 1                    |
| SRF          | Serum response factor                                  |
| TAB2/3       | TAK1 binding protein 2/3                               |
| TAK1         | Transforming growth factor $\beta$ -activated kinase 1 |
| TNF $\alpha$ | Tumour necrosis factor alpha                           |
| TnI          | Troponin-I   |
| TLR4         | Toll-like receptor 4                                   |
| TRAF6        | TNF-receptor associated factor 6                       |
| TRIM5        | Tripartite motif containing 5                          |
| TUBEs        | Tandem-repeated ubiquitin-binding entities             |
| Ub           | Ubiquitin  |
| UBA          | Ubiquitin associated domain                            |
| UBD          | Ubiquitin binding domain                               |
| UCH-L3       | Ubiquitin carboxyl-terminal hydrolase isozyme L3       |
| UIM          | Ubiquitin-interacting motif                            |
| UPS          | Ubiquitin proteasome system                            |
| USP2         | Ubiquitin specific peptidase 2                         |
| VCP          | Valosin-containing protein                             |
| WD repeats   | Trp-Asp repeats  |
| ZNF216       | Zinc finger protein 216                                |
| ZnF4         | Zinc finger 4  |

## **CHAPTER 1**

### **General Introduction**

## **1.1. Introduction**

Skeletal muscle atrophy describes a reduction in muscle size that often accompanies other disease states; associated weakness and reduced muscular function makes this a debilitating condition. This introduction highlights the importance of understanding the molecular mechanisms which underlie skeletal muscle atrophy, and describes the current understanding of the proteins and pathways involved. One such protein that has recently been identified for its role in muscle atrophy is zinc finger protein 216 (ZNF216). We note strategies that have been previously employed to proteomically analyse ubiquitinated proteins, and conclude with current information on ZNF216, the ubiquitin receptor we have characterised within this thesis *via* its expression and interactions.

## **1.2. Clinical importance of skeletal muscle atrophy**

The onset of skeletal muscle atrophy in combination with life threatening diseases, such as cancer and AIDS, is associated with longer recovery time and increased mortality [1, 2]. Pajak *et al.* 2008 state that almost a third of all cancer deaths are due to muscle cachexia, which causes cardiac and respiratory failure [3]. Muscle wasting may also be induced by catabolic states such as sepsis [4-6], denervation [7-10] and immobilisation or disuse [11-13], illustrating the various triggers of atrophy. Hasselgren *et al.* 2005 reviews various aspects of muscle atrophy initiated by sepsis, and briefly reviews the clinical implications, which include loss of ambulation and pulmonary complications [14]. Disuse induced muscle atrophy may also be relevant to astronauts, who suffer muscle loss during space flight due to the lack of gravity, or more commonly is experienced by

inactive patients who are hospitalised [15]. Loss of muscle strength and mass is additionally associated with old age, termed “sarcopenia” and reviewed in more detail elsewhere [16, 17]. Sarcopenia differs from other atrophy types as multiple factors induce this condition, through largely unknown mechanisms, which have been suggested to, in part, involve apoptosis, as reviewed in more depth by Marzetti *et al.* 2010 [17].

Muscle wasting has traditionally been recognised by reduced muscle size, induced by increased levels of protein degradation, coupled with down-regulated protein synthesis. In the case of fasting induced skeletal muscle atrophy, protein degradation into individual amino acids has been suggested as an advantage for providing a source of energy when carbohydrates and fats are at low levels. The reason for muscle atrophy onset under other conditions is unclear, as no apparent physiological advantage is evident. The muscle atrophy-inducing effect of immobilisation has been reversed by exercise, but this cannot be applied to muscle wasting caused by other triggers [18] and to date no drug has been produced that specifically inhibits atrophy onset.

Studies have previously focused on cytokines released that trigger muscle cells to shrink, but clearly there can be a number of upstream pathways that result in muscle wasting. Biochemical and genetic studies have revealed that muscle atrophy is not a random chaotic event, but that specific proteins are upregulated and involved in an “atrophy programme”, as detailed below in Section 1.5. While the initial biochemical pathways have been relatively well characterised, the downstream events, which multiple modes of skeletal muscle atrophy may share in common, are yet to be fully elucidated. By clearly characterising these

pathways, and identifying specific targets required for muscle atrophy under all conditions, potential drug targets may be identified that could ultimately improve the prognosis of patients affected by muscle wasting.

### **1.3. Models of skeletal muscle atrophy**

Ultimately, we are interested to understand modes of human skeletal muscle atrophy. However, while human studies involving immobilisation can be performed, atrophy triggers such as cancer and sepsis cannot be induced in humans. Samples from patients with cancer or from patients in intensive care are useful for validating potential mediators of skeletal muscle atrophy [19], but there can be multiple factors that vary between patients. Thus, animal models are of importance because these factors can be controlled for, as muscle atrophy can be induced, something that is ethically impossible to do in humans. The drawbacks of animal models arise as there are some differences in physiology between species. In addition there is some debate over the age of rats used for models, as juveniles may respond differently to atrophy stimuli.

Tumours can be introduced in animals for cachexia models, including C26-B adenocarcinoma implantation in mice [20] and Yoshida AH-130 ascites hepatoma inoculation in rats [21]. Models of sepsis in animals vary from infecting animals with live bacteria *via* cecal ligation and puncture (CLP) or by intravenously infusing animals with lipopolysaccharide (LPS), collected from Gram-negative bacteria that express LPS. LPS is recognised by a core tri-molecular complex of cluster of differentiation 14/toll-like receptor 4/MD2 (CD14/TLR4/MD2) in mammalian macrophage cells and induces anti-bacterial responses. Similarly,

studies into LPS-induced atrophy in C2C12 (mouse myoblast cell line) myotubes indicate that LPS is recognised by TLR4 and mediates downstream events [22]. The molecular events surrounding LPS recognition involve a number of protein-protein interactions, contrary to initial theories which regarded innate immune responses, such as LPS recognition, to be less complex than the acquired immune response, as discussed in more detail in Triantafilou & Triantafilou 2005 [23]. Sarcopenia models have primarily been based on *Caenorhabditis elegans* [24, 25], a well established and useful model, based on its short life cycle, low maintenance costs and small size (1mm in length). Additionally, *C. elegans* genome is relatively small and fully characterised and shares considerable homology with that of mammals, allowing identification of sarcopenia related genes through RNA interference (RNAi) in worms [26]. However, one group published findings supporting the suitability of the Rhesus monkey as a non-human primate model of sarcopenia [27], which has subsequently been utilised and produced data that suggested caloric restriction lessened age-related changes in Type II muscle fibres and fibre cross-sectional area in aging rhesus monkeys [28].

Diminished or ablated signalling from the nervous system to muscle triggers atrophy, thus animal models of denervation involve interrupting signalling to skeletal muscle *via* severing of the sciatic nerve. Animal models allow controls to be introduced and can reveal genes and proteins that are upregulated or required in different modes of atrophy. The human homologs of these candidates can then be assessed for their involvement in patients with muscle atrophy, to validate them in a human situation [19].

#### **1.4. Sensitivity to muscle atrophy is dependent on muscle type and species**

Skeletal muscle, which can be consciously controlled and is sometimes referred to as “voluntary muscle”, may be categorised as “slow-twitch” or “fast-twitch” muscle, containing type I or type II fibres, respectively. As the names suggests, slow-twitch muscle contracts slowly, metabolising aerobically and thus requiring a rich blood supply, hence its characteristic red appearance. Slow-twitch muscle contains numerous mitochondria for aerobic respiration, thus requiring large numbers of capillaries to deliver enough blood to meet the high oxygen demand. Fast-twitch muscle contracts rapidly and can produce a greater force than that of slow-twitch muscle. Fast-twitch muscle contains further subtypes IIa, IIb and IIx. Subtype IIa is similar to slow-twitch muscle in having a rich blood supply and large numbers of mitochondria and thus metabolising aerobically, but contracts more quickly than type I fibres. However, this subtype is rare in humans, in which the fastest fibre is type IIx. Unlike type I/type IIa fibres, this subtype metabolises anaerobically utilising glycolysis [29], contracting at a faster rate but exhausting sooner. Type IIb fibres similarly respire anaerobically, and are the major constituent of rodent skeletal muscle. Type IIx and IIb have considerably less mitochondria than types I and IIa, thus requiring less blood and having a paler appearance.

Severity of muscle atrophy is predominantly measured by percentage muscle loss. An alternative method for measuring the extent of muscle atrophy is by calculating changes in protein-to-DNA ratio, as a method for determining protein catabolism [30-32]. However, this ratio is less frequently measured than percentage muscle weight loss.

The severity of muscle wasting, as occurs in different modes of skeletal muscle atrophy, varies depending on muscle type. In a fasting-induced model of atrophy in rats, the authors noted a difference in the severity of wasting between muscle types, measured by weight loss in fast-twitch plantaris muscle (primarily type IIa) relative to slow-twitch soleus muscle (type I) [33]. Plantaris muscle was more sensitive to wasting relative to soleus, the former exhibiting increasing weight loss from one to three days of fasting, whilst weight loss of soleus muscle was first observed on the third day and to a lesser extent than that of plantaris muscle. This was attributed to a difference in autophagy signalling between different muscle types. The lysosomal based catabolic process autophagy contributes to some modes of muscle atrophy, as discussed later in Section 1.7. Conversely, a group utilising a denervation induced atrophy model in rats (in which the sciatic nerve was crushed), observed that slow-twitch soleus muscle was more sensitive to wasting than fast-twitch extensor digitorum longus (EDL) muscle (type IIb), when comparing muscle loss in denervated/innervated limbs [34]. This study was designed to measure the sparing effect of the proteasome inhibitor Velcade in a denervation model of atrophy, and the authors noted greater sparing of slow-twitch muscle upon Velcade treatment relative to fast-twitch muscle, implicating the involvement of the ubiquitin proteasome system (UPS) during denervation induced atrophy, primarily in soleus over EDL muscle. The UPS is one of the cells major processes responsible for degradation of cellular proteins (further details on the UPS later). A similar observation was made in a rat unloading model of muscle atrophy, in which soleus muscle was more severely wasted upon unloading relative to unloaded EDL muscle [35]. The authors also noted that unloaded soleus muscle had significantly higher ubiquitin levels relative to control, but no significant difference was observed in unloaded EDL muscle relative to control.

It would appear, from these models, that muscle atrophy involving the UPS affects slow-twitch muscle preferentially to fast-twitch muscle. However, earlier studies on a CLP induced sepsis model of muscle atrophy in rats provided evidence of UPS involvement in this mode of atrophy specifically in fast-twitch EDL relative to slow-twitch soleus, in which ubiquitin mRNA levels and energy-dependent protein breakdown were observed to increase only in the former [6]. This highlights the differences between different models of skeletal muscle atrophy, and emphasises the importance of studying multiple modes of wasting to clarify their different molecular regulation. Some muscles contain mixed fibre type, containing both fast-twitch and slow-twitch fibres, such as gastrocnemius (contains type I, IIa, IIx and IIb). Similarly to observations in other muscles, denervation induced muscle atrophy led to increases in ubiquitin-protein conjugates and ATP-dependent proteolysis in gastrocnemius muscle [36].

Skeletal muscle atrophy studies heavily rely on rodent models of atrophy. The differences in muscle fibre types between humans and rodents complicates the use of these animals in skeletal muscle atrophy models; as noted earlier, rodents predominantly contain type IIb skeletal muscle, whilst the fastest contracting human fast-twitch muscle is type IIx. Murton *et al.* 2008 reviews the involvement of the UPS during human skeletal muscle atrophy, and discusses differences between animal models and observations in humans [37]. The authors note differences between the physiology of rodents and humans, and the differences in severity of animal models and human studies, in which the former are more severe conditions that may induce stronger responses than that observed in humans. This emphasises the importance of validating the role of human homologs of atrophy related genes in rodent models, and vice versa.

## **1.5. Understanding molecular mechanisms that instigate muscle wasting**

The onset of skeletal muscle atrophy may be triggered by multiple stimuli, which may directly initiate atrophy signalling pathways in skeletal muscle, or alternatively stimulate immune cells, including macrophages, to release cytokines that subsequently induce an atrophy response in muscle cells. As extensively reviewed in Pajak *et al.* 2008, multiple inflammatory cytokines may promote downstream muscle atrophy signalling, including tumour necrosis factor alpha (TNF $\alpha$ ) and interleukin-1 (IL-1), which they note may be released from immune cells in response to a tumour, or from the tumour itself [3]. The authors review a number of papers with conflicting observations, in which TNF $\alpha$  has been observed to be sufficient to activate downstream atrophy signalling, whereas others noted the requirement of additional cytokines to facilitate TNF $\alpha$  signalling, including IL-1 $\beta$ , interleukin-6 (IL-6) and interferon-gamma (IFN- $\gamma$ ). They noted that TNF $\alpha$ , IL-1 $\beta$  and IL-6 can be produced and secreted from muscle fibres themselves. Li *et al.* 2009 observed that both IL-1 $\alpha$  and IL-1 $\beta$  could directly signal to C2C12 cells, stimulating p38 mitogen-activated protein kinase (p38 MAPK) phosphorylation and nuclear factor kappa-light-chain-enhancer of activated B cells (NF- $\kappa$ B) signalling, that resulted in significant shrinking of myotubes after 48 hours of stimulation [38]. NF- $\kappa$ B signalling is discussed in further detail in Section 1.9.1.5. Thus IL-1 $\alpha$  and IL-1 $\beta$  alone were sufficient to trigger an atrophy response in C2C12 myotubes.

As noted earlier in Section 1.3, LPS-induced atrophy in C2C12 cells stimulates TLR4 activation [22]. Similarly to observations in IL-1 $\alpha$  and IL-1 $\beta$  stimulated cells, Doyle *et al.* 2011 observed TLR4 signalling was propagated *via* p38 MAPK

activation, which mediated downstream atrophy events, and the authors demonstrated that TLR4 knockout or inhibition of p38 MAPK abolished myotube atrophy. Cachectic factors such as TNF $\alpha$  thus have a role in skeletal atrophy in stimulating downstream signalling to increase protein degradation, in part *via* increased activity of the UPS (see Section 1.7.) However, muscle size is determined by both catabolic signals and anabolic signalling, which is comprehensively described in Sandri *et al.* 2008 [39]. Anabolic signalling is regulated by growth factors, including insulin-like growth factor 1 (IGF1), which stimulates PI3-kinase (PI3K) generation of phosphatidylinositol-3,4,5-triphosphates, that subsequently activates Akt. IGF1 both induces muscle growth, also termed hypertrophy, by increasing protein synthesis and suppresses muscle protein breakdown (further information in Section 1.6) [40]. Under basal conditions, Akt inhibits the transcription factor forkhead box, class O (FoxO) by phosphorylating it and thus sequestering it in the cytoplasm. Upon dephosphorylation, FoxO can enter the nucleus and transcribe targeted atrophy related genes, suggesting a possible link between atrophy and hypertrophy signalling that might allow precise regulation of muscle size. Supporting this, a FoxO mutant resistant to Akt mediated phosphorylation prevented Akt mediated inhibition of downstream FoxO signalling targets [41]. Additionally, reduced circulating IGF-1 levels were observed in a rat model of sepsis [42] and in children diagnosed with cancer [43]. Conversely, mice bearing the C26 colon adenocarcinoma exhibited the same loss of muscle mass upon hyperexpression of IGF-1 [44] and whilst IGF-1 is down-regulated in a cancer cachexia in rats bearing the AH-130 hepatoma, muscle IGF-1 receptor increases [45]. Together, this suggests that the relationship between IGF-1/Akt signalling and muscle atrophy is yet to be fully elucidated and may be more complex than originally

considered. Figure 1.1, from Sandri *et al.* 2008, illustrates some of the pathways associated with muscle hypertrophy and atrophy that affect muscle fibre size.

Ultimately, muscle atrophy can be attributed to simultaneous decreased protein synthesis coupled with upregulated protein degradation *via* specific pathways in a co-ordinated manner, known as the atrophy programme. The relative contribution of depressed synthetic and promoted catabolic pathways differs between different modes of atrophy. Cancer induced atrophy was once believed to occur as a result of reduced protein synthesis rates [46], but more recent studies have identified a role for both depressed synthetic rates coupled with increased protein degradation during cancer cachexia [47]. Down-regulation of IGF-1 was noted in a sepsis model of atrophy in rats, causing a reduction in protein synthesis [48]. This supports the notion that atrophy may be induced by inverse regulation of the mediators of hypertrophy [49]. However, sepsis has been observed to also increase expression of genes required for protein degradation by the UPS [50, 51], and proteasome inhibitors inhibited sepsis-induced muscle proteolysis, strongly implicating the importance of protein degradation during muscle atrophy [52]. Upstream pathways, such as the release of cytokines and recognition of LPS to induce muscle atrophy signalling pathways have been extensively reviewed, although there is less information available about the downstream pathways. Evidence has emerged that while a decrease in protein synthesis, such as by IGF-1/Akt signalling is apparent, protein degradation is also upregulated. The common downstream pathways shared between different modes of muscle atrophy are unclear and studies have been performed to look for common genes/proteins that are upregulated across all models of muscle atrophy.

**Figure 1.1**

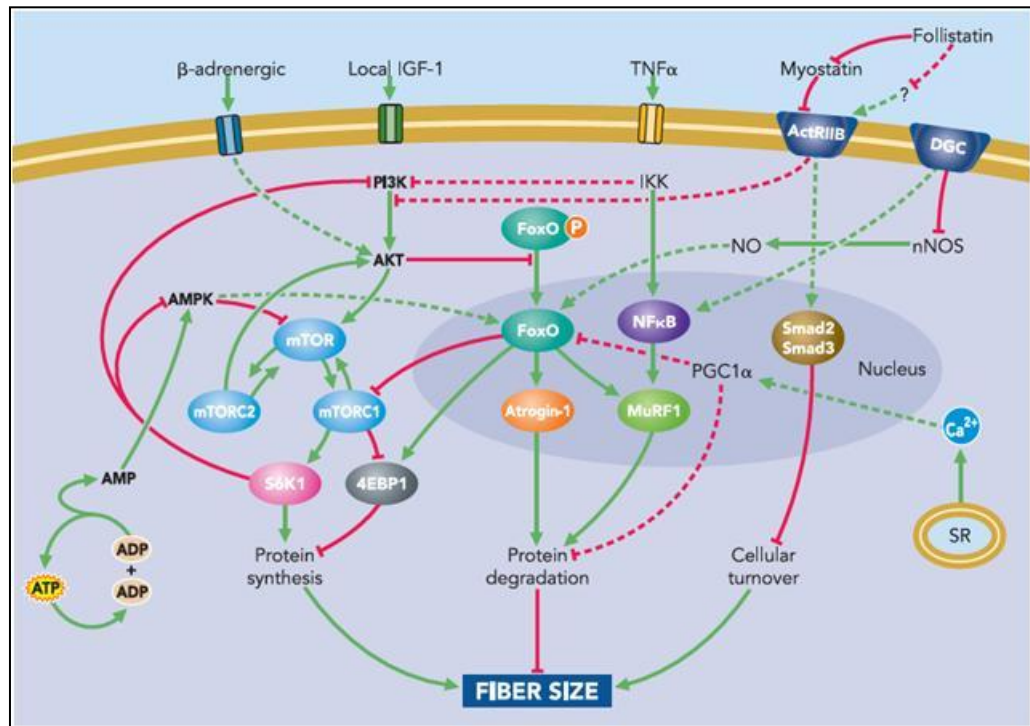


**Figure 1.1** Signalling pathways linked to hypertrophy and atrophy pathways that regulate muscle fibre size, taken from Sandri *et al.* 2008 [39].

## 1.6. Atrogenes

To address the question of whether there are common features of muscle atrophy, there has been investigation into the existence of atrophy related genes that are upregulated across multiple models of wasting. Whilst a number of transcripts are upregulated in response to a single model of atrophy, Bodine *et al.* 2001 identified transcripts upregulated in multiple rodent models, which included denervation, immobilisation and unweighting models [53]. Two transcripts were observed to be upregulated across all studied models (denervation, unweighting and immobilisation models); UPS components MAFbx and MuRF1, that are discussed in more detail in 1.8.1.1 and 1.8.1.2, respectively. To validate candidates, the authors utilised two further rats models of skeletal muscle atrophy, in which rodents were treated with either the cytokine IL-1 or a high dose of the glucocorticoid dexamethasone (Dex), in which both MAFbx and MuRF1 gene expression was upregulated over 10-fold. MAFbx and MuRF1 knockout in mice conferred resistance to denervation induced atrophy, further substantiating the importance of these proteins during atrophy. In recent knockout studies, in a mouse fasting model of muscle atrophy, small hairpin RNA (shRNA)-mediated MAFbx silencing reduced fasting-induced muscle loss [54]. Gomes *et al.* 2001 independently identified upregulation of a transcript in a fasting model of atrophy in mice using cDNA microarrays, which consistent with the observations of Bodine *et al.*, was identified to be MAFbx. This group validated MAFbx as a key component of the atrophy programme by confirming its increased expression in rodent models of fasting, diabetes, cancer and renal failure induced atrophy, and later coined the term “atrogenes”, relating to atrophy-related genes [40, 55]. MAFbx and MuRF1 are connected to the UPS, both being characterised as E3 ubiquitin ligases (see Section 1.9).

The concept of an atrophy programme, in which specific genes are up- or down-regulated was further evidenced by later cDNA microarray analysis of multiple models of muscle atrophy, again noting MAFbx and MuRF1 increased expression, as well as components of the UPS (see Section 1.7), and observing down-regulation of growth-related mRNAs, including IGF1-binding protein 5 (IGF1-BP5) [55]. More recently in 2006, a further protein ZNF216 was first studied for its involvement in denervation and fasting models of atrophy. Not only was ZNF216 mRNA and protein expression upregulated in these models, but ZNF216 knockout mice exhibited resistance to denervation-induced muscle atrophy. This implicated ZNF216 to be another key protein involved in the atrophy programme, which similarly to MAFbx and MuRF1 has a role in the UPS, and highlighted ZNF216 as a novel atrogene [56].

### **1.7. Skeletal muscle atrophy up-regulates components of the ubiquitin proteasome system (UPS)**

Skeletal muscle atrophy is associated with suppressed protein synthesis coupled with increased protein degradation, the latter of which is mediated by a number of different processes. Two of the main intracellular pathways for protein degradation are autophagy and the UPS. Autophagy is a mechanism that allows degradation of cellular proteins, including protein aggregates and damaged organelles, by forming a double membrane around the target that matures into an autophagosome upon fusion with lysosomes. Lysosomal cysteine proteases cathepsins B, D and L degrade the sequestered contents, the products of which are then recycled. Autophagy has been linked to fasting-induced atrophy (see Section 1.4), in which the difference in sensitivity between fast- and slow-twitch muscles was attributed to a difference in autophagy signalling [33]. Increased

autophagy has also been associated with denervation [57] and disuse [58] models of atrophy, in addition to upregulated UPS components and activity. Sandri 2010 comprehensively reviews the role of autophagy in skeletal muscle and notes that while it does have a role in several modes of muscle wasting, autophagy suppression may actually trigger muscle atrophy [59-61]. Interestingly, autophagy is activated under starvation conditions to prevent cell death, but excessive autophagic activity leads to this outcome, in a process distinct from apoptosis induced cell death. Maiuri *et al.* 2007 discusses the complex crosstalk between autophagy and apoptosis [62]. Autophagosome formation requires a number of autophagy-related (Atg) genes, including Atg5.

Interestingly, apoptosis has been associated with calpain-mediated cleavage of Atg5, in which truncated Atg5 localises with mitochondria and promotes apoptotic events *via* caspase activation [63]. Calpains and caspases are cysteine proteases associated with cell death, but have also been implicated having a potential role in disuse and sepsis induced muscle atrophy [64, 65], possibly by disrupting the sarcomere to allow degradation by the UPS. While autophagy clearly plays a role in skeletal muscle atrophy, ablation of this process is detrimental as it has a role in maintaining muscle mass, whereas proteasomal inhibition during denervation can reduce the severity of muscle wasting [34], suggesting that components of the UPS may be a more viable drug target for reducing the severity of muscle atrophy. Jagoe & Goldberg 2001 also suggest that muscle loss in cachexia is primarily due to increased UPS activity [66] and Donohoe *et al.* 2011 suggest that the UPS is the primary mechanism of protein degradation in cachexia [67].

The UPS targets proteins for degradation *via* the conjugation of a polyubiquitin tag, which is recognised by the 26S proteasome; further details are in Section 1.9. Earlier in this Chapter, multiple studies are cited in which UPS components have been observed to increase during muscle atrophy. Ubiquitin mRNA levels increase between 1.2-19-fold in denervation, sepsis, fasting, cancer, uremia and diabetes models of muscle atrophy in rodents and humans [6, 34, 50, 51, 55], as does proteasomal subunit mRNA expression between 1.5-5-fold [51, 55].

However, changes in UPS activity are not only associated with conditions such as muscle atrophy, but aberrant components of the UPS result in diseases such as Alzheimer's disease. The ability of ubiquitin to conjugate to other proteins, including other ubiquitin moieties, is vital for its function. A ubiquitin frameshift mutation is produced from misreading of mRNA for the human *Ub-B* gene, in which the reading frame is adjusted +1, and results in loss of the C-terminal Gly76 residue, essential for ubiquitin conjugation (see Section 1.9.1.5), which is replaced by a 20 amino acid nonsense extension sequence. This frameshift mutant is termed *Ubb*<sup>+1</sup>, which wild type ubiquitin is still able to conjugate to, and thus the *Ubb*<sup>+1</sup> mutant acts to "cap" polyubiquitin, preventing its conjugation to substrates. "Free" polyubiquitin chains, (not containing *Ubb*<sup>+1</sup>), have previously been observed to inhibit 26S proteasomal degradation of ubiquitinated substrates *in vitro* [68], and *Ubb*<sup>+1</sup> capped chains were shown to similarly inhibit the proteasome [69]. These *in vitro* studies in combination with evidence that *Ubb*<sup>+1</sup> capped polyubiquitin chains accumulate in patients with Alzheimer's disease suggest this frameshift mutant may contribute to the aetiology of this disease [69-71].

## **1.8. The importance of the ubiquitin proteasome system (UPS) during normal cellular function**

As mentioned previously, intracellular protein degradation may be carried out by a number of pathways, which includes the UPS. Components of the UPS may be upregulated or perturbed during disease, but protein degradation is also of fundamental importance for protein homeostasis during normal cellular function. Imai *et al.* 2003 reviews the link between molecular chaperones and the UPS in determining the fate of unfolded proteins [72]. The authors note that over a third of cellular proteins fold incorrectly when newly synthesised and that even correctly folded proteins are susceptible to damage. Chaperones can recognise unfolded/damaged proteins, for example by exposed stretches of hydrophobic residues, and cooperate with co-chaperones to refold proteins correctly. Conversely, the UPS can recognise misfolded/damaged proteins and proteolytically destroy them, to prevent protein aggregation, which is associated with a number of neurodegenerative diseases [73, 74]. Protein aggregates may be sequestered from other cellular components by the formation of aggresomes [75], which may fuse with lysosomes and be degraded *via* autophagy pathways [76, 77]. Kraft *et al.* 2010 discuss the pathways that link the autophagy system and the UPS, both of which utilise ubiquitin and ubiquitin-binding proteins [78]. For example, ubiquitin binding protein p62 is required for autophagy-mediated degradation of protein aggregates [79].

Imai *et al.* 2003 note that there is little known about how the fate of proteins, to be refolded or degraded, is determined. Ravid & Hochstrasser 2008 review the various mechanisms by which proteins are recognised for proteasomal degradation, and note that some proteins that do not fold correctly, termed

protein quality control (PQC) substrates, may expose “degrons” (degradation signals) that target them directly from the site of folding (often the endoplasmic reticulum (ER)) to the proteasome for degradation [80]. “N-degrons” are amongst the other degrons described by this review, which was discussed in further detail recently by Varshavsky 2011; the N-end rule describes observations that for certain proteins, their half-life *in vivo* is highly dependent on the identity of its N-terminal residue [80, 81]. N-terminal degrons, or destabilizing residues, include type I (basic) or type II (hydrophobic) residues. In eukaryotes, the N-end rule affects protein degradation *via* ubiquitin-dependent degradation, but interestingly similar observations are observed in prokaryotes which lack a UPS, reviewed in Mogk *et al.* 2007 [82]. Both eukaryotic and prokaryotic systems require recognition of the N-terminal residue of proteins by E3-ligase N-recogin or bacterial adaptor protein ClpS, respectively. Eukaryotic N-recogin mediates ubiquitination of the target, for proteasomal degradation (further details of UPS enzymes in Section 1.9.), while bacterial ClpS delivers the substrate to bacterial ClpAP protease complex [80, 82].

While ubiquitin is fundamental in general protein turnover for both UPS-mediated degradation and selective autophagy, ubiquitin is a protein that is also essential for signalling events and a host of non-degradative processes (see 1.9.1.5. for further details).

## 1.9. Components of UPS

### 1.9.1. Enzymes required for polyubiquitination

Ubiquitin conjugation to a substrate, *via* the C-terminal glycine residue of ubiquitin, is primarily controlled by 3 enzymes; classed as E1, E2 and E3 enzymes [83] (see Figure 1.2). A single ubiquitin may be conjugated, or alternatively multiple ubiquitin moieties may be added to form a polyubiquitin “tag”; both the number of attached ubiquitin proteins and isopeptide linkage determines the fate of the attached protein (see Section 1.9.1.5). The first event during ubiquitin conjugation is ATP-driven, in which an E1 ubiquitin-activating enzyme forms a thioester bond with ubiquitin. ATP is hydrolysed, and pyrophosphate is released upon AMP binding to the terminal carboxylate group of ubiquitin. Subsequently, ubiquitin is conjugated to a key cysteine residue within the E1 enzyme, *via* a sulfhydryl group. This “activated” ubiquitin can then be transferred to the sulfhydryl of an E2 conjugating enzyme.

E3 ubiquitin ligase enzymes then mediate transfer of ubiquitin to the  $\epsilon$ -amino group of a lysine residue within a substrate, forming an isopeptide bond. Interestingly, ubiquitin may occasionally be conjugated to the  $\alpha$ -amino group within the N-terminal residue of substrates [84]. E3 ligases, in combination with different E2 enzymes, confer substrate selectivity. It has been widely noted that while mammalian cells appear to have only two E1 enzymes, the enzymes responsible for specificity have been identified in greater numbers; 20-40 E2 enzymes and 500-1000 E3 ubiquitin ligases. The mode of ubiquitin transfer to a

**Figure 1.2**

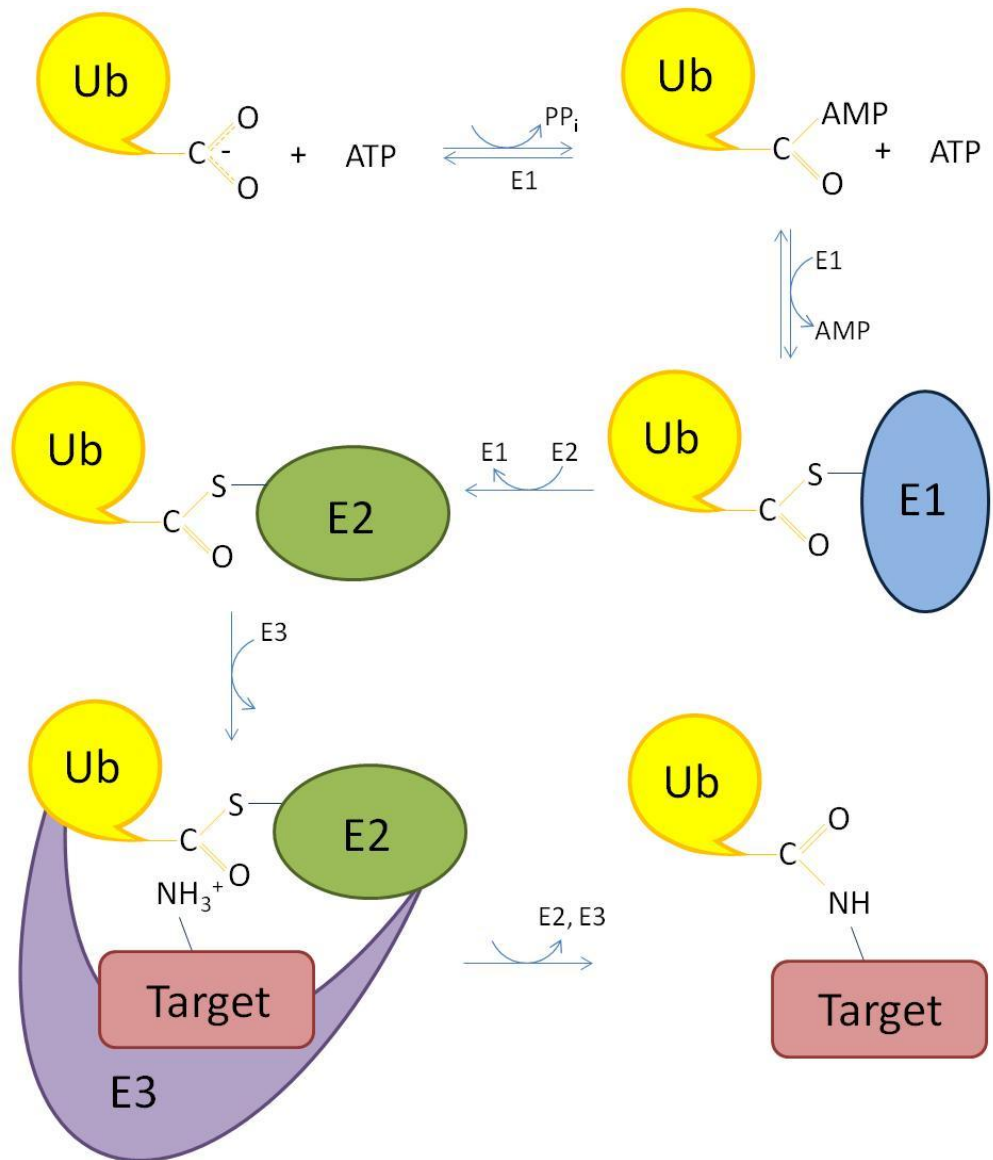


**Figure 1.2** Ubiquitin conjugation to a target protein. Ubiquitin is adenylated by an E1 activating enzyme and forms a thioester bond, *via* a key cysteine residue in the E1 enzyme. Ubiquitin is conjugated to an E2 conjugating enzyme, before an E3 ligase mediated transfer to a target protein, forming an isopeptide bond between ubiquitin and the target.

substrate varies depending on the E3 ligase involved, reviewed in more detail in Nagy & Dicik 2010 [85], and varies between the two major subtypes. HECT (homologous to the E6-AP carboxyl terminus)-type E3 ubiquitin ligases are one subtype of E3s, which contain catalytic activity and directly bind ubiquitin prior to transfer to a substrate. Nedd4 family members are included within this group, and mediate a number of physiological processes through ubiquitination, discussed in further detail in Rotin & Kumar 2009 [86]. The alternative major E3 subtype are RING- (really interesting new gene)-finger domain E3 ligases, that bring E2-conjugated ubiquitin within close proximity of target protein to mediate direct transfer from the E2 to the target. MuRF1 is a single subunit RING-finger E3 ligase, discussed in more detail in Section 1.9.1.2. However, RING E3-ligases may also include multi-subunit ligases such as the Skp1–Cul1–F-box protein (SCF) complex, reviewed in greater detail in Cardozo & Pagano 2004 [87]. F-box proteins within this complex are responsible for substrate recognition, and include MAFbx (see 1.9.1.1). RING-finger proteins contain zinc binding sites that support a finger-like structure (Figure 1.3). U-box E3 ligases have finger structures highly similar to RING E3 ligases, but lack zinc binding sites and stabilise the fold *via* hydrogen bonding [88] and are increasingly regarded as another major E3 ubiquitin ligase subtype [89, 90], although u-box ligases are predominantly associated with plants over other organisms [91].

Although not enzymes, a number of ubiquitin-binding proteins have been implicated in mediating translocation of ubiquitinated substrates to the proteasome for degradation. These may be considered as “shuttle factors”, often having a ubiquitin-like domain and a ubiquitin-binding domain, presumably to allow simultaneous binding to the proteasome and to polyubiquitinated

**Figure 1.3**

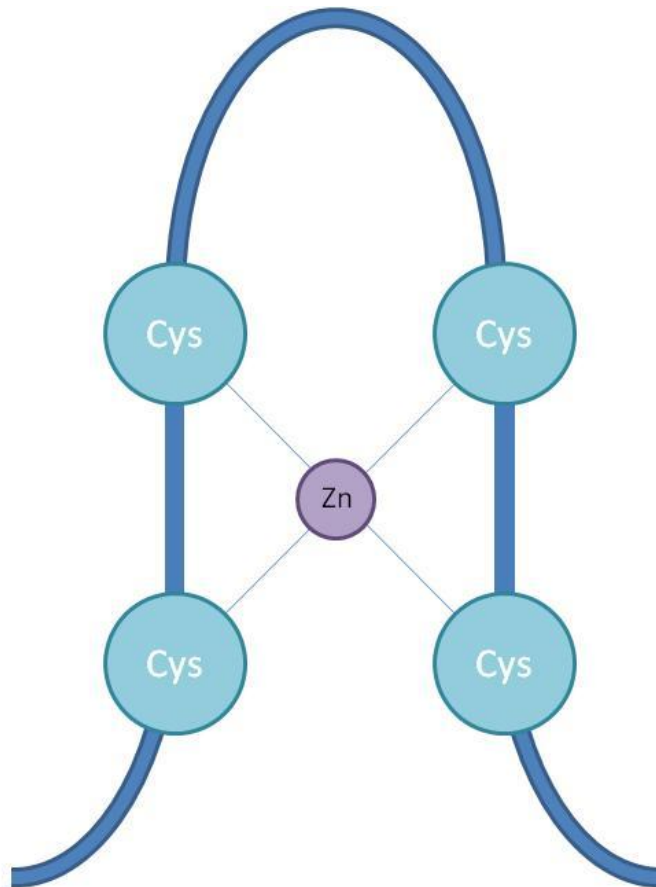


**Figure 1.3** Schematic representation of a zinc finger domain, in which four cysteine residues within a polypeptide bind a zinc cation to produce a finger-like structure. These are found in RING finger E3 ligases, as well as other ubiquitin-binding proteins and a number of proteins involved in DNA-binding.

substrates. Yeast proteins Rad23 and Dsk2 were suggested to be shuttle factors based on their ability to bind polyubiquitin and interact with the proteasome [92, 93]. Rad23 and Dsk2 mutants lacking ubiquitin-binding ability induced growth defects in yeast and provided evidence that shuttle factors play an important role in the UPS in yeast [92, 94]. However, shuttle proteins are not only present in yeast, as a mammalian shuttle factor valosin-containing protein (VCP)/p97 has been identified; reduced interaction of ubiquitinated substrates with this shuttle protein impairs proteolysis of the target, validating a role for shuttle proteins in the UPS in a mammalian context [95]. Zhang *et al.* 2009 suggested that shuttle factors preferentially associate with the proteasome when bound to a minimum ubiquitin chain length [96]. This was based on observations that ternary complexes involving yeast shuttle factor Dsk2 and proteasome subunit Rpn10 varied greatly depending on ubiquitin chain length. The atroгене ZNF216 has also been proposed to act as a shuttle protein during muscle atrophy, and is discussed further in Section 1.10.

MAFbx and MURF1 mRNA is predominantly expressed in skeletal muscle [53] and, as described in more detail in earlier sections, there is mounting evidence that these E3 ubiquitin ligases are both upregulated and required during multiple modes of muscle atrophy. This strongly implicates the importance of MAFbx and MuRF1 during skeletal muscle wasting, and prompted subsequent investigations into their biochemical roles and substrates.

### 1.9.1.1. MAFbx

MAFbx was initially identified independently by two groups [53, 97], and was noted to contain an F-box domain that could bind to other components of the SCF complex, implicating its function as an E3 ligase. The ~40 residue domain was first identified in cyclin F [98], and accordingly later named the F-box domain by the same group [99]. Bai *et al.* 1996 noted that Skp1 was required for ubiquitin-mediated proteolysis and bound cyclin F, and first associated F-box containing proteins with the UPS [99]. Human F-box proteins are divided into three subtypes, depending on the identity or presence of an additional domain; leucine-rich repeats (LRRs)- and WD (Trp-Asp) repeats are the most common, and F-box proteins containing these domains are named FBXL and FBXW proteins, respectively [100-102]. N-terminal to MAFbx's F-box domain are leucine zipper and leucine-charged residue-rich (LCD) domains. Like other F-box proteins that contain an alternative domain to that of the LRR or WD, or those that lack an additional domain, MAFbx is designated an FBXO protein; hence, MAFbx protein is derived from the *FBXO32* gene. Like other F-box proteins, MAFbx provides substrate specificity during SCF-mediated ubiquitination. The MAFbx containing SCF complex also includes Skp1, Cul1, Rbx1 proteins. This complex forms a horseshoe shape in which substrate binding *via* MAFbx brings the target within close proximity of E2-conjugated ubiquitin, mediating ubiquitin transfer from the E2 enzyme to the substrate (Figure 1.4). Multiple rounds of ubiquitination generates a polyubiquitin chain, and targets the substrate for 26S proteasomal degradation (see Section 1.9.1.3.).

Interestingly, another F-box protein, derived from *FBXO25*, shares high homology with MAFbx (see Chapter 3.2.), but expression is not induced during skeletal

**Figure 1.4**

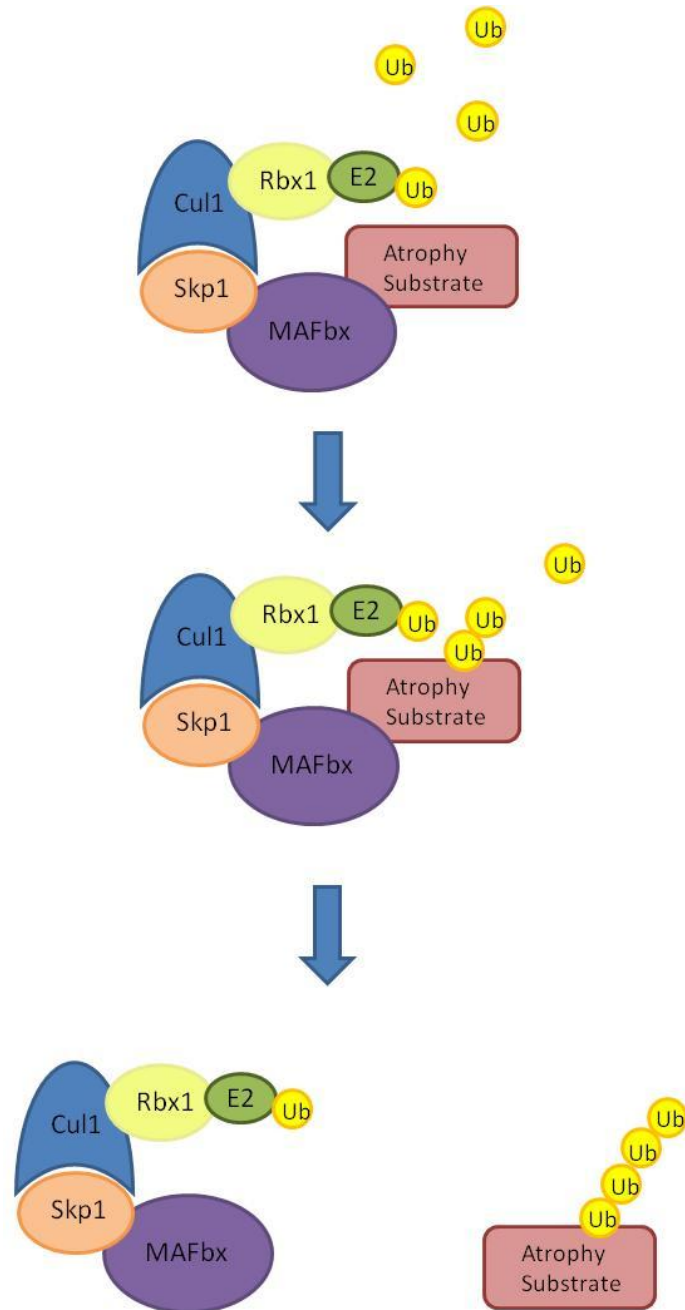


**Figure 1.4** MAFbx-mediated polyubiquitination of a muscle atrophy substrate. The SCF complex comprises of MAFbx, Skp1, Cul1 and Rbx1, forming a horseshoe shape. This binds an E2-conjugating enzyme, and holds a MAFbx selected substrate within close proximity of ubiquitin-conjugated E2's to mediate polyubiquitination.

muscle atrophy [103] and recent evidence implicates its involvement in targeting cardiac specific transcription factors [104]. MAFbx's role as an E3 ligase, and its requirement during muscle atrophy suggests that MAFbx substrates are amongst proteins specifically degraded under muscle atrophy conditions. One proposed MAFbx substrate is MyoD, a protein involved in myogenic differentiation [105]. Tintignac *et al.* 2005 identified that MAFbx LCD region is responsible for the MAFbx/MyoD interaction. The authors also observed reduced MyoD-induced differentiation upon MAFbx overexpression and provided evidence that a purified SCF complex containing MAFbx could ubiquitinate MyoD *in vitro*. Further evidence from another group implicates MAFbx's involvement during MyoD degradation, in which shRNA-mediated MAFbx down-regulation in fasted mice attenuated muscle loss was also associated with increased MyoD protein levels [54].

Skeletal muscle atrophy has been observed to not only result from increased protein degradation, but also reduced protein synthesis [47]. Indeed, there is evidence supporting theories of a link between muscle atrophy and hypertrophy molecular pathways [41]. Thus it was of great interest when Lagirand-Cantaloube *et al.* 2008 identified a novel link between synthetic and proteolytic pathways, providing evidence that eukaryotic initiation factor 3 subunit F (eif3-f) is ubiquitinated by MAFbx [106]. Similar to observations with MyoD, MAFbx's LCD domain mediates eif3-f binding and MAFbx down-regulation by shRNA in a C2C12 myotube model of atrophy prevents eif3-f degradation. The authors noted that this initiation factor can induce hypertrophy, by increasing levels of muscle structural proteins such as troponin T, desmin and myosin heavy chains and

suggest a novel mechanism where these two apparently distinct pathways are connected.

### **1.9.1.2. MuRF1**

MuRF1 was initially identified as a protein binding to the giant myofibrillar protein titin by yeast two-hybrid screening [107]. MuRF1 was noted for its involvement in muscle atrophy within the same year it was identified binding to titin, and recombinant MuRF1 was confirmed to have E3 ligase activity *in vitro* [53]. MuRF2 and MuRF3 make up the other two family members and are close homologs of MuRF1; all three contain a tripartite RING:B-box:coiled coil domain. MuRF2 and MuRF3 appear to be involved in maintaining normal contractile function [108, 109]. Similarly to MuRF1, MuRF2 was observed to be part of a complex with titin, although binding was indirect *via* binding to the ubiquitin binding and autophagy associated protein p62, which in turn bound the titin-binding zinc finger protein Nbr1 (next to BRCA1 gene 1) [110]. The authors hypothesised that titin, a protein that responds to mechanical load, may link sarcomere activity to downstream gene transcription. Lange *et al.* suggest that MuRF2 binding in this complex may sequester it from nuclear localisation, in which it may bind to the transactivation domain of transcription factor serum response factor (SRF) thus influencing SRF-mediate transcription, as opposed to functioning as an E3 ligase. MuRF1 is a RING-finger ligase, but monomeric as opposed functioning as part of a complex. However, similarly to MAFbx, MuRF1 does not bind ubiquitin directly, but mediates ubiquitin transfer from an E2 enzyme to a MuRF1-bound substrate. Yeast two-hybrid screens of skeletal muscle cDNA libraries identified eight myofibrillar proteins that interacted with MuRF1, but not all showed reduced levels in MuRF1 KO mice, suggesting they

may be regulators rather than substrates [109]. MuRF1 and MuRF3 have been suggested to ubiquitinate long lived sarcomeric proteins beta/slow myosin heavy chain (beta/slow MyHC) and MyHCIIa, in conjunction with E2 enzymes UbcH5a, -b and -c [108]. MyHC was observed to accumulate in MuRF1 and MuRF3 KO mice in this study, while another group also noted MuRF1's ability to bind MyHC was depleted upon Dex treatment of myotubes, but spared by inhibiting MuRF1 in myotubes or in MuRF1 KO mice [111]. Correspondingly, a more recent study observed MuRF1-dependent MyHC ubiquitination upon denervation and fasting, although they observed that myosin-binding protein C (MyBP-C) and myosin light chains 1 and 2 (MyLC1 and MyLC2) were ubiquitinated and degraded prior to MyHC [112]. MyLC2 was one of the eight MuRF1-binding protein candidates reported by Witt *et al.* 2005[109], who also reported binding of troponin-I (TnI). Further evidence from another group supported TnI as a MuRF1 substrate [113]. However, this yeast two-hybrid screen identified cardiac TnI, having utilised a heart cDNA library, and a study that analysed a proteins that bound a catalytic MuRF1 mutant failed to capture TnI [112]. Clearly further work is required to validate TnI as a MuRF1 substrate during skeletal muscle atrophy, while in contrast MyHC is better validated as a target. Interestingly, a very recent study observed that GST-tagged MuRF1 could interact with and polyubiquitinate actin *in vitro*, and ubiquitinated actin could be detected in C2C12 myotubes, in healthy volunteers and cancer patients, implicating actin as a novel MuRF1 substrate [114].

Despite MAFbx and MuRF1 having different modes of ubiquitination and targeting different proteins, both act to conjugate polyubiquitin chains to a

substrate and thus target them for degradation by the 26S proteasome (further details on polyubiquitin chains in 1.9.1.5.2.)

### **1.9.1.3. 26S Proteasome**

The 26S proteasome is an ATP-driven multisubunit complex consisting of the 20S proteasome, that contains proteolytic activity, and two 19S regulatory particles (see Figure 1.5). The 20S proteasome contains two alpha ( $\alpha$ ) and two beta ( $\beta$ ) rings stacked on top of each other, each ring containing seven subunits. The four rings form a barrel structure; the two inner rings are formed from  $\beta$  subunits, and the rings at the end of the barrel are formed from  $\alpha$  subunits. The fourteen subunits required for 20S proteasome (two copies of each are required) are structurally homologous, but unlike  $\alpha$  subunits, some of the inner ring-forming  $\beta$  subunits provide the proteolytic activity of the 20S proteasome.  $\beta$  subunits that have N-terminal threonine or serine residues provide the active sites of proteases, which are converted into nucleophiles that can attack the carbonyl groups in peptide bonds. Subunits  $\beta$ 1,  $\beta$ 2 and  $\beta$ 5 provide caspase-like, trypsin-like and chymotrypsin-like catalytic activities, respectively [115, 116], and are contained within the 20S proteasome barrel structure. Proteins that enter the proteasome are digested into peptides seven to nine residues in length, which are subsequently broken down further by cellular proteases upon release into the cytoplasm, which reduce short peptides into individual amino acids.

Substrate access to the proteasome for subsequent degradation is highly controlled to prevent non-specific proteolysis. The N-terminal residues of  $\alpha$  subunits in the outer rings block access to the 20S core and proteasomal entry is

**Figure 1.5**

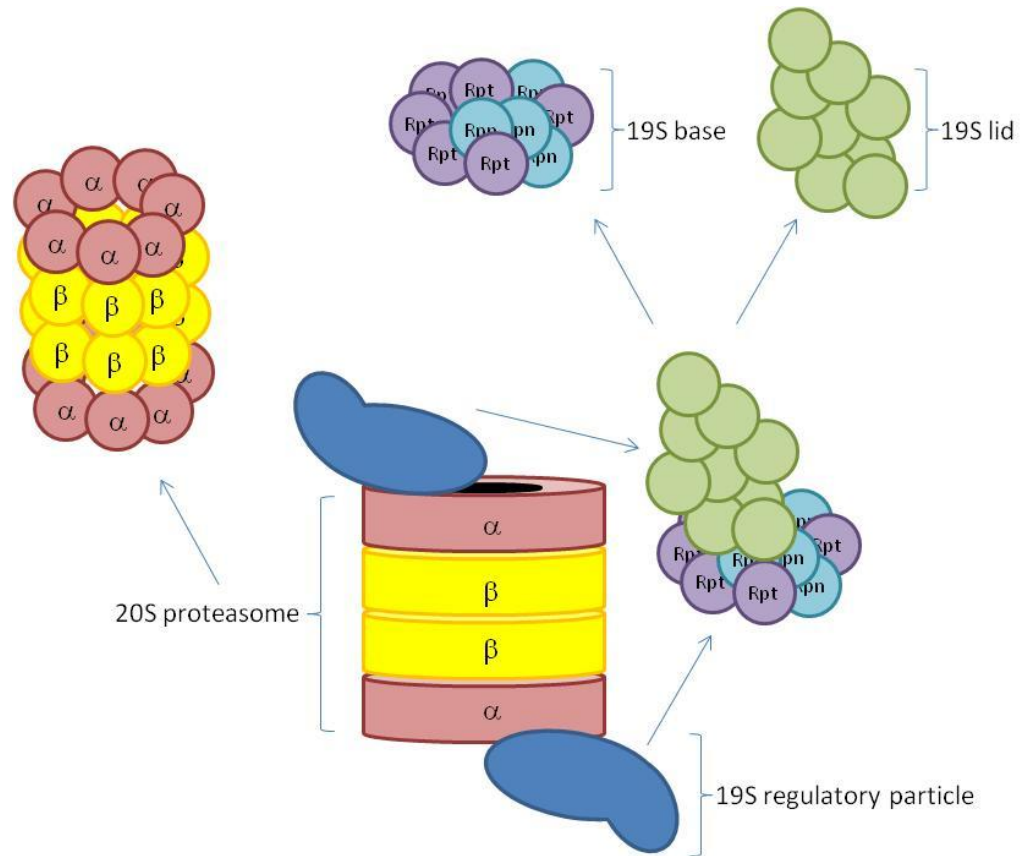


**Figure 1.5** Composition of the 26S proteasome. The 20S proteasome comprises of four stacked rings, the two central and two outer rings made of seven  $\beta$  subunits and  $\alpha$  subunits, respectively. The 19S regulatory particle is made of the 10 subunit base, and 9 subunit lid. While the base is known to consist of 6 ATPase subunits (Rpt subunits), and 4 non-ATPase subunits (Rpn subunits), the positions of subunits within the 19S regulatory particle are, to date, unknown.

tightly regulated by the 19S regulatory complex. The 19S regulatory particle contains 19 subunits, 10 of which form the 20S core-binding “base”, and 9 forming the “lid”. Six distinct ATPases are contained within the base component (Rpt1-6). The non-ATPase subunits, termed Rpn (regulatory particle non-ATPase) subunits, include Rpn1, Rpn2, Rpn10 and Rpn13; the latter two of which have been associated with polyubiquitin binding [117, 118]. The ATPases are of the ATPase associated with various cellular activities (AAA) class, and has been suggested to have a number of roles, described in greater detail in a recent review by Bar-Nun & Glickman 2011 [119]. Globular proteins cannot enter the proteasome in their native structure, and require unfolding; ATPases in the 19S base produce a mechanical force that unfolds substrates. ATPases have also been associated with translocation of the targeted protein into the proteasome and this process has been coupled with unfolding activity. However, to date it is unclear whether unfolding drives translocation, or whether the reverse is true. AAA ATPase subunits are also required to open the “gate”, formed by the N-terminal residues of  $\alpha$  subunits; gate opening is induced by a conformational change in the  $\alpha$  subunit ring, *via* a mechanism involving the C-terminus of 19S ATPase subunits (again, discussed further in Bar-Nun & Glickman 2011 [119]). The 19S “lid” is associated with an alternative function to the base, in deubiquitinating substrates *via* its Rpn11 subunit, which amputates the entire chain from substrates [120]. Deubiquitinating enzymes (DUBs) have enzymatic activities that reverse single ubiquitin (or ubiquitin-like) conjugation, or edit polyubiquitin (or ubiquitin-like) chains, thus regulating the fate of the target protein or potentially regulating a number of cellular processes [121]. Interestingly, a recent paper notes that proteasomal associated deubiquitinating enzymes ubiquitin C-terminal hydrolase 37 (Uch37) and ubiquitin specific peptidase 14 (Usp14) have an alternative chain “trimming” activity, which may

be required for removal of Rpn11 amputated polyubiquitin chains that may otherwise remain associated with the proteasome and compete with polyubiquitinated substrates for binding [122]. Deubiquitination and proteasomal degradation are coupled, but further work is required to fully understand the effect of different deubiquitinating activities with proteolysis. While some ubiquitin is inevitably degraded, much of it is recycled and return to the cytosol intact for further rounds of conjugation, prior to its own proteolysis.

However, a more complex mechanism for proteasomal recognition has emerged, in which a sequence within a substrate termed a proteasome initiation region, in combination to a polyubiquitin tag (proteasome binding tag), aids rapid proteasomal degradation [123-125]. Subsequent investigation revealed that presence of initiation region and proteasome binding tag on a target protein is not sufficient for degradation, but must be appropriately positioned and the initiation region be of a minimum length, to promote recognition by proteasomal receptors [126]. Further studies are required to understand proteasomal targeting.

#### **1.9.1.4. Deubiquitinating enzymes**

In addition to the 20-40 E2 enzymes and 500-1000 E3 ubiquitin ligases, nearly 100 DUBs have been identified in the human genome. Protein degradation is, in part, regulated by deubiquitination. However, DUBs are not exclusively proteasomal associated (see 1.9.1.3), and alternatively localised DUBs also have a role in determining a target protein's fate, as well as having a role in a number of other diverse cellular processes from generating active monoubiquitin from

precursors (see Section 1.9.1.5) to regulating cellular signalling [121, 127]. DUBs are divided into five families - UCH, USP, ovarian tumour (OTU), Josephin and Jab/MPN domain-associated metalloproteinase (JAMM) - and target a range of substrates, that may be mono- or polyubiquitinated, or alternatively conjugated to ubiquitin-like modifiers. The JAMM family are part of the zinc-dependent metalloprotease family, while the other four families are cysteine proteases; the latter family of DUBs can thus be irreversibly inactivated by reducing agents including N-ethylmaleimide (NEM) and iodoacetamide, which disrupt cysteine structures at the active site thiol group.

Here, we will focus on the regulation of protein degradation *via* deubiquitination of polyubiquitinated proteins. One of the most established examples of deubiquitinating enzymes is USP7, alternatively named HAUSP (herpes simplex virus associated ubiquitin-specific protease). This cysteine protease binds to and deubiquitinates the tumour suppressor protein p53 [128], a tumour suppressor protein that has a role regulating cellular stress response genes, including those involved in apoptosis, cell cycle arrest, senescence, DNA repair, cell metabolism and autophagy [129]. Removal of the polyubiquitin chain/proteasomal tag, increases p53 stability by reducing proteasomal degradation. In light of evidence that USP7 deubiquitinates polyubiquitinated p53, and that USP7 overexpression stabilised p53 [128], knock out of USP7 was predicted to destabilise p53 protein *via* increased proteasomal degradation. However, USP7 ablation *via* siRNA [130] or USP7 knock out by homologous recombination [131] also resulted in stabilisation of p53. It became evident that p53 stabilisation was more complex than initially thought. The E3 ubiquitin ligase murine double minute 2 (MDM2) both targets p53 and itself; the latter leading to destabilisation of MDM2 and its

subsequent degradation by the proteasome. The paradox that both USP7 knock down and overexpression resulted in p53 stabilisation was explained by USP7's ability to deubiquitinate both MDM2 and its p53 target.

DUBs may target a number of substrates, such as USP7 targeting MDM2 and p53; DUB activity may also be restricted to specific linkage polyubiquitin chains; for example, CYLD is a DUB associated with K63-linked polyubiquitin deubiquitination [132], while Otubain 1 (Otu1) preferentially cleaves K48-linked polyubiquitin [133]. Isopeptidase T (isoT) is a DUB that specifically recognises "unanchored" polyubiquitin, i.e. polyubiquitin with a free C-terminus [134]. More detail is provided about unanchored polyubiquitin in Section 1.9.1.5.3.

#### **1.9.1.5. Ubiquitin**

Ubiquitin is a 76 amino acid globular protein, that has been observed to remain stable even at high temperatures, likely due to its compact structure. Ubiquitin is translated as a protein-precursor in both yeast and higher eukaryotes, where ubiquitin copies are conjugated head-to-tail (C-terminal glycine to N-terminal methionine) in a linear fusion, or a single copy is fused to a ribosomal protein. Ubiquitin precursors are subsequently deubiquitinated by cellular DUBs to produce mature ubiquitin monomers [135-137]. Mammals contain four ubiquitin genes, two as ribosomal fusions and two as polyubiquitin-encoding genes; *Ubb* and *Ubc* [138].

Proteins may be post-translationally modified by the conjugation of ubiquitin, described in further detail below (Sections 1.9.1.5.1 and 1.9.1.5.2), but proteins may also bind ubiquitin non-covalently *via* at least one of 3 ubiquitin binding

surfaces. The key residues required for binding at these surfaces ; D58 [139], I44 [140] and GG (at the C-terminus) [141]. Ubiquitin binding proteins are discussed in more detail in 1.9.1.5.4.

NF- $\kappa$ B is a family of transcription factors that regulate various cellular processes involved in immunity responses, inflammation, apoptosis, cell adhesion, and proliferation [142-145]. There are five family members in mammals, including p50/p105, p52/p100, RelA(p65), c-Rel and RelB; these form homo- and hetero-dimers in different combinations to mediate gene transcription, but are mostly sequestered in the cytoplasm by binding of inhibitor of  $\kappa$ B family (I $\kappa$ Bs) proteins under non-stimulated conditions. I $\kappa$ Bs inhibit NF  $\kappa$ B dimers from entering the nucleus by masking the nuclear localisation signal (NLS), located at the N-terminus of NF- $\kappa$ B family members in the Rel homology domain (RHD). Liu & Chen 2011 comprehensively reviews ubiquitin's diverse roles in NF- $\kappa$ B signalling [144], which may be regulated by post-translational modification of proteins involved in NF- $\kappa$ B pathways by mono- and polyubiquitination (see Sections 1.9.1.5.1 & 1.9.1.5.2, respectively), or even by unanchored polyubiquitin chains, that are not conjugated to a substrate (Section 1.9.1.5.3). An overview of NF- $\kappa$ B signalling events described here are presented in Figure 1.6.

#### ***1.9.1.5.1. Monoubiquitination***

Proteins may be monoubiquitinated; this modification is not associated with proteasomal degradation, but is connected to a number of other cellular processes, which includes protein degradation *via* an alternative pathway.

**Figure 1.6**

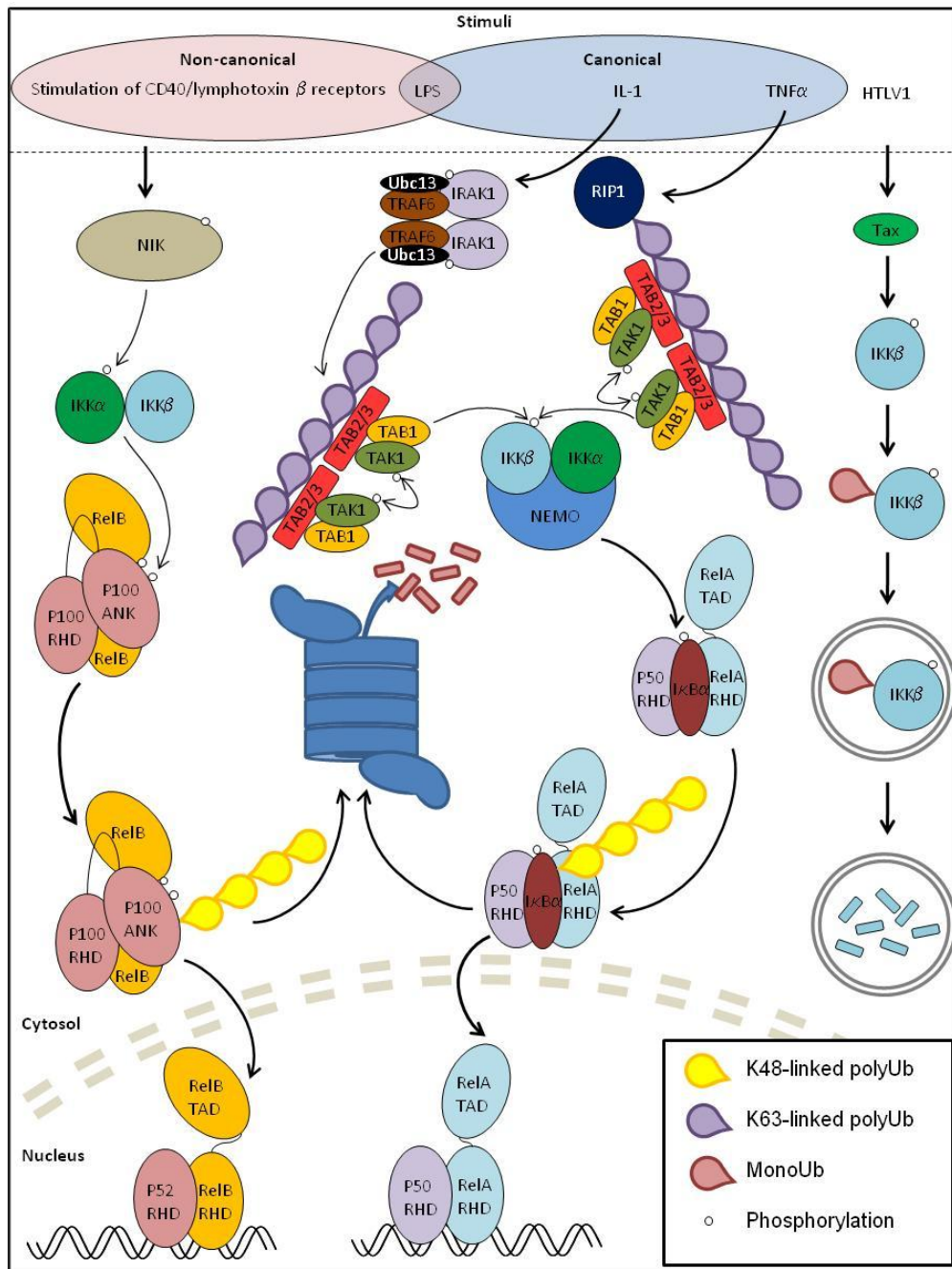


**Figure 1.6** Canonical NF- $\kappa$ B pathways may be stimulated by LPS, IL-1 or TNF $\alpha$ . TNF $\alpha$  and IL-1 induces RIP1 polyubiquitination or IRAK1/TRAF6/Ubc13-mediated synthesis of unanchored K63-linked polyubiquitin chains, respectively. Binding of TAK1 kinase *via* TAB2/TAB3 subunits, promotes self-activation and then phosphorylates IKK. IKK phosphorylates I $\kappa$ B $\alpha$ , which is polyubiquitinated and targeted for degradation by the 26S proteasome. Thus, the NLS of RelA within the RHD is unmasked, and promotes translocation of NF- $\kappa$ B to the nucleus to mediate gene transcription. Non-canonical pathways induce NIK activation, which in turn phosphorylates the P100 NF- $\kappa$ B precursor, inducing degradation of the ankryin repeat containing domain (ANK), unmasking the NLS of RelB and again allowing translocation to the nucleus. Transcriptional activation domains (TADs) allow binding of transcriptional co-activators/co-repressors. HTLV-1 induces Tax expression, inducing IKK $\beta$  phosphorylation and monoubiquitination. IKK $\beta$  is translocated to autophagosomes and degraded, reducing NF- $\kappa$ B mediated signalling.

Genomic DNA is packaged into chromatin, in which DNA is wrapped around histone proteins, and has been widely considered to inhibit gene transcription [146]. Post-translational modification of histone H2A by monoubiquitination was discovered over 30 years ago [147] but has only relatively recently been recognised for having a role in transcriptional repression and may be induced by DNA damage and have a role in DNA repair (reviewed in more detail in Zhou & Rosenfeld 2008 [148]).

Interestingly, NF- $\kappa$ B is widely assumed to be associated with polyubiquitin modification, but recent evidence indicates a minor role for monoubiquitination in NF- $\kappa$ B signalling. For NF- $\kappa$ B signalling to occur, the I $\kappa$ B inhibitory protein must be removed; I $\kappa$ B phosphorylation by IKK (I $\kappa$ B kinase) induces its degradation (further details in 1.9.1.5.2). Cells infected with human T-cell leukaemia virus type 1 (HTLV-1) express the oncogene protein Tax, and were observed to induce constitutive phosphorylation and monoubiquitination of IKK $\beta$  [149-151]. The monoubiquitination event was later associated with subcellular translocation of IKK $\beta$  to autophagosomes for subsequent degradation, and induced down-regulated NF- $\kappa$ B signalling [152].

The link between monoubiquitination and protein translocation is well established, having a role in membrane protein trafficking, regulating endocytosis and endosomal sorting [153]. Signal-inducing receptors are amongst the proteins that have been observed to undergo internalisation into clathrin coated pits, which are transported *via* vesicles to endosomes termed multi-vesicular bodies (MVB). Receptors may be recycled back to the cell surface, or

budding off from MVBs and fusion with lysosomes results in protein degradation in a proteasome-independent manner. Monoubiquitination of the receptor at the cytosolic domain has been observed to be sufficient for endocytosis to occur [154], which appears to be due to recruitment of ubiquitin-binding endocytic proteins (reviewed further in Mosesson & Yarden 2006 [153]).

#### ***1.9.1.5.2. Polyubiquitinated substrates***

E3 ubiquitin ligase enzymes mediate transfer of ubiquitin to the  $\epsilon$ -amino group of lysine residues or the  $\alpha$ -amino group of an N-terminal residue within a substrate; subsequently, further ubiquitin proteins may be conjugated to the substrate-attached ubiquitin to form polyubiquitin chains, *via* one of 7 lysine residues (K6, K11, K27, K29, K33, K48 or K63) or at the N-terminal methionine (known as linear polyubiquitin chains). Traditionally, proteasomal recognition of polyubiquitinated substrates was associated with K48-linked polyubiquitin chains. However, it has become evident that, with the exception of K63-linked chains, all other polyubiquitin linkages can target proteins for proteasomal degradation [155]. Indeed, earlier *in vitro* studies noted that even heterogeneous polyubiquitin chains of mixed linkage were sufficient for binding to ubiquitin receptors as well as promoting proteasomal degradation [156]. Histone post-translational modification and membrane protein trafficking requires a single ubiquitin, but it appears that tetraubiquitin is the minimum signal for proteasomal recognition [157].

Polyubiquitination, as has been previously noted, has a major role in NF- $\kappa$ B signalling. There are a number of pathways that ultimately lead to NF- $\kappa$ B

activation, reviewed in greater detail in Perkins 2007 [145]. NF- $\kappa$ B is mostly sequestered in the cytoplasm by binding of I $\kappa$ B. A number of stimuli induce the canonical pathway, including bacterial LPS, and cytokines TNF $\alpha$  and IL-1. IKK contains three subunits; two catalytic subunits, IKK $\alpha$  and IKK $\beta$  and one regulatory subunit IKK $\gamma$ /NEMO (NF- $\kappa$ B essential modifier). An example of the canonical pathway is the activation of IKK subunit IKK $\beta$ , which phosphorylates I $\kappa$ B $\alpha$ . This induces I $\kappa$ B $\alpha$  ubiquitination with K48-linked polyubiquitin, targeting it for degradation by the 26S proteasome. This unmaskes the NLS of NF- $\kappa$ B subunit RelA, in a heterodimer complex with p50 (see Figure 1.6), allowing nuclear translocation and binding to various co-activators/co-repressors to mediate gene transcription. However, K48-linked polyubiquitination and degradation has another role during NF- $\kappa$ B signalling, such as during the non-canonical/alternative pathway. LPS may also trigger this pathway, as can stimulation of CD40 and lymphotoxin- $\beta$  receptors. This pathway leads to IKK $\alpha$  activation by NF- $\kappa$ B-inducing kinase (NIK), which in turn phosphorylates the NF- $\kappa$ B precursor p100, of a p100/RelB dimer. Subunit p100 contains a C-terminal ankyrin repeat region, which acts similarly to I $\kappa$ B inhibitors, masking the NLS of the adjacent RelB NF- $\kappa$ B subunit. Phosphorylation of p100 induces K48-linked polyubiquitination, leading to proteasomal processing of p100 to p52. This unmaskes the NLS and allowing entry of the p52/RelB NF- $\kappa$ B dimer into the nucleus to mediate gene transcription.

However, K48-linked polyubiquitin is not the only linkage important for NF- $\kappa$ B signalling. TNF $\alpha$  induced canonical NF- $\kappa$ B signalling promotes the formation of a complex which includes RIP1 (receptor interacting protein 1) (see Figure 1.6), which is polyubiquitinated with K63-linked polyubiquitin chains, which in

turn recruits TAK1 (transforming growth factor  $\beta$ -activated kinase 1) and IKK complexes. TAK1 phosphorylates and activates IKK, again resulting in I $\kappa$ B $\alpha$  phosphorylation and degradation, and inducing nuclear localisation of the RelA/p50 dimer. TNF-receptor associated factor 6 (TRAF6) is a protein that is essential for IL-1 [158] and TLR- [159] mediated NF- $\kappa$ B signalling. It was later found to be an E3 ubiquitin ligase, which functions with Ubc13/Uev1a to form K63-linked polyubiquitin chains [160]. There is conflicting data regarding TRAF6 substrates and their role in NF- $\kappa$ B signalling, described in further detail in Liu *et al.* 2010 [144]. Candidates for TRAF6-mediated ubiquitination include TRAF6 itself and IKK's regulatory subunit NEMO, although further study is needed as K63-linked polyubiquitin is not the only linkage associated with NEMO (see below). There is recent evidence that TAK1 activation is not only *via* K63-polyubiquitinated RIP1, and that TRAF6/Ubc13 synthesised unanchored K63-polyubiquitin chains may also activate this kinase (see Section 1.9.1.5.3).

Interestingly, linear polyubiquitin chains appear to also have a role in NF- $\kappa$ B signalling [161-164]. Linear ubiquitin assembly complex (LUBAC), that forms linear polyubiquitin chains, has been found to activate canonical signalling by binding to NEMO and conjugating linear chains [165, 166] and more recently, genotoxic stress has been reported recently to induce NEMO linear ubiquitination, which is required for NF- $\kappa$ B activation [164]. Alternatively, another group observed K27-polyubiquitination of NEMO during viral induced NF- $\kappa$ B activation [167], indicating another potential polyubiquitin linkage involved in NF- $\kappa$ B signalling.

Other polyubiquitin linkages have been associated with a number of roles other than proteasomal degradation and NF- $\kappa$ B signalling; K6 with DNA repair [168] while K11-linked polyubiquitin has an emerging role in cell cycle control, reviewed in further detail in Bremm & Komander 2011 [169]. However, it is K63-linked polyubiquitin chains that have been studied the most out of the non-proteasomal related polyubiquitin linkages. DNA post-replication repair may be mediated by the *RAD6* pathway and the DNA-polymerase sliding clamp PCNA (proliferating cell nuclear antigen) was identified a substrate in this pathway [170]. Hoege *et al.* 2002 noted PCNA could be modified at the same site by SUMO (small ubiquitin-related modifier), monoubiquitin, or K63-linked polyubiquitin chains. The authors suggested that DNA damage triggers monoubiquitination at this site, in preference to SUMOylation. Monoubiquitination then allows recruitment of enzymes that assemble K63-linked polyubiquitin which induces error-free DNA repair. K63-linked polyubiquitin mediated activation appears to be proteasome-independent, as it was shown that K63-polyubiquitinated PCNA was not subjected to proteasomal degradation [171], although the mechanism of activation remains unknown.

Traditionally, polyubiquitin has been considered for its role as a “linear” structure, but its ability to link *via* any of 7 lysine residues/N-terminal methionine opens the possibility of it forming branched structures. Indeed, E3 ligase RING1B has been observed to auto-ubiquitinate and form branched ubiquitin chains for self-activation [172] and evidence suggests that branched polyubiquitin chains may inhibit protein degradation [173].

In summary, polyubiquitination may be a very complex post-translational modification beyond the complexity of phosphorylation, even if only considering linkage, let alone the vast number of possible conformations polyubiquitin can form. Multiple groups have performed quantitative analyses of polyubiquitin linkages present across different tissues and under different conditions [155, 174-176]. Together, these studies revealed varied linkage compositions, that can be associated with multiple cellular processes from regulation of degradation to protein trafficking.

#### ***1.9.1.5.3. Unanchored polyubiquitin***

Polyubiquitin has been largely studied for its role in regulating the proteins it post-translationally modifies. As was noted earlier, proteasomal associated DUBs act to remove polyubiquitin bound to the proteasome to allow subsequent binding of further polyubiquitinated proteins [122]. Indeed, earlier groups had observed the ability of unanchored polyubiquitin chains of tetraubiquitin and above to inhibit proteasome degradation *in vitro* [68], while deletion of the UBP14 DUB induced accumulation of free polyubiquitin chains that inhibited proteasomal degradation in yeast [134]. Unanchored polyubiquitin chains were further validated in a human context. Knockdown of isoT in human cells, a DUB that recognises and cleaves unanchored polyubiquitin, increased levels of free ubiquitin chains and competed with ubiquitinated p53 tumour suppressor protein for proteasomal binding; thus stabilising p53 by inhibiting its degradation [177].

A recent suggestion for the physiological role of unanchored polyubiquitin chains was as a source of monoubiquitin for the cell [178], but K63-linked unanchored polyubiquitin has also been implicated in having a role both activating kinases [179] and during innate immunity [180, 181]. TAK1, a kinase previously mentioned for its ability to phosphorylate and activate kinase IKK, is activated by unanchored K63-linked polyubiquitin; the model proposed a mechanism where multiple TAK1 kinases are brought within close proximity to activate each other, when binding to unanchored K63-linked chains *via* TAB2/3 (TAK1 binding protein 2/3) accessory proteins [179]. As previously noted, TRAF6/Ubc13 mediate synthesis of unanchored K63-linked polyubiquitin chains upon IL-1 pathway stimulation. Recruitment of myeloid differentiation primary gene 88 (MyD88) at IL-1 receptors induces recruitment of two IL-1 receptor-associated kinases, IRAK4 and IRAK1. IRAK1 is activated and binds to TRAF6, which oligomerises and catalyses K63-polyubiquitination with Ubc13. Activated TAK1, induced by binding to TRAF6-synthesised unanchored K63-linked polyubiquitin chains, can subsequently activate IKK. This suggests that unanchored polyubiquitin is yet another ubiquitin species associated with NF- $\kappa$ B signalling (see Figure 1.6) and that TRAF6 may be the source of these species.

#### **1.9.1.5.4. Ubiquitin binding proteins**

Non-covalent binding to ubiquitin is key to all ubiquitin-mediated processes, including deubiquitination, protein trafficking and autophagy. Ubiquitin binding proteins may bind *via* at least one of 3 binding surfaces, defined by key residues D58 [139], I44[140] or GG (at the C-terminus) [141]. Dikic *et al.* 2009 reviews the various ubiquitin-binding domains (UBDs) and how binding specificity for certain polyubiquitin chain lengths and linkages relates to their functions [182].

The authors note that most UBDs bind at the I44 surface, a hydrophobic patch on the  $\beta$ -sheet surface that is solvent exposed, but due to the multiple modes of binding at this surface I44 binding-UBDs are still structurally diverse. I44 binding proteins include ubiquitin conjugating enzyme UBCH5C [183], Alpha4 *via* a ubiquitin-interacting motif (UIM) (a protein that regulates protein serine/threonine phosphatase 2A catalytic subunit (PP2Ac) polyubiquitination) and p62 *via* its ubiquitin associated (UBA) domain, ubiquitin-binding mutants of which are associated with Paget's disease of the bone [184].

Alternatively, proteins may bind to ubiquitin at the polar surface of ubiquitin, centred around the D58 residue; for example, the Znf\_A20 domain of RAB5 guanine nucleotide exchange factor (RABEX5) [185]. Finally, isoT specifically deubiquitinates unanchored polyubiquitin, recognition of which has been attributed to the Znf\_UBP/BUZ domain of isoT; this domain forms a pocket into which the free C-terminal tail of unanchored ubiquitin (the proximal ubiquitin) can enter [141].

Radiation sensitivity abnormal 23 (RAD23) is a shuttle protein, that aids translocation of polyubiquitinated proteins to the proteasome *via* binding to the polyubiquitin tag and direct proteasome binding. Considering the association of K48-linked polyubiquitin to proteasome recognition, in favour of K63-linked chains, it is interesting to note that RAD23 showed preferential binding to K48-over K63-linked polyubiquitin [186]. Alternatively, the nuclear protein localization 4 ZnF (NZF) domain of TAB2, specifically binds K63-linked chains [187]; as was discussed in the previous Section.

#### **1.9.1.5.5. Methods for purifying polyubiquitinated proteins**

Specific polyubiquitination of targets is key to a number of processes, as exemplified by NF- $\kappa$ B signalling in which a specific inhibitor is degraded to allow NF- $\kappa$ B entry to the nucleus, or during the regulation of polyubiquitinated proteins by DUBs like USP7 which mediate MDM2-catalysed auto- or p53-polyubiquitination. The concept of a regulated “atrophy programme” involves polyubiquitination of specific targets, and subsequently protein degradation is not a random process but aimed to remove particular substrates. The majority of muscle atrophy targets are yet to be catalogued. To fully understand the muscle atrophy process, these polyubiquitinated proteins need to be identified.

Different methods have been employed for purifying polyubiquitinated substrates. Tagged ubiquitin has been expressed in yeast [188] and human cells [189] allowing purification *via* this tag, subsequent trypsinolysis and analysis by liquid chromatography tandem mass spectrometry (LC-MS/MS). Jeon *et al.* 2007 generated a transgenic mouse that expressed tagged ubiquitin in the heart, and similarly purified and analysed ubiquitination substrates [190]. This has revealed a number of ubiquitin conjugation sites and substrates. An alternative strategy that has been employed is utilising the ubiquitin-binding S5a proteasomal subunit [191] or a ubiquitin-specific antibody [192].

Subsequently, tandem-repeated ubiquitin-binding entities (TUBEs) that are based on UBA domains were engineered in which multiple ubiquitin-binding domains are in close proximity, both promoting binding to polyubiquitin and protecting them from cellular enzymatic activities [193]. However, despite the

use of different UBA domains, it is unclear whether there is a level of selectivity using this method in terms of ubiquitin linkage.

MS methods that have been employed to identify ubiquitination sites have taken advantage of trypsin's inability to cleave after lysine residues in substrates that have ubiquitin attached [188]. This induces a mass shift of 114.1Da in the tryptic peptide derived from the linkage site, due to the isopeptide linked di-glycine stub remaining from the previously conjugated ubiquitin, aiding identification of substrates. As an alternative method for identifying ubiquitinated substrates, *via* binding to the S5a proteasomal subunit, but specifically eluting immobilised ubiquitinated proteins using USP2 catalytic core [194]. Eluted proteins were resolved by two-dimensional gel electrophoresis (2DE) and analysed by MS. More recently, a strategy was devised which utilised a monoclonal antibody that recognises the diglycine isopeptide on tryptic peptides; diglycine remains on ubiquitin-modified proteins after trypsinolysis [195]. This strategy allowed identification of around 19000 sites within 5000 human proteins that were diglycine modified, a method that can be used to assess ubiquitination-modification quantitatively. Therefore, a number of different strategies have been employed to proteomically analyse ubiquitinated proteins in a range of cells and tissues, which may be utilised to address the unknown substrates of the atrophy programme.

## **1.10. ZNF216**

### **1.10.1. Structure of ZNF216**

ZNF216 is a 213 residue protein (rat sequence), containing Znf\_A20 and Znf\_AN1 domains at the N- and C- termini, respectively [196]. The N-terminal Znf\_A20 domain, located between amino acids 11-35, shares significant homology with the A20 protein, an inhibitor of TNF-induced NF- $\kappa$ B signalling. This is the domain that has subsequently been associated with polyubiquitin binding [56]. The C-terminal Znf\_AN1 domain was named for its homology with a ubiquitin-like protein AN1 in *Xenopus Laevis*. ZNF216 protein exists in only one form, but two alternatively spliced transcripts exist in humans, as two different sequences exist upstream of the start ATG in exon [197]. However, no apparent difference in expression or regulation of these splice forms has been found to date.

### **1.10.2. Biochemical function**

Initially, bioinformatic approaches were used to identify candidate genes responsible for hearing loss in humans, which mapped to the location of *ZNF216* [197]. Despite the position of *ZNF216* on the human chromosome implicating a causal relationship to hearing loss, it could not be validated as a candidate. This was concluded when no disease causing mutations were identified in *ZNF216*, and transcripts were not observed to vary in length or abundance between control and deaf mice (*dn*) mice.

Huang *et al.* 2004 later identified ZNF216 as NEMO interacting protein *via* a yeast two-hybrid system [196]. Luciferase reporter assays indicated that ZNF216 inhibits TNF-, IL1-, and TLR4-induced NF- $\kappa$ B activation in a dose-dependent manner. More recently, ZNF216 was studied in the context of osteoclast differentiation [198]. Receptor and activator of NF-kappa B (RANK) and its ligand RANKL are known to be intimately involved in osteoclast differentiation. DNA microarray techniques showed that ZNF216 was upregulated as a result of RANKL stimulation in macrophages, and inhibited osteoclast formation (although not through the NF- $\kappa$ B pathway). Hishiya *et al.* 2005 found no evidence that ZNF216 inhibits the NF- $\kappa$ B pathway and in 2006 suggested that ZNF216 may not act directly on the NF- $\kappa$ B pathway but act as a downstream effector as a component of the UPS [56]. Interestingly, AWP1 (protein associated with PRK1) is a protein highly homologous to ZNF216, having an N-terminal Znf\_A20 domain that binds ubiquitin, and a C-terminal Znf\_AN1 domain, and may be a regulator of NF- $\kappa$ B signalling [199]. However, its role during NF- $\kappa$ B signalling remains undefined to date.

To reveal ZNF216's biochemical role and function, Hishiya *et al.* 2006 used yeast two-hybrid screening to identify binding partners and thus potential substrates of ZNF216 [56]. This yielded several clones of polyubiquitin C, binding ZNF216 specifically through its Znf\_A20 domain. The same study established ZNF216's localisation within the cell and was found to mostly be cytoplasmic. MS/MS was used to analyse proteins that co-immunoprecipitated with FLAG-tagged ZNF216 and was found to associate 26S proteasome subunits. Interestingly, ubiquitin binding activity conferred by the A20 domain was not required for this association .

Hishiya *et al.* 2006 thus reasoned that ZNF216 may bind to polyubiquitinated substrates of the atrophy programme and shuttle targeted proteins to the 26S proteasome for degradation (Figure 1.7) [56]. Shuttle proteins may act to increase the efficiency of degradation by the 26S proteasome. Reduced interaction of the proteasome shuttle protein VCP leads to down-regulation of degradation of inactive ataxin-3, a deubiquitinating enzyme responsible for spinocerebellar ataxia type 3 [95]. Therefore shuttle proteins may play an important role in efficiently delivering substrates for degradation. Hishiya *et al.* 2006 noted that although Dsk-2 has been identified as a shuttle protein in yeast, that similarly binds polyubiquitin and can associate with the proteasome, ZNF216 is not an orthologue [56]. The authors also inhibited COS-7 cell proteasomes with MG132, inducing accumulation of polyubiquitinated proteins that could not be degraded, and thus accumulated in an 'aggresome' [56]. The authors noted the association of ZNF216 with aggresomes, providing *in vivo* evidence of ZNF216 colocalising with polyubiquitinated proteins.

Significant upregulation of ZNF216 mRNA levels was measured by Northern blotting in both a Dex induced myotube model and a fasting induced rat model of muscle atrophy [56]. Strikingly, ZNF216 knockout mice exhibited resistance to denervation induced atrophy, substantiating observations of increased ZNF216 expression and accumulated ubiquitinated substrates in rats and myotubes under different atrophy stimuli. Together, these data implicated ZNF216 as having a critical role during skeletal muscle atrophy and supported ZNF216's status as an atrogene. However, unlike the well established atrogenes MAFbx and MuRF1, further muscle atrophy models have yet to be analysed for the involvement of ZNF216, which may further validate it as a *bona fide* atrogene.

**Figure 1.7**

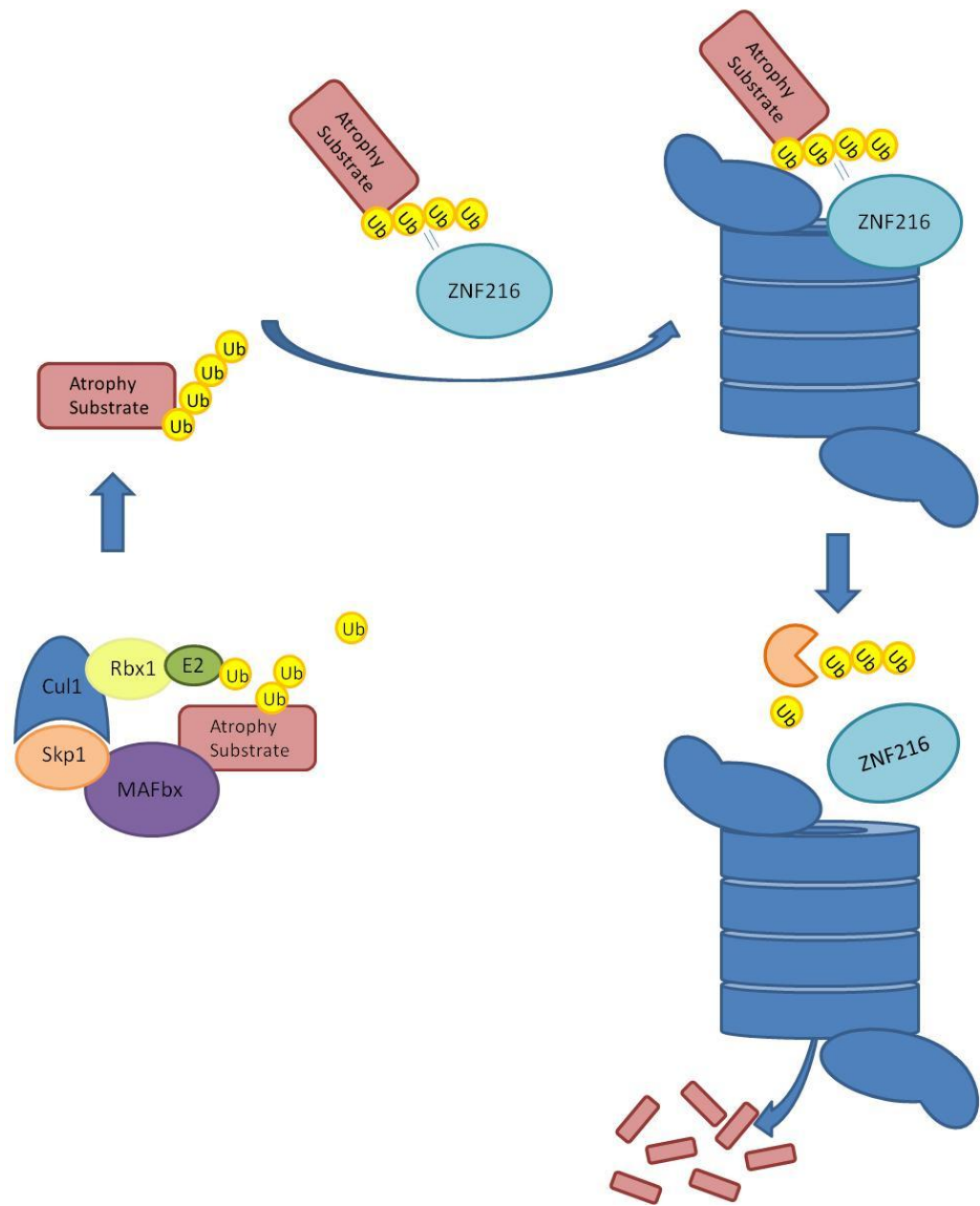


**Figure 1.7** Schematic of proposed function of ZNF216, which may bind polyubiquitinated proteins during skeletal muscle atrophy (such as those targeted by MAFbx), and shuttle them across to the 26S proteasome for degradation. ZNF216 may then continue to shuttle polyubiquitinated targets, and polyubiquitin is deubiquitinated and recycled for further rounds of conjugation.

### **1.11. Aims**

The atrogenes MAFbx and MuRF1 have been extensively researched in various models of skeletal muscle atrophy. Here, we aim to measure ZNF216 expression levels in different models of muscle atrophy, and compare to that of the established atrogenes MAFbx and MuRF1 to investigate ZNF216's role as an atroгене. ZNF216's affinity for polyubiquitin provides a method for purifying polyubiquitinated proteins *via* binding to the Znf\_A20 domain. Considering its potential role as a shuttle protein that translocates atrophy substrates, ZNF216-bound polyubiquitinated proteins may be muscle atrophy substrates. Thus we aim to purify and identify polyubiquitinated proteins from muscle that bind ZNF216, and potentially elucidate the elusive substrates degraded during skeletal muscle atrophy.

## **CHAPTER 2**

### **Materials and Methods**

## **2.1. Experimental animals**

### **2.1.1. Intravenous endotoxin and chemical reagents**

- 1) lipopolysaccharide (LPS) (*E. Coli*, serotype 0127: B8, Sigma-Aldrich)
- 2) thiobutabarbital sodium ((Inactin), Sigma-Aldrich)

### **2.1.2. Protocol**

Chronically-instrumented male Sprague-Dawley Rats were continuously infused intravenously (i.v.) with either lipopolysaccharide (LPS) ( $15 \mu\text{g kg}^{-1} \text{h}^{-1}$ ; n=6) or saline (n=8) for 24 hr at  $0.4 \text{ml h}^{-1}$ .

The extensor digitorum longus (EDL) muscle was then removed and freeze-clamped while the animals were under terminal anaesthesia, using thiobutabarbital sodium ( $80 \text{mg kg}^{-1} \text{i.v.}$ ). Muscles were stored in liquid nitrogen. Procedures were carried out by Julie March and Philip Kemp and were approved by the University of Nottingham Ethical Review Committee and were performed under Home Office Project and Personal license authority.

## **2.2. Protein-to-DNA ratio**

### **2.2.1. Protein and DNA extraction**

#### **2.2.1.1. Solutions**

- 1) perchloric acid: 0.2M, 0.1M and 1.2M PCA
- 2) potassium hydroxide solution; 0.3M KOH

### 2.2.1.2. Protocol

Alkaline soluble protein and DNA were extracted and quantified from EDL muscle from either saline or LPS-infused rats. Specifically, approximately 20mg of muscle was freeze-dried overnight and any visible blood and connective tissue was removed prior to powdering. 3 mg of powdered muscle was required for analysis. For precipitation of protein, 500 $\mu$ l of perchloric acid (0.2M PCA) was added to 3mg of muscle, and incubated in an ice-bath for 10 min. Samples were centrifuged at 3000 rcf for 15 min at 4°C. The remaining pellet was washed twice with 500 $\mu$ l PCA (0.2M) and the supernatant and washes were discarded. The precipitate was dissolved in 1ml potassium hydroxide (0.3M KOH) and incubated at 37°C for 1 hr, with gentle mixing. This solution was used to determine quantification of soluble protein and DNA by methods in Forsberg *et al.* 1991 [200]. This allowed calculation of the protein-to-DNA ratio, a proposed method of calculating the magnitude of protein loss in muscle by Gamrin *et al.* 1996 [30]. Specifically, three 10  $\mu$ l aliquots of solution were extracted for protein quantification (see Section 2.2.2.) and the remaining solution was transferred to a glass tube. To precipitate DNA, 1ml of PCA (1.2M) was added to the remaining solution and was incubated in an ice-bath for 30 min. Samples were centrifuged at 3000 rcf for 15 min at 4°C. The pellet was washed twice with 500 $\mu$ l PCA (0.2M), and the supernatant, which contained the RNA, and washes were discarded. DNA was hydrolysed by incubating the pellet in 250 $\mu$ l PCA (1M) at 70°C for 1 hr. Samples were centrifuged at 3000 rcf for 10 min at 4°C, and 200 $\mu$ l was required for DNA quantification (see Section 2.2.3.)

## 2.2.2. Protein quantification: Lowry method

### 2.2.2.1. Solutions

- 1) NaOH solution: 0.1M NaOH
- 2) potassium hydroxide solution; 0.3M KOH
- 3) NaOH and KOH solution: NaOH solution, KOH solution, mixed 9:1
- 4) BSA standard: 1mg/ml, in NaOH and KOH solution
- 5) sodium carbonate solution: 2% (w/v) Na<sub>2</sub>CO<sub>3</sub>
- 6) sodium potassium tartrate solution: 2% (w/v) sodium potassium tartrate. 4H<sub>2</sub>O
- 7) copper sulphate solution: 1% (w/v) CuSO<sub>4</sub>. 5H<sub>2</sub>O
- 8) Lowry reagent: sodium carbonate solution, sodium potassium tartrate solution, copper sulphate solution, mixed 10:1:1 (v/v)
- 9) Folin reagent: 10% (v/v) Folin and Ciocalteu's phenol reagent (Fisher Scientific), in NaOH solution

### 2.2.2.2. Protocol

Protein quantification was performed on samples from Section 2.2.2. Samples (10µl each) were diluted in NaOH solution (1:9). Similarly, BSA standards were used in triplicate in a range of 0-80µg. 100µl of samples were dispensed into a 96 well plate, and samples/standards were made up to 200µl with NaOH, and 50µl of Lowry reagent was added. After 10 min incubation, 50µl of Folin reagent was added. The plate was incubated for 30 min at room temperature. Once colour had developed, the absorbance was measured using a plate reader (DYNEX technologies), and protein concentration was determined by comparing to the BSA protein standard curve.

### **2.2.3. DNA quantification**

#### **2.2.3.1. Solutions**

- 1) perchloric acid: 1.7 M PCA
- 2) diphenylamine solution: 4% (w/v), in glacial acetic acid
- 3) acetaldehyde solution: 1.6mg/ml acetaldehyde
- 4) DNA quantification reagent: diphenylamine, acetaldehyde, mixed 25:1 (v/v)
- 5) calf thymus DNA (Sigma-Aldrich; D4522): 45µg/ml, in 1M PCA

#### **2.2.3.2. Protocol**

To quantify DNA concentration, 50µl of PCA (1.7M) and 250µl of DNA quantification reagent were added to 200µl of the sample (see Section 2.2.2), and incubated overnight at 30°C. Absorbances were then analysed on a spectrophotometer (Spectramax® 190; Molecular Devices) at 595nm, in addition to a standard curve generated from calf thymus DNA that was treated identically to samples; the assay detected 0-11.25µg DNA.

### **2.3. RNA extraction**

#### **2.3.1. Solutions**

- 1) TRIzol® solution (Invitrogen)
- 2) glycogen solution (10µg/µl), dissolved in TRIzol® solution
- 3) CHCl<sub>3</sub> (Sigma-Aldrich): iso-amyl alcohol (Sigma-Aldrich) (49:1)
- 4) iso-propanol (Sigma-Aldrich)
- 5) 75% EtOH
- 6) RNase free water (Invitrogen)

### **2.3.2. Protocol**

Approximately 20-30mg of LPS (n=6) or control (n=8) EDL muscle was homogenised in 800µl of ice cold TRIzol solution, containing 5µl of glycogen solution. A polytron was used to homogenise the EDL muscle for approximately 30s. Homogenate was incubated at room temperature for 5 min. To the homogenate, 160µl CHCl<sub>3</sub> : iso-amyl (49:1) was added to the muscle extract and the tube then manually shaken followed by a 2s vortex. Incubation took place at room temperature for 2-3 min and was centrifuged at 12000 rcf for 15 min at 4°C. The aqueous phase containing RNA was added to 400µl of ice-cold iso-propanol, to have a 1:1 water phase:alcohol ratio and the organic phase and inter-phase were discarded. The samples were frozen at -20°C overnight to precipitate RNA, and the next day centrifuged at 12000 rcf for 15 min at 4°C. Pellets were washed in 800µl of 75% EtOH and were centrifuged again at 10000 rcf for 10 min. RNA pellets were allowed to air-dry and then resuspended in 35µl of RNase free water. Resuspended RNA was quantified by measuring absorbance at 260nm and 280nm and was stored at -80°C (to undergo cDNA synthesis; see Section 2.4.)

## **2.4. cDNA synthesis**

### **2.4.1. Solutions**

- 1) RNase free water (Invitrogen)
- 2) random hexamer primers (Promega C1181)
- 3) 10 x MMLV reverse transcriptase buffer
- 4) 10mM dNTPs: 10mM dATP, 10mM dCTP, 10mM dTTP, 10mM dGTP, in RNase free water (Invitrogen)

- 5) RNA-ase inhibitor (Promega N2511)

### **2.4.2. Protocol**

Reverse transcription was carried out using 1µg total RNA and 50ng of random hexamer primers was added to 15µl of diluted mRNA. An extra sample was made to act as a reverse transcription minus (-RT) control. Samples were incubated at 70°C for 5 min to denature secondary structures and then placed on ice. To each sample was added 0.5µl of RNase inhibitor, 5µl 10 x MMLV reverse transcriptase buffer, 1.25µl of a pooled nucleotide mix and 1µl MMLV reverse transcriptase was added to each tube with the exception of the -RT sample, in which 1µl of RNase free water was added instead. Samples were made to a final volume of 30µl and incubated at room temperature for 10 min, followed by a 42°C incubation for 1 hr. Reverse transcriptase enzyme was inactivated by heating samples at 70°C for 15 min. RNA-ase free water was added to samples to dilute them 1:3 (RNA:water), and stored at -80°C.

## **2.5. TaqMan analysis**

### **2.5.1. Solutions**

- 1) PCR Universal Master Mix (Applied Biosystems)
- 2) primer and FAM (6-carboxyl-fluorescin) probe sets (Applied Biosystems): HMBS (Cat # Rn00565886\_m1), MAFbx (Cat # Rn00591730), MuRF1 (Cat # Rn00590197\_m1), ZNF216 (Cat # Rn01479599\_m1), Fbxo25 (Cat # Rn01478634\_m1)
- 3) primers: AWP1 (See Appendix I)
- 4) probe: AWP1 (See Appendix I)

- 5) RNase free water (Invitrogen)
- 6) cDNA samples from control and LPS tissue – diluted 1:3 with RNase free water

### **2.5.2. Protocol**

Primer/probe sets for mRNA transcripts were shown to amplify with equal efficiency (data not shown; one example in Figure 3.2a), thus a comparative cycle-threshold ( $C_t$ ) method was used for relative quantification of gene expression. Reactions were performed in the ABI Prism 7700 Sequence Detection System (Applied Biosystems) in MicroAmp 96-well reaction plates. Each well contained 12.5 $\mu$ l of master mix, 1.25 $\mu$ l primer and probe mix and 2 $\mu$ l of cDNA template in a reaction volume of 25 $\mu$ l in triplicate. Optimisation of AWP1 primers and probe was carried out to find conditions for the most efficient PCR. Wells measuring AWP1 contained 200nM probe, 900nM forward primer, 450nM reverse primer and again 12.5 $\mu$ l of master mix, and 2 $\mu$ l of cDNA template in a reaction volume of 25 $\mu$ l in triplicate. Cycling conditions were as follows: 50°C for 2 min, 95°C for 10 min followed by 40 cycles of 95°C for 15s and 60°C for 1 min. Amplicons produced during cycling were analysed by DNA electrophoresis (on a 4% agarose gel; see Section 2.6). The data from the LPS-treatment group was normalised to the average for the saline (control) group, using the  $2^{-\Delta\Delta C_t}$  method.  $\Delta\Delta C_t$  was calculated using the difference in  $\Delta C_t$  of LPS-treated samples and the mean  $\Delta C_t$  of controls, following normalization of  $C_t$  values for the target gene to the  $C_t$  values of HMBS. The saline control group was given a value of 1, and fold changes in mRNA expression for the LPS-treated group were calculated, relative to the control group.

All data reported as means  $\pm$ SEM. Comparisons between LPS and control tissue were performed by one-way analysis of variance (ANOVA). Significance was accepted at the 5% level.

## **2.6. DNA electrophoresis**

### **2.6.1. Solutions**

- 1) Tris -acetate-EDTA (TAE) buffer: 0.04M Tris-acetate 1mM EDTA, pH 8 (HCl)
- 2) ethidium bromide solution: 1% (w/v) water
- 3) agarose gel solution: 1%/4% (w/v) agarose in TAE
- 4) sample loading buffer: 5 x sample buffer (BioRad Cat 161-0767)

### **2.6.2. Protocol**

Agarose gel solution was microwaved until the agarose had melted; either 1% or 4% agarose was used, the latter required for separation of smaller gel products, including amplicons produced from TaqMan analysis in Section 2.5. The solution was mixed to ensure even temperature throughout. After cooling (but prior to setting), 1 $\mu$ l ethidium bromide solution was added and the mixture poured into a gel tank. Wells were formed by insertion of a comb before the gel set. The gel tank was filled with TAE buffer and sample loading buffer added to samples. Samples were loaded and the gel run at a constant voltage of 70V. DNA bands were detected on a UV transilluminator.



- 4) 10mM dNTPs: 10mM dATP, 10mM dCTP, 10mM dTTP, 10mM dGTP, in deionised water
- 5) deionised water
- 6) GoTaq® DNA polymerase (5U/μl) (Promega)

### **2.8.1.2. Protocol**

To clone the protein coding sequence of the Znf\_UBP domain of iso T, 50ng human U20S cDNA (kindly donated by D. Foxler) was utilised as a template, and incubated with 1μl each of Znf\_UBP forward/reverse primers, 0.5μl GoTaq, 4μl 5 x Green GoTaq® Flexi buffer and 1μl dNTPs. A separate reaction was made up in the absence of GoTaq, and reaction mixtures were made up to 20μl with water. The cycling steps were as follows: 95°C for 1 min, followed by 40 cycles of 95°C for 1 min, 60°C for 1 min and 72°C for 1 min. Reactions were finally heated at 72°C for 3 min for final extension, then held at 4°C. PCR reactions were separated by DNA electrophoresis on a 1% agarose gel (see Section 2.6); samples did not require the addition of sample buffer, as Green GoTaq Flexi buffer increases the density of samples to allow sinking to the bottom of the agarose gel well, and contains loading dye necessary for monitoring migration. The agarose gel purified PCR product was extracted using the QIAquick Gel Extraction Kit (QIAGEN), according to the manufacturer's instructions, and was double digested and ligated (see Section 2.8.2.)

## **2.8.2. Restriction digest and ligation**

### **2.8.2.1. Solutions**

- 1) *Bam*HI restriction enzyme (20U/μl) (NEB)

- 2) *XhoI* restriction enzyme (20U/ $\mu$ l) (NEB)
- 3) NEBuffer 3 (10x) (NEB)
- 4) T4 DNA ligase (3U/ $\mu$ l) (NEB)
- 5) T4 DNA ligase reaction buffer (10x) (NEB)
- 6) deionised water
- 7) PCR product from Section 2.8.1. (Znf\_UBP sequence)
- 8) pGEX-4T-1 plasmid (100ng/ $\mu$ l)

### 2.8.2.2. Protocol

The PCR product purified from Section 2.8.1 was amplified to have *Bam*HI and *Xho*I specific DNA sequences at 5' and 3' ends, respectively. 16 $\mu$ l PCR product or 5 $\mu$ l pGEX-4T-1 were double digested by the addition of 1 $\mu$ l *Bam*HI, 1 $\mu$ l *Xho*I and 2 $\mu$ l NEBuffer 3. The plasmid digestion was made up to a final volume of 20 $\mu$ l using deionised water. Digests were incubated for 2 hours at 37°C. Digested products were separated by DNA electrophoresis on a 1% agarose gel (see Section 2.6). The double digested PCR product or plasmid was extracted from agarose gel pieces using the QIAquick Gel Extraction Kit (QIAGEN), according to the manufacturer's instructions.

Purified double-digested products were quantified using a NanoDrop® ND-1000 spectrophotometer (NanoDrop Technologies Inc., Wilmington, USA). The PCR product was ligated into the pGEX-4T-1 plasmid by incubating 50ng plasmid with between 3.5-10.5ng of double digested PCR product, together with 2.5 $\mu$ l T4 DNA ligase reaction buffer and 0.5 $\mu$ l T4 DNA ligase. Reactions were made up to a final volume of 25 $\mu$ l, and incubated overnight at 22°C, to allow ligation of the PCR

product into the pGEX-4T-1 plasmid. The ligation product was then put onto ice prior to transformation of the newly ligated plasmid into XL10-Gold bacteria.

## 2.9. Site-directed mutagenesis

### 2.9.1. Solutions

- 1) 10 x *Pfu* reaction buffer (Stratagene)
- 2) plasmid pGEX-4T-1-WT-rZNF216 (50ng/μl)
- 3) primers (10μM) (Appendix I) ZNF216 C30/33A sense  
ZNF216 C30/33A antisense  
ZNF216 (1-60) sense (Znf\_A20)  
ZNF216 (1-60) antisense (Znf\_A20)
- 4) dimethyl sulphoxide (DMSO) (Sigma-Aldrich D2650)
- 5) 10mM dNTPs: 10mM dATP, 10mM dCTP, 10mM dTTP, 10mM dGTP, in deionised water
- 6) deionised water
- 7) *Pfu* DNA polymerase (2.5U/μl; Stratagene)
- 8) *Dpn1* restriction enzyme ( 20U/μl; NEB)

### 2.9.2. Protocol

This protocol follows instructions in QuikChange® Site-Directed Mutagenesis Kit (Stratagene.) Mutagenesis reactions were set up using the pGEX-4T-1-WT-rZNF216 plasmid as a template, to generate a FL ZNF216 C30/33A mutant, and a truncated Znf\_A20 construct. To each reaction, 5μl 10 x *Pfu* buffer, 1.25μl of sense and antisense primers and 1μl of 10mM dNTPs was added. Either 5ng, 20ng or 50ng of plasmid was also added to each reaction, each in combination with either

0µl, 2.5µl or 5µl of DMSO. 1µl *Pfu* was added to each of these reactions at the denaturation step during cycling (see cycling information), with the exception of one reaction which contained 50ng plasmid and 0µl DMSO, and also lacked *Pfu* enzyme. The final reaction mixtures were made up to a final volume of 50µl. The cycling steps were; 95°C for 30s, after which *Pfu* was added to the necessary reactions, followed by 18 cycles of 95°C for 30s, 55°C for 1 min, 68°C for 6 min. Reactions were then held at 4°C.

After site-directed mutagenesis, PCR products were treated with *Dpn1* restriction enzyme to remove any non-mutated plasmid: 0.5µl *Dpn1* was added to 25µl PCR products. The reaction was incubated at 37°C for 2 hours and put onto ice prior to transformation of the mutated plasmids into XL10-Gold bacteria.

## **2.10. Transformation of *E. coli* with plasmid DNA**

### **2.10.1. Solutions**

- 1) XL10-Gold® ultracompetent cells (Stratagene)
- 2) Luria Broth medium: 2.5% (w/v) LB (Sigma-Aldrich) – autoclaved to sterilise
- 3) LB-agar ampicillin plates: 3.5% (w/v) LB-agar in H<sub>2</sub>O, 100µg/ml ampicillin

### **2.10.2. Protocol**

Between 5µl-20µl of newly ligated plasmid (Section 2.8) or *Dpn1*-digested mutated plasmid (Section 2.9) was added to 100µl XL10-Gold competent cells

and incubated on ice for 30 min. Cells were heat shocked at 42°C for 30s before incubation on ice for 5 min. Cells and mutant plasmid were made up to 1ml with LB, and incubated at 37°C whilst shaking for 1 hr. Cells were plated out on agar ampicillin plates and incubated at 37°C overnight. pGEX-4T-1 plasmids confer ampicillin resistance, thus colonies that had grown after incubation are likely to contain intact plasmid. Single colonies were picked and used to inoculate 10ml LB overnight cultures. Plasmid preps using QIAprep® Spin Miniprep Kit (Cat # 27104) were used to harvest plasmid from bacteria, and sequenced to identify successful mutagenesis and transformation. Glycerol stocks were made of successfully transformed cells.

## **2.11. Glycerol stocks of *E. coli***

### **2.11.1. Solutions**

- 1) 30% glycerol

### **2.11.2. Protocol**

30% glycerol was filter sterilised, and 0.5ml added to 0.5ml bacterial culture. Glycerol stocks were then frozen at -80°C.

## **2.12. GST-fusion protein overexpression**

### **2.12.1. Solutions**

- 1) Luria Broth: 2.5% LB (w/v) - autoclaved to sterilise
- 2) ampicillin (100mg/ml)

- 3) 200mM isopropyl-1-thio- $\beta$ -D-galactopyranoside (IPTG)
- 4) Tris-buffered saline (TBS)- Triton: 10mM Tris, 150mM sodium chloride, pH7.5 (HCl) 0.1% (v/v) Triton X-100

### **2.12.2. Protocol**

Cells were obtained from glycerol stocks of XL10-Gold *E. coli* containing pGEX-4T-1 plasmids with inserts that allow expression of GST-fused proteins. The plasmid confers ampicillin resistance to host cells, and cells either express recombinant GST-tagged WT ZNF216, C30/33A ZNF216, Znf\_A20 or Znf\_UBP proteins/constructs. These cells were grown overnight at 37°C whilst shaking in 10ml LB amp (100 $\mu$ g/ml). The following day, cultures were diluted (1/100) in LB ampicillin (100 $\mu$ g/ml) contained in baffled flasks. Cells were grown whilst shaking at 37°C for 3 hours. Cultures were induced to overexpress protein by the addition of IPTG to a final concentration of 200 $\mu$ M and grown for a further 3 hours while shaking at 37°C. These cultures were centrifuged in the Cellsep centrifuge at 4500 rcf, 4°C for 15 min, cell pellets resuspended in 10ml TBS 0.1% Triton X100 and stored at -20°C.

## **2.13. Sodium dodecyl sulphate polyacrylamide-gel electrophoresis (SDS PAGE)**

### **2.13.1. Solutions**

- 1) 30% (w/v) acrylamide to bis-acrylamide 37.5:1
- 2) 0.1% sodium dodecyl sulphate (SDS)
- 3) buffer A: 1.1M Tris, 0.1% (w/v) SDS, 30% (w/v) glycerol, pH8.8(HCl)
- 4) buffer B: 1.1M Tris, 0.1% (w/v) SDS, pH8.8(HCl)

- 5) stacking gel buffer: 0.14M Tris, 0.1% (w/v) SDS, pH6.8(HCl)
- 6) ammonium persulphate (AMPS): 10% (w/v) ammonium persulphate
- 7) deionised water
- 8) tetramethylethylenediamine (TEMED): undiluted
- 9) gel application buffer (GAB): 0.15M Tris, 8M urea, 2.5% (w/v) SDS, 20% (v/v) glycerol, 10% (w/v) 2-mercaptoethanol, 3% (w/v) DTT, 0.1% w/v bromophenol blue, pH6.8(HCl)
- 10) electrode buffer: 0.025M Tris, 0.19M glycine, 0.1% w/v SDS
- 11) Coomassie Blue stain: 50% (v/v) methanol, 20% (v/v) glacial acetic acid, 0.12% (w/v) Coomassie Brilliant Blue R-250
- 12) Coomassie Blue destain: 10% (v/v) methanol, 10% (v/v) glacial acetic acid

### **2.13.2 Protocol**

5-20% polyacrylamide resolving gels were poured using a gradient caster, producing a continuous gradient. 100µl SDS was added to each resolving gel mixture, made to a total volume of 10ml with deionised water; the 5% polyacrylamide gel is composed of 1.67ml 30% acrylamide, 3.33ml buffer B and the 20% polyacrylamide gel contains 6.67ml 30% acrylamide, 3.33ml buffer A. Prior to pouring the gel, 100µl AMPS and 10µl TEMED were added to the gel mixtures to catalyse polymerisation. Water saturated butanol was used to cover the surface of the gradient gel. Subsequently, the 5% stacking gel was also polymerised using 100µl AMPS and 10µl TEMED (final concentration 0.12M Tris, 0.1% SDS). GAB was added to protein samples, typically adding 20µl GAB to 50µl sample (containing around 5µg protein), which were heated to 90°C for 5 min. The gel was run at 40mA (E-C Apparatus Corporation). BIO-RAD All Blue

Precision Plus Protein™ Standards were run on the gel in order to approximate the size of proteins within the samples. Gels were mostly either incubated for 1 hr in Coomassie Blue stain and destained using Coomassie Blue destain solution, or proteins from the gel were transferred *via* Western blotting (see Section 2.15). Some gels were stained using Silver Staining Kit (GE Healthcare), according to the manufacturer's instructions.

## **2.14. Two-dimensional gel electrophoresis (2DE)**

### **2.14.1. Solutions**

- 1) 30% (w/v) acrylamide to bis-acrylamide 37.5:1
- 2) 0.1% sodium dodecyl sulphate (SDS)
- 3) buffer A: 1.1M Tris, 0.1% (w/v) SDS, 30% (w/v) glycerol, pH8.8(HCl)
- 4) buffer B: 1.1M Tris, 0.1% (w/v) SDS, pH8.8(HCl)
- 5) ammonium persulphate (AMPS): 10% (w/v) ammonium persulphate
- 6) tetramethylethylenediamine (TEMED): undiluted
- 7) isoelectric focussing (IEF) sample buffer: DeStreak™ Rehydration Solution (GE Healthcare), 0.5% (v/v) pH 3 – 11NL ampholyte solution (GE Healthcare)
- 8) mineral oil (BioRad)
- 9) 70% EtOH
- 10) equilibration buffer I (6M urea, 2% (w/v) SDS, 0.375M Tris-Cl, 2% (w/v) DTT, pH 8.8, 20% (v/v) glycerol)
- 11) equilibration buffer II (6M urea, 2.5% (w/v) iodoacetamide, 0.375M Tris-Cl, 2% (w/v) DTT, pH 8.8, 20% (v/v) glycerol)
- 12) electrode buffer: 0.025M Tris, 0.19M glycine, 0.1% w/v SDS

- 13) agarose gel solution: 1% (w/v) agarose, 0.1% (w/v) bromophenol blue,  
in 1 x electrode buffer
- 14) fixative: 40% (v/v) methanol, 10% (v/v) glacial acetic acid
- 15) deionised water
- 16) colloidal Coomassie Blue stain: 0.0125% (w/v) Coomassie G250, 3%  
(v/v) phosphoric acid, 8% (w/v) ammonium sulphate, 20% (v/v) ethanol

#### **2.14.2 Protocol**

5-20% polyacrylamide resolving gels were poured using a gradient caster, in a protocol identical to Section 2.13, except that the stacking gel was omitted, and GAB was not added to samples. Instead, 150µl isoelectric focussing (IEF) sample buffer was added to samples and incubated at room temperature for 15 min. Immobilised pH gradient (IPG) strips (11cm; pH 3-11NL) were actively rehydrated at 50V with the sample/IEF buffer, under 2ml mineral oil, overnight at 20°C. An 11cm focusing tray was washed with 70% ethanol, and dampened electrode wicks were placed on the electrodes. Excess mineral oil was drained from IPG strips, placed in the focusing tray and covered in 1ml mineral oil. To isoelectrically focus strips, the isoelectric focuser (BioRad) was set to a linear ramping programme (Step 1: 250V – 15 min; Step 2: 8000V – 2 hr 30 min; Step 3: 8000V – 35000 Vh, Step 4: 500V – Hold).

When focusing was complete, wicks were removed and mineral oil drained from IPG strips. Strips were washed 3 x 5 min with 1ml equilibration buffer I and 3 x 5 min with 1ml equilibration buffer II. Finally, strips were mounted on the 5-20% gradient polyacrylamide gel, and a 1% agarose solution was pipetted onto the gel strip to monitor protein migration through the gel, and to seal the strip in

position. Gels were run at 40mA (E-C Apparatus Corporation). BIO-RAD All Blue Precision Plus Protein™ Standards were run on the gel, adjacent to the IPG strip, in order to approximate the size of proteins within the samples.

Proteins were either visualised by colloidal Coomassie staining, silver staining or were transferred *via* Western blotting (see Section 2.15). To colloidal Coomassie stain proteins, gels were fixed in fixative for one hr at room temperature with gentle rocking, prior to two 10 min washes with deionised water. Gels were then immersed in 100ml colloidal Coomassie Blue stain overnight with gentle rocking, and finally destained by further washes with deionised water. Some spots were excised and tryptically digested and analysed by peptide mass fingerprinting (PMF; Section 2.23). Gels were silver stained using Silver Staining Kit (GE Healthcare), according to the manufacturer's instructions.

## **2.15. Western blotting**

### **2.15.1. Solutions**

- 1) Western transfer buffer: 0.025M Tris, 0.192M glycine, 20% (v/v) methanol
- 2) Ponceau S solution: 0.1% (w/v) Ponceau S, 10% (v/v) glacial acetic acid
- 3) Renaissance Enhanced Chemiluminescence (ECL): (Amersham)
- 4) developing solution: (Calumet Photographic LTD 757314)
- 5) fixing solution: (Calumet Photographic LTD 2000RT)

### **2.15.2. Protocol**

The gel and nitrocellulose (Hybond-C, Amersham) were soaked in Western transfer buffer prior to contact. Protein on the gel was transferred to the membrane by blotting overnight at room temperature (Fisherbrand Electrophoresis Unit) at 40mA. To confirm successful transfer, the blot was stained with Ponceau S solution for 1 min (until bands were visible), then destained with distilled water. Information about antibodies (manufacturer and dilutions), incubation times, wash buffer and blocking buffer can be found in Appendix II. Ponceau S stain was removed by washing in wash buffer. Membranes were incubated in blocking solution prior to incubating in either primary antibody, or horseradish peroxidase (HRP)-conjugated antibody. Membranes were washed 3 x 5 min with wash buffer to remove excess and unbound antibodies. Blots incubated in primary antibody were then incubated with secondary antibody, and subsequently washed 3 x 5 min in wash buffer. Washed membranes (both those incubated in secondary and HRP-conjugated antibodies) were then immersed for 1 min in Renaissance ECL solutions. Hyperfilm ECL (Amersham Biosciences) was exposed to the blot for between 1-20 min prior to developing (with developing solution). Film was then washed in distilled water, fixed (in fixing solution), washed again in water and finally air-dried.

## **2.16. Thrombin cleavage**

### **2.16.1. Solutions**

- 1) Tris-buffered saline (TBS)-Triton: 10mM Tris, 150mM sodium chloride, pH 7.5 (HCl) 0.1% (v/v) Triton x100

- 2) glutathione-Sepharose beads (stored in ethanol)
- 3) thrombin cleavage buffer: 20mM Tris, 150mM sodium chloride, 2.5mM calcium chloride dihydrate, pH 8.4 (HCl)
- 4) thrombin 0.5units/ $\mu$ l

### **2.16.2. Protocol**

Cell pellets resulting from protein overexpression were sonicated on ice 7 x 15s at 6-7 microns (30s cooling.) The sample was centrifuged at 35000 rcf at 4°C for 30 min in an Avanti JA-25-50 rotor. 1ml glutathione-Sepharose beads (per sample) were equilibrated with 5ml TBS-Triton, in a polyprep column (BioRad). Once centrifuged, the pellet formed was discarded and the supernatant incubated with beads for a minimum of 1 hr, at 4°C while rotating. Beads were washed with 3 x 10ml TBS Triton and 1 x 10ml thrombin cleavage buffer (to equilibrate). For thrombin cleavage of the GST tag, 10 units of thrombin were added per column in 1ml thrombin cleavage buffer and incubated overnight at 4°C whilst rotating. The following day, recombinant protein was collected from the beads in solution. The purified protein was resolved by SDS PAGE and stained with Coomassie Blue for 1 hr, and destained with Coomassie destain (see Section 2.13).

## **2.17. Coupling protein to Sepharose beads**

### **2.17.1. Solutions**

- 1) cyanogen bromide-activated-Sepharose-4B (CNBr Seph 4B) (GE Healthcare)
- 2) 1mM HCl
- 3) coupling buffer: 100mM NaHCO<sub>3</sub>, 500mM NaCl, pH8.3 (HCl)

- 4) 1M ethanolamine, pH8.0 (HCl)
- 5) acetate buffer: 100mM NaOAc, 500mM NaCl, pH4 (acetic acid)
- 6) Tris buffer: 100mM Tris (hydroxymethyl) methylamine pH8 (HCl)
- 7) column storage buffer: 25mM Tris (hydroxymethyl) methylamine, 1mM sodium azide, pH7.4(HCl)

### **2.17.2. Protocol**

Cyanogen bromide Sepharose 4B (CNBr Seph 4B) was hydrated for 15 min in HCl solution, and transferred to a polyprep column (BioRad.) Beads were washed with 5 bed volumes of coupling buffer. Protein that was coupled with Sepharose beads was either ubiquitin or thrombin cleaved protein (either FL ZNF216 WT, FL ZNF216 C30/33A, Znf\_A20 or Znf\_UBP). Thrombin cleaved proteins/ubiquitin were diluted to the appropriate concentration with coupling buffer and incubated with the beads for 3 hours at 4°C (see Results for final concentrations of mg protein/ml Sepharose). Protein solution was passed through the beads, which were then washed with 5 bed volumes of ethanolamine and incubated in ethanolamine overnight at 4°C. The following day, this solution was removed, and beads were washed with 5 bed volumes of coupling buffer 3 x. Beads were washed alternately with 5 bed volumes of acetate or Tris buffer 4 x. Beads were finally washed with column storage buffer, and stored in a 50% slurry in column storage buffer. Control Sepharose (protein omitted, replaced by coupling buffer) was prepared in parallel to protein coupled beads.

## **2.18. Deubiquitination assay**

### **2.18.1. Solutions**

- 1) USP2, catalytic core (rat, recombinant); (0.5µg/µl; Enzo Life Sciences)
- 2) TBSA: 50mM Tris, 0.1% (w/v) bovine serum albumin (BSA) pH7.5
- 3) Polyubiquitin chains: Lys48 (K48) or Lys63 (K63) linked polyubiquitin chains, (Enzo Life Sciences) in TBSA, 0.125µg/30µl
- 4) gel application buffer (GAB): 0.15M Tris, 8M urea, 2.5% (w/v) SDS, 20% (v/v) glycerol, 10% (w/v) 2-mercaptoethanol, 3% (w/v) DTT, 0.1% w/v bromophenol blue, pH6.8 (HCl)

### **2.18.2. Protocol**

FL ZNF216 WT-Sepharose (17.75mg/ml), FL ZNF216-C30/33A-Sepharose (17.75mg/ml) and control-Sepharose were produced by covalently immobilising proteins on CNBr Seph 4B (see Section 2.17.) 0.125µg K48-linked polyubiquitin chains (in TBSA buffer) were incubated overnight at 37°C with 30µl Sepharose (as noted above), in the absence of Sepharose or with 0.5µg USP2. 50µl GAB was added to beads/solutions, and the remaining protein was resolved by SDS PAGE (Section 2.13) and proteins were immunoblotted with anti-ubiquitin antibodies (Section 2.15).

## **2.19. Ubiquitin-Sepharose binding assay**

### **2.19.1. Solutions**

- 1) Tris-buffered saline (TBS)- Triton: 10mM Tris, 150mM sodium chloride, pH7.5 (HCl) 0.1% (v/v) Triton X-100

- 2) gel application buffer (GAB): 0.15M Tris, 8M urea, 2.5% (w/v) SDS, 20% (v/v) glycerol, 10% (w/v) 2-mercaptoethanol, 3% (w/v) DTT, 0.1% (w/v) bromophenol blue, pH6.8 (HCl)

### **2.19.2. Protocol**

Previous to this protocol, pellets were spun down from 10ml overnight *E. coli* cultures. These cultures were previously induced to overexpress the following recombinant proteins: GST, GST-WT-ZNF216 and GST- ZNF216-C30/33A. Pellets were thawed and resuspended in 1ml TBS-Triton, sonicated 4 x 15s (with 30s cooling intervals) and centrifuged at 16000 rcf for 10 min. The pellet that resulted was discarded and the supernatant collected. 50µl glutathione, control and ubiquitin-Sepharose (10mg/ml) beads (see Section 2.17) were equilibrated in 1ml TBS-Triton. For all supernatants, except for GST, 50µl supernatant was added to each type of Sepharose bead. Only 25µl of the GST supernatant was added as it is more efficiently expressed in *E. coli* relative to the other proteins. The beads were incubated with supernatant for 30 min at 4°C while rotating. After incubation, beads were washed 2 x 1ml TBS-Triton, and bead-bound protein was eluted with 50µl gel application buffer. Samples were boiled for 5 min and resolved by SDS PAGE (Section 2.13). 20µl sample was loaded per lane. One gel was stained for protein using Coomassie (Section 2.13) and one was transferred overnight by Western blotting (Section 2.15) and subsequently probed with anti-GST antibodies.

## 2.20. Polyubiquitin chain-binding assay

### 2.20.1. GST-tagged proteins

#### 2.20.1.1. Solutions

- 1) Tris-buffered saline (TBS)- Triton: 10mM Tris, 150mM sodium chloride, pH7.5 (HCl) 0.1% (v/v) Triton X-100
- 2) TBSA: 50mM Tris, 0.1% (w/v) Bovine serum albumin (BSA) pH7.5 (HCl)
- 3) polyubiquitin chains: Lys48 (K48)- or Lys63 (K63)-linked polyubiquitin chains, (Enzo Life Sciences) in TBSA, 0.5µg/50µl
- 4) gel application buffer (GAB): 0.15M Tris, 8M urea, 2.5% (w/v) SDS, 20% (v/v) glycerol, 10% (w/v) 2-mercaptoethanol, 3% (w/v) DTT, 0.1% w/v bromophenol blue, pH6.8 (HCl)

#### 2.20.1.2. Protocol

Previous to this protocol, pellets were spun down from 10ml overnight *E. coli* cultures. These cultures were previously induced to overexpress the following recombinant proteins: GST, GST-WT-ZNF216 and GST-C30/33A-ZNF216. Pellets were thawed and then resuspended in 1ml TBS-Triton, sonicated 4 x 15s (with 30s cooling intervals) and centrifuged at 16000 rcf for 10 min. The resultant pellet was discarded and supernatant collected. 50µl glutathione Sepharose beads were equilibrated in 1ml TBS-Triton. For all supernatants, except GST, 50% supernatant was added to each type of Sepharose bead. Only 25% of the GST supernatant was added as it is more efficiently expressed in *E. coli* relative to the other proteins. The beads were incubated with supernatant for 30 min at 4°C while rotating. After incubation, beads were washed 2 x 1ml TBS-Triton and equilibrated with TBSA. K48/K63 polyubiquitin chains (0.5µg) were added to

each set of beads in 50µl Tris BSA buffer. Beads were incubated for 30 min at 4°C with gentle agitation every 5 min. Solution was discarded and beads were washed 2 x 1ml Tris BSA. Bound protein was eluted with 50µl GAB. Proteins were resolved by SDS PAGE (Section 2.13), transferred to nitrocellulose overnight by Western blotting and probed with anti-ubiquitin (Section 2.15).

## **2.20.2. Thrombin cleaved proteins**

### **2.20.2.1. Solutions**

- 1) binding buffer: 50mM Tris, 150mM NaCl, 0.5% (v/v) NP-40, 0.1% (w/v) bovine serum albumin (BSA; Sigma-Aldrich), 1mM DTT, pH 7.5 (HCl)
- 2) polyubiquitin chains: Lys48 or Lys63 linked polyubiquitin chains, (Enzo Life Sciences) in binding buffer, 0.25µg/50µl
- 3) ubiquitin 5 +1: Ub<sub>5</sub>+1 (Enzo Life Sciences), in binding buffer, 0.125µg/50µl
- 4) gel application buffer (GAB): 0.15M Tris, 8M urea, 2.5% (w/v) SDS, 20% (v/v) glycerol, 10% (w/v) 2-mercaptoethanol, 3% (w/v) DTT, 0.1% w/v bromophenol blue, pH6.8 (HCl)

### **2.20.2.2. Protocol**

Znf\_A20- (5mg/ml), Znf\_UBP- (10mg/ml) or control-Sepharose (50µl each) were equilibrated in binding buffer. Beads were incubated with 0.25µg of K48-/K63-linked polyubiquitin chains or 0.125µg Ub<sub>5</sub>+1 (in binding buffer) for 30 min at 4°C, with gentle agitation every 5 min (see Results for further detail). Beads were washed twice in 1ml binding buffer and bound proteins were eluted with 50µl GAB, resolved by SDS PAGE (Section 2.13) and immunoblotted with anti-ubiquitin (Section 2.15).

## **2.21. MG132 treatment of U2OS cells**

### **2.21.1. Solutions**

- 1) dimethyl sulphoxide (DMSO): (Sigma-Aldrich D2650)
- 2) MG132: 10mM MG132 (Enzo Life Sciences), in DMSO
- 3) Penicillin/Streptomycin: (Sigma-Aldrich). Penicillin/Streptomycin solution contained 10,000 units of Penicillin and 10mg/ml Streptomycin in 0.9% (w/v) NaCl
- 4) Dulbecco's Modified Eagle's Medium (DMEM): 4500mg/L glucose, 2mM L-glutamine and 100mg/L sodium pyruvate (Sigma-Aldrich)
- 5) Fetal Bovine Serum (FBS): (Sigma-Aldrich).
- 6) media: DMEM, 10% (v/v) foetal calf serum (FCS), 1% (v/v) penicillin/streptomycin
- 7) Phosphate Buffer Saline (Sigma-Aldrich)

### **2.22.2. Protocol**

U2OS cells (derived from a human osteosarcoma cell line) were grown to ~80% confluence in 2 x 75cm<sup>2</sup> cell culture flasks (Corning®, cell culture flask, 75cm<sup>2</sup>). One flask was then treated with MG132 (to a final concentration of 1µM) and the other with the same volume of DMSO, in fresh media, for 16 hours and incubated at 37°C. Cells were then targeted for affinity capture, as detailed in Section 2.22.3.

## **2.22. Pulldown Assays**

### **2.22.1. Rat muscle**

#### **2.22.1.1. Affinity chromatography**

### ***2.22.1.1.1. Solutions***

- 1) dimethyl sulphoxide (DMSO): (Sigma-Aldrich D2650)
- 2) MG132: 10mM MG132 (Enzo Life Sciences), in DMSO
- 3) mammalian protease inhibitor cocktail (Sigma-Aldrich)
- 4) Tris DTT: 50mM Tris, 1mM DTT, 20 $\mu$ M MG132, 0.1% (v/v) mammalian protease inhibitor cocktail, pH 7.5 (HCl)
- 5) gel application buffer (GAB): 0.15M Tris, 8M urea, 2.5% (w/v) SDS, 20% (v/v) glycerol, 10% (w/v) 2-mercaptoethanol, 3% (w/v) DTT, 0.1% w/v bromophenol blue, pH6.8 (HCl)

### ***2.22.1.1.2. Protocol***

Affinity chromatography was typically utilised to capture polyubiquitinated proteins/unanchored polyubiquitin, using CNBr Seph 4B immobilised FL ZNF216 WT, FL ZNF216 C30/33A, Znf\_A20 and Znf\_UBP (Section 2.17). In the first instance, approximately 7g of control, mixed rat muscle was homogenised in 50ml Tris DTT buffer. Rat muscle was kindly donated by L. Lyons; muscle was taken from rat hind legs and includes EDL, soleus, biceps femoris, tibialis anterior, gastrocnemius and gluteus superficialis muscles. Rat muscle homogenate was centrifuged at 35000 rcf at 4°C for 30 min in an Avanti JA-25-50 rotor. The insoluble pellet was discarded, and the supernatant passed through glass wool to remove any debris. Supernatant was split three ways between either 150 $\mu$ l FL ZNF216 WT-Sepharose, 150 $\mu$ l ZNF216 C30/33A-Sepharose or 150 $\mu$ l control-Sepharose (in polyprep column; BioRad) at 4°C. Muscle lysate was passed through Sepharose twice and then washed three times with 10ml Tris DTT. Bound proteins were eluted with GAB and resolved by SDS PAGE and visualised either by Coomassie staining (Section 2.13), stained using Silver

Staining Kit (GE Healthcare; according to the manufacturer's instructions), or the gel was transferred *via* Western blotting and immunoblotted with anti-ubiquitin antibodies (see Section 2.15). Subsequent rat muscle pulldowns were a variation of this protocol, and details can be found in the appropriate Results and Figure legends. Some affinity captured proteins were resolved instead by 2DE and colloidal Coomassie stained (Section 2.14) or captured on Znf\_A20- or Znf\_UBP-Sepharose. Rat muscle was subsequently homogenised in optimised buffers, and Sepharose was washed in varying buffers and details of analysis are detailed in Figure legends; i.e. SDS PAGE or 2DE, antibodies used, use of deubiquitination and PMF/liquid chromatography tandem mass spectrometry (LC-MS/MS), rat muscle (total mass, muscle type), Sepharose (type, volume, concentration) and buffer (volume, composition). Some affinity captured ubiquitinated proteins were subjected to deubiquitination, as detailed below in Section 2.22.1.2.

### **2.22.1.2. Deubiquitination**

#### **2.22.1.2.1. Solutions**

- 1) USP2, catalytic core (rat, recombinant); (0.5µg/µl; Enzo Life Sciences)
- 2) Deubiquitination (DUB) buffer: 50mM Tris, 1mM DTT, pH 7.5 (HCl)
- 3) gel application buffer (GAB): 0.15M Tris, 8M urea, 2.5% (w/v) SDS, 20% (v/v) glycerol, 10% (w/v) 2-mercaptoethanol, 3% (w/v) DTT, 0.1% w/v bromophenol blue, pH6.8 (HCl)

#### **2.22.1.2.2. Protocol**

Rat muscle proteins were captured on Znf\_A20- /Znf\_UBP-Sepharose, as described in Section 2.22.1.1. To elute ubiquitinated proteins specifically, rather

than eluting all bound proteins using GAB, Sepharose was deubiquitinated using USP2. Typically, 800µl of Sepharose that has been washed three times in the appropriate wash buffer was then washed 1 x 10ml DUB buffer. An equal volume of DUB buffer (800µl) to beads was added, +/- 10µg USP2 core for 2hrs at 37°C. Limited deubiquitination was also performed, in which beads were incubated for only 1hr. Solutions were collected from beads, and two further equal volume DUB buffer washes were performed, and the washes pooled. Proteins bound to beads were eluted with GAB, resolved by SDS PAGE, Coomassie stained (Section 2.13) and some proteins were excised for tryptic digestion and PMF (Section 2.23). Alternatively, SDS PAGE gels were transferred overnight and immunoblotted with a number of antibodies (Section 2.15; see Results for information on antibodies used.) Solutions were treated the same as beads, or were tryptically digested and analysed by LC-MS/MS.

## **2.22.2. Mouse cortex**

### **2.22.2.1. Affinity chromatography**

#### ***2.22.2.1.1. Solutions***

- 1) dimethyl sulphoxide (DMSO): (Sigma-Aldrich D2650)
- 2) MG132: 10mM MG132 (Enzo Life Sciences), in DMSO
- 3) mammalian protease inhibitor cocktail (Sigma-Aldrich)
- 4) homogenising buffer: 50mM Tris, 150mM NaCl, 0.5% (v/v) NP-40, 5mM N-ethylmaleimide, 20µM MG132, 0.1% (v/v) mammalian protease inhibitor cocktail (Sigma), pH 7.5
- 5) wash buffer: 50mM Tris, 150mM NaCl, 0.5% NP-40, 1mM DTT, pH 7.5

- 6) gel application buffer (GAB): 0.15M Tris, 8M urea, 2.5% (w/v) SDS, 20% (v/v) glycerol, 10% (w/v) 2-mercaptoethanol, 3% (w/v) DTT, 0.1% w/v bromophenol blue, pH6.8 (HCl)

#### **2.22.2.1.2. Protocol**

Mouse cortexes from wild type and *Psmc1* knockout mouse brain (~15mg each) were donated by L. Bedford. Cortexes were homogenised in 5ml homogenising buffer. Homogenate was centrifuged, supernatant passed through glass wool. DTT was added to the supernatant to a final concentration of 10mM, and mixed at 4°C for 15 minutes. Supernatant was passed twice through 50µl Znf\_A20-/control-Sepharose for 1 hour at 4°C. Beads were washed three times in wash buffer and bound proteins eluted with GAB, resolved by SDS PAGE (Section 2.13) and immunoblotted with anti-ubiquitin (Section 2.15).

### **2.22.3. U2OS cells**

#### **2.22.2.1. Affinity chromatography**

##### **2.22.2.1.1. Solutions**

- 1) dimethyl sulfoxide (DMSO): (Sigma-Aldrich D2650)
- 2) MG132: 10mM MG132 (Enzo Life Sciences), in DMSO
- 3) mammalian protease inhibitor cocktail (Sigma-Aldrich)
- 4) homogenising buffer: 50mM Tris, 150mM NaCl, 0.5% (v/v) NP-40, 5mM N-ethylmaleimide, 20µM MG132, 0.1% (v/v) mammalian protease inhibitor cocktail (Sigma), pH 7.5
- 5) wash buffer: 50mM Tris, 150mM NaCl, 0.5% NP-40, 1mM DTT, pH 7.5

- 6) gel application buffer (GAB): 0.15M Tris, 8M urea, 2.5% (w/v) SDS, 20% (v/v) glycerol, 10% (w/v) 2-mercaptoethanol, 3% (w/v) DTT, 0.1% w/v bromophenol blue, pH6.8 (HCl)

#### **2.22.2.1.2. Protocol**

U2OS cells were grown to >80% confluence in 3 x 75cm<sup>2</sup> cell culture flasks (Corning®, cell culture flask, 75cm<sup>2</sup>). Cells were scraped into 8ml homogenising buffer, while the MG132-treated/DMSO-only cells (Section 2.21), each from 1 x 75cm<sup>2</sup> cell culture flask, was scraped into 4ml homogenising buffer. All samples were then sonicated 3 x 30s (with 30s cooling), centrifuged at 12000 rcf and the supernatant was passed through glass wool. Insoluble material that pelleted was discarded and DTT was added to the supernatant to a final concentration of 10mM, and mixed at 4°C for 15 min. Protein concentration was approximately 4mg protein per flask. Lysate was either passed through Sepharose twice (+/- MG132 cells), or incubated overnight (untreated U2OS cells only) at 4°C. Untreated cell lysate was incubated with either FL ZNF216 WT- or FL ZNF216 C30/33A-Sepharose, while +/- MG132 treated cells were passed through either Znf\_A20-, Znf\_UBP- or control-Sepharose (Section 2.17) (further details in Results). Beads were then washed 3 x 10ml wash buffer, proteins were eluted with GAB, resolved by SDS PAGE (Section 2.13) and immunoblotted (Section 2.15), as detailed in the Results chapters.

### **2.22.3. Human muscle**

#### **2.22.2.1. Affinity chromatography**

##### **2.22.2.1.1. Solutions**

- 1) dimethyl sulphoxide (DMSO): (Sigma-Aldrich D2650)
- 2) MG132: 10mM MG132 (Enzo Life Sciences), in DMSO
- 3) mammalian protease inhibitor cocktail (Sigma-Aldrich)
- 4) homogenising buffer: 50mM Tris, 150mM NaCl, 0.5% NP-40, 5mM N-ethylmaleimide, 20 $\mu$ M MG132, 0.1% (v/v) mammalian protease inhibitor cocktail (Sigma), pH 7.5
- 5) wash buffer: 50mM Tris, 150mM NaCl, 0.5% NP-40, 1mM DTT, pH 7.5
- 6) gel application buffer (GAB): 0.15M Tris, 8M urea, 2.5% (w/v) SDS, 20% (v/v) glycerol, 10% (w/v) 2-mercaptoethanol, 3% (w/v) DTT, 0.1% w/v bromophenol blue, pH6.8 (HCl)

#### ***2.22.2.1.2. Protocol***

Human muscle biopsy samples (~10mg each), taken from 5 healthy volunteers (donated by P. Atherton), were homogenised in 1ml homogenising buffer.

Homogenate was centrifuged, supernatant passed through glass wool and DTT added to the supernatant to a final concentration of 10mM, and mixed at 4°C for 15 minutes. Supernatant was incubated with 50 $\mu$ l Znf\_A20-Sepharose for 1 hour at 4°C. Beads were washed three times in wash buffer and bound proteins eluted with GAB, resolved by SDS PAGE (Section 2.13) and immunoblotted with anti-ubiquitin (Section 2.15).

### **2.23. Trypsinolysis and mass spectrometry analysis**

#### **2.23.1. Solutions**

- 1) Trypsin: 5 $\mu$ g.mL<sup>-1</sup> sequencing grade porcine trypsin (Promega)
- 2) acetonitrile

- 3) ammonium bicarbonate: 0.1M ammonium bicarbonate, 50% (v/v)  
acetonitrile, pH 8.0
- 4) DTT: 1mM DTT, in ammonium bicarbonate
- 5) iodoacetamide: 2mM iodoacetamide, in ammonium bicarbonate
- 6) 0.1% formic acid<sub>(aq)</sub>
- 7) 0.1% formic acid in 70% acetonitrile<sub>(aq)</sub>

### **2.23.2. Protocol**

All detected components were manually excised and then trypsinolysed using standard automated robotic procedures. Briefly; bands/spots were incubated with 1mM DTT followed by 2mM iodoacetamide with interim washing. Gel pieces were then washed with acetonitrile, dried and then rehydrated with sufficient trypsin in aqueous 0.1M ammonium bicarbonate. Proteolytic peptides were extracted by recovering sequential washes with 0.1% formic acid<sub>(aq)</sub> and 0.1% formic acid in 70% acetonitrile<sub>(aq)</sub> and then dried.

For PMF analysis, extracted tryptic peptides were analysed by MALDI-TOF-MS and the resulting peak-list was used to interrogate genome databases using the Peptide-Mass-Fingerprint application in MASCOT software (Matrix Science). Alternatively, to analyse mixtures proteins eluted by deubiquitination (Section 2.22.1.2.), mixtures of tryptic peptides were analysed by LC-MS/MS.

## **CHAPTER 3**

### **Expression profiling of ZNF216 in different models of skeletal muscle atrophy**

### 3.1. Introduction

Skeletal muscle atrophy may be activated by a number of different stimuli, for example in acidosis conditions as occurs during diabetes or chronic renal failure [201, 202], during sepsis in which macrophages release cytokines that then trigger specific signalling cascades [4-6, 48, 51], and upon treatment with the cholesterol-lowering drugs, statins [203]. Burn injury may also induce muscle wasting [204], as can the onset of cancer [47, 205] and infection with human immunodeficiency virus (HIV) [206]. Fasting, disuse and denervation may also trigger skeletal muscle atrophy [207], but unlike other atrophy modes, is triggered by a lack of nutrients and inactivity. Different atrophy triggers may induce muscle wasting *via* different molecular pathways that regulate protein synthesis and breakdown. When considering protein degradation, the E3 ubiquitin ligase enzymes, muscle atrophy F-box protein (MAFbx) and muscle RING-finger 1 (MuRF1) (both classified as 'atrogenes'), have been shown to play a critical role in a number of different atrophy models, suggesting that there are likely to be common downstream molecular pathways. The zinc finger protein 216 (ZNF216) protein is another 'atrogene' implicated in skeletal muscle atrophy, thought to act at a later stage of the atrophy programme by shuttling ubiquitinated substrates (presumably modified by the actions of MAFbx and/or MuRF1) to the 26S proteasome for their degradation [56]. This proposal is based on evidence that ZNF216 localises (*via* its Znf\_AN1 domain) with the 26S proteasome and simultaneously can bind to polyubiquitin (*via* its Znf\_A20 domain) [56]. ZNF216 has previously been shown to be up-regulated in denervation and starvation-induced mouse models of skeletal muscle atrophy, and indeed is required for muscle atrophy to occur (based on gene knock-out studies in mice) [56]. However, changes in ZNF216 expression have yet to be determined in other models of muscle atrophy or in pathophysiological

conditions in which skeletal muscle atrophy is a feature. In this Chapter, ZNF216 mRNA expression levels were determined in a rat model of lipopolysaccharide (LPS)-induced endotoxaemia, in which indices of muscle atrophy are apparent [32]. We also measured ZNF216 mRNA expression in rat muscle in which LPS-induced muscle mass loss was blunted by low dose dexamethasone (Dex) co-administration without altering MAFbx and MuRF1 mRNA expression [208], and in an *in vivo* rat model of statin-induced myopathy [209]. Given that ZNF216 is thought to function in the same pathway as MAFbx and MuRF1, we hypothesise that ZNF216 expression changes may mirror those of MAFbx and MuRF1.

### **3.2. Primer and probe sets specifically target ZNF216, MAFbx, MuRF1, Fbxo25, AWP1 and HMBS mRNA sequences**

Primer and probe sets designed to specifically amplify rat ZNF216, MAFbx, MuRF1, F-box protein 25 (Fbxo25) and hydroxymethylbilane synthase (HMBS) mRNAs were selected from the Applied Biosystems TaqMan® inventoried database. No inventoried primer/probe set existed within the database that guaranteed specific targeting of rat sequence protein associated with PRK1 (AWP1) mRNA sequences as of the start of the study, but primers/probes were manually designed by Dr. Tim Constantin-Teodosiu (School of Biomedical Sciences) to prevent genomic DNA amplification. Rat AWP1 shares 55.8% protein sequence homology with rat ZNF216 (Fig 3.1a), but the former has not been reported for its involvement in muscle atrophy. The atrogene MAFbx shares 59.1% amino acid sequence identity with Fbxo25 (rat sequences) (Fig 3.1b), but while MAFbx expression has been observed to increase in multiple atrophy models, similarly to AWP1, is not induced during atrophy [103]. The housekeeping gene HMBS was selected as the internal control, as expression is

### Figure 3.1

a)

55.8% identity in 226 residues overlap

```
rZNF216,      1 MAQETNQTTPGMLCSTGCGFYGNPRNMGCSVCYKEHLQRQONS-GRMSPMGTASGSNSP
rAWP1,        1 MAQETNHSQAPMLCSTGCGFYGNPRNMGCSVCYKEHLQRQONSNGRISP---PAASVSS
*****      *****

rZNF216,      60 TSDSASVQRADATLNNCEGAAGSTSEKSRNVFV-----AALPVTQQMTEMSISRE
rAWP1,        58 LSESLPVQCADGSPDAQSAALDSTSSSMQPGPVSNSQLLSESVAPSQVDSTSVDKAVSET
* * * * *      * * * * *

rZNF216,      110 DKITSPKTEVSEPVVTQPPSPVSQPSSSQSEE--KAPELPKPKKNRCFMCRRKVGLTGFD
rAWP1,        118 EDLQGPRAEGLVPLECDPPSSVSDTTQQPSEEQSKSLEKPKQKKNRCFMCRRKVGLTGFE
* * * * *      * * * * *

rZNF216,      168 CRCGNLFCGLHRYSDKHNCYPDYKAEAAAKIRKENPVVVAEKIQRI
rAWP1,        178 CRCGNVYCGVHRYSDVHNCYNYKADAAEKIRKENPVVVGEKIQKI
*****      ** * * * * * * * * * * * * * * * * * * * * * * *
```

b)

59.1% identity in 357 residues overlap

```
rMAFbx,      1 MPFLGQDWRS PGQSWVKTADGWKRFLDEKSGTFVSDLSSYCNKENLFNLSLNDV-----
rFbxo25,     1 MPFLGQDWRS PGWSWIKTEDGWKRCDPCSHEIRSEDNQYPVNHSHIILNSGEEEIFNNDCE
*****      * * * * * * * * * * * * * * * * * * * * * * *

rMAFbx,      55 -AAKRRKKDIQNSKTKTQYFHQEKWIYVHKGSTKERHGYCTLGEAFNRLDFSTAILDSRR
rFbxo25,     61 YAAKRRKKQHFGNDTAAHSFYREKWIYVHKESTKERHGYCTLGEAFNRLDFSSAIQDIRR
*****      * * * * * * * * * * * * * * * * * * * * * * *

rMAFbx,      114 FNYVVRLELELIAKSQTLSLGGIAQKNFMNILEKVVVKVLEDQQNIRLIRELLQTLTSLC
rFbxo25,     121 FTYVVKLLQLLAKSQTLSLGVQKNFYFNILDKIVQKVLDDHQNPRLIKDLLQDLSSTLC
* * * * *      * * * * * * * * * * * * * * * * * * * * * * *

rMAFbx,      174 TLVQRVGVKSVLVGNINMWVYRMETTLHWQQQLNSIQISRPAFKGLTITDLPVCLQLNIMQ
rFbxo25,     181 LLVRGVGVKSVLVGNINIWICRLETVLNWQEKQLNLQMTKQVNTGLTSLDPLHMLNLIY
** * * * * *      * * * * * * * * * * * * * * * * * * * * * *

rMAFbx,      234 RLSGDRDLVSLGQAAPDLHVLSERDLRWKRLCQYHFSEQRKRLIISDKGQLDWKKMYF
rFbxo25,     241 RFSGWDIVTLGQVPTLYMLSEDRRLWKRLCQYHFAEKQFCRHLILSEKGHIEWKLMYF
* * * * *      * * * * * * * * * * * * * * * * * * * * * * *

rMAFbx,      294 KLVRCYPREQYGVTLQLCKHCHILSWKGTDPCTANNPESCSVSLSPQDFINLFKF
rFbxo25,     301 TLQKYPTKEQYGDTLHFCHCSILFWKDSGHPCTAADPDCSFTPVSEHFIDLKFKF
* * * * *      * * * * * * * * * * * * * * * * * * * * * * *
```

**Figure 3.1** Rat sequences of a) ZNF216 vs. AWP1 and b) MAFbx vs. Fbxo25 were aligned using <http://expasy.org/tools/sim-prot.html>. Matching residues are denoted by an asterisk (\*). ZNF216 and AWP1 shared 55.8% sequence identity and MAFbx and Fbxo25 sequences were 59.1% identical.

unaffected by the LPS insult [31]. The database contains primers and probes designed to cross exon-exon boundaries which selectively amplify mRNA sequences and not genomic DNA; mammalian genomic DNA contains non-coding sequence (introns) between exons that is removed upon mRNA processing. Primers cannot bind to both halves of the genomic sequence simultaneously, greatly reducing binding of primers to genomic DNA relative to binding to mRNA. A TRizol based method, which separates RNA, DNA and protein based on solubility after the addition of chloroform, was utilised to extract mRNA from extensor digitorum longus (EDL) muscle of control and LPS-infused animals. Male Sprague-Dawley rats were split into two groups and intravenously infused continuously for 24 hours with either LPS dissolved in saline ( $15 \mu\text{g kg}^{-1} \text{h}^{-1}$ ;  $n=6$ ) or an equal volume of saline ( $0.4 \text{ ml h}^{-1}$ ;  $n=8$ ) *via* inserted catheters. The EDL muscles were then removed from the hindlimbs and freeze-clamped while the animals were under terminal anaesthesia after administration of thiobutabarbital sodium (Section 2.1). Muscles were stored in liquid nitrogen. Procedures were carried out by Julie March and Philip Kemp and were approved by the University of Nottingham Ethical Review Committee and were performed under Home Office Project and Personal license authority. We measured mRNA expression specifically in fast-twitch EDL muscle, because it has previously been noted for its sensitivity to sepsis relative to slow-twitch soleus muscle, *via* observed upregulated energy-dependent protein degradation and ubiquitin mRNA expression [31, 32, 210]. To control for genomic DNA contamination, when mRNA samples were reverse transcribed to cDNA a control sample lacking reverse transcriptase was included, which was tested against all primer/probe sets and no significant contamination was observed. Efficiency of primer and probe sets were tested by producing standard curves of amplification in the presence of pooled cDNA of varying concentrations (the pooled cDNA generated

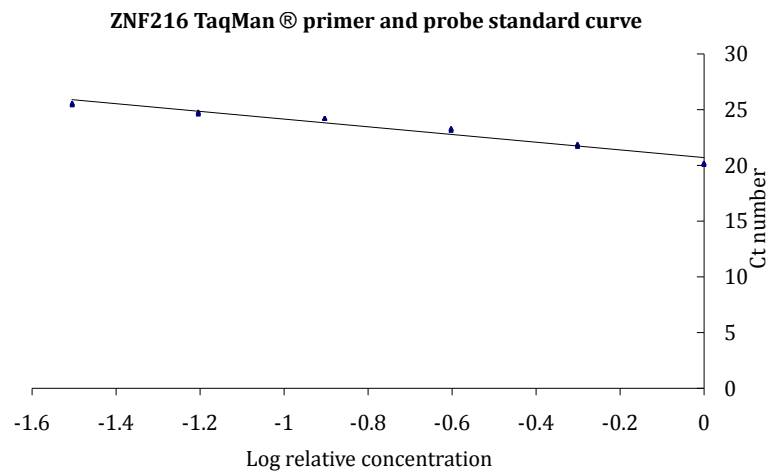
from equal amounts of all of the LPS cDNA samples), such as ZNF216 primer and probe set in Figure 3.2a, and subsequently cDNA samples were diluted to a concentration at which efficiency of amplification was between 90-110%. Housekeeping and target gene amplification efficiencies are approximately equal, allowing the use of the cycle-threshold ( $C_t$ ) method for relative quantification of gene expression [31]. Finally, end point PCR products from each primer/probe set were resolved by agarose gel electrophoresis, and amplicons were found to migrate at the correct predicted molecular weights (Fig 3.2b). The raw data, in the form of amplification curves, produced for all experimental samples and –RT control samples for each primer and probe set are shown in Figure 3.3.

### **3.3. Continuous infusion of LPS for 24h decreases the protein-to-DNA ratio of rat EDL muscle**

Expression of the atrogenes MAFbx and MuRF1 has previously been noted to increase at the mRNA level in EDL muscle in LPS-induced endotoxaemia; Crossland *et al.* 2008 & 2010 similarly used an LPS-infusion rat model (also at  $15 \mu\text{g kg}^{-1} \text{h}^{-1}$ ) and assessed expression levels at 24 hours [32, 208]. Decreased muscle size, resulting from reduced muscle protein synthesis and increased degradation, is also a recognised feature of muscle atrophy. Crossland *et al.* observed a decrease in the protein-to-DNA ratio in EDL using this model, in which protein concentration reduces relative to DNA concentration, as would be expected from shrinking cells. This ratio may be considered as an index of muscle atrophy measuring net protein catabolism [30-32]. Consistent with these previous observations, we also observe a decrease in the protein-to-DNA ratio by 43% ( $p = 0.028$ ) in EDL muscle from animals after 24 hours of LPS infusion, relative to control saline- infused animals (Fig 3.4). The magnitude of this change

**Figure 3.2**

**a)**



**b)**

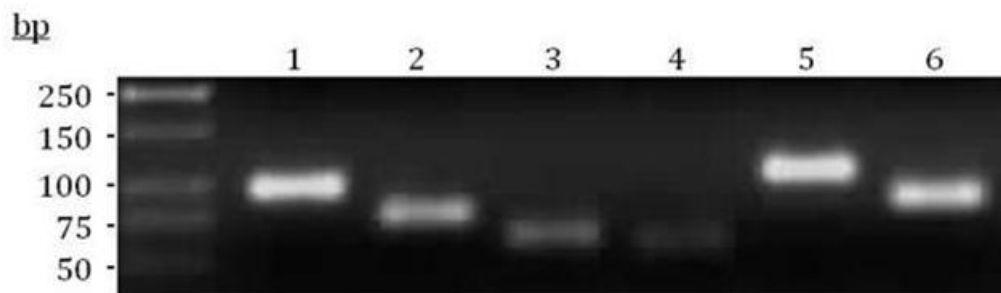
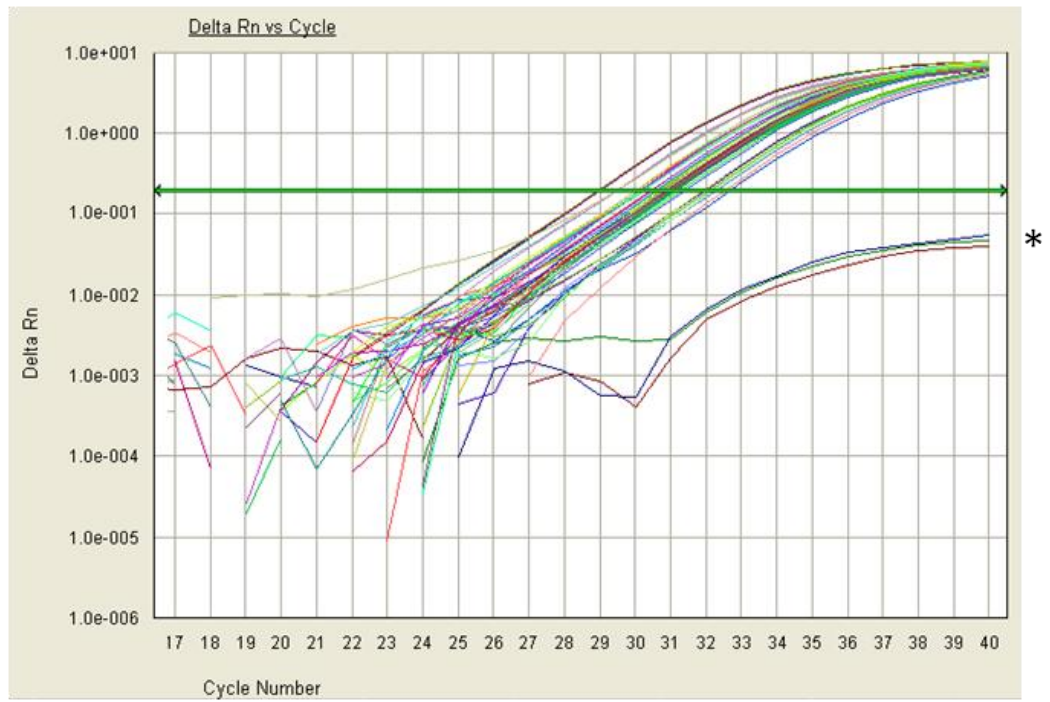


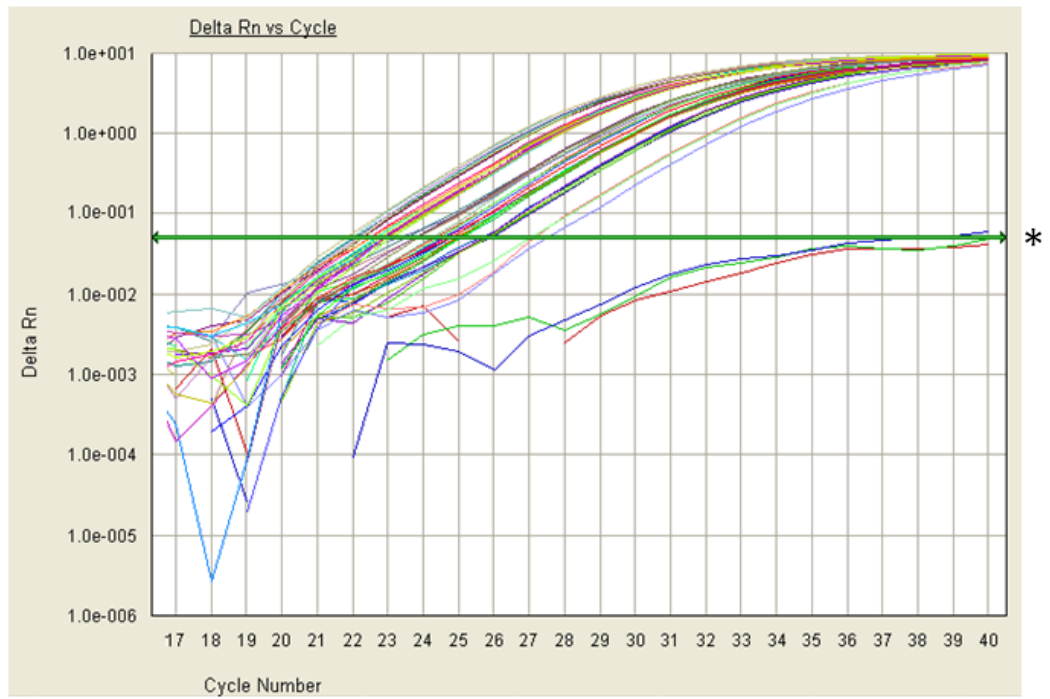
**Figure 3.2** Validating the use of the C<sub>t</sub> method and confirming amplification of amplicons of the correct molecular weight. **a)** The ZNF216 TaqMan primer and probe set was validated by performing RT-PCR with a series of 2-fold dilutions of pooled cDNA, obtained from equal volumes of each LPS cDNA sample, to obtain a standard curve of C<sub>t</sub> number vs. Log relative concentration. C<sub>t</sub> relates to the cycle in the reaction at which the products fluorescence is detected above the background during the exponential phase of amplification. Efficiency is determined via a calculation involving the gradient of the slope: Efficiency = 100 \* (10<sup>-1/slope</sup> - 1), thus in this case the slope = 3.21 and efficiency = 104.9%. Standard curves for all primer and probe sets were found to amplify with approximate equal efficiencies, allowing use of the C<sub>t</sub> method. **b)** RT-PCR amplicons produced using specific primer and probe sets to amplify targeted sequences in pooled cDNA (generated by combination of equal volumes of each LPS cDNA sample) were resolved by agarose gel electrophoresis (4% w/v agarose) to confirm amplicons migrated at the correct predicted molecular weights. Electrophoresis was at 70V for approximately 1 hour and the gel was stained with ethidium bromide. DNA was detected under UV. Lane 1: HMBS (99bp), Lane 2: ZNF216 (76bp), Lane 3: MAFbx (61bp), Lane 4: MuRF1 (56bp), Lane 5: AWP1 (107bp), Lane 6: Fbxo25 (86bp)

**Figure 3.3**

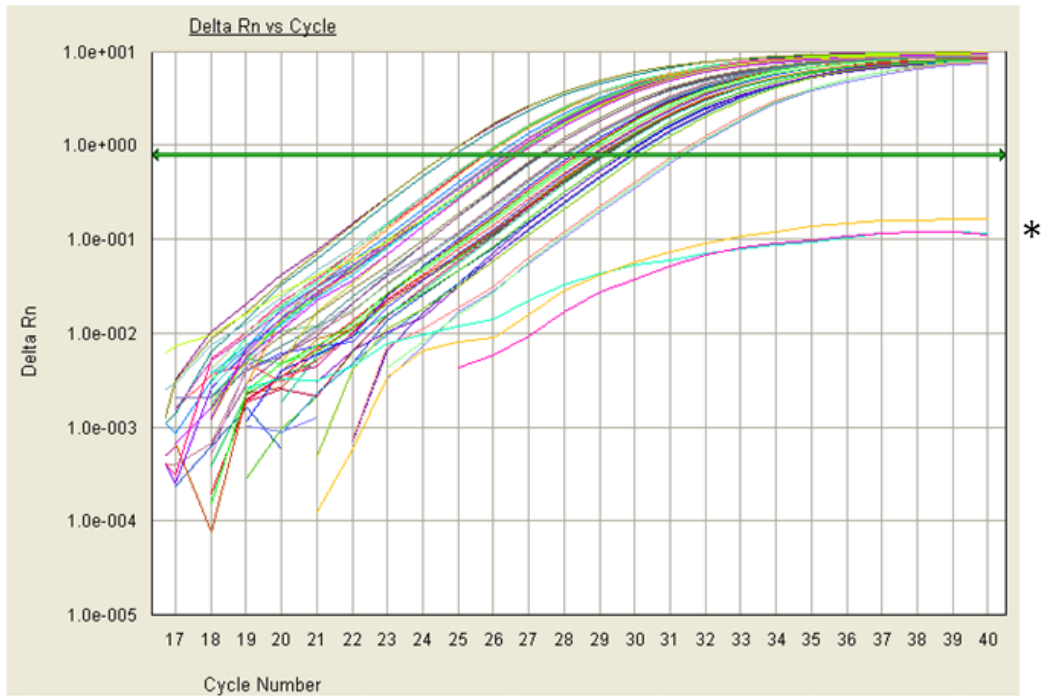
**a)**



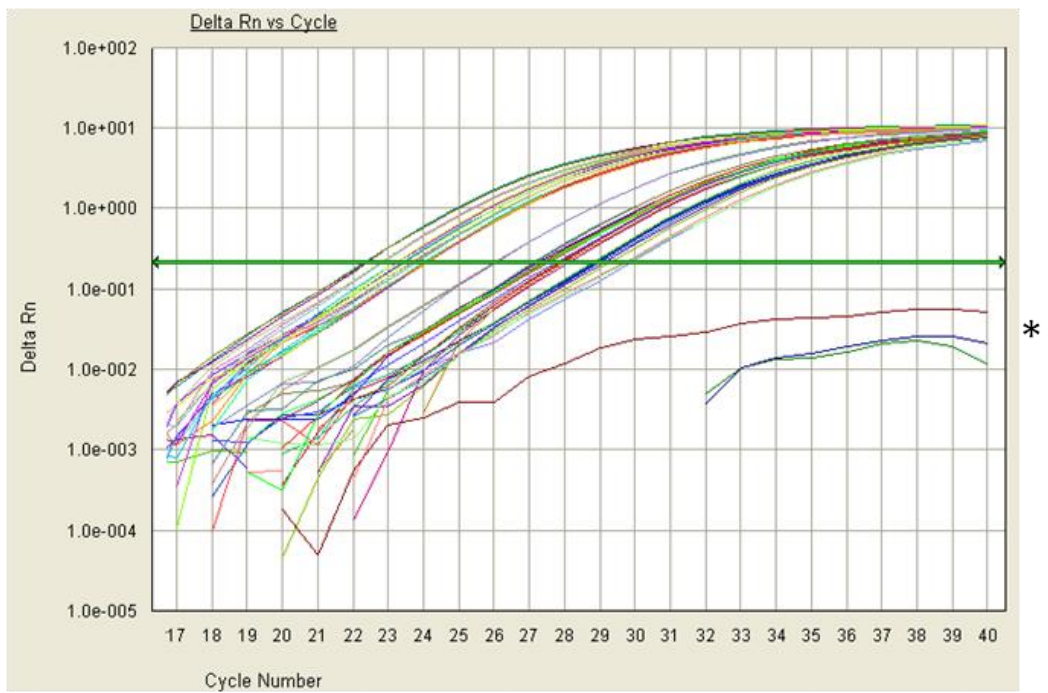
**b)**



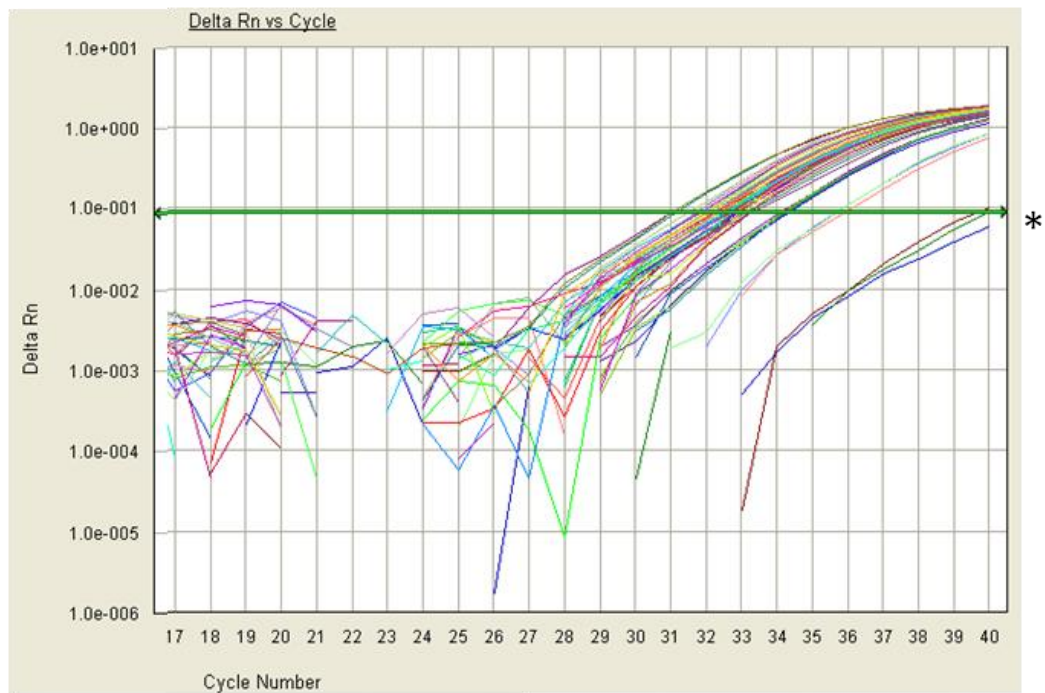
c)



d)



e)



f)

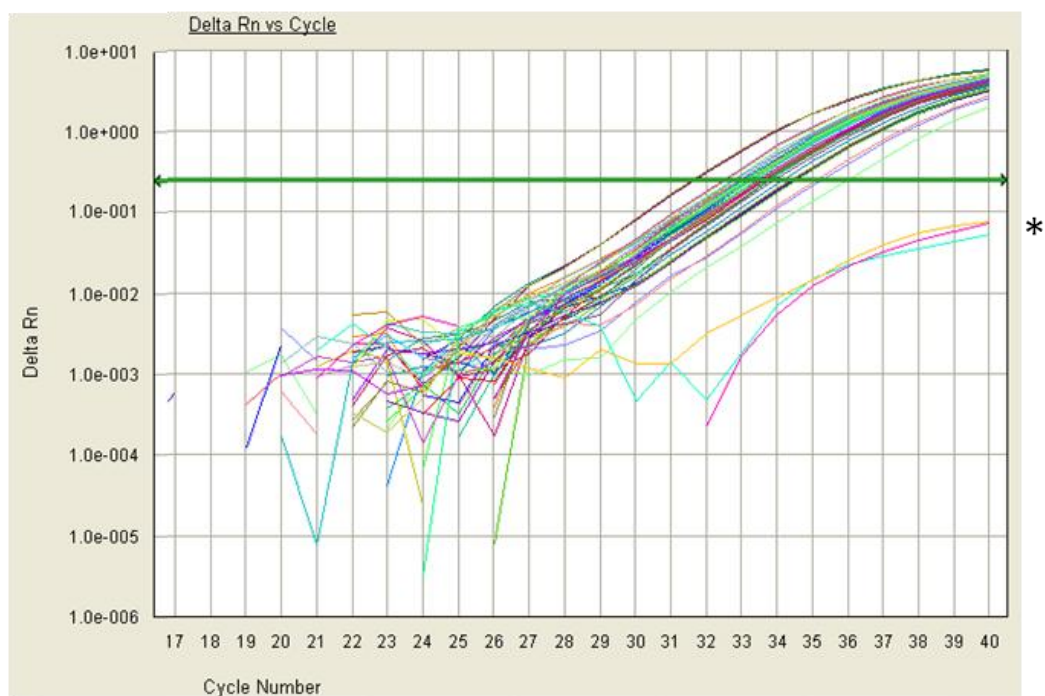


**Figure 3.3** Amplification curves produced by RT-PCR for **a)** HMBS, **b)** ZNF216, **c)** MAFbx, **d)** MuRF1, **e)** AWP1 and **f)** Fbxo25. Delta Rn represents the magnitude of the signal produced *via* fluorescence, corrected for background signal. \* Denotes the -RT control amplification curves, which amplify at a considerably later cycle number, relative to sample amplification curves.

Figure 3.4

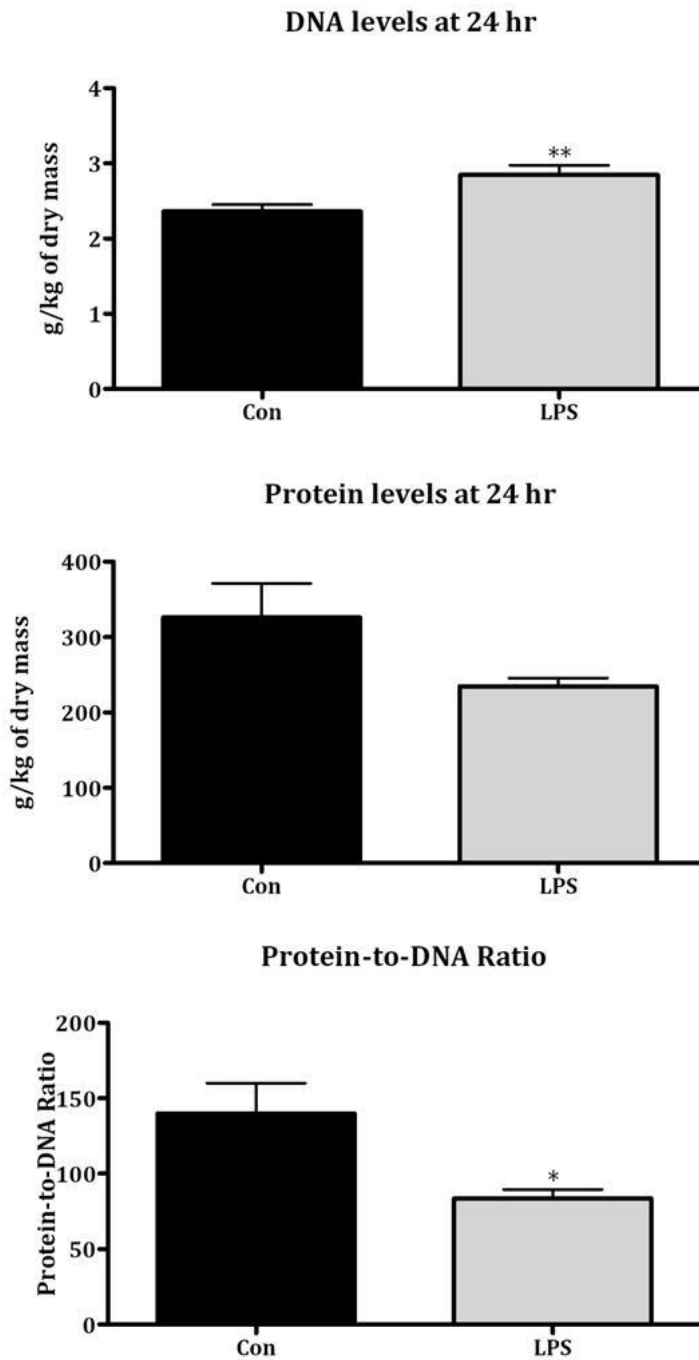


**Figure 3.4** Total alkaline soluble protein and DNA was extracted from approximately 3mg of freeze-dried and powdered Saline- or LPS-infused EDL muscle using perchloric acid (PCA). Protein was isolated using KOH and total content measured *via* a Lowry assay. DNA quantification was performed using a diphenylamine reaction, as detailed in Forsberg *et al.* 1991 [200]. Values represent  $\pm$  SEM. \* Significantly different from control animals  $p \leq 0.05$  (\*\*  $p \leq 0.01$ ). LPS n=6, Con n=8

was very similar to the observations of Crossland *et al.*, who also noted a 40% reduction in this ratio [208]. Notably however, Crossland *et al.* reported no significant change in the DNA concentration but only a decrease in protein concentration. In contrast we found that that DNA concentration significantly increased by 22% ( $p < 0.01$ ) and whilst there was a trend for reduced protein levels in EDL muscle from the LPS animals relative to controls of 31%, the change did not reach statistical significance ( $p = 0.09$ ). Although we observed a similar reduction in protein-to-DNA ratio, we see an increase in DNA as opposed to a decrease in protein, although the reasons for the differences between our observations and those of Crossland *et al.* are unclear.

### **3.4. Continuous infusion of LPS for 24h increases ZNF216 mRNA levels in rat EDL muscle**

We compared relative mRNA expression levels of selected genes in saline-infused and LPS-infused EDL muscle after 24 hours relative to the housekeeper HMBS, which was selected for its fixed levels regardless of the LPS insult [31]. Crossland *et al.* 2008 observed significant increases in MAFbx (5.5-fold,  $P < 0.001$ ) and MuRF1 mRNA expression (21-fold,  $P < 0.001$ ), relative to saline controls, after 24 hours [32]. Using Real Time PCR (RT-PCR) we similarly observed MAFbx and MuRF1 mRNA levels to significantly increase in response to LPS in the EDL, in this study by 3.8-fold ( $p < 0.001$ ) and 10.4-fold ( $p < 0.001$ ), respectively, relative to saline-infused control muscle (Fig 3.5). Fbxo25 has not previously been found to play a role in skeletal muscle atrophy, and showed no increase in expression levels in EDL after 24 hours of LPS-infusion. Interestingly, a small but significant decrease of Fbxo25 expression by 0.8-fold ( $p < 0.05$ ) was noted in LPS-infused EDL relative to control, contrasting that of its structural homologue MAFbx. We

Figure 3.5

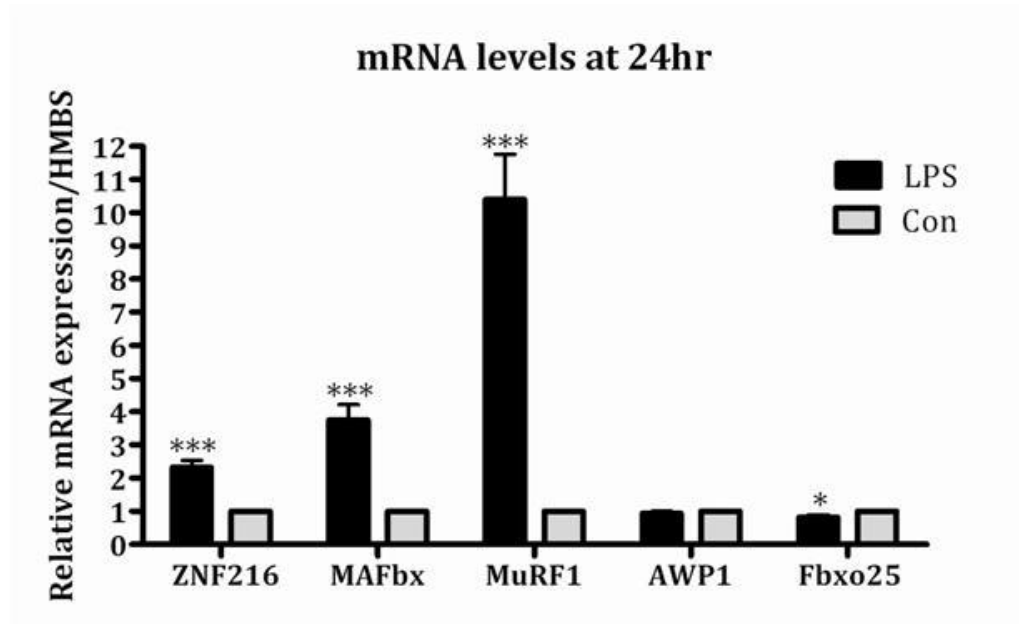


**Figure 3.5** Relative mRNA expression levels of LPS or saline (Con) infusion in rats. Significant fold increase changes are observed in ZNF216, MAFbx and MuRF1 mRNA levels in response to LPS infusion over control, saline-infused animals in EDL muscle after 24 hours. Fold changes are normalised relative to HMBS mRNA expression levels. Values represent  $\pm$  SEM. \* Significantly different from control animals  $p \leq 0.05$  (\*\*  $p \leq 0.01$ ); \*\*\* ( $p \leq 0.001$ )). LPS n=6, Con n=8

observed, for the first time in this model, an increase of ZNF216 mRNA levels in EDL in response to LPS-infusion by 2.3-fold ( $p < 0.001$ ) relative to control muscle. The structural homologue of ZNF216, AWP1, contains Znf\_A20 and Znf\_AN1 domains at its N- and C-termini respectively, but unlike ZNF216 it has not been implicated in muscle atrophy. Supporting this, we saw no significant change in AWP1 mRNA expression levels after 24 hours of LPS-infusion.

### **3.5. Low dose Dex treatment fails to blunt increases in ZNF216 mRNA levels induced by LPS in rat EDL muscle**

Intravenous LPS-infusion induces skeletal muscle atrophy in rats, but simultaneous treatment with a low dose of the corticosteroid Dex ( $12.5 \mu\text{g kg}^{-1} \text{h}^{-1}$ ) during LPS ( $15 \mu\text{g kg}^{-1} \text{h}^{-1}$ ) (LPS+Dex) has previously been observed to prevent the atrophy response in EDL muscle observed using LPS alone, indicated by a lack of change in protein-to-DNA ratio in LPS+Dex [32]. Crossland *et al.* 2010 investigated whether coadministration of the anti-inflammatory agent Dex with LPS prevented muscle atrophy *via* the Akt/Forkhead box, class O (FOXO) pathways [208]. However, despite the diminished atrophy response (i.e. sparing of muscle loss) *via* prevention of reduced protein-to-DNA ratio, decreased Akt phosphorylation and partial prevention of reduction in FOXO1 phosphorylation, Crossland *et al.* observed that Dex+LPS failed to affect the increased MAFbx and MuRF1 mRNA levels that result from LPS infusion relative to saline-treated animals. Infusion of Dex alone was shown to have no effect on MAFbx and MuRF1 relative to saline-infused control muscle. Similarly, we found that Dex alone did not induce increases in ZNF216 expression and measurements of ZNF216 mRNA levels in Dex+LPS animals relative to LPS alone revealed no blunting in expression levels (Fig 3.6). Thus Dex fails to blunt the increase in MAFbx,

Figure 3.6

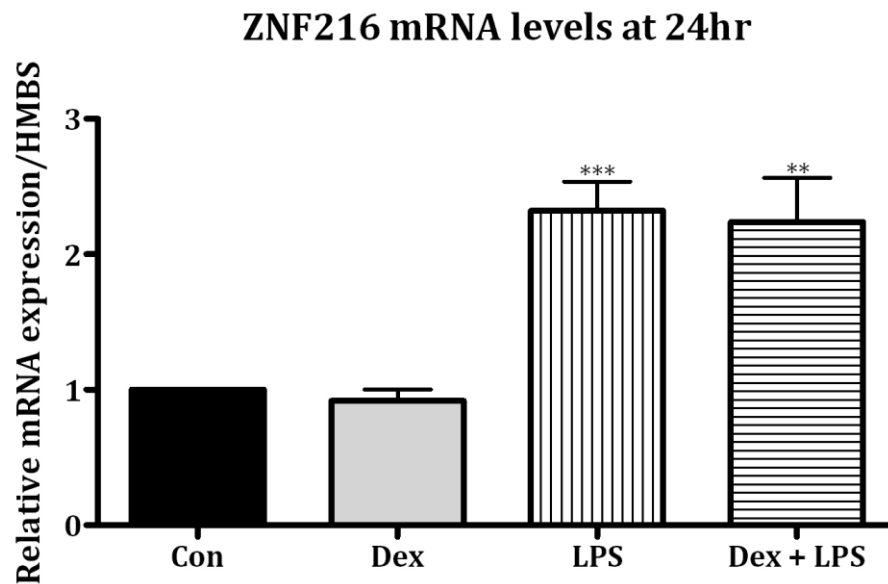


**Figure 3.6** Relative ZNF216 mRNA expression levels in saline (Con), Dex, LPS and Dex+LPS infusion in rats. Significant fold increase changes are observed in ZNF216 in response to LPS infusion over control, saline-infused animals in EDL muscle after 24 hours. Low doses of Dex alone does not induce atrophy and no significant change in ZNF216 expression is observed. A low dose of Dex administered to LPS treated rats (Dex+LPS) blunts the atrophy response, however, no significant change in ZNF216 expression is observed relative to levels in LPS treated rats, thus the pathway by which Dex acts appears to be independent of ZNF216. Fold changes are normalised relative to HMBS mRNA expression levels. Values represent  $\pm$  SEM. \* Significantly different from control animals  $p \leq 0.05$  (\*\*  $p \leq 0.01$ ); \*\*\* ( $p \leq 0.001$ )). LPS n=6, Dex=5, Dex+LPS=7, Con n=7

MuRF1[208] and ZNF216 mRNA levels associated with LPS infusion. This implies that Dex exerts a muscle sparing effect *via* a mechanism excluding affecting mRNA expression of the measured atrogenes (see Crossland *et al.* 2010 for mechanism suggested [208]).

### **3.6. Daily simvastatin treatment for 12 days increases ZNF216 mRNA levels in rat EDL muscle**

Statins are commonly prescribed to reduce cholesterol but patients may suffer unwanted side effects from these drugs including muscle myopathy [211]. Reasons for this response are unclear and so Mallinson *et al.* 2009 previously performed a study to identify the elusive molecular mechanisms responsible for the adverse effects of statins [209]. Their focus was on the transcription factor FOXO1's downstream targets, due to their interest in PI3-Kinase (PI3K)/Akt signalling, which includes FOXO regulation. After 12 days of 88mg kg<sup>-1</sup> day<sup>-1</sup> simvastatin treatment by gavage they noted increased levels and activation (as observed by decreased phosphorylation) of FOXO1 protein in the nuclear fraction of biceps femoris muscle, and increased atrogenes MAFbx and MuRF1 mRNA levels. Additionally, they noted a 29% decrease in protein-to-DNA ratio compared with control ( $p < 0.05$ ) and plasma creatine kinase levels increased 315-fold relative to control ( $p < 0.01$ ). Cellular injury liberates cytoplasmic creatine kinase into surrounding serum, and thus acts as an indicator of muscle damage. Thus 12 days of statin treatment using the dosing regime of Mallinson *et al.* produced a severe myopathic response in rats. Consistent with previous observations, we noted MAFbx and MuRF1 showed elevated levels greater than those in the LPS-infusion model, presenting increases of 16.1-fold ( $p < 0.05$ ) and 30.0-fold ( $p < 0.05$ ), respectively (Fig 3.7) in the same cDNA. Similarly to increases

Figure 3.7

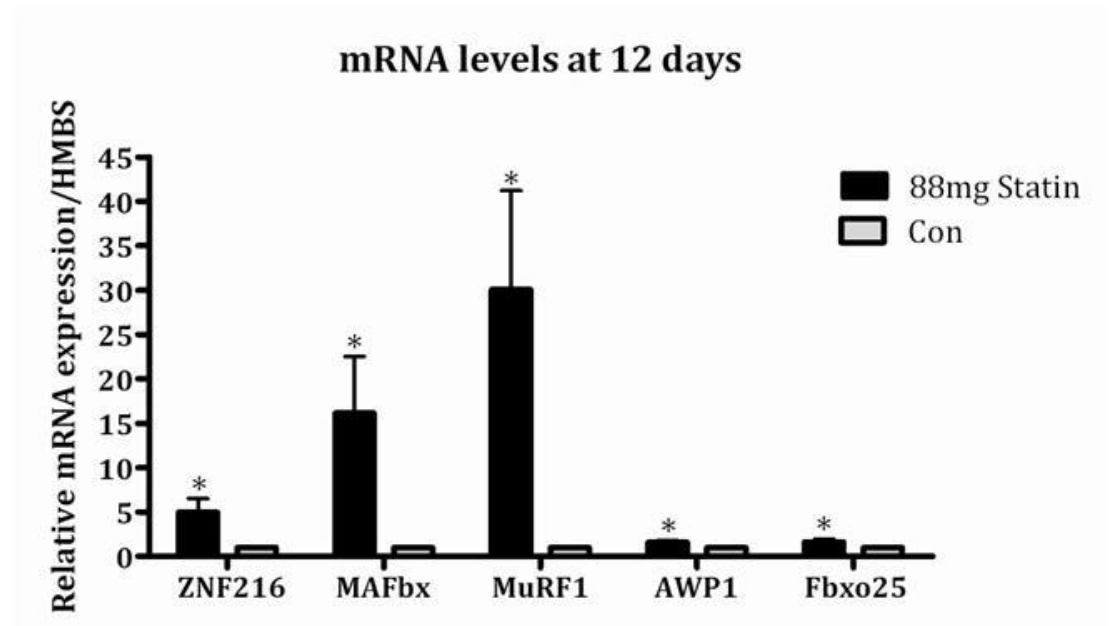


**Figure 3.7** Relative mRNA expression levels of Statin or saline (Con) infusion in rats. Significant fold increase changes are observed in all mRNA expression levels in response to 88mg Statin over control, saline-infused animals in EDL muscle after 12 days. Creatine Kinase levels are vastly increased at this time point indicative of muscle damage. Atrogenes ZNF216, MAFbx and MuRF1 levels are particularly elevated by Statin infusion between 5 and 30 fold, whereas non-atrophy related AWP1 and Fbxo25 show a lesser, yet statistically significant, increase in expression. Fold changes are normalised relative to HMBS mRNA expression levels. Values represent  $\pm$  SEM. \* Significantly different from control animals  $p \leq 0.05$  (\*\* ( $p \leq 0.01$ ); \*\*\* ( $p \leq 0.001$ )). Statin n=4, Con n=6

seen in MAFbx and MuRF1 which exceed those observed in the LPS model, ZNF216 showed an increase of 5.0-fold ( $p < 0.05$ ) in simvastatin treated muscle relative to control after 12 days. It should be noted that AWP1 and Fbxo25 also showed significant, but lower, increases in expression both by 1.6-fold ( $p < 0.05$ ). The severity of this model is likely to explain reasons behind the significant, although slight, increase in AWP1 and Fbxo25. While a number of pathways are likely to be activated under such severe conditions, increases in MAFbx, MuRF1 and ZNF216 implicates that protein degradation pathways are amongst those triggered in this model. Indeed atrogene mRNA are expressed at a significantly higher level than AWP1 and Fbxo25, and strongly mirror the pattern of expression levels measured in our LPS-infusion model.

### **3.7. Discussion**

#### **3.7.1. ZNF216 mRNA expression is upregulated in EDL muscle in an LPS-infusion model of sepsis**

For the first time in this model we have noted upregulated ZNF216 mRNA levels in response to LPS-infusion by 2.3-fold ( $p < 0.001$ ) relative to saline control. This is, to our knowledge, the first quantitative measurement of ZNF216 mRNA levels, *via* real-time PCR. Our observations support previous findings by Northern blotting that ZNF216 expression was noticeably upregulated in a Dex-induced atrophy model in differentiated C2C12 myotubes from the earliest time point of 24 hours up until the latest at 96 hours [56]. Dex treatment was at a high concentration of 100 $\mu$ M to induce atrophy, unlike lower levels of Dex which spares muscle from wasting, as discussed in Section 3.5. Our data additionally

supports increased ZNF216 mRNA levels noted in fasting and denervation models of atrophy in mice, after 2 days and 7 days respectively [56]. Supporting the hypothesis that ZNF216 is upregulated during a specific atrophy programme, rather than *via* non-specific transcription, the structural homologue AWP1 showed no significant change of expression in this model. We also noted increases in MAFbx and MuRF1 that are consistent with previous findings in the same model [32], authenticating the accuracy of our methodology, in which we noted an increase in ZNF216 mRNA expression.

### **3.7.2. ZNF216 mRNA expression is induced to a lesser level than other atrogenes under LPS-induced atrophy and statin-induced myopathy conditions**

We have observed an increase in ZNF216 mRNA expression to a lesser degree than that of MAFbx and MuRF1, but this does not mean that the role of ZNF216 is less important than the other atrogenes during the atrophy response. The importance of ZNF216 during denervation-induced atrophy has previously been demonstrated, as Northern blotting revealed an increase in ZNF216 mRNA levels in wild type animals during denervation induced atrophy, but while upregulation was apparent it appears to increase to a lesser extent than MuRF1 expression, and yet animals lacking ZNF216 demonstrated resistance to denervation-induced wasting [56]. Hishiya *et al.* measured ZNF216 mRNA and protein expression in RAW264.7 cells treated with LPS and number of cytokines and observed a rapid increase in ZNF216 mRNA expression within an hour of LPS treatment, which had declined by the 24 hour time point [198]. Should our rat model mirror expression patterns observed in LPS treated cells, then ZNF216 mRNA expression may have peaked at an earlier time point. Lacking an efficient ZNF216

antibody against rat ZNF216 protein has limited us to measuring mRNA expression, but interestingly Hishiya *et al.* measured both protein levels and mRNA levels in cells after RANKL treatment and observed that mRNA expression declined after 48 hours but protein expression persisted even at 96 hours [198]. At 24 hours in our rat LPS-induced sepsis model we may be measuring mRNA levels after they have already peaked but ZNF216 protein may still be expressed at peak levels. Alternatively, ZNF216's role as a shuttling protein implies it is downstream of the MAFbx and MuRF1, and so upregulated expression may occur at a later time point than 24 hours. However, ethical considerations limit us to the 24 hour time point when using the LPS-infusion model, so future additional observations could only be made at earlier time points. However, expression levels alone are not the only consideration for the importance of a gene in a specific process. Frost *et al.* measured MAFbx and MuRF1 expression in gastrocnemius muscle from rats exposed to polymicrobial sepsis by cecal ligation and puncture (CLP) (n=7/8 per group) [212]. Samples were taken over a time course up to 72 hours, during which MAFbx expression reached its peak around 12 hours after CLP and remained elevated throughout the 72 hour time course. The authors suggest MAFbx to be more important than MuRF1 in contributing to muscle proteolysis in this model due to the maintenance of expression, thus future measurements of ZNF216 over a time course would elucidate how expression changes over time. Should ZNF216 expression be maintained at around a 2.3 fold in LPS-infused rats, this may indicate its importance throughout sepsis. Further measurements of temporal expression levels would also confirm whether ZNF216's mRNA peak has already been reached earlier, or possibly show a continuing increase in expression throughout the time course.

### **3.7.3. Fbxo25 may compete with MAFbx for binding to components of SCF-type E3s in rats**

Fbxo25 is a highly similar structural homologue of MAFbx, but has not been shown to be involved in skeletal muscle atrophy and accordingly we observed no significant increase in mRNA expression in this sepsis model. Indeed, Fbxo25 showed a slight but significant decrease of expression 0.8-fold ( $p < 0.05$ ) in LPS-infused muscle relative to control, contrasting that of structural homologue atroгене MAFbx. Maragno *et al.* noted that Fbxo25 could bind to Skp1, Cul1 and Roc1 and assemble an SCF<sup>Fbxo25</sup> complex with E3 ligase activity [103]. MAFbx also requires the formation of this complex for ligase activity, so Fbxo25 and MAFbx may compete for binding to these components, or Maragno *et al.* suggest they may bind the same substrate considering their homology, and could explain the reduction in Fbxo25 mRNA expression in response to the LPS insult and upregulated MAFbx expression. However, observations in mice show that tissue specific expression of Fbxo25 and MAFbx differ, as Fbxo25 mRNA and protein is more strongly expressed in tissues such as brain, kidney and intestine and while Fbxo25 mRNA has been found at a lower level in muscle and brain compared to other tissues, protein is undetectable in muscle tissue in mice [103, 213]. Conversely, MAFbx mRNA expression has been observed mostly in muscle and to a lesser extent the heart in mice [97]. Thus evidence from mice tissues suggests MAFbx and Fbxo25 may not compete should they be expressed differentially, although there is no information specifically on Fbxo25 expression in rats which may express Fbxo25 and MAFbx simultaneously in muscle, as we have detected Fbxo25 mRNA in rat EDL muscle. Since Fbxo25's substrate specificity and function has yet to be confirmed, and considering that mice exhibit differential tissue expression for Fbxo25 and MAFbx, there may be other reasons for its

downregulation during sepsis-induced atrophy in rats than reducing competition for SCF complex components or substrates.

#### **3.7.4. ZNF216 may be activated by the same pathways as atrogenes MAFbx and MuRF1**

A recent study measured the effects on downstream targets of FOXO (including MAFbx and MuRF1) when the LPS-induced atrophy response in rats was impaired by co-administration of low-dose Dex with LPS [208]. In the present study, ZNF216 mirrors MAFbx and MuRF1 expression changes, inasmuch as Dex did not blunt increased ZNF216 expression induced by LPS-infusion, and nor did it blunt expression of other atrogenes. Interestingly, Crossland *et al.* noted lower levels of dephosphorylated (and thus active) FOXO1, which lead them to conclude that an alternative Akt-FOXO mechanism may be responsible for observed MAFbx and MuRF1 levels, and they suggested MAFbx upregulation may be in response to FOXO4, concordant with other findings [214]. Constitutively active FOXO4 has also been shown to upregulate ZNF216 mRNA expression [56] and together this suggests that ZNF216 may be upregulated by a similar pathway to MAFbx.

#### **3.7.5. Statin-induced myopathy induces ZNF216 expression**

A recent study used a rat model of statin-induced myopathy to better characterise the elusive molecular mechanisms behind myopathic changes observed in some patients taking statins [209]. Observations included measurements of mRNA expression of genes associated with proteasomal-mediated proteolysis, to better understand the effect of statins on PI3k/Akt

signalling, a pathway involved in FOXO regulation. As the authors hypothesised, after 12 days of 88mg kg<sup>-1</sup> day<sup>-1</sup> simvastatin they noted increased FOXO1 in the nuclear fraction of biceps femoris muscle and decreased phosphorylation (and thus increased activation) and increased MAFbx and MuRF1. We confirmed MAFbx and MuRF1 mRNA having elevated expression levels greater than those in the LPS-infusion model (and concordant with levels recorded previously), and similarly ZNF216 showed a greater degree of upregulation compared to the sepsis model. It should be noted that AWP1 and Fbxo25 also showed significant, but lower, increases in expression. Considering the muscle damage, as indicated by elevated creatine kinase measurements and exhibition of minimal-mild necrosis, increased expression of AWP1 and Fbxo25 may result from some loss of transcriptional control. Increased expression of ZNF216 is consistent with it playing a role coupled with that of E3 ubiquitin ligases in situations where muscle undergoes proteolysis. Interestingly, we noted a positive correlation between creatine kinase levels and atrogene expression; where creatine kinase levels were high and muscle damage was thus more severe, we observed increased ZNF216, MAFbx and MuRF1 expression in individual animals within the simvastatin-treated group (not shown). In addition to high levels of muscle damage, 12 days of 88mg kg<sup>-1</sup> day<sup>-1</sup> simvastatin treatment increased the risk of mortality, as only four of six rats survived. Less samples were available for analysis as a direct result of the models severity, thereby reducing statistical power and revealing the limitations of this model.

### **3.7.6. Protein-to-DNA ratio may not be a sensitive indicator of skeletal muscle atrophy**

Reduced muscle size is an indicator of muscle atrophy, but reduced protein-to-DNA ratio has since been shown to be an additional index of wasting and has been measured in all of the models discussed in this Section. We noted an increase in DNA levels, that differs from observations by Crossland *et al.* 2008, and may be a result of increased muscle satellite cell activation in this LPS-infusion model. While reduced protein-to-DNA ratio has been observed in the LPS model, this has been recorded as a reduction between 29%-40% in the same model [32, 208] and only a 29% reduction in protein-to-DNA ratio was noted in the statin-induced myopathy model, despite evidence of muscle damage, *via* increased creatine kinase levels [209]. However, atrogene levels are notably elevated in the more severe statin-induced myopathy model relative to the sepsis-infused model, each more than doubling in the statin model relative to the sepsis model. It seems that atrogene expression may act as a more sensitive index of skeletal muscle atrophy, as loss of protein-to-DNA ratio appears to have an upper limit. Preliminary data mentioned above in 3.7.5. corresponds with this notion, as muscle damage, measured by creatine kinase levels, and atrogene expression appear to positively correlate. However, it should be noted that in some situations atrogenes are expressed without any muscle damage, as noted earlier during co-administration of LPS+Dex [208]. Further to this, MAFbx and MuRF1 expression was upregulated during both PPARdelta agonist administration [215] and acute alcohol intoxication in rats [216], but did not induce UPS-mediated proteolysis.

Atro gene expression studies are important for elucidating the proteins that are involved in various modes of skeletal muscle atrophy. However, information on atro gene function is also critical for understanding the pathways involved in skeletal muscle atrophy.

## **CHAPTER 4**

### **Functional characterisation of the ZNF216 protein**

#### 4.1. Introduction

In Chapter 3 we observed that zinc finger protein 216 (ZNF216) mRNA expression levels increased in rat extensor digitorum longus (EDL) tissue in the lipopolysaccharide (LPS)-infused model of skeletal muscle atrophy as well as in the statin-induced myopathy model. This mirrored increases in muscle atrophy F-box protein (MAFbx) and muscle RING-finger 1 (MuRF1) mRNA expression, suggesting that ZNF216 may be involved in the atrophy programme. However, these findings provide limited insights into ZNF216's precise role(s) at the molecular level. In order to understand the biological significance of increases in ZNF216 expression, we sought to identify proteins that interact with ZNF216 to reveal its possible substrates. Previous work has demonstrated that ZNF216 is able to bind to polyubiquitin, presumably mediating delivery of polyubiquitinated substrates to the 26S proteasome [56]. However, the specific polyubiquitinated substrates of ZNF216 have yet to be determined.

In order to attempt the direct identification of ubiquitinated proteins that bind to ZNF216, we expressed recombinant GST-tagged rat ZNF216 (rZNF216) protein and used this to 'capture' interacting proteins from rat skeletal muscle *via* affinity chromatography. The cDNA sequence encoding the 213 amino residue rZNF216 was previously cloned in the lab into the bacterial expression plasmid pGEX-4T-1, and was provided at the outset of this study; this plasmid was transformed into XL10 gold *E. coli*. The rZNF216 sequence was verified by DNA sequencing and confirmed to encode the full length (FL) rZNF216 protein as shown in Figure 4.1. Residues 11-35 of rZNF216 encode the zinc finger A20 domain (Znf\_A20) which has been previously shown to bind to polyubiquitin [56]; in contrast, ZNF216's AN1 zinc finger domain (Znf\_AN1), between residues 154-194, binds to TNF-

**Figure 4.1**

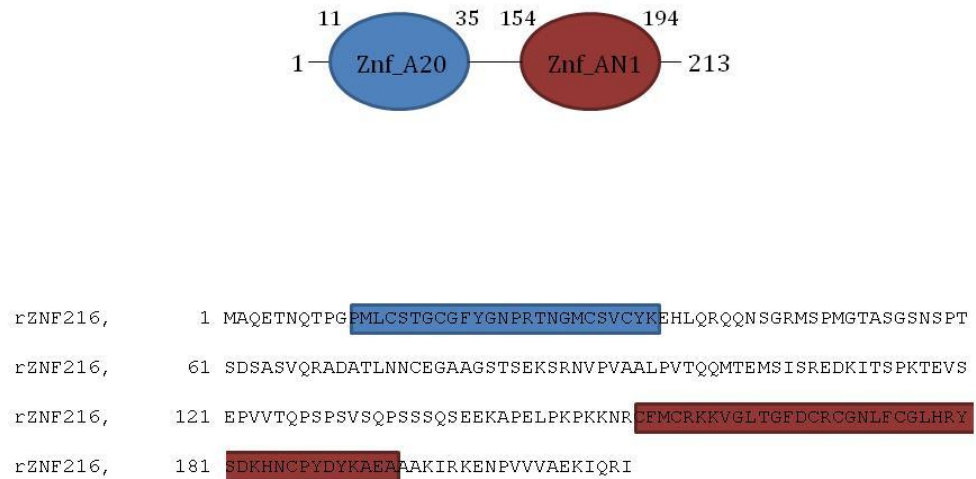


**Figure 4.1** Schematic representation and peptide sequence of 213 residue wild-type rat ZNF216. The N-terminal Znf\_A20 domain is encoded by amino acids 11-35 while residues 154-194 contain the C-terminal Znf\_AN1 domain, highlighted in blue and red, respectively.

receptor associated factor 6 (TRAF6) but its precise function remains unknown [196]. Characteristic of many zinc fingers, both the Znf\_A20 and the Znf\_AN1 domains contain 4 cysteine residues that chelate a single zinc atom to form the distinctive zinc finger structure. Previous studies showed that mutation of two cysteines to alanine in the Znf\_A20 domain is sufficient to disrupt zinc binding and abolish formation of the zinc finger structure, impairing polyubiquitin binding [56]. Therefore, as a negative control for ubiquitin-binding, the rZNF216 plasmid was mutated using site-directed mutagenesis to convert cysteines 30 and 33 to alanines (C30/33A mutant).

#### **4.2. Recombinant GST-rZNF216 protein binds to ubiquitin-Sepharose**

In order to test the functionality of recombinant GST-rZNF216 protein with respect to ubiquitin-binding, commercially available purified bovine ubiquitin was covalently immobilised (at 10mg/ml) on cyanogen bromide activated Sepharose-4B (CNBr Seph 4B) beads (ubiquitin-Sepharose); control Sepharose was produced in parallel using the same coupling process but omitting ubiquitin. GST, GST-rZNF216 (wild type) or GST-rZNF216 (C30/33A) proteins were expressed in 10ml overnight *E. coli* cultures from plasmids encoding GST/GST-tagged proteins. Bacterial pellets were lysed by sonication in TBS-Triton prior to centrifugation (10 min, 16000 rcf, 4°C), after which the pelleted insoluble material was discarded and GST/GST-tagged proteins in the supernatant were incubated with an excess (50µl) of ubiquitin-Sepharose (10mg/ml), glutathione-Sepharose (commercially available) or control-Sepharose beads at 4°C for 30 minutes. Unbound proteins were removed by extensive washing and bound proteins were eluted with gel application buffer. Proteins were either visualised *via* SDS PAGE and Coomassie staining, or Western blotting using an anti-GST

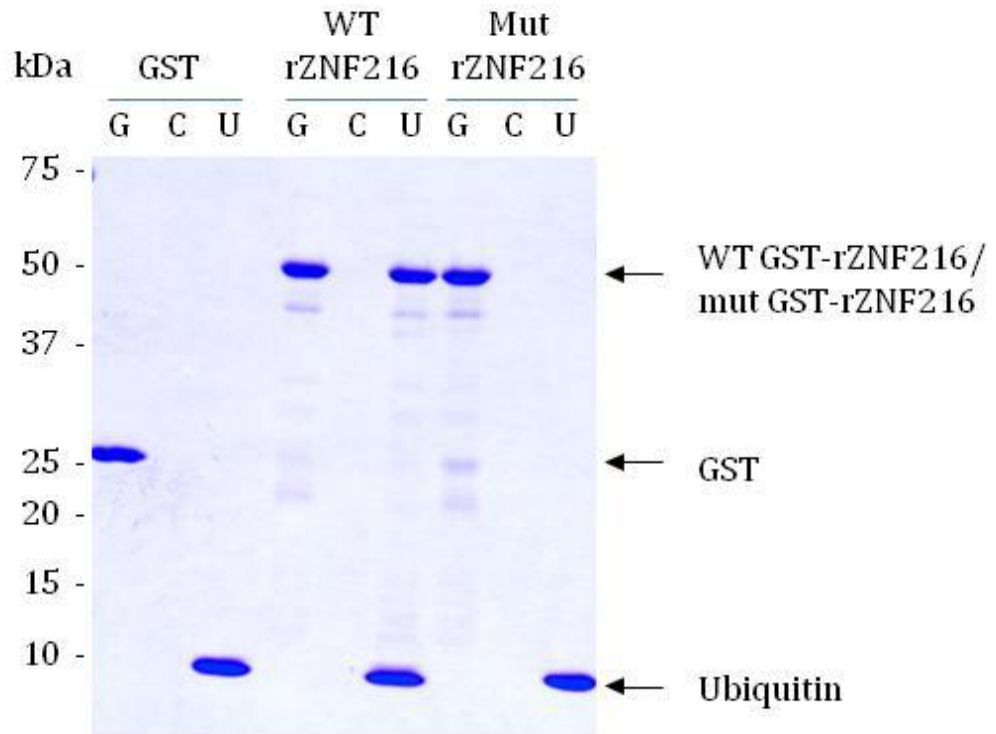
antibody; approximately 10 $\mu$ g and 1 $\mu$ g bound protein were loaded per lane for Coomassie staining (Fig 4.2ai) or Western blotting (Fig 4.2aii), respectively. All of the GST-tagged proteins tested bound glutathione-Sepharose consistent with the presence of the GST tag (schematic diagram in Fig 4.2b), however whilst wild type GST-rZNF216 bound to ubiquitin-Sepharose as predicted, the C30/33A mutant was unable to bind ubiquitin. Protein binding to the control-Sepharose was not seen; thus our recombinant GST-tagged wild type rZNF216 retains its specific monoubiquitin-binding function.

### **4.3. Recombinant GST-rZNF216 protein binds to K48- and K63-linked polyubiquitin chains**

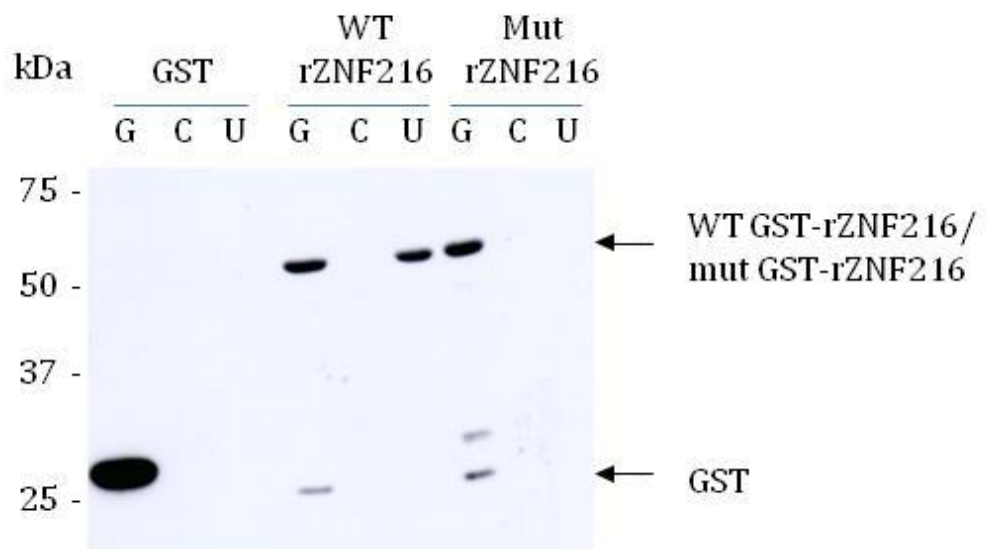
Our analyses in Section 4.2 confirm that recombinant wild type GST-rZNF216 can bind to immobilised monoubiquitin. As one of ZNF216's proposed functions is to shuttle polyubiquitinated substrates to the 26S proteasome [56], we next assessed rZNF216's ability to bind ubiquitin polymers, which more closely resembles its proposed physiological substrates. GST, GST-rZNF216 or GST-rZNF216(C30/33A) proteins were purified from 10ml cultures of *E. coli* by immobilising on glutathione-Sepharose and incubated with 1 $\mu$ g commercial Lysine 48 (K48)-linked or K63-linked unanchored polyubiquitin chain mixtures. Bound polyubiquitin chains were eluted with gel application buffer, resolved by SDS PAGE, transferred overnight to nitrocellulose membrane and probed with anti-ubiquitin (Fig 4.3). Ponceau S staining confirmed approximately equal expression of the GST fusions. Wild type GST-rZNF216 alone bound both K48- and K63-linked polyubiquitin chains whereas the C30/33A mutant did not, further demonstrating rZNF216's ability to bind ubiquitin *via* its Znf\_A20 domain and confirming that the recombinant protein was functional. Figure 4.3 clearly

Figure 4.2

a i)

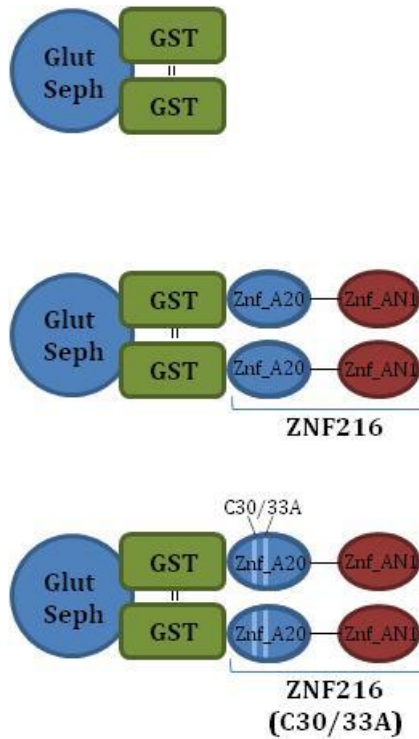


ii)



**Figure 4.2**

**b)**



**c)**

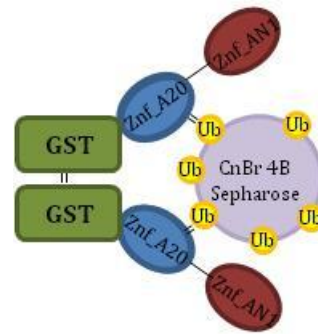
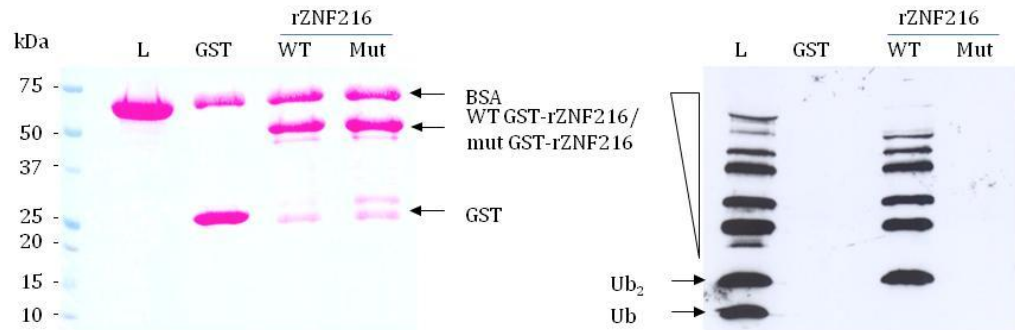


**Figure 4.2** Recombinant GST-tagged rZNF216, but not C30/C33A mutant, binds to ubiquitin-Sepharose. **a)** IPTG-induced 10ml overnight *E. coli* cultures produced recombinant proteins GST, GST-rZNF216 (WT rZNF216) or GST-rZNF216 (C30/33A) (Mut rZNF216), were extracted in TBS-Triton (TBS-T) and incubated with 50µl of glutathione- (G), control- (C) or ubiquitin- (U) Sepharose beads at 4°C for 30 min (in TBS-T). Subsequently, Sepharose was washed twice with TBS-T and bound proteins eluted in gel application buffer. 50 % of proteins that bound to glutathione-, control- or ubiquitin-Sepharose beads were detected by i) Coomassie staining and 50% by ii) immunoblotting using anti-GST. **b) & c)** Models of glutathione-Sepharose and ubiquitin-Sepharose-bound proteins, respectively (no protein bound to control-Sepharose). Note that GST forms a strong dimer.

**Figure 4.3**

**a)**



**b)**

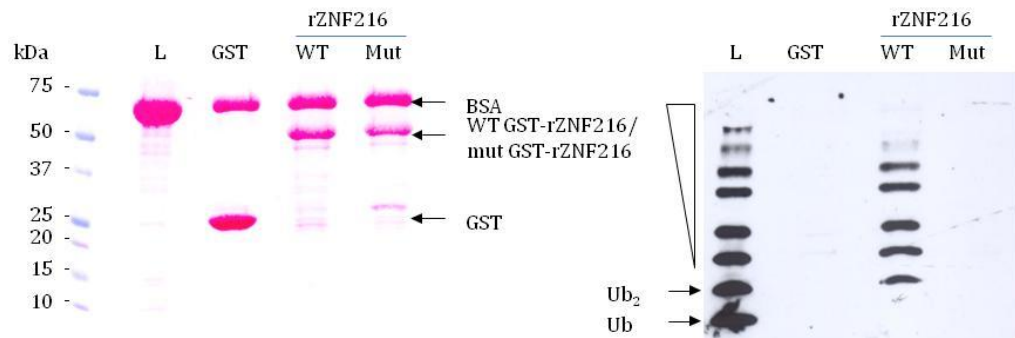


**Figure 4.3** Immobilised GST-rZNF216 binds to K48- and K63-linked polyubiquitin chains. GST, GST-rZNF216 (WT rZNF216) or GST-rZNF216 (C30/33A) (Mut rZNF216) proteins were extracted from 10ml *E. coli* cultures that were grown overnight and induced with IPTG to overexpress GST-tagged proteins. GST-tagged proteins were captured on 50 $\mu$ l of glutathione-Sepharose (in TBS-T) for 30 min at 4 $^{\circ}$ C and washed twice in TBS-T. Subsequently, 0.25 $\mu$ g of **a)** K48- or **b)** K63-linked polyubiquitin chains were then incubated with glutathione-captured GST-tagged proteins in 50mM Tris, 0.1% BSA (pH 7.5) (TBSA) for a further 30 minutes at 4 $^{\circ}$ C. Beads were washed twice in TBSA and bound proteins eluted with gel application buffer. Load (L) represents 100% of the polyubiquitin load. Western blots were Ponceau stained to ensure equal loading (left panel) and subsequently immunoblotted with anti-ubiquitin (right panel).

demonstrates that whilst diubiquitin and longer polyubiquitin chains readily bind wild type rZNF216, monoubiquitin does not in this assay.

These observations, and those in Section 4.2, are consistent with the findings of Hishiya *et al.* [56] who showed that FLAG-tagged ZNF216 and HA-tagged ubiquitin interacted *via* co-immunoprecipitation experiments in HEK293 cells, confirming their initial observations that ZNF216 and polyubiquitin C clones interacted *via* yeast two-hybrid experiments. Additionally, the authors identified that polyubiquitin binding was dependent on the Znf\_A20 domain, as the N-terminal mutant which lacked the Znf\_A20 domain and the Znf\_A20 C30/33A mutant (noted earlier in Section 4.1) lacked polyubiquitin binding ability. Whilst rZNF216 can bind to single ubiquitin moieties, the interaction is weak ( $K_d = 8 \mu\text{M}$  at 298K [217]) relative to avidity effects afforded by multiple ubiquitin-binding domain (UBD)-ubiquitin interactions. Indeed, our own work (Fig 4.2a) demonstrates that wild type rZNF216 can indeed bind to immobilised monoubiquitin, but this probably occurs *via* avidity effects. GST is known to form strong dimers [218] and it is likely that GST-tagged rZNF216 will dimerise *via* the GST-tag in solution, allowing two rZNF216 proteins to bind simultaneously to two single ubiquitins brought into close proximity when immobilised at high protein concentration (Fig 4.2c). In experiments when GST-rZNF216 is immobilised on beads (as in Figure 4.3), the high concentration of rZNF216 protein presumably places multiple UBDS in close proximity, allowing simultaneous interactions with multiple ubiquitins within the same polyubiquitin chain. Notably Huang *et al.* 2004 suggested that ZNF216 forms homodimers [196] pointing to a possible mechanism by which it may attain higher affinity polyubiquitin-binding *in vivo*.

#### **4.4. Recombinant GST-rZNF216 protein does not exhibit deubiquitinating activity**

As noted earlier Hishiya *et al.* proposed that ZNF216 may act as a shuttle protein transporting ubiquitinated proteins to the 26S proteasome for their degradation. This suggestion was based on its ability to bind polyubiquitin chains, and its co-precipitation with the 26S proteasome [56]. However, the complete physiological significance of the ZNF216 protein has not yet been fully determined. ZNF216's N-terminal zinc finger Znf\_A20 domain was accordingly named because of similarity to the A20 protein, which contains seven zinc fingers at its C-terminus. A20 has both deubiquitinating activity and E3 ligase activity, but despite ZNF216's similarity to the A20 protein, Hishiya *et al.* 2006 [56] detect no deubiquitinating or E3 ligase activity. Our interest in ZNF216, as further detailed in Section 4.5, developed into exploiting its ubiquitin-binding ability for purifying ubiquitinated proteins. To confirm that ZNF216 does not have deubiquitinating activity, which would impede purification of ubiquitinated proteins, we performed a deubiquitinating assay with our recombinant rZNF216 proteins. In this case GST-rZNF216 and GST-rZNF216 (C30/33A) were first purified using glutathione-Sepharose affinity chromatography and thrombin cleaved (within a thrombin site at the C-terminus of the GST-tag), eluting FL wild type or C30/33A mutant rZNF216 with 2 additional N-terminal residues (GS; see Fig 4.4). This is because subsequent affinity purifications (in this Chapter) involve thrombin-cleaved GST-ZNF216. The double cysteine mutation only substitutes two amino acids, and does not change the overall length of the protein, thus only fractionally changing the size by the mass difference between two cysteines/alanines. Resolving the wild type and mutant GST-tagged recombinant rZNF216 proteins by SDS PAGE revealed no difference in denatured molecular weight, however notably upon thrombin cleavage and removal of the GST-tag,

**Figure 4.4**

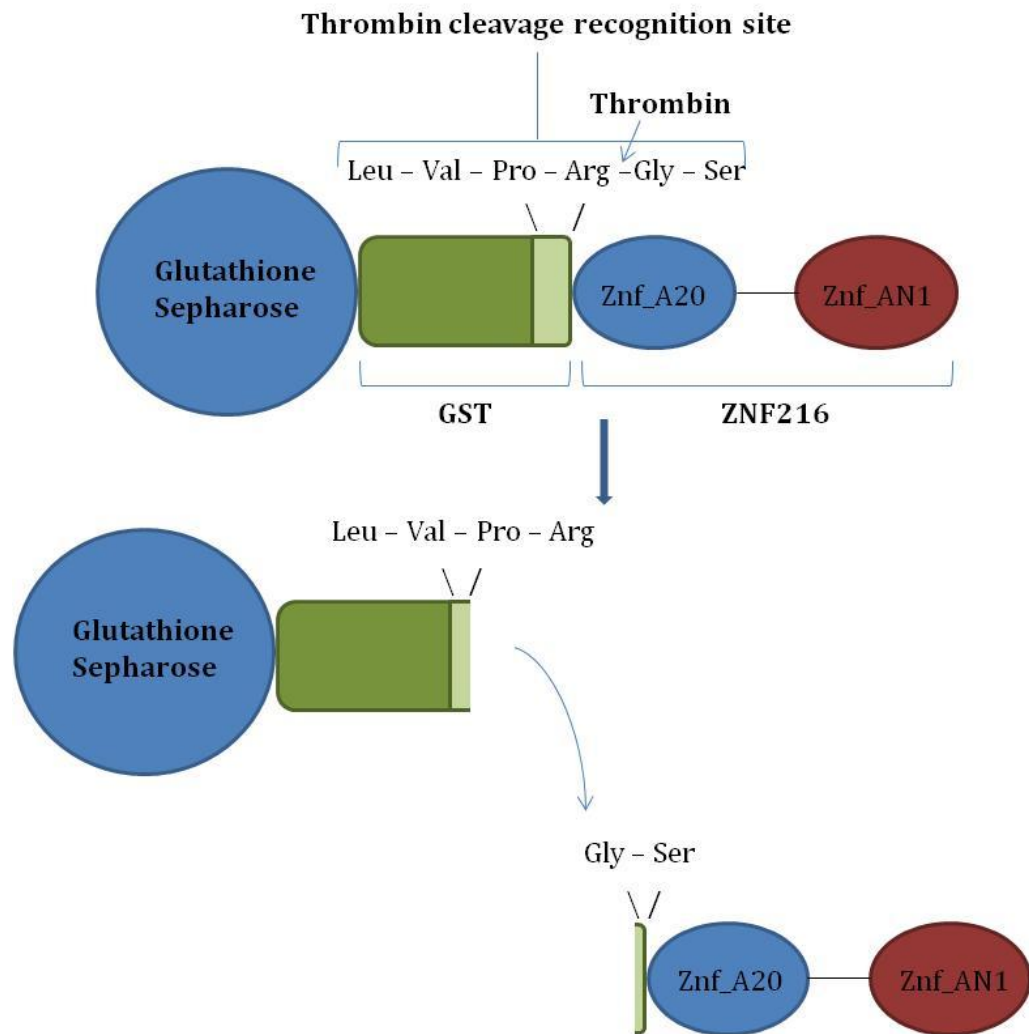


**Figure 4.4** Thrombin cleavage of GST-rZNF216. Recombinant rZNF216 protein was expressed to have a GST-tag at its N-terminus, immediately prior to rZNF216's start codon. GST-rZNF216 was captured on glutathione-Sepharose *via* its GST-tag, the C-terminus of which contains a sequence of 6 amino acids (Leu-Val-Pro-Arg-Gly-Ser) that is absent within the wild-type rZNF216 sequence. The sequence is recognised by thrombin, which cleaves this site within GST to liberate the recombinant rZNF216 protein that consequently gains an additional 2 residues from the GST-tag after cleavage. The residual GST-tag remains bound to glutathione-Sepharose.

wild type and mutant rZNF216 proteins migrated differently with the mutant appearing smaller by approximately 4-5kDa (Fig 4.5). This apparent difference in size after cleavage was confirmed not to be truncation of the mutant protein by thrombin, as no thrombin cleavage site was introduced by the double mutation, and antibodies recognising epitopes at the N- and C-terminus (not efficient for recognising endogenous rat ZNF216 in Chapter 3, but proficient for recognising recombinant ZNF216) still recognised mutant rZNF216 (not shown). In addition, peptide mass fingerprinting (PMF) could not discern any differences in primary sequence (with the exception of the engineered C/A mutations; not shown) between the wild type and mutant proteins. Interestingly, rZNF216's calculated denatured molecular weight is approximately 25kDa, but wild type recombinant rZNF216 migrates at greater than 30kDa when resolved by SDS PAGE. Hence the double cysteine mutant is in fact closer to the predicted molecular weight of the protein. We speculate that, when liberated from GST fusion, the wild type Znf\_A20 domain may fail to fully denature during SDS PAGE despite the presence of denaturing agents in the gel application buffer, and the additional positive charge resulting from zinc ion binding may impede protein migration on the gel. This effect may be negligible within the larger GST-tagged protein, potentially explaining why no differences in migration are observed for tagged versions.

K63-linked polyubiquitin is generally associated with non-degradative signalling events including DNA repair [170], nuclear factor kappa-light-chain-enhancer of activated B cells (NF- $\kappa$ B) signalling [160] and innate immunity [181], whilst K48-linked polyubiquitin can be recognised by the 26S proteasome and targets proteins for degradation [219]. Based on ZNF216's reported association with the 26S proteasome, we selected K48-linked polyubiquitin as a substrate for the

**Figure 4.5**

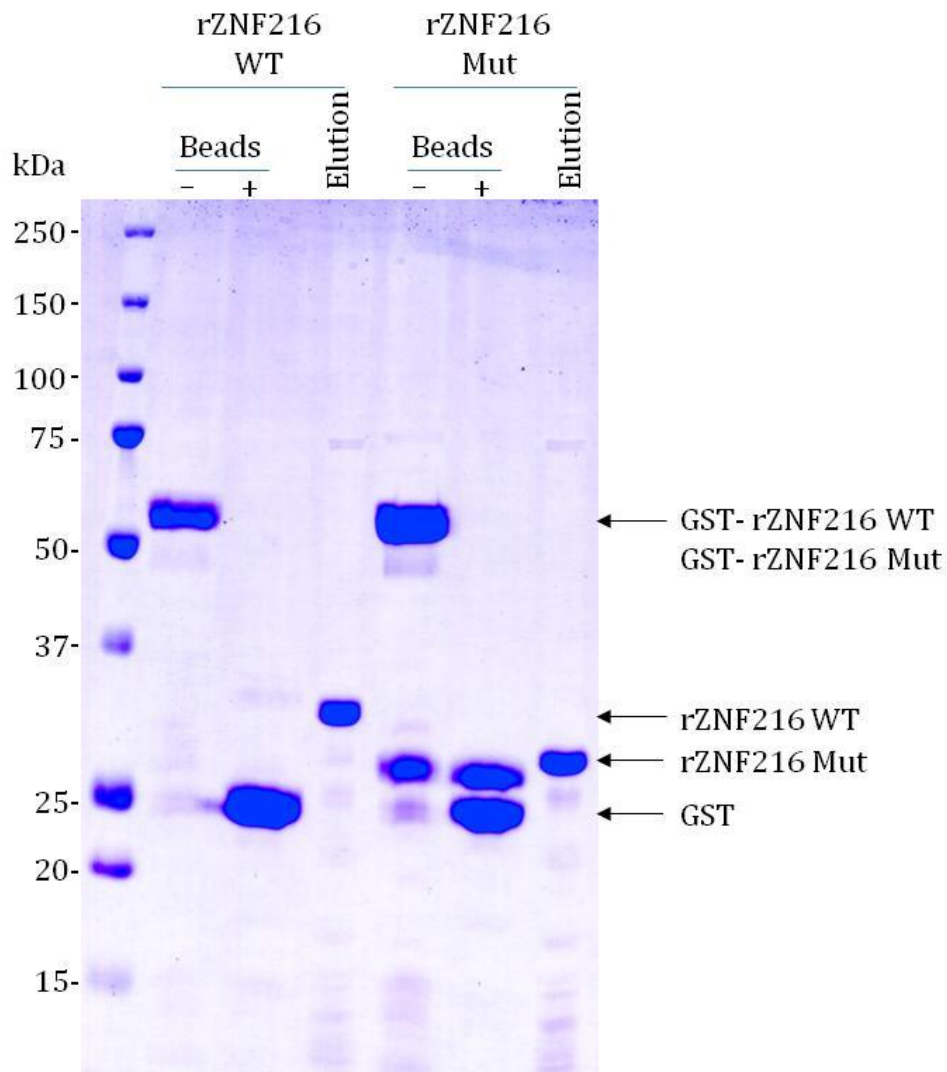


**Figure 4.5** Thrombin cleavage of GST-rZNF216 and GST-rZNF216 (C30/33A). GST-tagged proteins expressed from 5l of IPTG-induced *E. coli* were purified in TBS-T on glutathione-Sepharose beads, after incubation for 1 hr at 4°C and subsequent washing. A small sample of glutathione-beads were retained to ensure GST-tagged protein binding (Beads -). The remaining GST-rZNF216 (GST-rZNF216 WT)/GST-rZNF216 (C30/33A) (GST-rZNF216 Mut) bound to glutathione-Sepharose was then incubated with 10 units thrombin in thrombin cleavage buffer (20mM Tris, 150mM Sodium Chloride, 2.5mM Calcium Chloride Dihydrate, pH 8.4) overnight at 4°C. The GST-tag remained on beads after thrombin cleavage (Beads +), and recombinant rZNF216 WT/rZNF216 Mut was eluted into solution (Elution), and proteins were detected by Coomassie staining.

deubiquitinating assay. Cleaved rZNF216 proteins were covalently immobilised using CNBr Seph 4B beads. K48-linked polyubiquitin chain mixtures were incubated with control-Sepharose, rZNF216-Sepharose or rZNF216 (C30/33A)-Sepharose or in the absence of any Sepharose beads overnight at 37°C (Fig 4.6). Wild type or mutant rZNF216 was covalently coupled to CNBr Seph 4B at a high concentration in case deubiquitinating activity was weak (17.75mg/ml), and a bead volume of 15µl was incubated with 0.125µg of polyubiquitin chains in a reaction volume of 25µl for 30 minutes at 4°C, prior to overnight incubation at 37°C. Ubiquitin specific peptidase 2 (USP2) catalytic core, which has broad spectrum deubiquitinating activity was used here as a positive control and readily disassembled K48-linked polyubiquitin chains to monoubiquitin under these conditions. Wild type rZNF216 (or mutant) beads had no effect on polyubiquitin chain composition, confirming that immobilised rZNF216 has no deubiquitinating activity. To verify that rZNF216 immobilisation does not abrogate deubiquitinating activity, an assay was performed using wild type and mutant rZNF216 in solution, rather than covalently immobilised on beads, and again no activity was observed (data not shown).

#### **4.5. Using immobilised rZNF216 protein to purify *in vivo* ubiquitinated skeletal muscle proteins**

Should ZNF216 assist translocation of ubiquitinated proteins to the 26S proteasome for their degradation and be a *bona fide* atrogene, we reasoned that endogenously ubiquitinated proteins that bind recombinant rZNF216 may represent its substrates which are degraded during muscle atrophy. The identity of the ubiquitinated substrates of ZNF216 has not yet been determined, thus we sought to identify them by directly purifying them with recombinant rZNF216.

**Figure 4.6**

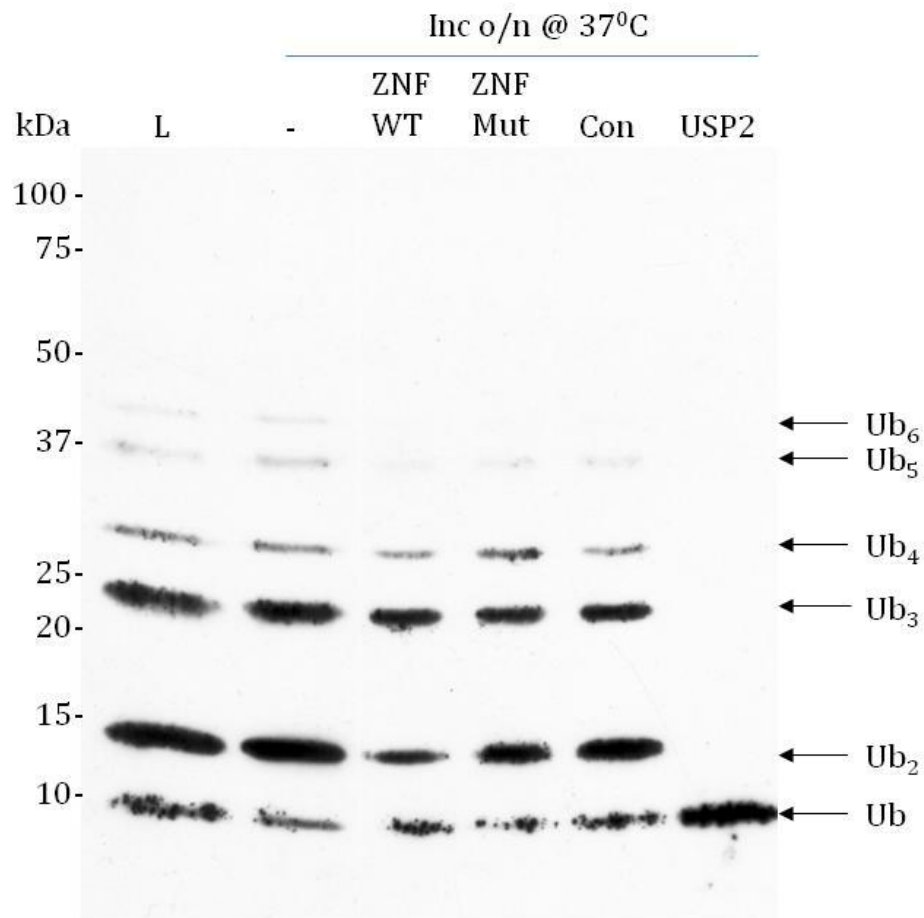


**Figure 4.6** Recombinant immobilised rZNF216 exhibits no deubiquitinating activity. 0.125µg K48-linked polyubiquitin chains were incubated overnight at 37°C with 30µl rZNF216 WT-Sepharose (ZNF WT; 17.75mg/ml), rZNF216 (C30/33A)-Sepharose (ZNF Mut; 17.75mg/ml), control-Sepharose (Con), in the absence of Sepharose (-) or with 0.5µg USP2. Remaining protein was immunoblotted with anti-ubiquitin. Load (L) represents 100% of the polyubiquitin load.

For these experiments the rZNF216 (C30/33A) mutant acts as a control, as proteins binding the Znf\_A20 domain mutant must bind in a ubiquitin-independent manner. Thus this provided a method of disregarding proteins that bind in the absence of an intact Znf\_A20 domain. To allow the preparative purification of rZNF216-binding proteins in sufficient quantities to allow protein identification we required substantial amounts of muscle tissue. Rat EDL muscle was used for expression profiling of ZNF216 (Chapter 3), however, the limited size of this muscle type led us to use “mixed” muscle which was more readily accessible in large amounts. Increased expression of atrogenes has been observed in muscle types other than EDL. Hindlimb suspension increased MuRF1 levels in soleus muscle [220], tibialis anterior muscle and gastrocnemius muscle have exhibited upregulation of MAFbx and MuRF1 under denervation conditions [53] and MAFbx increases as a result of fasting in gastrocnemius [97]. Mixed muscle was taken from rat hind legs, and includes all of the aforementioned muscles as well as a number of other muscles including biceps femoris and gluteus superficialis. Rates of protein breakdown increase in atrophy conditions, however, under normal or “basal” conditions protein degradation still occurs [221], and therefore we reasoned that polyubiquitinated proteins which ZNF216 binds during atrophy conditions would still be present in basal muscle but at lower concentrations. We thus aimed to optimise purification methods using mixed “control” muscle under basal conditions, which could subsequently be applied to identifying changes in ubiquitinated proteins in atrophying muscle.

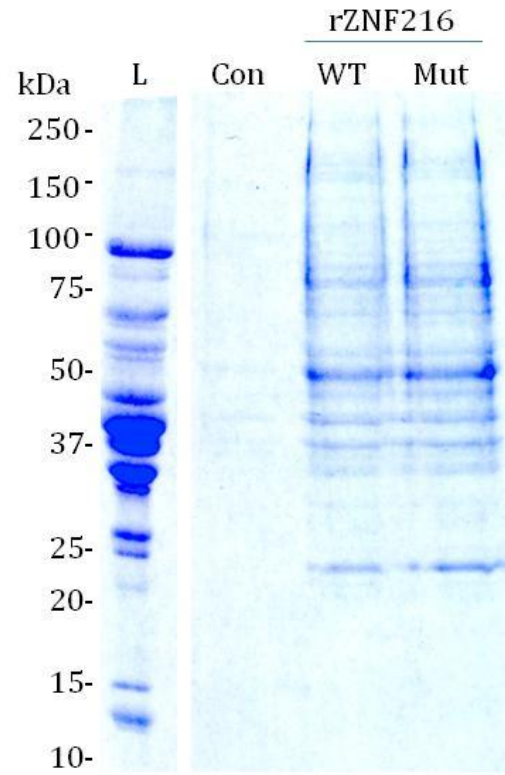
#### **4.5.1. Profile of rat skeletal muscle proteins binding to wild type or C30/33A mutant rZNF216 are indistinguishable by SDS PAGE**

To affinity capture rZNF216-binding proteins from rat muscle, tissue was homogenised in the presence of protease inhibitors and the proteasome-specific inhibitor MG132 to reduce levels of protein degradation by inhibiting *in vivo* proteases and proteasomes that might eliminate the ubiquitinated proteins we were aiming to purify. The clarified supernatant was incubated with either immobilised wild type recombinant rZNF216 or C30/33A mutant rZNF216 covalently coupled to CNBr Seph 4B, as described earlier (Section 4.4).

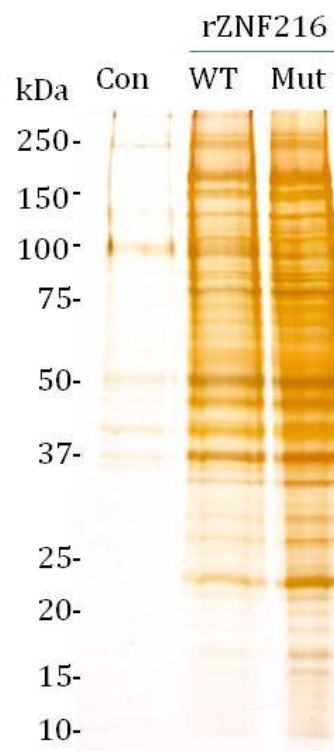
After extensive washing to remove unbound material, proteins retained on the beads were resolved by SDS PAGE and stained with both Coomassie Blue and by silver staining. Despite the difference in ubiquitin-binding ability between the wild type and C30/33A mutant rZNF216 proteins, a subjective visual analysis of the resulting gels revealed no distinguishable differences between the profile of purified proteins (Fig 4.7a and b). However, immunoblotting with anti-ubiquitin clearly demonstrated the ability of the wild type rZNF216 alone to enrich ubiquitinated proteins from rat muscle (Fig 4.7c). Ubiquitin-independent binding proteins thus appear to mask wild-type rZNF216 specific ubiquitin-dependent binding proteins when visualised by Coomassie staining, or even using more sensitive staining methods such as silver staining.

**Figure 4.7**

**a)**



**b)**



c)

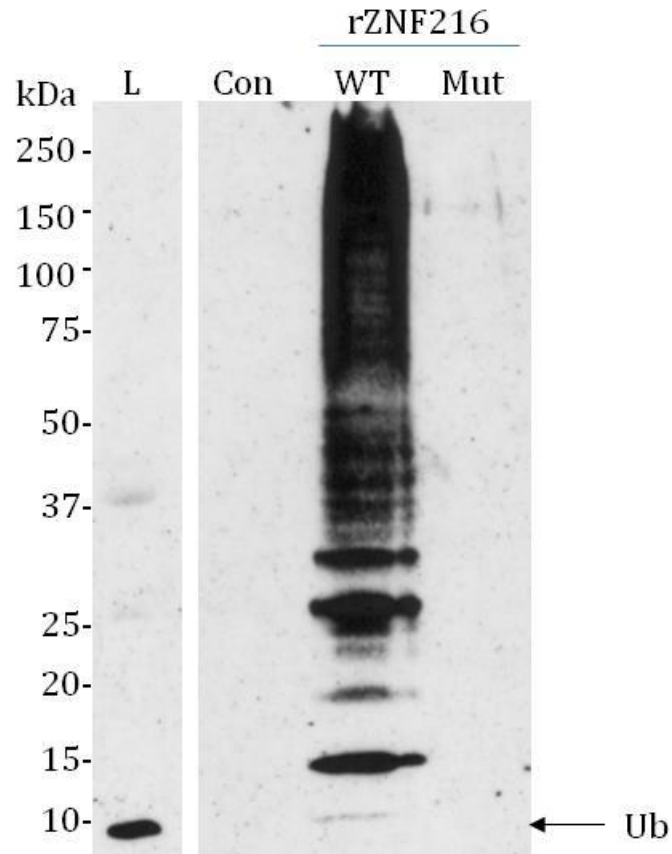


**Figure 4.7** Rat muscle proteins that bound to recombinant rZNF216 (WT) and rZNF216 (C30/33A) mutant (Mut). Mixed, control rat muscle (~7g) was homogenised in 50ml Tris DTT (50mM Tris, 1mM DTT, 20 $\mu$ M MG132, 0.1% mammalian protease inhibitor cocktail (Sigma), pH 7.5) at 4°C. Homogenate was centrifuged and the supernatant was split three ways and passed twice through either 150 $\mu$ l rZNF216-Sepharose (WT), 150 $\mu$ l rZNF216-Sepharose (C30/33A) or 150 $\mu$ l control-Sepharose (Con) at 4°C. Beads were washed three times in Tris DTT, bound proteins were eluted with gel application buffer and 1/15<sup>th</sup> visualised by **a)** Coomassie staining, **b)** silver staining and **c)** immunoblotting with anti-ubiquitin. Load (L) represents approximately 1/200<sup>th</sup> of the proteins loaded.

#### **4.5.2. Two-dimensional gel electrophoresis (2DE) preferentially resolves lower molecular weight rZNF216-binding proteins**

As noted in Section 4.5.1, ubiquitin-independent binding partners of rZNF216 were predominantly visualised when purified protein samples were analysed by SDS PAGE and Coomassie staining. We next used 2DE to resolve rZNF216-binding proteins by both denatured molecular weight and protein iso-electric point (pI), in an attempt to identify subtle differences in proteins interacting with wild type compared to mutant rZNF216. Coomassie Blue and silver staining of resulting 2DE gels revealed broadly similar spot patterns (Fig 4.8a for Coomassie staining, silver staining not shown). Ubiquitin-positive spots were also visualised by anti-ubiquitin immunoblotting, with discrete spots that bound wild type rZNF216 only clearly visible (Fig 4.8a). However in contrast to the immunoblots of samples resolved by SDS PAGE, in which a smear of ubiquitin-positive proteins were evident up to 250kDa (Fig 4.7c), there was an absence of ubiquitinated proteins over 75kDa on anti-ubiquitin blots of the 2DE gels. This suggests that the higher molecular weight ubiquitinated proteins probably do not efficiently enter the first dimension immobilised pH gradient (IPG) strip and that lower molecular weight ubiquitin-positive proteins are preferentially included, limiting the applicability of this approach. However, lower molecular weight discrete ubiquitin-reactive spots (binding to rZNF216) are readily discernible *via* immunoblotting of 2D gels.

**Figure 4.8**

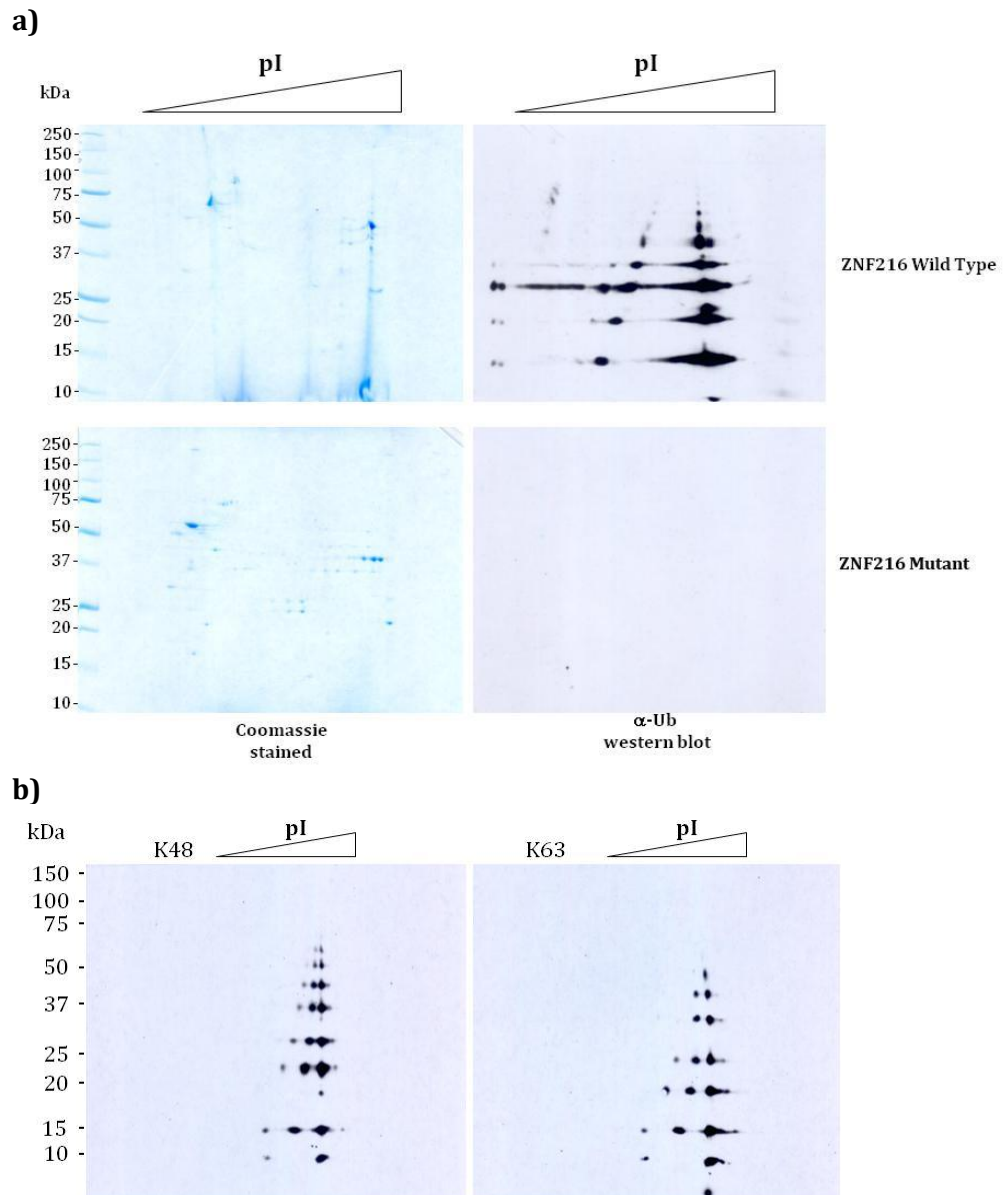


**Figure 4.8** Coomassie staining and anti-ubiquitin immunoblotting of two-dimensional gel electrophoresis of rat muscle proteins bound to recombinant wild type rZNF216 and anti-ubiquitin immunoblotting of commercial K48 and K63-linked polyubiquitin chains. **a)** Mixed rat muscle (~1.5g) was homogenised in 10ml Tris DTT (50mM Tris, 1mM DTT, 20 $\mu$ M MG132, 0.1% mammalian protease inhibitor cocktail (Sigma), pH 7.5) at 4 $^{\circ}$ C. Homogenate was centrifuged and the supernatant was passed twice through 100 $\mu$ l wild type rZNF216-Sepharose at 4 $^{\circ}$ C. Beads were washed three times in Tris DTT and bound proteins were eluted with isoelectric focussing (IEF) sample buffer. **b)** IEF buffer was also added to 0.5 $\mu$ g of commercial K48- or K63-linked polyubiquitin chains. 100% of all samples were incubated with immobilised IPG pH gradient strips (pH 3-11NL) and actively rehydrated at 50V at 20 $^{\circ}$ C overnight and isoelectrically focused. Strips were washed 3 x 5 min with equilibration buffer I (6M urea, 2% SDS, 0.375M Tris-Cl, 2% DTT, pH 8.8, 20% glycerol) and then 3 x 5 min with equilibration buffer II (6M urea, 2.5% iodoacetamide, 0.375M Tris-Cl, 2% DTT, pH 8.8, 20% glycerol) prior to resolving isoelectrically focused proteins by SDS PAGE, and either Coomassie staining or immunoblotting with anti-ubiquitin.

#### **4.5.3. Spot pattern of ubiquitin-positive rZNF216-binding proteins resolved by 2DE is similar to that of unanchored polyubiquitin chains**

Anti-ubiquitin immunoblotting of wild type rZNF216 binding proteins purified from rat skeletal muscle and separated by 2DE revealed several series of protein spots resolved at the same pI but migrating at different molecular weights (Fig 4.8a). When commercial K48- or K63-linked polyubiquitin chain mixtures were resolved using 2DE and blotted with anti-ubiquitin antibodies, a strikingly similar pattern was seen (Fig 4.8b). The lower molecular weight spots within the ladder derived from the rZNF216-binding proteins, at the corresponding positions of the mono (spot 1) and diubiquitin (spot 2) standards, were excised from a Coomassie Blue-stained gel (Fig 4.9) and submitted for matrix-assisted laser desorption/ionisation time-of-flight (MALDI-TOF) PMF analysis. Briefly, in this analysis, protein sample is first digested in gel into peptide fragments using trypsin, and the resulting peptides are ionised. A TOF analyser measures how long ions take to reach a detector (through a flight tube) when accelerated through a fixed potential. The resulting trace, contains information about  $m/z$  values of resulting ions formed and the relative abundance of the ions, producing a mass fingerprint. This fingerprint can be compared to theoretical fingerprints of proteins, determined based on known sequences. The statistically most similar matching fingerprint provides the most likely identity of the test protein.

Analysis of PMF data derived from the two rZNF216-binding protein spots revealed them to contain the ubiquitin sequence, each containing four matching peptides (not shown). The higher molecular weight protein (spot 2) additionally contains an unmatched peptide. This may represent sequence from a ubiquitin-modified target, although further identification of a ubiquitinated target is not

**Figure 4.9**

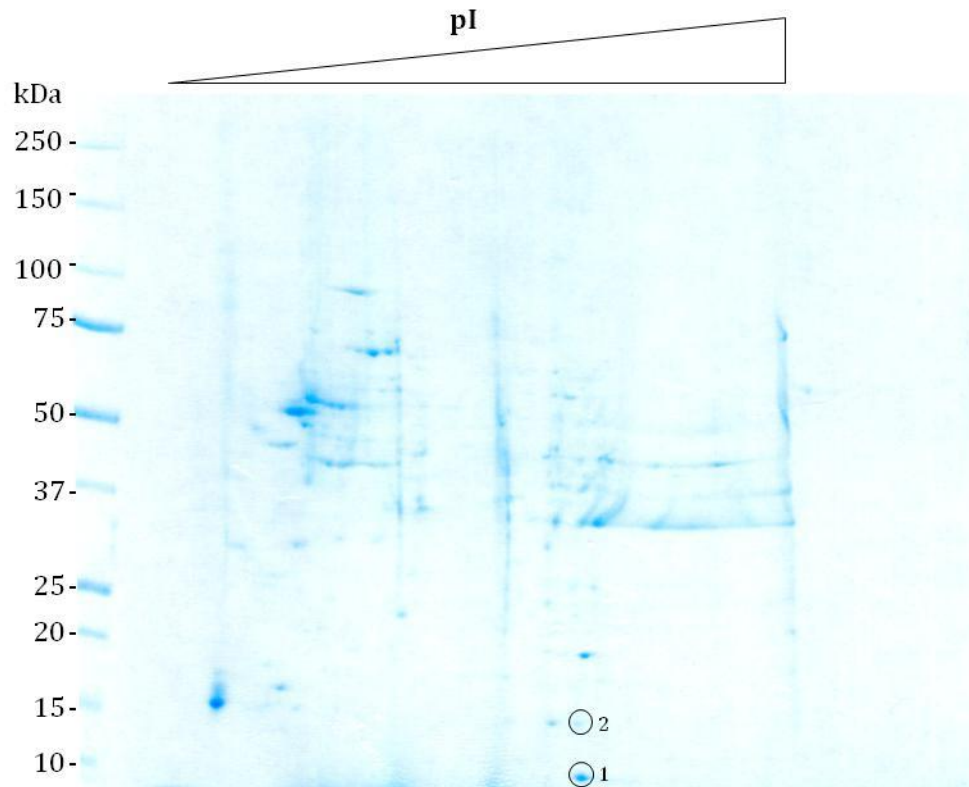


**Figure 4.9** Two-dimensional gel electrophoresis of rat muscle proteins bound to recombinant wild type rZNF216. Mixed rat muscle (~1.5g) was homogenised in 10ml Tris DTT (50mM Tris, 1mM DTT, pH 7.5) at 4°C. Homogenate was centrifuged and the supernatant was passed twice through 100µl wild type rZNF216-Sepharose at 4°C. Beads were washed three times in Tris DTT, bound proteins were eluted with isoelectric focussing (IEF) sample buffer (100% of sample loaded onto immobilised IPG pH gradient strips (pH 3-11NL)) and treated identically to samples in Figure 4.8 up to the stage that proteins were resolved by SDS PAGE, and colloidal Coomassie-stained. Spots 1 and 2 were excised and analysed by PMF.

feasible as there is only one unmatched peptide, and multiple peptides are required to confirm protein identity. Protein spots above this molecular weight were not discernable *via* Coomassie Blue staining of 2D gels, but presumably can be visualised using anti-ubiquitin antibodies on Western blot because longer polyubiquitin chains have more epitopes available for antibody binding, increasing the signal.

Binding assays of wild type ZNF216 against control muscle, analysed by anti-ubiquitin Western blotting of SDS PAGE (Fig 4.7c) and anti-ubiquitin Western blotting and PMF analysis of 2DE (Fig 4.8a and Fig 4.9 respectively), revealed the insubstantial but definite presence of monoubiquitin. However, as noted earlier, binding assays of rZNF216 against commercial ubiquitin chain mixtures confirmed ubiquitin binding, but only when 2 or more ubiquitins were conjugated in a chain, which we previously reasoned was a result of avidity effects. We would expect this avidity effect when rZNF216 is immobilised on CNBr Seph 4B (Fig 4.10) as well as when using glutathione Sepharose (Fig 4.2c). We reasoned that monoubiquitin was unlikely to bind from control muscle, based on our observations using commercial ubiquitin chains. Thus we rationalised that in this case, in the absence of N-ethylmaleimide (NEM) (see Section 4.5.5), co-purification of deubiquitinating enzymes from control muscle may generate monoubiquitin by deubiquitination of longer chains in the purified samples.

#### **4.5.4. Optimising affinity capture by ZNF216 of ubiquitinated proteins using different buffers**

We noted previously, in Section 4.5.1, that while the C30/33A mutation ablates

**Figure 4.10**

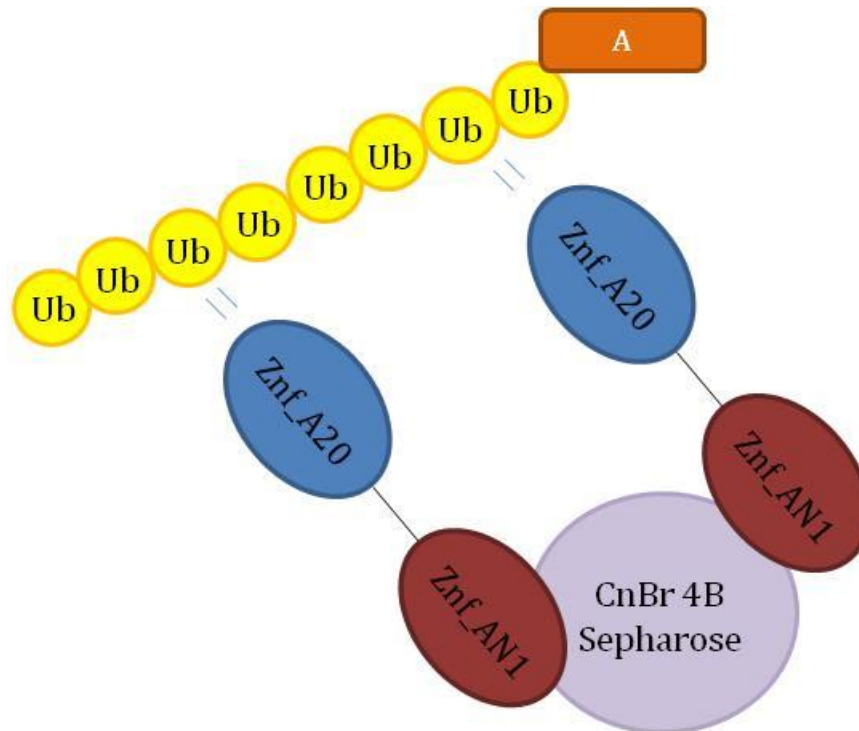


**Figure 4.10** A model of polyubiquitin binding to immobilised rZNF216. Avidity effects may enhance binding to polyubiquitin, as multiple ubiquitin proteins within a chain may bind to multiple Znf\_A20 domains. “A” represents a polyubiquitinated protein, that binds the Znf\_A20 domain *via* its polyubiquitin tag.

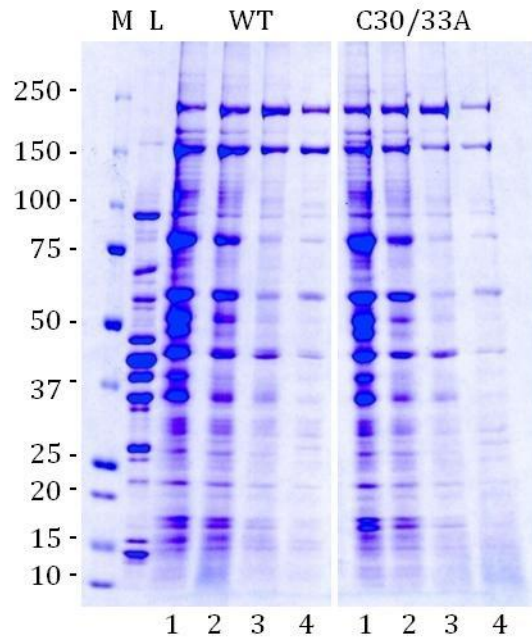
the ubiquitin binding ability of ZNF216, there were no discernable differences in the profile of proteins binding to wild type or C30/33A mutant by Coomassie staining, thus we aimed to optimise binding conditions to reduce non-specific binding. Rat skeletal muscle proteins that bound to wild type rZNF216 or to the C30/33A mutant rZNF216 using four different homogenising/binding buffers were compared using Coomassie staining and anti-ubiquitin immunoblotting (Fig 4.11). No ubiquitinated proteins were detected binding to the C30/33A mutant under any conditions, by immunoblotting with anti-ubiquitin (Fig 4.11b). Notably, the most stringent of the four buffers was considered the most favourable (containing salt and detergent – 50mM Tris, 1mM DTT, 150mM NaCl, 0.5% NP40, pH 7.5) as it reduced the intensity and number of “non-specific” proteins binding to both wild type and mutant rZNF216 bound proteins, as evidenced by Coomassie Blue staining, (Fig 4.11a) and simultaneously enhanced ubiquitin-positive binding partners to wild type rZNF216, evidenced *via* immunoblotting, relative to the other three buffers (Fig 4.11b).

#### **4.5.5. Using on bead deubiquitination to identify ubiquitinated muscle proteins bound to FL rZNF216 and the Znf\_A20 domain under optimised affinity capture conditions**

Despite improvements in our affinity capture method, subjective visual analysis of Coomassie Blue-stained SDS PAGE gels still proved not to be sensitive enough to distinguish ubiquitinated proteins that selectively bound to wild type rZNF216 compared to the C30/33A mutant. Thus an alternative strategy was devised. It has previously been established that the Znf\_AN1 domain of ZNF216 is not required for polyubiquitin-binding [56]. Hence we reasoned that removing this C-terminal domain from our recombinant rZNF216 protein used for our

**Figure 4.11**

**a)**



**b)**

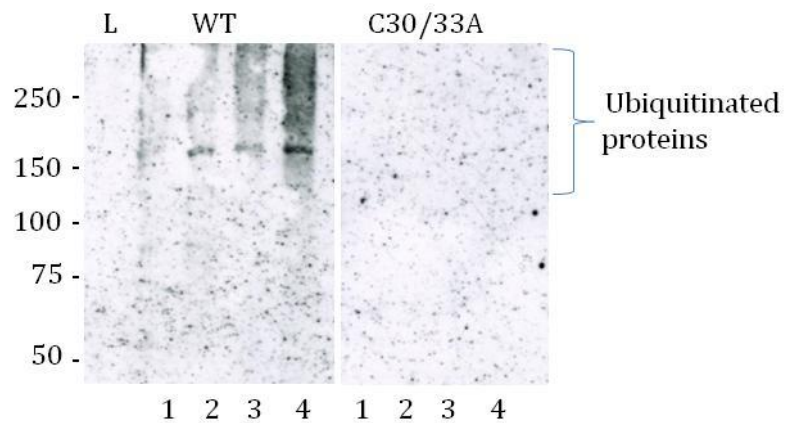


**Figure 4.11** Optimising binding of ubiquitinated rat muscle proteins to recombinant rZNF216 wild type (WT). Mixed rat muscle (~1g each) was homogenised in 4 different buffers (10ml) at 4°C of different compositions; buffers were 1) 50mM Tris, 1mM DTT, 20µM MG132, 0.1% mammalian protease inhibitor cocktail (Sigma), pH 7.5; 2) Buffer 1 + 150mM NaCl, pH 7.5; 3) Buffer 1 + 0.5% NP-40, pH 7.5 and; 4) Buffer 1 + 150mM NaCl, 0.5% NP-40, pH 7.5. (Buffer 1) is the composition of the previously used buffer, in Figures 4.7-4.9). Homogenate was centrifuged and the supernatant was passed twice through 50µl of wild type rZNF216-Sepharose (WT) or rZNF216 (C30/33A) at 4°C. Beads were washed three times in the same buffer that muscle was homogenised in, and bound proteins were eluted with gel application buffer. Proteins were resolved by SDS PAGE and **a)** 50% Coomassie-stained or **b)** 50% immunoblotted with anti-ubiquitin. Load (L) represents approximately 1/200<sup>th</sup> of the proteins loaded.

polyubiquitin-binding experiments might reduce the number of “non-specific” proteins (that bound independently of ubiquitin; Fig 4.12) and mask the specific interactors. The Znf\_A20 domain is contained within the first 60 amino acids (residues 11-35) of the rZNF216 wild type sequence. Site directed mutagenesis was used to introduce an early stop codon after residue 60. The Znf\_A20 domain was expressed as a GST-fusion, purified using glutathione-Sepharose and thrombin cleaved (Fig 4.13a). The resulting Znf\_A20 peptide was immobilised (with CNBr Seph 4B; at 5 mg/ml) and found to retain binding to commercial K48-linked polyubiquitin chains; control-Sepharose produced in tandem did not (Fig 4.13b). We reasoned that proteins binding in a ubiquitin-dependent manner would no longer interact with rZNF216 or the Znf\_A20 domain after deubiquitination; a similar approach was used by Ventadour *et al.* [194] in which ubiquitinated proteins from C2C12 cells were bound to immobilised ubiquitin binding domains of proteasomal S5a subunit, before subsequent deubiquitination with the catalytic domain of USP2. Our new approach was to combine previously optimised conditions (using a more stringent homogenising buffer) in combination with on bead deubiquitination to selectively elute ubiquitin-dependent binding proteins, and to include the use of the Znf\_A20 domain alone as well as FL ZNF216.

For these experiments during homogenisation of the muscle sample, we permanently inactivated any co-purifying deubiquitinating enzymes through the addition of NEM to our previously determined optimal binding buffer. NEM is a thiol-reactive compound that irreversibly modifies cysteine residues in proteins, and can be used as an inhibitor of many deubiquitinating enzymes (DUBs) which use this residue catalytically. Muscle homogenate was subsequently treated with

**Figure 4.12**

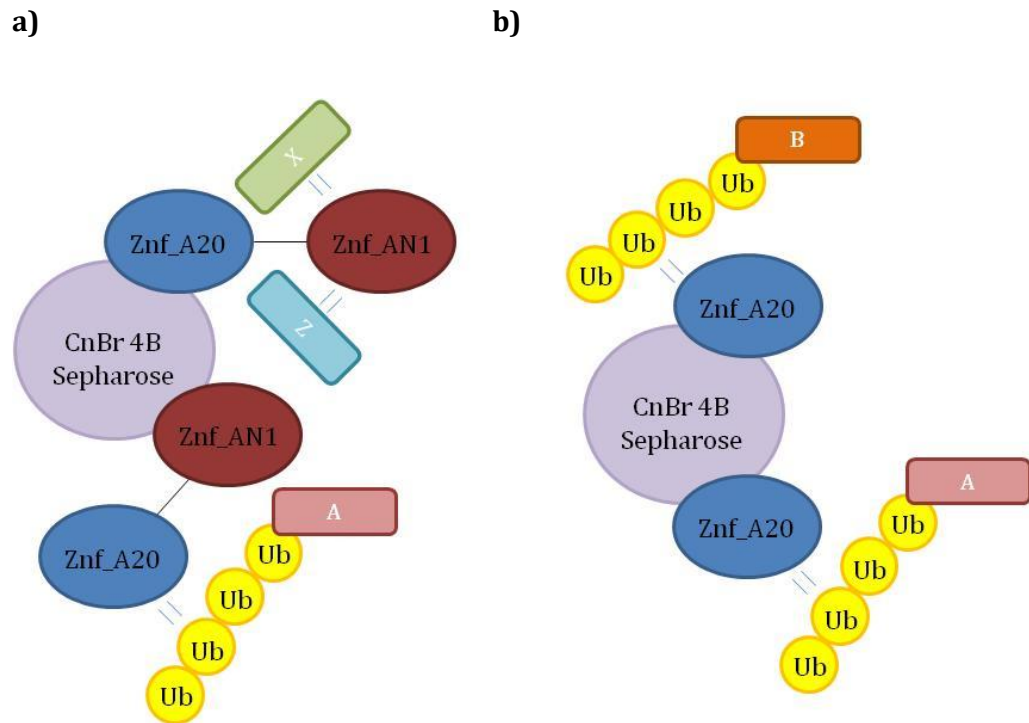


**Figure 4.12** Model of **a)** FL rZNF216 and **b)** the Znf\_A20 domain binding to rat muscle proteins. Increased ubiquitin-dependent binding may result from using the Znf\_A20 domain for pulldown assays, as proteins that bind FL rZNF216 *via* its Znf\_AN1 domain might sterically block ubiquitinated proteins binding the Znf\_A20 domain. “A” and “B” represent polyubiquitinated proteins that bind the Znf\_A20 domain, “X” and “Z” represent “non-specific” proteins that bind independently of ubiquitin *via* the Znf\_AN1 domain of ZNF216.

**Figure 4.13**

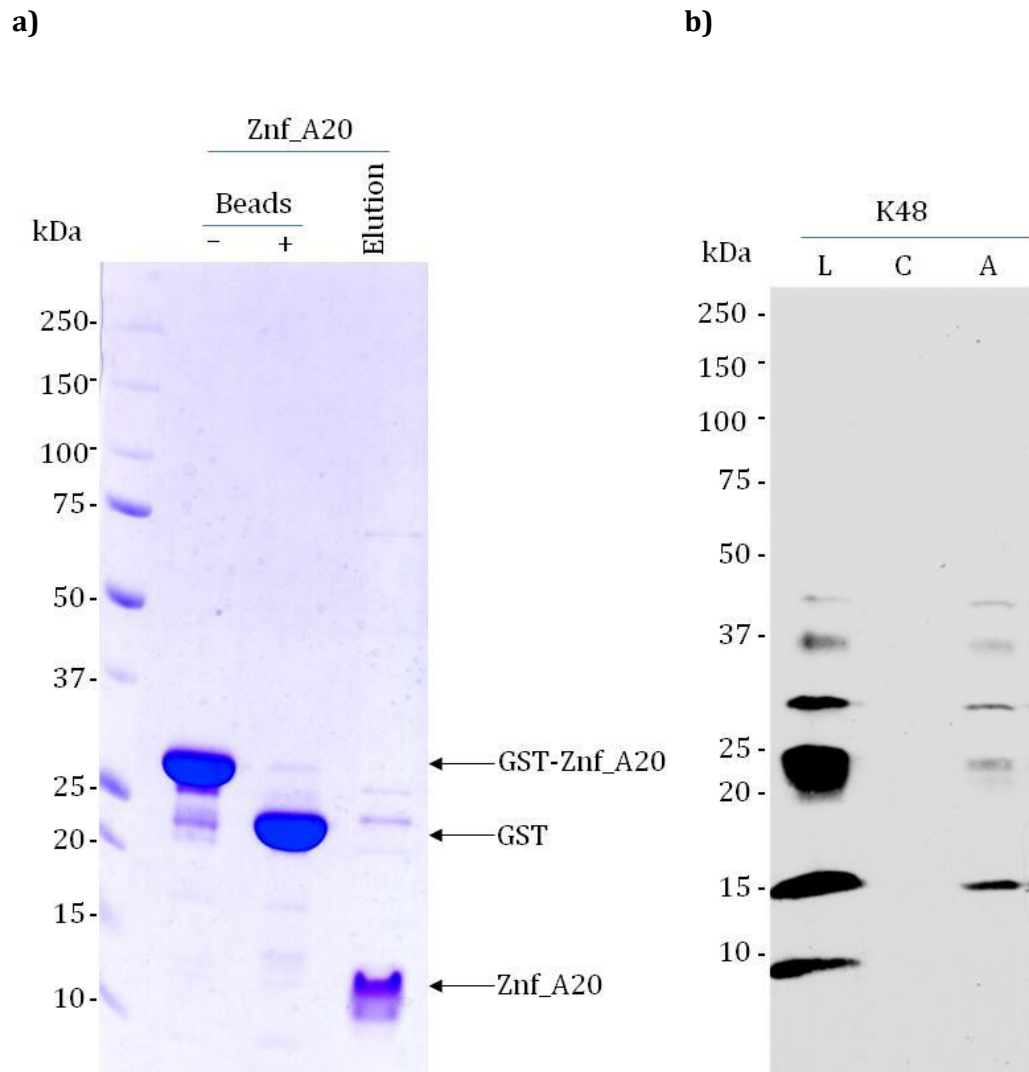


**Figure 4.13** Thrombin cleavage of the GST-tagged Znf\_A20 domain (GST-Znf\_A20) and binding to K48-linked polyubiquitin. **a)** GST-Znf\_A20 expressed from 5l of IPTG-induced *E. coli* was purified in TBS-T on glutathione-Sepharose beads, after incubation for 1 hr at 4°C and subsequent washing. A small sample of glutathione-beads were retained to ensure GST-tagged protein binding (Beads -). The remaining GST-Znf\_A20 domain bound to glutathione-Sepharose was then incubated with 10 units thrombin in thrombin cleavage buffer (5mM Tris, 150mM Sodium Chloride, 2.5mM Calcium Chloride Dihydrate, pH 8.4) overnight at 4°C. The GST-tag remained on beads after thrombin cleavage (Beads +), and recombinant Znf\_A20 WT was eluted into solution (Elution), and SDS PAGE resolved proteins were stained with Coomassie Blue. **b)** Znf\_A20-Sepharose (A) or control-Sepharose (C) was incubated with 0.25µg of K48-linked polyubiquitin chains in binding buffer (50mM Tris, 150mM NaCl, 0.5% NP-40, 0.1% bovine serum albumin (BSA), 1mM DTT, pH 7.5) for 30 minutes at 4°C. Beads were washed twice in binding buffer, bound proteins were eluted with gel application buffer, resolved by SDS PAGE and immunoblotted with anti-ubiquitin. Load (L) represents 100% of the polyubiquitin load.

an excess of DTT to quench the NEM, as cysteine linking is vital for the Znf\_A20 zinc finger domain structure and would affect the affinity capture. Using this protocol we captured ubiquitinated proteins from skeletal muscle with FL rZNF216-Sepharose or Znf\_A20-Sepharose, and treated the proteins on beads with the catalytic core of USP2 deubiquitinating enzyme. The anti-ubiquitin immunoblotting profile of Znf\_A20 bound ubiquitinated proteins (Fig 4.14a) mirrored previous observations of rZNF216 captured material (Fig 4.7c). Anti-ubiquitin immunoblotting revealed that deubiquitination of Znf\_A20 bound proteins (Fig 4. 14a) and FL rZNF216 bound proteins (not shown), diminished the smear of bound ubiquitinated proteins following 2 hours of USP2 treatment and monoubiquitin was produced as a result of deubiquitination in the eluted fraction. Ubiquitinated proteins that bound FL rZNF216 or Znf\_A20 *via* their polyubiquitin tag may thus also be released into solution and no longer retained on the beads (fraction iv in Figure 4.14), rendering them amenable to further analysis.

#### **4.5.6. LC-MS/MS analyses of deubiquitinated FL rZNF216/Znf\_A20 domain-binding proteins**

While PMF is a useful technique, and was used previously when identifying ubiquitin-positive protein spots which bound to rZNF216 (Fig 4.9), it is not applicable to a complex mixture of proteins, such as those liberated from FL rZNF216 or the Znf\_A20 domain binding *via* deubiquitination with USP2. In order to identify proteins within this mixture, we used liquid chromatography tandem mass spectrometry (LC-MS/MS). This technique is often employed to identify individual proteins within a complex mixture of proteins. Initially, the mixture of proteins is digested using trypsin, generating a complex mixture of resultant

**Figure 4.14**

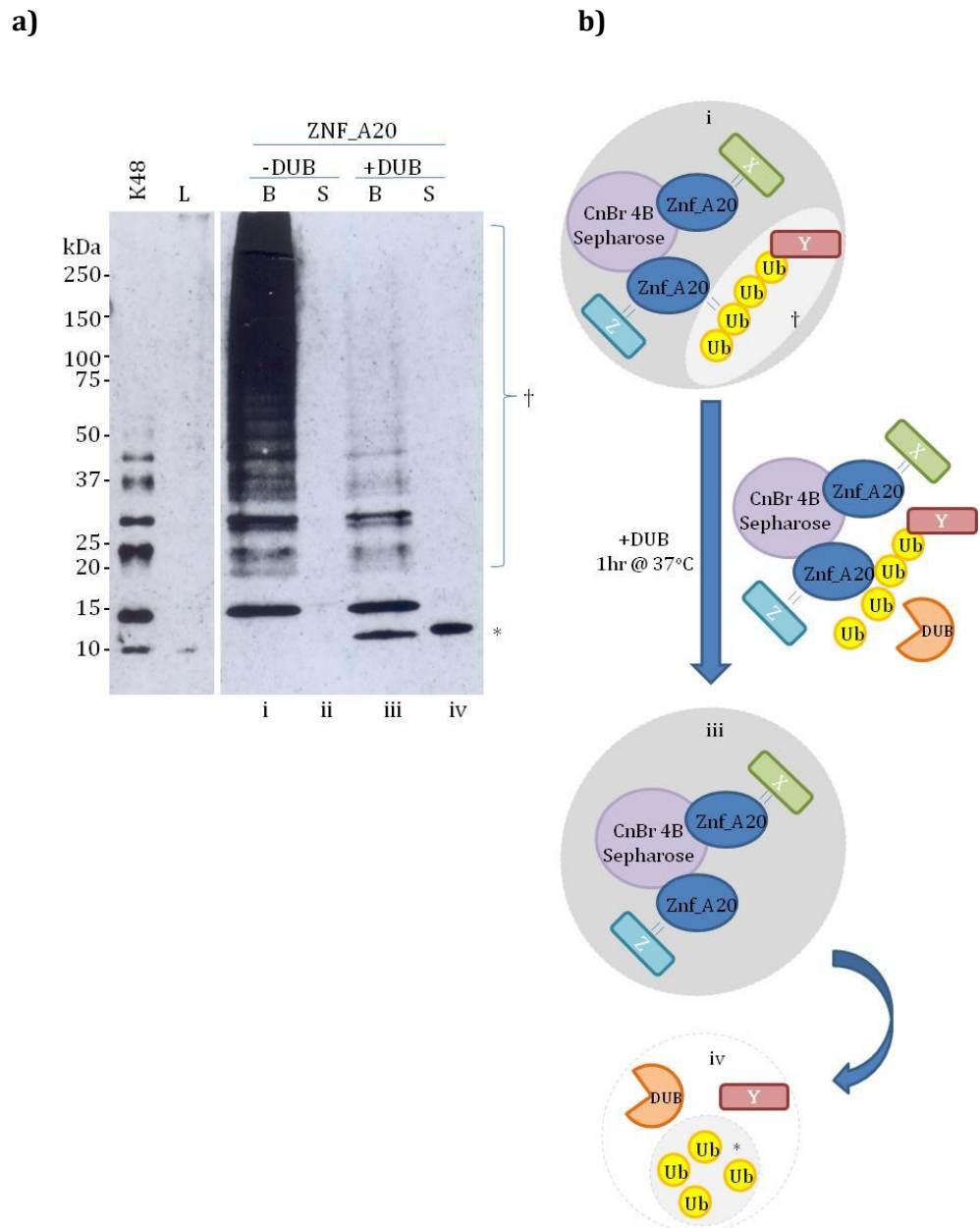


**Figure 4.14** Elution of Znf\_A20-Sepharose-bound ubiquitinated rat muscle proteins *via* deubiquitination. Mixed, control rat muscle (~15g) was homogenised in 100ml homogenising buffer (50mM Tris, 150mM NaCl, 0.5% NP-40, 5mM N-ethylmaleimide, 20 $\mu$ M MG132, 0.1% mammalian protease inhibitor cocktail (Sigma), pH 7.5). Homogenate was centrifuged and DTT added to the supernatant to a final concentration of 10mM, and mixed at 4 $^{\circ}$ C for 15 minutes. Supernatant was passed twice through 800 $\mu$ l Znf\_A20-Sepharose at 4 $^{\circ}$ C. Beads were washed three times in wash buffer (50mM Tris, 150mM NaCl, 0.5% NP-40, 1mM DTT, pH 7.5) and incubated in DUB buffer (50mM Tris, 1mM DTT, pH 7.5) (an equal volume solution to beads), incubated +/- 10 $\mu$ g USP2 core for 2hrs at 37 $^{\circ}$ C. Solution was collected, and gel application buffer was added separately to 1/40<sup>th</sup> beads/solutions (the remaining was frozen). **a)** Proteins eluted from beads in the absence (i) and presence (iii) of USP2 core, and their respective solutions were resolved by SDS PAGE and immunoblotted with anti-ubiquitin. Part **b)** represents proteins present in lanes i – iv and proteins highlighted by † (smear of ubiquitinated proteins) and \* (monoubiquitin). (K48)=0.25 $\mu$ g K48-linked polyubiquitin, (L)=Load 1/250<sup>th</sup> lysate applied to beads, (B)=beads, (S)=solution.

peptides. These are then separated using LC, separating peptides based on differences in hydrophobicity, upstream of a tandem mass spectrometer. During tandem MS, peptides are ionised and detected in the first mass spectrometer, and selected fragments can be further fragmented and analysed in a second mass spectrometer which generates peptide sequence information. This information can be interrogated against sequence databases affording protein identification. Although sequence coverage is typically low using this approach, it can be extensive and broadly representative of the protein components within a complex mixture.

Protein mixtures released by USP2 treatment of rat skeletal muscle proteins captured on rZNF216 or Znf\_A20-Sepharose were analysed using LC-MS/MS. Analysis exclusively focused on peptide sequences that are unique to a single protein hit within the database, in this case within the mammalia taxonomy of the NCBI nr protein sequence database (containing all non-redundant GenBank CDS translations). Proteins identified within samples were analysed based on number of unique peptides and function, the latter including possible binding to atrogenes and/or involvement in skeletal muscle atrophy. We additionally inputted sequences into Ubipred [222] to detect predicted ubiquitination sites and substantiate evidence that these proteins were indeed ubiquitinated targets. Proteins identified from control experiments (eluted from beads treated in parallel but -USP2) were presumed to be non-ubiquitinated and resulting from leaching from beads into solution, and were discounted from +USP2 analysis. Additionally, “bait” sequence (from ZNF216), and sequences from ubiquitin, trypsin and USP2 sequences were omitted. Tables 4.1 and 4.2 lists proteins identified that were eluted into solution only in the presence of USP2 from

**Table 4.1**

| Subsection | GI number | Protein name  | GenBank <sup>TM</sup> accession no | Total peptides | Function                                   |
|------------|-----------|---|------------------------------------|----------------|--|
| i          | 149036532 | actin, gamma 2, isoform CRA_b   | EDL91150.1                         | 2              | Z disc component                           |
|            | 49868     | put. beta-actin (aa 27-375)   | CAA27396.1                         | 2              | Dystrophin binding                         |
|            | 20521786  | KIAA1180 protein  | BAA86494.2                         | 1              | Erk activation in brain                    |
|            | 149494200 | PREDICTED: similar to KIAA1582 protein  | XP_001517138.1                     | 1              | MicroRNA regulation                        |
|            | 56188     | glyceraldehyde 3-phosphate-dehydrogenase  | CAA26150.1                         | 1              | Apoptosis/Autophagy/Glycolysis             |
| ii         | 73992595  | PREDICTED: similar to serologically defined colon cancer antigen 33 like        | XP_543057.2                        | 1              | Transcription factor during development    |
|            | 73948200  | PREDICTED: similar to carcinoembryonic antigen-related cell adhesion molecule 5 | XP_541572.2                        | 1              | Mutated in autosomal dominant hearing loss |
|            | 22129749  | protein CASC3   | NP_671485.1                        | 1              | Nonsense-mediated mRNA decay (NMD)         |
| iii        | 7106864   | HSPC237   | AAF36157.1                         | 1              | Unknown                                    |
|            | 109094596 | PREDICTED: cysteine-rich with EGF-like domain protein 2-like                    | XP_001116152.2                     | 1              | Unknown                                    |
|            | 71043870  | tudor domain-containing protein PHF20L1   | NP_001020873.1                     | 1              | Unknown                                    |
|            | 194041852 | PREDICTED: CWF19-like protein 1   | XP_001929566.1                     | 1              | Unknown                                    |
|            | 220829516 | novel protein similar to mouse B230396012Rik                                    | CAQ10653.2                         | 1              | Unknown                                    |
|            | 26342434  | unnamed protein product   | BAC34879.1                         | 1              | Unknown                                    |
|            | 149634714 | PREDICTED: similar to C10orf63 protein  | XP_001506317.1                     | 1              | Unknown                                    |
|            | 5929884   | nucleolin-related protein NRP   | AAD56625.1                         | 1              | Unknown                                    |
|            | 58331230  | DALR anticodon-binding domain-containing protein 3 isoform 1                    | NP_001009996.1                     | 1              | Unknown                                    |
|            | 10438978  | unnamed protein product   | BAB15392.1                         | 1              | Unknown                                    |

**Table 4.1** Proteins eluted into solution after USP2-mediated deubiquitination of Znf\_A20-Sepharose-bound rat muscle proteins, identified by LC-MS/MS. All peptides sequences were unique to the identified proteins. Peptides from “bait” protein (from Znf\_A20 domain), ubiquitin, trypsin and USP2 were omitted from analysis, and none of the above proteins were detected in –USP2 control samples. Subsection i); proteins of known function of particular interest; ii) other proteins of known function; iii) proteins with unknown function.

**Table 4.2**

| Subsection | GI number | Protein name  | GenBank <sup>TM</sup> accession no | Total peptides | Function                                  |
|------------|-----------|---|------------------------------------|----------------|---|
| i          | 10945605  | perforin  | AAG24611.1                         | 1              | Apoptosis                                 |
|            | 194664014 | PREDICTED: hypothetical protein isoform 5   | XP_879713.4                        | 1              | Microtubule stabilisation                 |
|            | 119921446 | PREDICTED: TSPY-like 2 isoform 2  | XP_874476.2                        | 1              | Chromatin remodelling                     |
|            | 74001392  | PREDICTED: similar to Nucleolar preribosomal-associated protein 1                     | XP_544859.2                        | 1              | Ribosome biogenesis                       |
|            | 8918488   | adenylate kinase isozyme 1  | BAA97655.1                         | 1              | Possible MuRF1 binder, AMP signalling     |
| ii         | 149728930 | PREDICTED: ATR interacting protein  | XP_001494950.1                     | 1              | Involved in DNA damage checkpoint pathway |
|            | 1098543   | interleukin-2 receptor alpha  | AAC48487.1                         | 1              | Signal transduction                       |
|            | 194220872 | PREDICTED: zinc finger protein 513  | XP_001500950.2                     | 1              | Transcription factor                      |
|            | 29825889  | small conductance calcium-activated potassium channel subfamily N member 3 variant 1B | AAN46636.1                         | 1              | Potassium channel                         |
|            | 126273765 | PREDICTED: similar to Blooms syndrome protein   | XP_001368666.1                     | 1              | Helicase                                  |
| iii        | 149487896 | PREDICTED: hypothetical protein, partial  | XP_001519894.1                     | 1              | Unknown                                   |
|            | 149642231 | PREDICTED: similar to phosphoglucomutase 2  | XP_001511051.1                     | 1              | Unknown                                   |
|            | 6330472   | KIAA1205 protein  | BAA86519.1                         | 1              | Unknown                                   |
|            | 149633328 | PREDICTED: hypothetical protein   | XP_001505775.1                     | 1              | Unknown                                   |
|            | 149618229 | PREDICTED: similar to dual specificity phosphatase 19, partial                        | XP_001508319.1                     | 1              | Unknown                                   |
|            | 90076816  | unnamed protein product   | BAE88088.1                         | 1              | Unknown                                   |
|            | 159570900 | novel protein   | CAP19250.1                         | 1              | Unknown                                   |
|            | 126283044 | PREDICTED: hypothetical protein   | XP_001378841.1                     | 1              | Unknown                                   |

**Table 4.2** Proteins eluted into solution after USP2-mediated deubiquitination of FL rZNF216-Sepharose-bound rat muscle proteins, identified by LC-MS/MS. All peptides sequences were unique to the identified proteins. Peptides from “bait” protein (from ZNF216), ubiquitin, trypsin and USP2 were omitted from analysis, and none of the above proteins were detected in –USP2 control samples. Subsection i); proteins of known function of particular interest; ii) other proteins of known function; iii) proteins with unknown function.

Znf\_A20 and FL rZNF216, respectively. Where possible, the rat sequence was selected over other mammalian species. All proteins identified were predicted to have ubiquitination sites, ranging from a single possible site to forty-five (not shown). Each table is split into 3 subsections; i) proteins of known function of particular interest ii) other proteins of known function iii) proteins with unknown function. Proteins within subsections ii) and iii) have either yet to be established for their roles within the cell, or have no obvious connections with muscle atrophy, and thus our analysis concentrates on subsection i). Five proteins of particular interest were identified in subsections i) of both Znf\_A20 and FL rZNF216 eluted proteins, although interestingly we observed no overlap of proteins binding to the Znf\_A20 domain alone and to FL ZNF216. Two apoptosis related proteins were identified, one each binding Znf\_A20 and FL rZNF216 (GI 56188 and GI 10945605, respectively). Two proteins binding Znf\_A20 were identified that are key components of muscle cells, including a Z disc component (GI 149036532) and a dystrophin binding protein (GI 49868), and whilst all other bound proteins were identified by only by a single unique peptide, 2 unique peptides identified these two proteins. Proteins binding the Znf\_A20 domain include one involved in Erk signalling (GI 20521786) and microRNA regulation (GI 149494200). FL rZNF216 binders further included a microtubule stabilising protein (GI 194664014), one involved in chromatin remodelling (GI 119921446) and ribosome biogenesis (GI 74001392). Interestingly, adenylate kinase 1 protein (AK1) (GI 8918488), identified in fractions of deubiquitinated FL rZNF216 binding proteins, has previously been identified as a MuRF1 binder (and presumed substrate) by yeast two-hybrid interaction studies [109]. We attempted to validate our LC-MS/MS approach by probing rat muscle proteins bound to rZNF216 wild type, rZNF216 (C30/33A) and Znf\_A20 +/- DUB with an antibody specific for AK1 (Fig 4.15). AK1 was only

identified in the FL rZNF216 elution and not the Znf\_A20 elution by LC-MS/MS, and accordingly we see AK1 binding specifically to FL and not the Znf\_A20 domain alone by immunoblotting, although the failure to detect AK1 in solution indicates a lack of sensitivity of Western blotting. AK1 appears to be unmodified as evidenced by the presence of only a single band and binds both the FL wild type ZNF216 and the C30/33A mutant. Together these results suggest that binding is, in fact, *via* a ubiquitin independent mechanism, and reduces the confidence in the LC-MS/MS approach.

## **4.6. Discussion**

### **4.6.1. ZNF216 polyubiquitin binding and linkage specificity**

Lysine-48 (K48)-linked chains have, until recently, been widely recognised as the signal for proteasomal degradation [219], whereas K63-linked chains tend to have non-proteolytic functions (see Chapter 1.9.1.5.). Our results indicate that recombinant GST-rZNF216 has no K48-linkage specificity preferentially to K63-chains, as might be expected from a proteasomal shuttle protein. The UBA domain of shuttle protein Rad23 shows considerable preference for K48-linked ubiquitin chains by surface plasmon resonance analysis over K63- and K29-linked polyubiquitin [223]. While our binding assay and immunoblotting method allows us to detect presence or absence of ubiquitin binding, this method is less sensitive or quantitative than surface plasmon resonance that can quantify association and dissociation between two proteins. This more sensitive method may detect a preference of ZNF216 for a specific ubiquitin linkage that is not detectable under our conditions. However, Li & Yi 2008 [224] notes that the

**Figure 4.15**

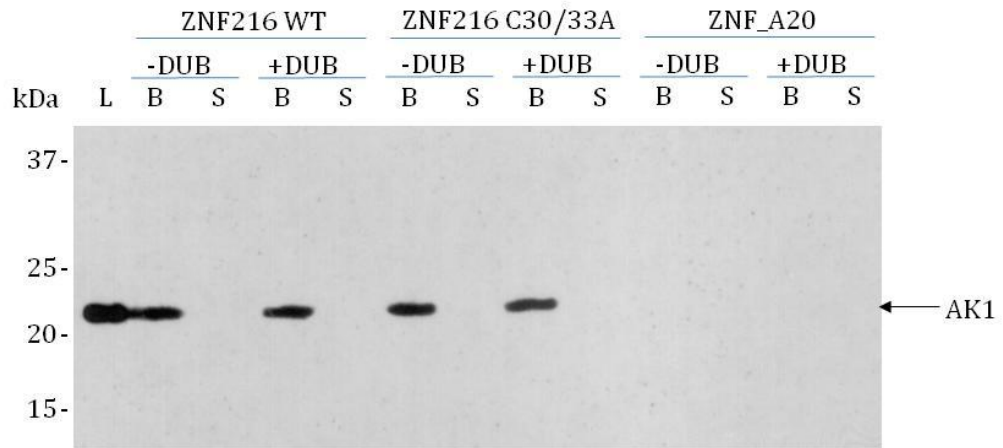


**Figure 4.15** Anti-adenylate kinase 1 (AK1) immunoblotting of rat muscle proteins bound to rZNF216 wild type, rZNF216 C30/33A and Znf\_A20 beads and elutions +/- deubiquitination (-/+DUB) with USP2. As previously for LC-MS/MS samples, mixed rat muscle (~7g) was homogenised in 50ml homogenising buffer (50mM Tris, 150mM NaCl, 0.5% NP-40, 5mM N-ethylmaleimide, 20µM MG132, 0.1% mammalian protease inhibitor cocktail (Sigma), pH 7.5) prior to centrifugation. DTT was added to the resulting supernatant to a final concentration of 10mM and mixed at 4°C for 15 minutes. Supernatant was passed twice through 150µl rZNF216 WT/ rZNF216 C30/33A or Znf\_A20-Sepharose at 4°C. Beads were washed three times in wash buffer (50mM Tris, 150mM NaCl, 0.5% NP-40, 1mM DTT, pH 7.5) and incubated in DUB buffer (50mM Tris, 1mM DTT, pH 7.5) (an equal volume solution to beads), +/- USP2 core for 2hr at 37°C. Solution was collected, and gel application buffer was added separately to beads/solutions. (L)=Load 1/200<sup>th</sup> lysate loaded onto beads, (B)=1/15<sup>th</sup> beads, (S)=1/15<sup>th</sup> solution.

ubiquitin receptor p62 shows no polyubiquitin linkage specificity *in vitro*, as observed by our lab where p62 binds K48- and K63-linked chains *in vitro* [184], but *in vivo* evidence implicates a preference of p62 for K63-linked polyubiquitin [225]. Similarly, ZNF216 may exhibit polyubiquitin linkage specificity *in vivo*, possibly *via* association with other ubiquitin binding proteins and factors that confer selectivity.

#### **4.6.2. ZNF216 as a shuttle protein for polyubiquitinated proteins**

ZNF216 has been established as a polyubiquitin binding protein, but lacks deubiquitinating (Figure 4.6 and Hishiya *et al.* 2006 [56]) or E3 ubiquitin ligase activity [56]. Whilst these activities can be straightforward to assay *in vitro*, testing ZNF216's proposed function as a shuttle protein is more challenging. Further evidence from Hishiya *et al.* [56] supporting the shuttle protein hypothesis included ZNF216's reported association with the proteasome and the accumulation of polyubiquitinated proteins in atrophying ZNF216 knockout mice. As discussed in Chapter 1.9, ubiquitin ligases MAFbx and MuRF1 polyubiquitinate substrates during muscle atrophy to target proteins for proteasomal degradation. Mounting evidence of ZNF216's involvement in muscle atrophy, as observed by increased expression under various atrophy conditions and resistance of ZNF216 knockout animals to atrophy, led us to reason that ZNF216 may function to shuttle MAFbx and MuRF1 ubiquitinated substrates to the proteasome. Should this be the case, then any evidence of MAFbx or MuRF1 substrates binding to ZNF216 might provide further support for ZNF216's role as a shuttle protein. UBDs can be utilised as tools for capturing ubiquitinated proteins [193, 194] and similarly we have successfully captured polyubiquitinated proteins using FL rZNF216, or ZNF216's ubiquitin-binding

Znf\_A20 domain alone. Interestingly, we observed that AK1 was apparently eluted in solution from FL rZNF216 *via* deubiquitination with USP2, a protein which has previously been reported as a MuRF1 binding protein in yeast two-hybrid studies [109], further substantiating the shuttle protein hypothesis. As observed from our LC-MS/MS data, AK1 was only eluted from FL rZNF216, and not to the Znf\_A20 domain alone, which suggests that the FL protein may provide increased specificity of binding relative to the UBD alone. However, while AK1 has been identified as a MuRF1 binder in yeast two-hybrid experiments, there is currently no evidence of MuRF1 specifically polyubiquitinating AK1. In addition, as discussed later, Western blotting evidence indicates that AK1 captured on FL rZNF216 may not be polyubiquitinated.

There are limitations to our polyubiquitinated proteins purification methods. ZNF216 may require additional association with other ubiquitin binding proteins for higher specificity, as discussed in the previous Section. Consequently, the observed binding of polyubiquitinated substrates to rZNF216/Znf\_A20, may lack the *in vivo* specificity. To eliminate the effect of co-purifying DUBs, we treated homogenate with NEM to irreversibly inactivate *in vivo* DUBs, as confirmed by the lack of monoubiquitin in the -USP2 sample. Prior to incubation with the Znf\_A20 domain, homogenate had to be treated with DTT to quench NEM and prevent it modifying the zinc finger of the Znf\_A20 domain itself. Similarly, structures of zinc finger proteins within the homogenate are irreversibly disrupted by NEM treatment. It is possible that some zinc finger proteins that would bind polyubiquitin *in vivo* might aid ZNF216 binding, and NEM-induced disruption of these zinc fingers might then change the complement of proteins that binds ZNF216 under these conditions. These limitations could reduce the

number of identified genuine *in vivo* ZNF216 binding proteins, which may account for only identifying two proteins as a known atrogenic E3 ligase binding protein out of the thirty-six proteins identified.

#### **4.6.3. Znf\_A20 and ZNF216-binding polyubiquitinated protein candidates revealed by LC-MS/MS**

As revealed by the LC-MS/MS data, a number of proteins of known function bound FL rZNF216 and the Znf\_A20 domain, such as glyceraldehyde 3-phosphate-dehydrogenase (GAPDH) that bound Znf\_A20. GAPDH has been used as a real time-PCR and protein internal standard in some muscle wasting studies [226-228], on the assumption that its mRNA and protein expression levels remain constant under basal and atrophying conditions. However, GAPDH has been observed to stabilise an E3 ubiquitin ligase Siah1 after apoptotic stimulation, which mediates nuclear protein degradation during apoptosis [229]. Mounting evidence links apoptosis to a number of atrophy models, including denervation induced muscle atrophy [230] and to hindlimb unloading-induced muscle atrophy in rats [231]. Should GAPDH be involved in apoptosis, a pathway that may promote muscle atrophy, then its elution by deubiquitination may seem counter-intuitive as it would implicate GAPDH as an atrophy substrate. However, studies that have linked apoptosis and atrophy have, to date, not included sepsis-induced muscle atrophy models, which may induce different pathways to other stimuli. Alternatively, the presence of polyubiquitinated forms may be rationalised by GAPDH being an abundant protein *in vivo*, that like other proteins needs to be turned over.

GAPDH was not the only apoptosis related protein identified by LC-MS/MS, as perforin was also eluted from FL rZNF216, a protein that forms transmembrane pores in cells during apoptosis to allow granzymes to enter and induce apoptosis. Negative feedback may be an alternative explanation for targeted polyubiquitination and possible downstream proteasomal degradation of apoptosis related proteins. A protein eluted from the Znf\_A20 domain (GI 149494200) has been implicated in microRNA regulation. Whilst this specific protein has not been linked with muscle atrophy, Güller *et al.* 2010 [232] review the involvement of microRNAs in skeletal muscle, in which they consider that microRNA and atrogenes may be involved in a “regulatory loop” during muscle atrophy. More intuitively, two proteins that are known constituents of all cell types as part of the cytoskeleton, gamma-actin and beta-actin, were eluted from the Znf\_A20 domain. These were the only two candidates identified by more than a single unique peptide. Interestingly, in support of our findings, a very recent study published after completion of our experiments, has not only provided evidence of actin polyubiquitination *via* methods highly similar to our own, but also presents data that indicates both MuRF1 interaction with actin, and MuRF1-dependent ubiquitin polymerisation [114]. MuRF1 knockout in C2C12 myotubes, *via* transfection with MuRF1 targeting siRNA, stabilised flag-actin under Dex induced atrophy conditions relative to atrophying myotubes transfected with scrambled siRNA control, implicating a role for MuRF1 in destabilising actin. However, this study refers to the alpha form of actin, rather than beta and gamma forms that we have detected. In relation to beta actin, Prins *et al.* 2011 observed that specific ablation of beta actin in skeletal muscle results in quadriceps myopathy, highlighting its involvement with another form of muscle wasting [233]. Interestingly, a further MuRF1 binder was eluted from FL rZNF216 and not from the Znf\_A20 domain alone; AK1. However, AK1 immunoblotting indicated

that AK1 was not polyubiquitinated, as only a single band was observed as opposed to a smear of polyubiquitinated AK1, which bound both the FL rZNF216 and the C30/33A mutant. AK1 failed to bind Znf\_A20, which suggests that AK1 binding was *via* the Znf\_AN1 domain and thus may have been eluted into solution by leaching. It is possible that a small fraction of AK1 is indeed ubiquitinated, but below the detectable limit, although its ability to bind independently of ubiquitin and the lack of detectable AK1 eluted into solution after deubiquitination makes this unlikely. This highlights the importance of immunoblotting candidates to validate that they bound *via* polyubiquitination.

#### **4.6.4. Limitations of the LC-MS/MS approach**

Ion scores are calculated for lists of peptides during LC-MS/MS analysis, and those above a threshold of 20 are considered significant and certain when above 30. The greater the chance of random protein hits, the lower the score. Scores for peptides identified in Tables 4.1 and 4.2 are all below 20, the threshold of significance, with the exception of the two Znf\_A20 bound proteins that have 2 unique peptides, identified as gamma-actin (GI 149036532) and beta-actin (GI 49868) which have scores of 90 and 61, respectively. Using this approach the majority of proteins identified were from only a single peptide; for a more assured confirmation, two or more peptide sequences from the same protein are ideally required (which increases the total ion score). This approach is limited in success as many of the single peptides used for the identifications had low “scores”, so further validation of purified proteins, for example by immunoblotting, is clearly desirable. Our attempted validation of the LC-MS/MS method by immunoblotting for the candidate AK1 was unsuccessful, as various analysis indicated that AK1 was not polyubiquitinated. It is likely that AK1

leached from rZNF216 WT beads during overnight incubation and indicates that other candidates could also be ubiquitin-independent binding proteins. The lack of binding to the Znf\_A20 domain suggests that AK1 may bind *via* the Znf\_AN1 domain of ZNF216, but the functional significance of this is unclear.

#### **4.6.5. Utilising the Znf\_A20 domain of ZNF216 to bind polyubiquitinated proteins**

The caveat to the LC-MS/MS approach is that other regions of ZNF216, other than the Znf\_A20 polyubiquitin binding domain, may impart substrate specificity. This is supported by the observed binding of AK1 to FL rZNF216 in a ubiquitin-independent manner, of which binding is lost upon removal of ZNF216's Znf\_AN1 domain. What is apparent from this analysis is that the two confident protein matches were eluted from Znf\_A20 beads, substantiating the notion that FL rZNF216 may bind fewer ubiquitinated proteins due to non-ubiquitinated proteins binding in other regions, including the C-terminal Znf\_AN1 domain. Identifying ubiquitinated substrates may be limited using this approach because of the broad range of ubiquitinated proteins that can bind (evidenced by anti-ubiquitin Western blot), which reduces the concentration of individual ubiquitinated proteins and reduces the chances that peptide sequences are identified using LC-MS/MS, which has limited sensitivity. However, use of the Znf\_A20 domain alone may provide a method of comparing global ubiquitination profiles by binding polyubiquitinated proteins indiscriminately (see Chapter 5). While there is little evidence *via* LC-MS/MS of highly concentrated specific ubiquitinated FL rZNF216 binding proteins, this does not rule out the possibility that FL rZNF216 may have more specificity than Znf\_A20 domain alone. This, combined with our elution of actin specifically from the Znf\_A20 Sepharose,

supports that using the UBD alone may be more useful when capturing ubiquitinated species to observe global ubiquitination profiles.

## **CHAPTER 5**

### **Polyubiquitinated protein profiling and the purification of unanchored polyubiquitin chains**

## 5.1. Introduction

Our affinity purification strategy, using covalently immobilised full length rat sequence ZNF216 (FL rZNF216) protein or the Znf\_A20 domain alone, allowed enrichment of polyubiquitinated proteins from rat skeletal muscle (Chapter 4). Liberation of proteins that bound these immobilised proteins *via* a polyubiquitin tag was achieved through USP2-mediated deubiquitination and eluted proteins were analysed *via* liquid chromatography tandem mass spectrometry (LC-MS/MS). This approach had a number of limitations. Only a single unique peptide was detected for all except 2 purified candidates, indicating that this method provided limited coverage of eluted proteins present. Despite removing “background” proteins identified in a control sample (eluted even in the absence of USP2) LC-MS/MS still identified proteins that leached from beads, as evidenced by the absence of a smear of polyubiquitinated adenylate kinase 1 protein (AK1) in the purified fractions by Western blotting, and AK1 binding to the double cysteine C30/33A rZNF216 mutant, which lacks ubiquitin-binding ability. Failure to detect multiple peptides for the majority of candidates suggests this approach may not be sensitive enough to identify proteins for proteomic analysis.

## 5.2 The Znf\_A20 domain can be used to profile global ubiquitination changes in proteasome-knockout mouse brains

Although identification of ubiquitinated binding partners of rZNF216 (or more specifically the Znf\_A20 domain) has been restricted by experimental limitations, given the high affinity with which the Znf\_A20 domain binds to polyubiquitinated proteins ( $K_d = 8 \mu\text{M}$  at 298K [217]) we also investigated whether it may be used

more generally as a tool to globally profile changes in ubiquitinated targets. In this case, the quantitative capture of ubiquitinated proteins from different biological samples is required. Although the intention was to apply this method to uncover global changes in ubiquitination of skeletal muscle proteins from tissue undergoing atrophy, in the first instance the approach was used to analyse biological samples where changes in the pool of ubiquitinated proteins were known or expected to show significant alterations.

To determine whether our affinity capture and blotting method is sensitive enough to detect changes in global ubiquitination, we first applied the Znf\_A20 domain purification method to brains from 26S proteasome-depleted mice, in which ubiquitin neuropathology is observed two weeks after proteasomal depletion in the forebrain relative to wild type controls [174]. This model was developed by Bedford *et al.* 2008, who depleted 26S proteasomal activity *in vivo* without using pharmacological inhibitors. Conditional knockout using a Cre/loxP system was employed to inactivate the *Psmc1* gene in selected neurons of the forebrain, leading to polyubiquitin accumulation (assessed by Western blotting) and atrophy of the forebrain. We found that polyubiquitin accumulation in proteasomal knockout mice relative to wild type controls is evident in crude protein extracts from the brains (denoted by the loads in Fig 5.1a and by Bedford *et al.* 2008), but that the Znf\_A20 domain affinity purification allows differences in smaller ubiquitin-positive species that were previously undetectable to be observed, *via* enrichment of the same samples (Fig 5.1a). Clearly the 26S proteasome fails to efficiently degrade ubiquitinated proteins in the knockout mouse, and the accumulation of ubiquitinated proteins captured by the Znf\_A20

**Figure 5.1**

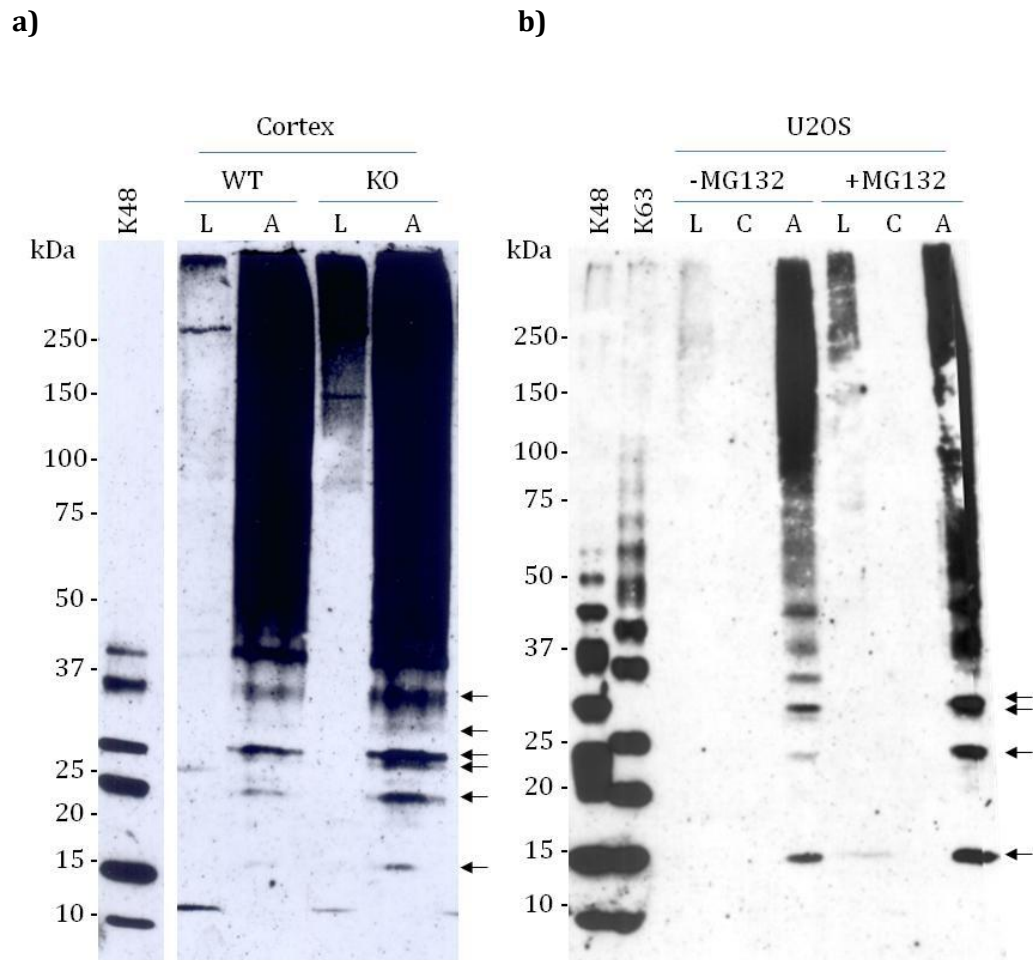


**Figure 5.1** Anti-ubiquitin immunoblotting of **a)** wild type and *Psmc1* knockout mouse brain (~15mg each) and **b)** +/- MG132 treated U20S cell proteins (~4mg each) (cells treated with 1 $\mu$ M MG132 for 16 hours) bound to Znf\_A20 beads. Samples were homogenised in a) 5ml or b) 4ml homogenising buffer (50mM Tris, 150mM NaCl, 0.5% NP-40, 5mM N-ethylmaleimide, 20 $\mu$ M MG132, 0.1% mammalian protease inhibitor cocktail (Sigma), pH 7.5), centrifuged, and the supernatant collected. DTT was added to the lysate to a final concentration of 10mM and mixed at 4°C for 15 minutes. Lysate was passed twice through a) 50 $\mu$ l Znf\_A20-Sepharose or b) split between 80 $\mu$ l of control or Znf\_A20 Sepharose at 4°C. Beads were washed three times in wash buffer (50mM Tris, 150mM NaCl, 0.5% NP-40, 1mM DTT, pH 7.5). Bound proteins were eluted in gel application buffer. **a)** (K48)=0.25 $\mu$ g K48-linked polyubiquitin, (L)=Load 1/100<sup>th</sup> lysate loaded onto beads, (A)=100% of Znf\_A20 bound proteins, WT=wild type mouse cortex, KO=*Psmc1* knockout mouse cortex. **b)** (K48)=0.25 $\mu$ g K48-linked polyubiquitin, (K63)=0.25 $\mu$ g K63-linked polyubiquitin, (L)=Load 1/80<sup>th</sup> lysate loaded onto beads, (C)=50% of Control Sepharose bound proteins (A)=50% of Znf\_A20 bound proteins. Arrows denote ubiquitin positive species that increase upon *Psmc1* knockout or MG132 treatment.

domain confirms that this protocol is sensitive to changes in global ubiquitination in the samples.

### **5.3. The Znf\_A20 domain can be used to profile global ubiquitination changes in cells following pharmacological proteasome inhibition**

As a further demonstration that our Znf\_A20 domain affinity-capture method can be used to detect changes in overall ubiquitination, we treated U2OS cells (a human osteosarcoma-derived cell line) with a pharmacological inhibitor of the proteasome, MG132. This provides a pharmacological equivalent of the genetic ablation of the proteasome, although MG132 treatment is performed in cells as opposed to tissue specific genetic knockout *in vivo*. An increase of ubiquitinated proteins similar to that seen upon genetic proteasomal inhibition in mice may be expected, due to reduced proteasomal activity and thus less degradation of ubiquitinated substrates. As predicted, overnight treatment of U2OS cells with a relatively low (1 $\mu$ M) concentration of MG132, followed by capture of ubiquitinated proteins with the Znf\_A20 domain, resulted in purification of increased levels of ubiquitinated proteins relative to untreated cells; (Figure 5.1b). Therefore, it appears that this approach is able to detect and amplify gross changes in protein ubiquitination. Changes in global ubiquitination have in the past been analysed by simply resolving crude (unpurified) samples by SDS PAGE and probing with anti-ubiquitin antibodies [174]. Our protocol provides a method of pre-fractionating and enriching ubiquitinated material, potentially increasing the sensitivity with which changes in protein ubiquitination can be detected.

#### **5.4. The Znf\_A20 domain reveals subtle changes in the profile of ubiquitinated proteins in rat EDL muscle after 24 hours of LPS infusion**

In sections 5.2 and 5.3, affinity capture of ubiquitinated proteins using immobilised Znf\_A20 domain confirmed global differences in protein ubiquitination between proteasomal knockout mouse brains compared to wild type, and in MG132-treated U2OS cells relative to untreated cells. Previously, in Chapter 3, we used rat extensor digitorum longus (EDL) muscle for mRNA expression profiling from lipopolysaccharide (LPS)- or saline-infused animals at a 24 hour time point. Subsequent to these analyses, we additionally gained access (from other investigators in the group) to EDL muscle from rats infused with the same concentration LPS or saline for 2 and 6 hours. Procedures were again carried out by Julie March and Philip Kemp (the same investigators as previously) and were approved by the University of Nottingham Ethical Review Committee and were performed under Home Office Project and Personal license authority. EDL muscle protein extracts from animals treated for 2, 6 and 24 hours with saline or LPS infusion were incubated with Znf\_A20-coupled Sepharose, and purified ubiquitinated proteins were identified using anti-ubiquitin immunoblotting (Fig 5.2). Similarly to earlier observations, we saw an enrichment of ubiquitinated proteins bound to Znf\_A20 when compared to blotting crude muscle lysate alone (Fig 5.3). Notably, we saw a clear increase in a species (band 1 in Fig 5.3) migrating at the same level as K48- and K63-linked diubiquitin standards (commercial unanchored polyubiquitin chains) after 24 hours of LPS infusion relative to saline infusion, a change not seen at the earlier LPS-infusion time points i.e. 2 and 6 hours only in the Znf\_A20 purified samples. (Fig 5.2). A further ubiquitin-positive species above the presumed diubiquitin (band 2 in Fig 5.3) also appears to show increased levels after 24 hours of LPS

**Figure 5.2**

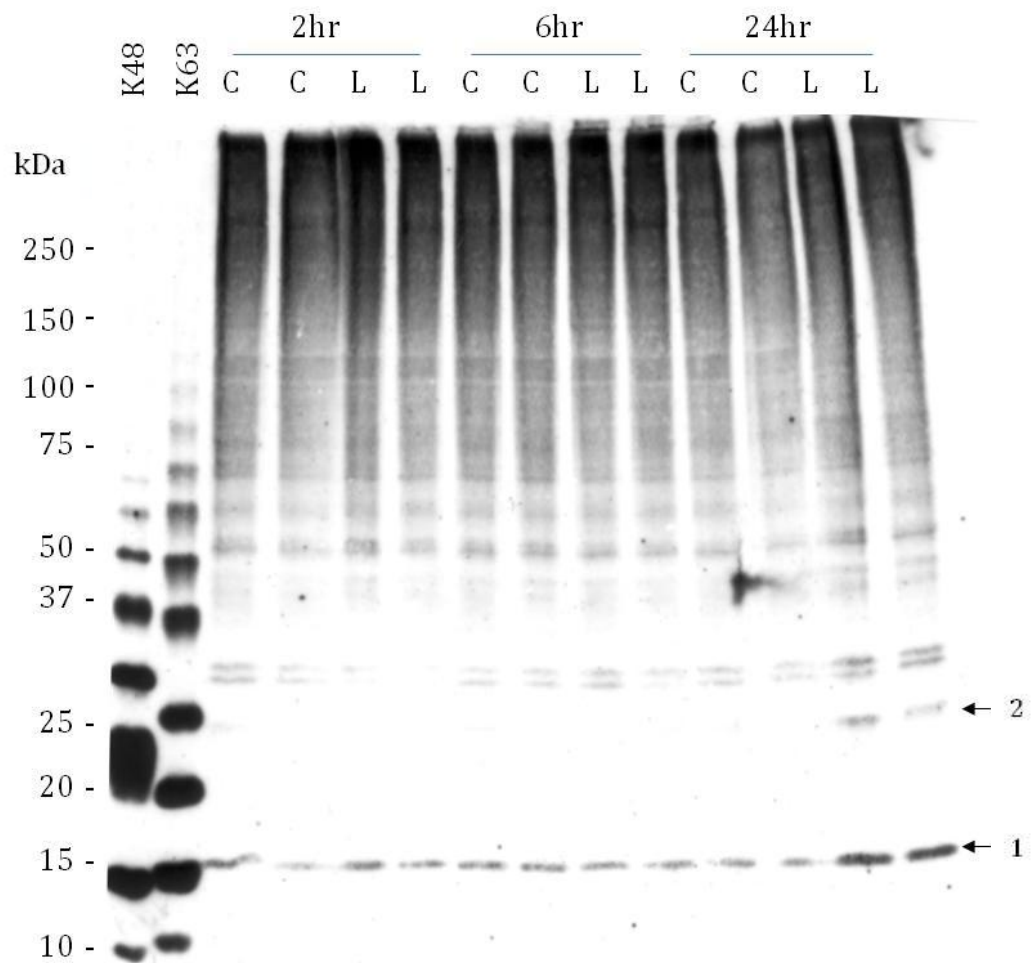


**Figure 5.2** Anti-ubiquitin Western blot of ZnA20 captured proteins from EDL muscle, from control rats (C) (infused with saline) or LPS-infused rats (L), after either 2, 6 or 24 hours of infusion. Samples (approximately 20mg each) were homogenised in 1.5ml homogenising buffer, NEM quenched with DTT and bound to 40 $\mu$ l beads, that were then washed with wash buffer (as detailed in Fig 5.1). 50% of ZnA20 captured proteins were probed with anti-ubiquitin. (K48)=0.25 $\mu$ g K48-linked polyubiquitin, (K63) =0.25 $\mu$ g K63-linked polyubiquitin. Arrows labelled 1 and 2 denote ubiquitin positive species that increase after 24 hours of LPS infusion.

**Figure 5.3**

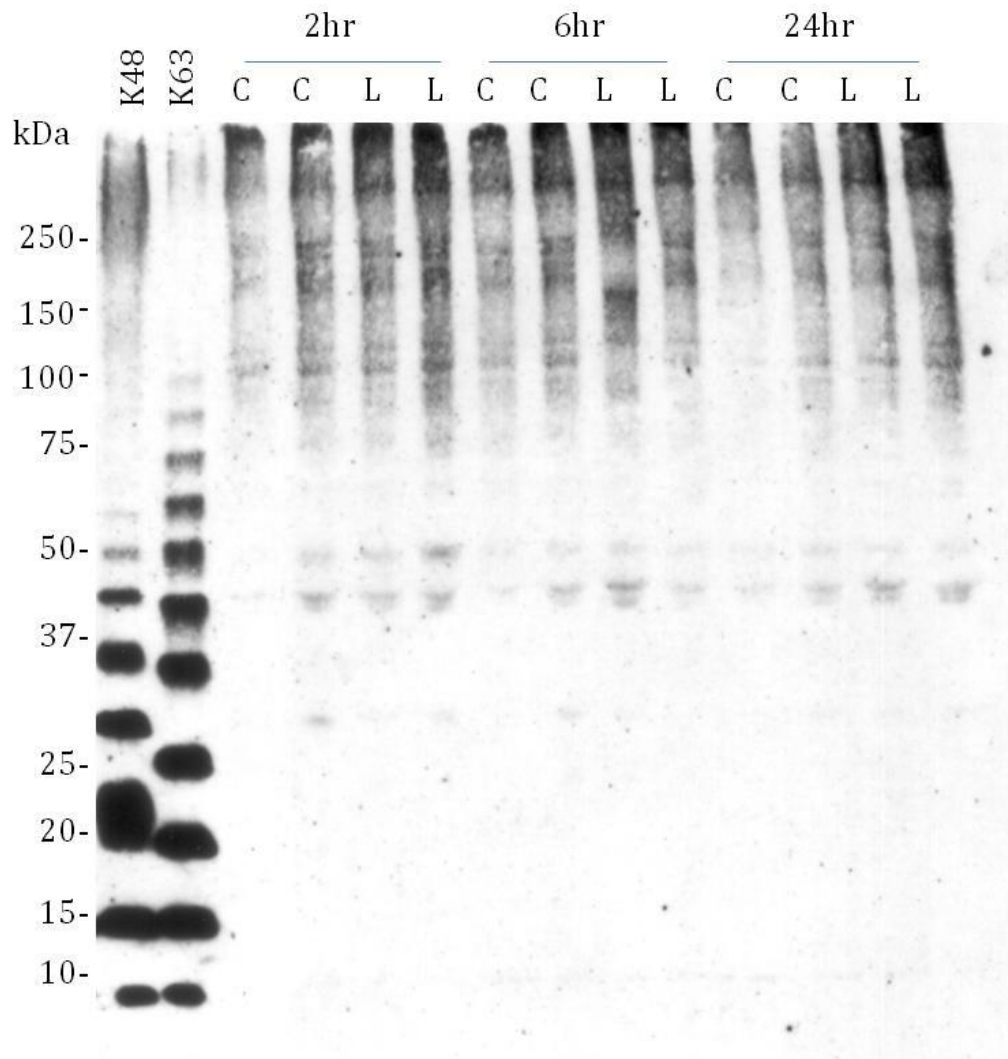


**Figure 5.3** Anti-ubiquitin Western immunoblotting of EDL muscle homogenate, from control rats (C) (infused with saline) or LPS-infused rats (L), after either 2, 6 or 24 hours of infusion, that was incubated with Znf\_A20 Sepharose in Fig 5.2. (K48)=0.25 $\mu$ g K48-linked polyubiquitin, (K63)=0.25 $\mu$ g K63-linked polyubiquitin. Represents 1/300<sup>th</sup> of protein loaded on beads in Fig 5.2.

infusion. In contrast to these increases in lower molecular weight ubiquitin-positive species after 24 hours of LPS infusion in EDL, levels of higher molecular weight species appear to remain unchanged, indicating that gross changes in global ubiquitination do not change in this model. This is in contrast to observations of the increased higher molecular weight ubiquitin species that accumulated during proteasomal inhibition in U20S cells by MG132. Further to this, we probed the Znf\_A20-purified fractions with an antibody that specifically recognises only K48-linked polyubiquitin (Fig 5.4) [234]. Anti-K48 specific antibody specifically recognises commercial K48-linked and not K63-linked polyubiquitin chains. This antibody appears to preferentially bind longer polyubiquitin chains, as diubiquitin in the commercial chain mixture is not as strongly detected by anti-K48-ubiquitin antibodies relative to our pan anti-ubiquitin antibody which detects all linkages. No clear change in global K48-linked ubiquitination between the purified samples from LPS-infused compared to saline-infused tissue was observed, although K48-linked polyubiquitinated proteins were readily detected in our samples.

### **5.5. Reassessment of the presumed diubiquitin band purified by the Znf\_A20 domain**

The obvious change in the ubiquitin-reactive band co-migrating with the diubiquitin standard, that was elevated in the ubiquitinated fraction purified from LPS-infused EDL tissue, drew our attention to its existence. Retrospective analysis of previous Figures (Figs 4.7c, 4.8a & 4.15a) demonstrates that it was consistently captured by rZNF216/Znf\_A20 domain from a diverse range of biological samples, including human U20S cells, rat muscle and mouse brain. In addition, peptide mass fingerprinting (PMF) analysis of a protein spot resolved

**Figure 5.4**

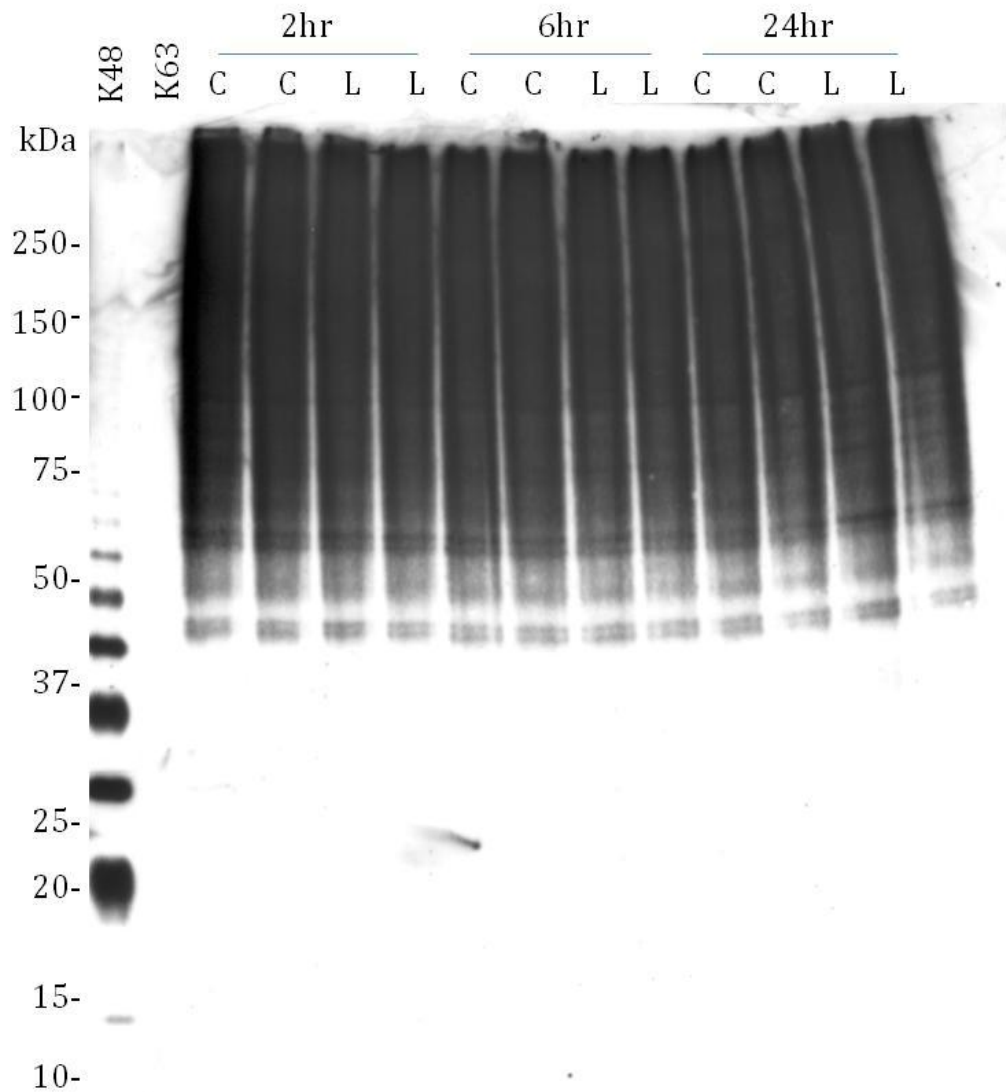


**Figure 5.4** Immunoblotting of ZnF\_A20 captured proteins using anti-K48 (that detects only K48-linked polyubiquitin) from EDL muscle, from control rats (C) (infused with saline) or LPS-infused rats (L), after either 2, 6 or 24 hours of infusion, as in Fig 5.2. 50% of ZnF\_A20 captured proteins were probed with anti-K48. (K48)=0.25 $\mu$ g K48-linked polyubiquitin, (K63) =0.25 $\mu$ g K63-linked polyubiquitin.

by two-dimensional gel electrophoresis (2DE), previously purified from rat muscle using rZNF216 (Fig 4.9) and presumed to be equivalent to the ubiquitin dimer indicated the ubiquitin protein sequence to be present (Section 4.5.3). This poses the question of whether this ubiquitin-reactive species does indeed represent diubiquitin, or alternatively a small protein that is monoubiquitinated and consistently purified on rZNF216/Znf\_A20 Sepharose. Having previously established that monoubiquitin from commercial ubiquitin chain mixtures and monoubiquitin from rat muscle (under our optimised affinity capture conditions) does not bind to immobilised rZNF216 or Znf\_A20 domain (Fig 4.3 & Fig 4.14a), it seemed more likely that the protein represented a ubiquitin dimer. Our observations that only Ub<sub>2</sub> species and above are efficiently captured by the Znf\_A20 domain suggests a preference of the domain for polyubiquitin over monoubiquitin, which we investigate later using gas phase MS analyses (Chapter 5.8.3) and structural modelling (Chapter 5.10). Remarkably, we noted that this presumed ubiquitin dimer is spared from deubiquitination when Znf\_A20-immobilised rat muscle proteins are treated with USP2, as demonstrated by anti-ubiquitin immunoblotting in Figure 4.14a (repeated in Figure 5.5a, with a corresponding Coomassie stained sample of USP2 treated beads in Figure 5.5b), suggesting a non-covalent interaction with the UBD may in fact protect this species from deubiquitination. We investigate the rationale behind sparing of the ubiquitin dimer during deubiquitination in Section 5.6.6.

**Figure 5.5**

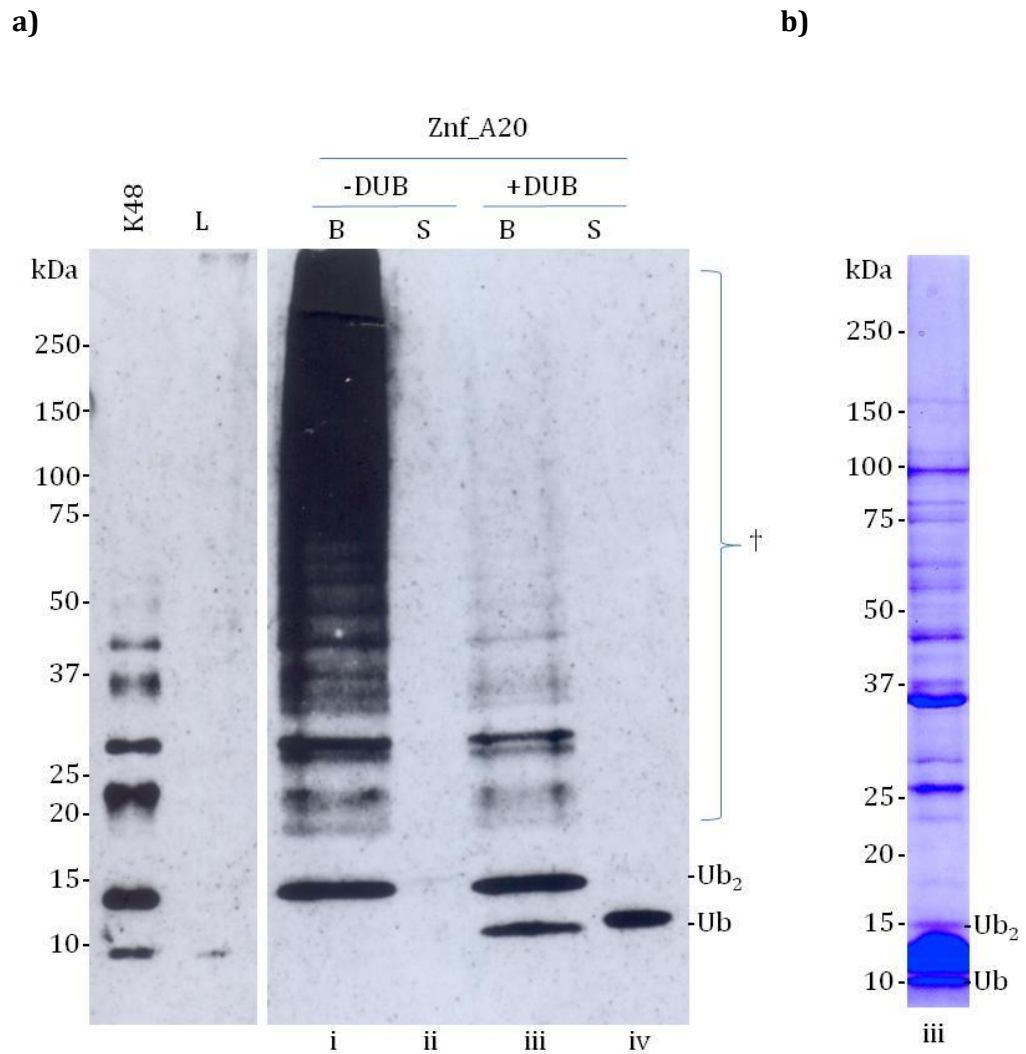


**Figure 5.5 a)** Anti-ubiquitin Western blot from Figure 4.14 (details of purification in Fig 4.14) and corresponding **b)** Coomassie stained gel of lane iii, of deubiquitinated Znf\_A20 captured rat muscle proteins, from 100 $\mu$ l Znf\_A20 beads (10-fold more protein loaded than equivalent lane iii in part a)). Proteins highlighted by † are a smear of ubiquitinated proteins. (K48)=0.25 $\mu$ g K48-linked polyubiquitin, (L)=Load 1/80<sup>th</sup> lysate loaded onto beads, (B)=beads, (S)=solution.

## 5.6. Unanchored polyubiquitin chains

### 5.6.1. Physiological significance of unanchored polyubiquitin chains

Studies into the molecular binding and structure of polyubiquitin are often based on the simplest possible model, Ub<sub>2</sub> [235-239], as opposed to considering it as a valid *in vivo* species. Polyubiquitin structure varies depending on ubiquitin linkage. This is evident in anti-ubiquitin blots of commercially produced K48- and K63-linked polyubiquitin. *In vitro* produced K48 or K63 chains contain practically identical molecular weight polyubiquitin chains that vary by only 28Da per monomer, as commercial K63-linked polyubiquitin chains are synthesised from wild type ubiquitin, but K48-linked chains are synthesised using a ubiquitin K29R mutant to prevent polymerisation at this residue. However, despite the negligible mass difference, chains longer than Ub<sub>2</sub> in K48- or K63-linked chains migrate differently, as linkage affects structure and thus migration through the polyacrylamide gel. Whilst structures of linear, K48-, K63-, K6- and K11-linked Ub<sub>2</sub> have been revealed by crystallography/nuclear magnetic resonance (NMR) analysis using *in vitro* synthesised polyubiquitin chains [187, 236, 239, 240], there is very little evidence confirming successful identification of “unanchored” ubiquitin dimers or polyubiquitin chains from an *in vivo* source to date.

Unanchored polyubiquitin chains have become of increasing interest as potential regulators of ubiquitin-mediated processes. Free chains synthesised *in vitro* were found to compete with polyubiquitinated substrates for binding to the proteasome [68] and accumulation of free chains in cells as a result of isopeptidase T (isoT) knockdown inhibited degradation of polyubiquitinated p53

by the 26S proteasome [177]. Free chains were additionally proposed to act as a source of monoubiquitin, which is depleted by increased polyubiquitination under heat stress conditions in *S. cerevisiae*, regulated by deubiquitinating enzyme Doa4 and its inhibitor regulator of free ubiquitin chains 1 (Rfu1) [178]. Further to this, recent studies have highlighted a potential role of unanchored K63-linked chains in both activating kinases [179] and in signalling during innate immunity [180, 181]. Studies have mostly focused on longer unanchored polyubiquitin chains, but interestingly a possible role has been identified for Ub<sub>2</sub>; *in vitro* studies into the deubiquitinating enzyme ubiquitin carboxyl-terminal hydrolase isozyme L3 (UCH-L3) revealed its hydrolase activity was reduced in the presence of K48-linked Ub<sub>2</sub> [241]. Further detail on the physiological significance of unanchored chains is provided in Section 5.7.2. Similarly to conjugated ubiquitin chains, in which different linkages are associated with different biological processes, the roles of unanchored chains also seem to exhibit linkage specificity. This highlights the importance of identifying ubiquitin linkage, should analysis confirm the spared ubiquitin species to be a ubiquitin dimer.

#### **5.6.2. PMF analysis confirms ubiquitin sequence in the presumed ubiquitin dimer purified using Znf\_A20 domain**

Previous PMF data confirmed the presence of both monoubiquitin and diubiquitin from rat muscle captured on FL rZNF216 Sepharose (Chapter 4). However, subsequently revised affinity capture conditions included inhibition of endogenous deubiquitinating enzyme (DUB) activity using N-ethylmaleimide (NEM), and consequently monoubiquitin was not captured. This suggests that monoubiquitin may have previously been liberated post-affinity capture from longer polyubiquitin chains by co-purifying catalytically active DUBs. In the

absence of polyubiquitin processing by *in vivo* DUBs, a species co-migrating with the ubiquitin dimer of commercial unanchored polyubiquitin chains is still captured, as observed by anti-ubiquitin immunoblotting. Interestingly, this species resists the deubiquitinating activity of USP2 (Fig 5.5a). Affinity capture was performed using the Znf\_A20 domain alone, as opposed to FL rZNF216, from rat muscle. To confirm the capture of Ub<sub>2</sub> on the Znf\_A20 domain and identify the protein spared from deubiquitination, we excised the corresponding band from a Coomassie stained gel of Znf\_A20 captured rat muscle proteins treated with USP2 core (Fig 5.5b). Bound proteins were eluted from beads by the addition of gel application buffer and approximately 10 times more sample was loaded for Coomassie staining relative to anti-ubiquitin immunoblotting, to account for lower sensitivity. The Coomassie-stained gel from which bands were excised and analysed by matrix-assisted laser desorption/ionisation (MALDI) PMF (from USP2 treated Znf\_A20 Sepharose beads) and the corresponding anti-ubiquitin Western blot (from Figure 4.14) are shown in Figure 5.5 (b and a, respectively). PMF analysis of the band corresponding to the presumed ubiquitin dimer confirmed the presence of five peptides corresponding to ubiquitin (referred to later, in Figure 5.8c), covering 55% of the ubiquitin sequence. This provides strong evidence that the purified protein indeed represents diubiquitin. To substantiate PMF results, we analysed the sample using electrospray ionisation (ESI)-MS (Fig 5.6) in the absence of tryptic digest to perform intact mass analysis with high accuracy. The ubiquitin species was eluted directly from beads using formic acid. Purification of a free ubiquitin dimer was confirmed as the intact mass was identical to that of an unanchored and unmodified ubiquitin dimer, with a monoisotopic mass of 17120Da.

**Figure 5.6**

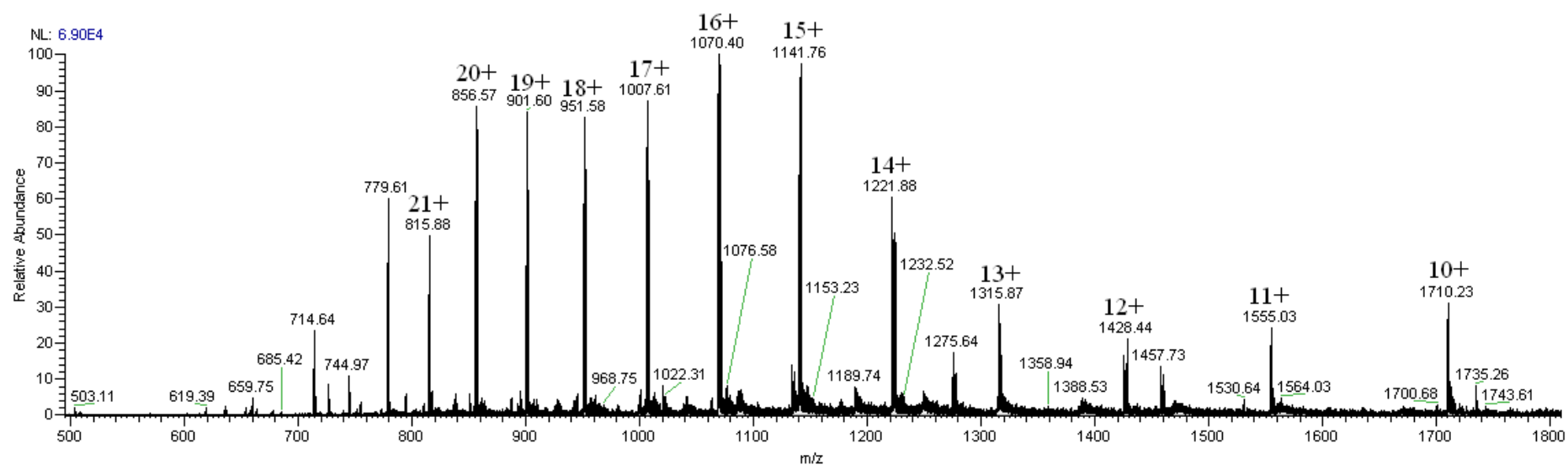


**Figure 5.6** ESI-MS of Ub<sub>2</sub> purified from rat skeletal muscle. The observed mass is identical to that of unanchored, unmodified Ub<sub>2</sub>, with a monoisotopic mass of 17120Da.

### **5.6.3. The Znf\_A20-purified ubiquitin dimer from skeletal muscle is K48-linked**

#### **5.6.3.1 Evidence from K48-polyubiquitin specific immunoblotting of the ubiquitin dimer**

Evidence of an isopeptide linkage between two ubiquitin proteins would further substantiate the purification of an endogenous ubiquitin dimer, as well as possibly providing information related to ubiquitin linkage selectivity of the Znf\_A20 domain (and by extension ZNF216's substrates). We used an antibody that only binds to K48-linked polyubiquitin [234] and anti-ubiquitin (that recognises all linkages) to probe rat skeletal muscle proteins bound both to untreated Znf\_A20 Sepharose and partially deubiquitinated Znf\_A20 Sepharose (incubated +/- USP2 core for 1 hour rather than the previous 2 hour deubiquitination in Figures 4.15 and 5.5) (Fig 5.7). The anti-K48 antibody does not detect commercial K63 polyubiquitin chains or monoubiquitin, but does detect commercial K48 chains, as expected. Interestingly, the ubiquitin dimer was detected weakly by the K48 antibody. The corresponding band was detected in both +/- USP2 treated samples, by both antibodies. This provides evidence that the ubiquitin dimer that is spared from deubiquitination may be K48-linked. This then raises the question of whether other linkage dimers are also spared from deubiquitination. The smear of longer polyubiquitinated proteins bound to Znf\_A20 Sepharose that was not deubiquitinated is both anti-ubiquitin and anti-K48 positive, as is a ladder that appears in the partially deubiquitinated sample. Should this ladder in the partially deubiquitinated sample represent unanchored polyubiquitin, then it appears chains of up to 13 ubiquitin moieties in length can be detected. The significance of this ladder will be discussed later (Section

**Figure 5.7**

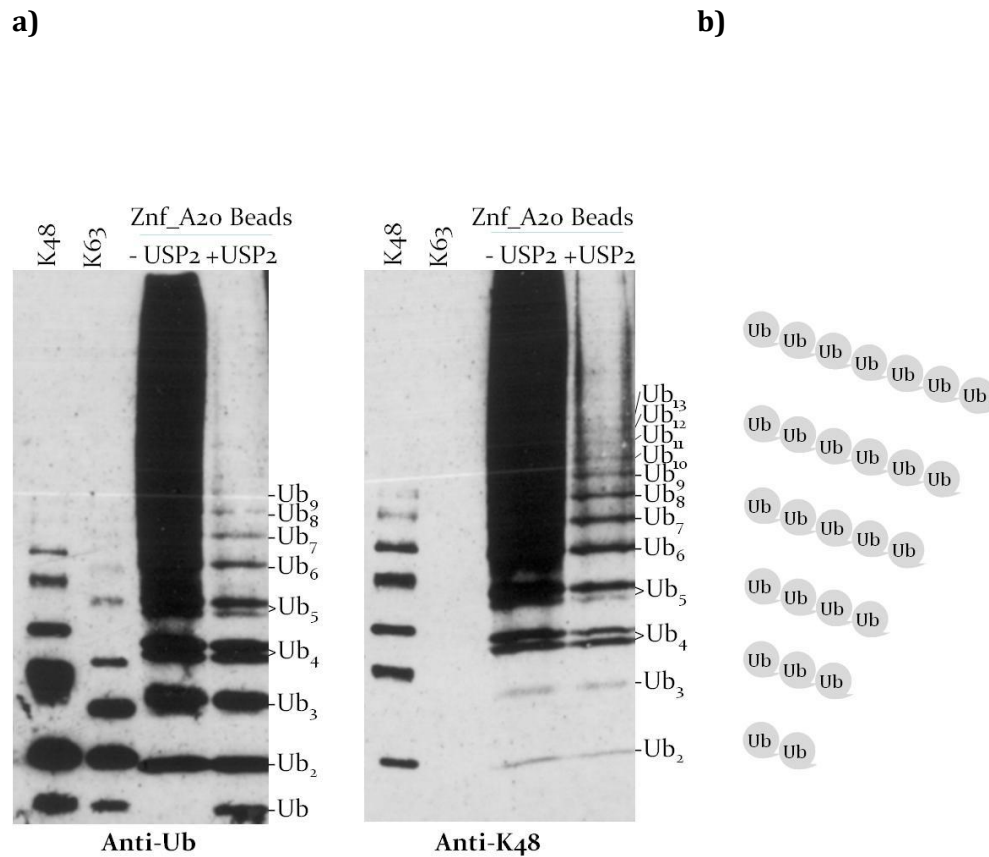


**Figure 5.7** Limited deubiquitination of Znf\_A20 Sepharose-captured ubiquitinated proteins reveals a ladder consistent with free polyubiquitin chains. **a)** Rat muscle proteins were captured on Znf\_A20 Sepharose, as in Fig 4.14, but instead incubated +/- USP2 core for only 1hr at 37°C, and 2-fold more protein loaded. Limited deubiquitination revealed a number of ubiquitin bands as opposed to a smear of polyubiquitinated proteins, observed using both anti-ubiquitin and anti-K48 linkage specific antibodies. (K48)=0.25µg K48-linked polyubiquitin, (K63)=0.25µg K63-linked polyubiquitin. **b)** Diagrammatic representation of free ubiquitin chains from Ub<sub>2</sub> to Ub<sub>7</sub>.

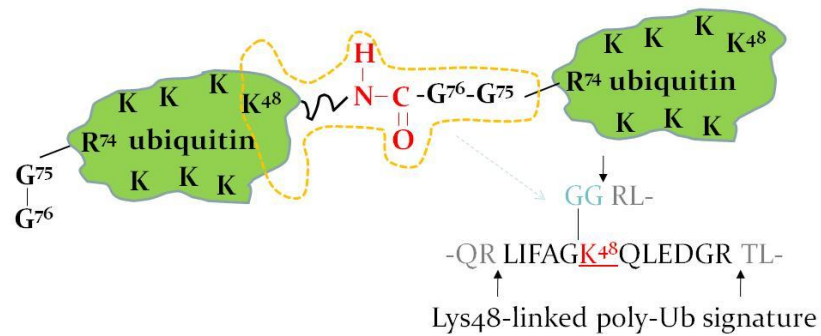
5.6.10). It is also notable that the bands that may correspond to free polyubiquitin up to Ub<sub>5</sub> in length are also detectable in non-deubiquitinated beads by both anti-ubiquitin and anti-K48 antibodies. Interestingly, we noted a doublet of both anti-ubiquitin and anti-K48 positive bands, one band within the doublet comigrating with K48-linked tetraubiquitin, suggesting we may have also purified unanchored tetraubiquitin. The other band within the doublet may be a ubiquitinated substrate or may possibly be an unanchored polyubiquitin chain of mixed linkage (i.e. including, but not exclusively, the K48 linkage). Having established that ubiquitin linkage effects chain migration, this variance in migration may be due to the presence of different linkages altering the structure enough to retard its migration through the polyacrylamide gel.

#### **5.6.3.2. Mass spectrometry analysis confirms the K48 linkage within the ubiquitin dimer**

To confirm immunoblotting results that indicate the presence of the K48-linkage in the Znf\_A20-purified ubiquitin dimer, we reanalysed earlier PMF data. Other ubiquitin linkage specific antibodies were not available to us at this time to test for other linkages, and so MS analysis provided an unbiased method to identify the presence of other linkages and validate immunoblotting data. As discussed previously, MALDI PMF analysis involves initial trypsin cleavage of proteins to distinctive peptides, as this enzyme cuts proteins specifically at the carboxyl side of lysine or arginine residues, with the exception of those followed by a proline residue. Polyubiquitin chains typically form *via* linkage of the C-terminus of one ubiquitin to a lysine residue within another ubiquitin. Alternatively ubiquitin can link in a linear manner, by condensation of the C-terminal glycine (Gly76) of one ubiquitin to the N-terminal methionine (Met1) of another. Ubiquitin isopeptide

**Figure 5.8**

**a)**



**b)**

| Name | Seq*                    | exp MH <sup>+</sup> |
|------|-------------------------|---------------------|
| K6   | MQIFVKTLTGKGG           | 1379.77             |
| K11  | TLTGKTITLEVEPSDTIENVKGG | 2402.26             |
| K27  | TITLEVEPSDTIENVKAKGG    | 2101.10             |
| K29  | AKIQDKGG                | 816.45              |
| K33  | IQDKEGIPPDQQRGG         | 1637.81             |
| K48  | LIFAGKQLEDGRGG          | 1460.88             |
| K63  | TLSDYNIQKESTLHLVLRGG    | 2244.19             |

**c)**

| Observed  | Mr (expt) | Mr (calc) | Delta   | Start | End | Miss | Peptide                |
|---|-----------|-----------|---------|-------|-----|------|------------------------|
| 1039.5300   | 1038.5227 | 1038.5094 | 0.0133  | 34    | 42  | 0    | K.EGIPPDQQR.L          |
| 1067.6200   | 1066.6127 | 1066.6135 | -0.0008 | 64    | 72  | 0    | K.ESTLHLVLR.L          |
| 1523.7500   | 1522.7427 | 1522.7740 | -0.0312 | 30    | 42  | 1    | K.IQDKEGIPPDQQR.L      |
| 1787.8700   | 1786.8627 | 1786.9200 | -0.0573 | 12    | 27  | 0    | K.TITLEVEPSDTIENVK.A   |
| 2130.0600   | 2129.0527 | 2129.1480 | -0.0953 | 55    | 72  | 1    | R.TLSDYNIQKESTLHLVLR.L |
| <b>No match to:</b> <span style="border: 1px solid black;">1460.7700</span> 1566.7500, 2173.0600, 2399.2800 |           |           |         |       |     |      |                        |

**Figure 5.8** PMF analysis of USP2 spared Ub<sub>2</sub> species captured from rat skeletal muscle on Znf\_A20-Sepharose (Ub<sub>2</sub> in Figure 5.5b). **a)** A diagrammatic representation of the unique branched peptide resulting from trypsin cleavage of K48-linked polyubiquitin. **b)** Expected monoisotopic “signature” masses from branched peptides liberated by trypsin cleavage for different polyubiquitin linkages. **c)** Results of PMF analysis of the USP2 spared ubiquitin band. Five ubiquitin peptides were identified, and one of the “unmatched” peptides matches the expected monoisotopic mass of the branched peptides generated by tryptic cleavage of the K48-linkage (as highlighted).

linkage can occur at any of 7 lysine residues within ubiquitin. Upon trypsin cleavage, isopeptide bonds between ubiquitins are not broken and the lysine involved in the linkage is not proteolysed, and so for each type of linkage a specific branched peptide, or unique “signature” peptide, remains (a di-glycine “stub”, characteristic of different polyubiquitin linkages) (Fig 5.8a). Although the MASCOT database contains information linking peptide mass to predicted amino acid sequences liberated by trypsin cleavage, it does not contain predicted masses for the branched polyubiquitin signature peptides that result from tryptic digestion. A table in Figure 5.8b contains calculated monoisotopic masses of theoretical branched peptides resulting from cleavage of polyubiquitin of specific linkages. The original PMF results of the ubiquitin dimer are in Figure 5.8c, in which we saw five peptides that matched ubiquitin and covered 55% of the ubiquitin sequence (see Section 5.6.2), but additionally some peptides were “unmatched” to the ubiquitin fingerprint within the MASCOT database. Manual analysis of peptide masses that previously identified diubiquitin in the Znf\_A20-purified fraction revealed an unmatched peptide of mass 1460.77 Da. This closely matches the calculated size of the branched peptide liberated from trypsin cleaved K48-linked polyubiquitin (Fig 5.8b). Molecular masses generated by this type of MS are accurate within 0.01%, thus an expected peptide of mass 1460.88 may be detected +/- 0.14 Da (between 1460.74-1461.02 Da), which places the unmatched peptide within range. Interestingly, manual analysis of earlier PMF data from 2DE analysis of FL rZNF216 captured proteins reveals the presence of an unmatched peptide of 1460.81 Da (not shown) (also within range) in the presumed diubiquitin spot that is absent from the monoubiquitin spot (Fig 4.9), again supporting that notion that this unmatched peptide represents the K48-linked signature peptide. The presence of ubiquitin peptides, combined with a peptide mass matching that derived from the K48-linkage that was additionally

absent from a monoubiquitin sample provides strong evidence that the Znf\_A20 domain binds to a K48-linked dimer. Peptides with masses equivalent to other ubiquitin signature peptides were not detected, perhaps indicating that the Znf\_A20 domain specifically binds K48-linked diubiquitin. However, previously rZNF216 was shown to bind equally well to commercial K48 and K63-linked polyubiquitin chain mixtures (Fig 4.3) including dimers from the mix. Alternatively, it may be that other linkages could bind to Znf\_A20 but are not present in high enough concentrations *in vivo* to be detected or may not exist at all. Finally, the sensitivity of detection of other ubiquitin linkage signature peptides by MALDI MS is not known. To definitively confirm that the unmatched peptide identified by PMF was indeed the signature peptide predicted from K48-ubiquitin linkage tryptic digestion, peptides were fragmented using collision induced dissociation (CID) (Fig 5.9) and electron-capture dissociation (ECD) (not shown). Peptides were positively ionised and sequenced using MS/MS, performed by Lucy Roach. MS/MS confirmed the sequence of the K48-linkage signature peptide, and validated accumulating data that we have purified an *in vivo* unmodified (see Section 5.7) K48-linked diubiquitin species from rat muscle.

#### **5.6.3.4. The Znf\_A20 domain shows no apparent ubiquitin linkage specificity in the gas phase**

Our observations that immobilised Znf\_A20 readily precipitates *in vitro* generated K48- and K63-linked polyubiquitin chains including dimers suggests the domain has no clear intrinsic binding specificity for (these) polyubiquitin linkages (binding to K48 linkages shown in Figure 4.13b, K63 binding not shown). Consistent with this proposal, ESI-MS, used to monitor the interaction between the Znf\_A20 domain and monoubiquitin or diubiquitin (K48- and K63-

**Figure 5.9**

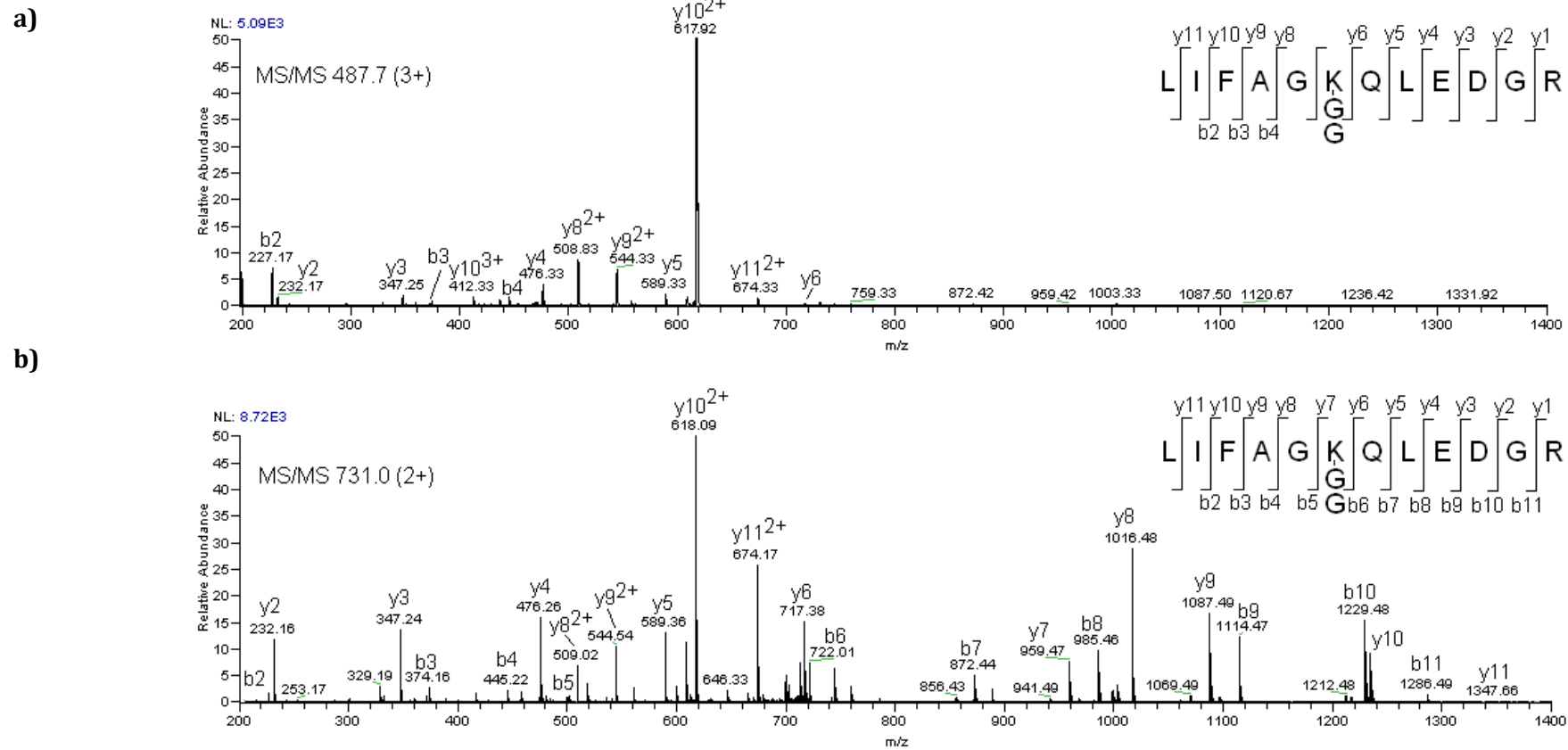


**Figure 5.9** Evidence for K48-linkage within Ub<sub>2</sub> purified from rat skeletal muscle by CID analysis. CID tryptic peptide LIFAGKQLEDGR containing the K48 (gly-gly) tag a) MS/MS of [M+3H]<sup>3+</sup> at m/z 487.7 b) MS/MS of [M+2H]<sup>2+</sup> at m/z 731.0.

linked) in the gas phase, indicated almost identical  $K_d$ 's for the 1:1 complexes, with no apparent linkage selectivity (performed in collaboration with Neil Oldham, not shown).

To further investigate the structural basis of ubiquitin recognition by ZNF216 and its Znf\_A20 domain, we performed a collaborative analysis (Mark Searle, School of Chemistry) to investigate how the Znf\_A20 domain binds to ubiquitin.

#### **5.6.4. The Znf\_A20 domain binds *via* the acidic D58 interaction surface on ubiquitin**

While many proteins are covalently monoubiquitinated or polyubiquitinated, there are also proteins (such as ZNF216) that non-covalently bind to ubiquitin *via* one of 3 binding surfaces, which are described according to the key residues required for interaction; D58 [139], I44 [140] and GG (at the C-terminus) [141]. Point mutations at these key residues interfere with ubiquitin-binding, and provide a simple route to determine which ubiquitin binding surfaces receptor proteins interact with. Ubiquitin mutants with mutations in these sites (I44A, D58A, des-G75-G76) were dot-blotted onto a membrane and incubated with GST-rZNF216 protein (work by previous lab member James Cavey [217]). Unbound protein was removed by washing, and anti-GST used to identify which ubiquitin mutants GST-rZNF216 would bind to (Fig 5.10). The double cysteine mutant GST-rZNF216 did not bind to any ubiquitin proteins, whilst wild type GST-rZNF216 bound all mutant ubiquitin with the exception of D58A, indicating that rZNF216 binds ubiquitin at the D58 face of ubiquitin. Interestingly, this corresponds with

**Figure 5.10**

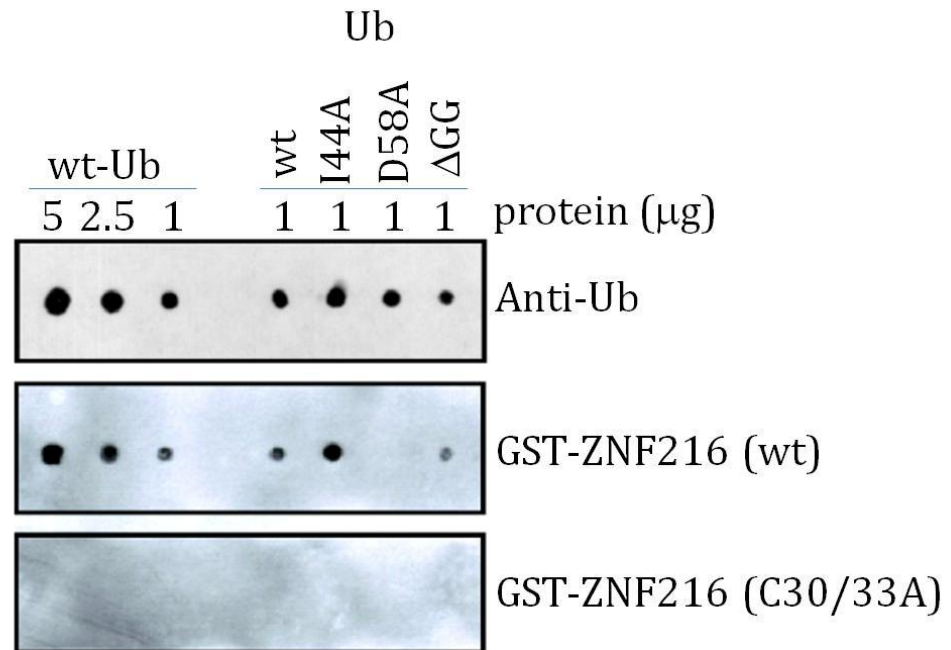


**Figure 5.10** ZNF216 binds *via* the D58 binding surface. Wild type ubiquitin and ubiquitin mutants I44A, D58A and  $\Delta$ -G75-G76 were dot-blotted onto a membrane, as observed by anti-ubiquitin, and incubated with GST-rZNF216 (wt) or GST-ZNF216 (C30/33A), from the equivalent of  $\sim$ 1ml of overexpressed bacterial cultures. Unbound protein was removed by washing and bound protein was probed with anti-GST. The double cysteine mutant GST-rZNF216 did not bind to any ubiquitin proteins, but wild type GST-rZNF216 bound all mutant ubiquitin except for D58A. (Work by James Cavey [217])

other reports of Znf\_A20 domains binding at the D58 surface, such as zinc finger 4 (ZnF4) of the A20 protein [139] and the Znf\_A20 domain of Rabex-5 [185, 242].

#### **5.6.5. Structural models of monoubiquitin and diubiquitin binding Znf\_A20**

Evidence of rZNF216 binding ubiquitin *via* its D58 surface and the notion that Znf\_A20 does not bind with linkage specificity (as shown by ESI-MS, Section 5.8.3) is supported by structural models of the Znf\_A20 domain in complex with ubiquitin and diubiquitin; the structure of the Znf\_A20-Ub complex was experimentally determined in a parallel collaborative project (Fig 5.11). Further analysis of this complex showed that Znf\_A20 binding does not occlude any of the seven lysine residues of ubiquitin involved in isopeptide linkages within polyubiquitin chains and binds at the D58 binding surface. Further, close inspection of models of Znf\_A20 domains in complex with different ubiquitin dimers (K48 open and closed conformations, K63, K11, K6 and linear; PDB structures 2PE9, 2PEA, 2JF5, 2XEW, 2XK5, 2W9N respectively) generated by replacing monoubiquitin units from the published structures of the dimers with ubiquitin-Znf\_A20 structures, did not indicate additional contacts of a single Znf\_A20 with the second ubiquitin in the dimers (Fig 5.12) (work done by Tom Garner). In each case the D58 surfaces of ubiquitin moieties within the dimers, required for recognition by the Znf\_A20 domain, were surface exposed. Thus, given that our purification strategy using the Znf\_A20 domain resulted in the isolation of exclusively K48-linked diubiquitin from skeletal muscle, when all seven of ubiquitin's lysine residues can participate in polyubiquitin chain formation, this suggests that the K48-linked form may be the predominant dimer *in vivo* since other dimers should have been purified were they present.

**Figure 5.11**

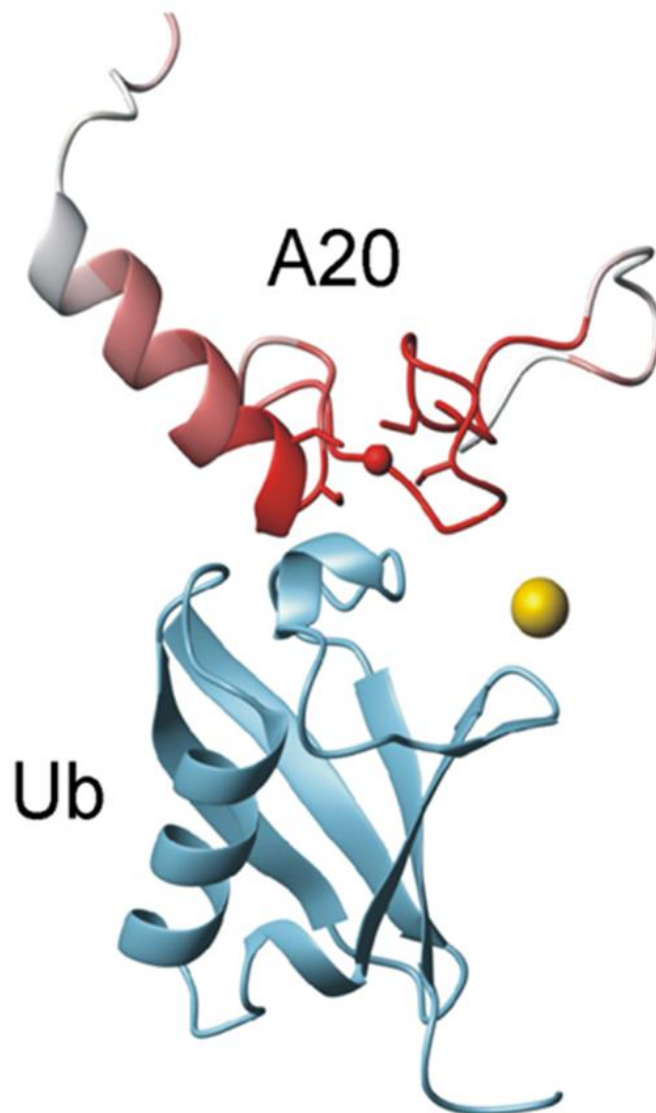


**Figure 5.11** Structural model of the Znf\_A20 domain in complex with ubiquitin, which binds at the D58 binding surface. (Work by Tom Garner [217])

**Figure 5.12**

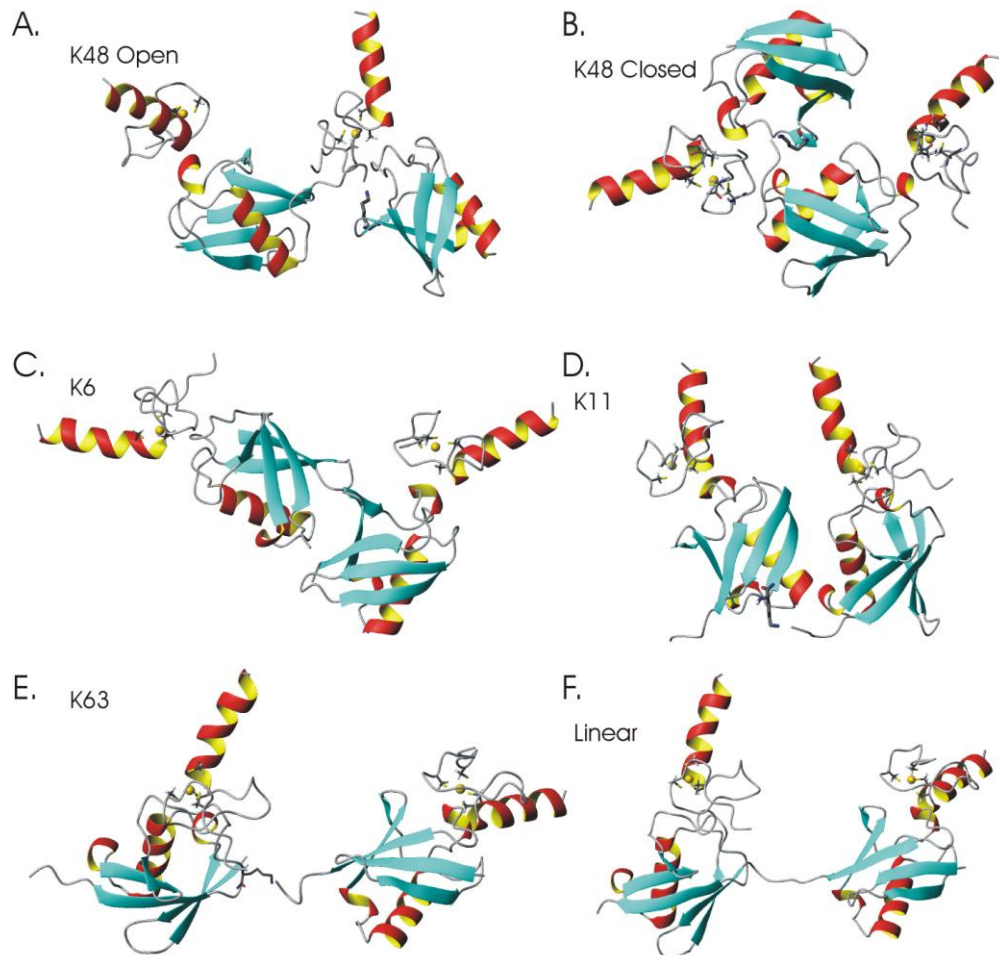


**Figure 5.12** Model of the Znf\_A20 in complex with K48-linked diubiquitin in its open (A) and closed (B) conformation and with diubiquitin linked through K6 (C) and K11 (D) and K63 (E) and to linear diubiquitin (F). Models are based on the complex presented in Figure 5.11 and PDB structures 2PE9, 2PEA, 2XK5, 2XEW, 2JF5 and 2W9N. (Work by Tom Garner).

Inspection of the structures of Znf\_A20 domains in complex with the open conformation of K48-Ub<sub>2</sub> did, however, reveal the possibility of steric clashes between the distal ubiquitin of the dimer and the Znf\_A20 in complex with the proximal ubiquitin, suggesting preferential binding of two Znf\_A20 domains to the closed conformation. Interestingly, within this closed conformation the I44 surface of ubiquitin, which is commonly recognised by many other ubiquitin-binding domains (UBDs)/ubiquitin-binding receptors, is occluded. Indeed pull-down analyses from skeletal muscle samples using commercial “TUBEs” (tandem-repeated ubiquitin-binding entities) based on head to tail repeats of UBA domains which recognise I44 of ubiquitin – at an equimolar concentration to the Znf\_A20 domain - did not result in the purification ubiquitin dimers (Fig 5.13), as assessed by Western blotting. The lack of diubiquitin binding to TUBEs, which did not bind K48-linked diubiquitin, supports that notion that other linkages within ubiquitin dimers may not exist (or predominate) *in vivo*.

#### **5.6.6. Sparing of K48-Ub<sub>2</sub> from USP2-mediated deubiquitination**

We next sought to rationalise why the Znf\_A20-bound K48-Ub<sub>2</sub> was spared from processing by the USP2 core enzyme, which has previously been shown to be a versatile tool for the *in vitro* removal of ubiquitin from ubiquitin conjugates [243]. As noted earlier, examination of the structural models of K48-Ub<sub>2</sub> in complex with two Znf\_A20 domains (Fig 5.12) showed no evidence of steric hindrance of the isopeptide bond within the ubiquitin dimer by either of the Znf\_A20 domains. Consequently, we predicted that other co-precipitating ubiquitin receptors from the muscle sample, which are able to form ternary complexes with a single Znf\_A20:Ub moiety through other interaction surfaces on ubiquitin, may provide the steric block which protects the ubiquitin dimer from

**Figure 5.13**

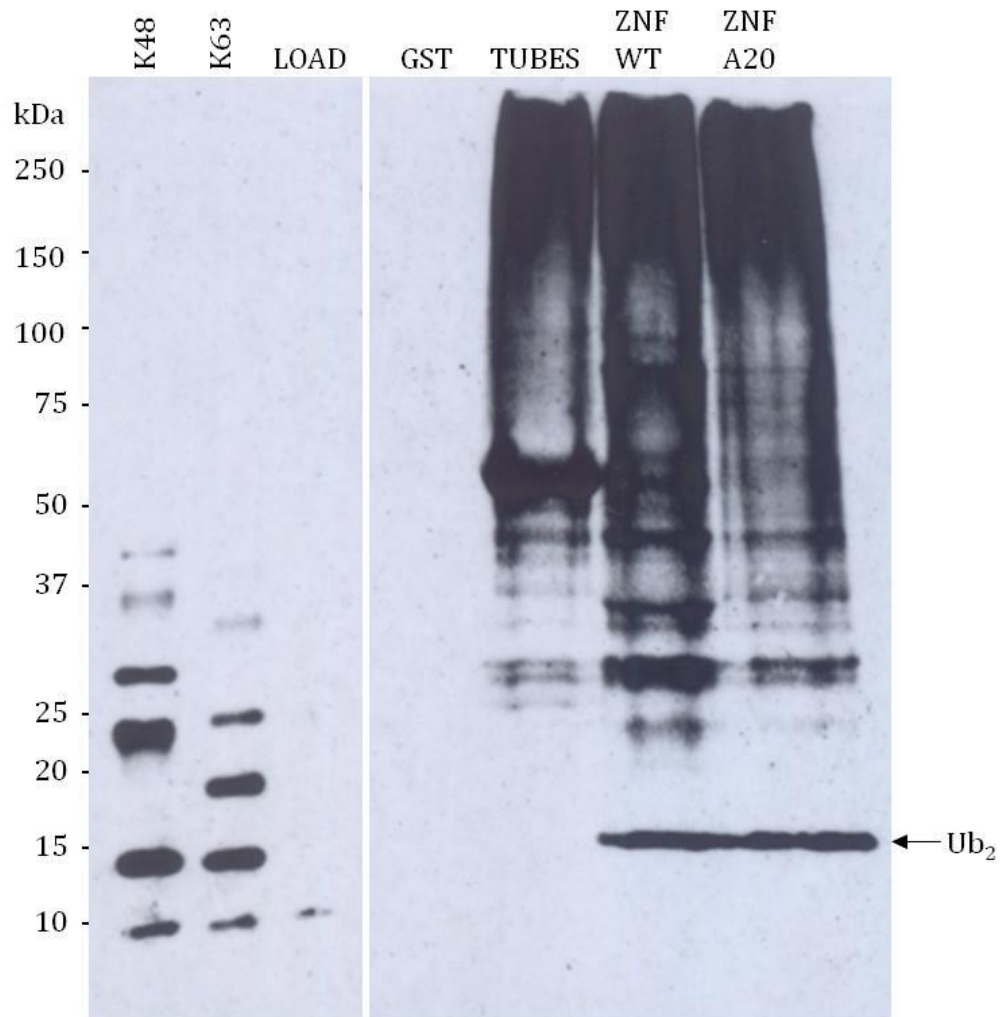


**Figure 5.13** Commercial TUBEs fail to purify diubiquitin from skeletal rat muscle (~1.5g) that was homogenised in 4ml homogenising buffer and treated identically to that described in Figure 4.14, up to and including wash steps. Supernatant was split 4 ways and incubated with 20 $\mu$ l TUBEs-, GST-, ZNF216 WT- or Znf\_A20-Sepharose overnight at 4°C. TUBEs (GST-RAD23; 35mg/ml) and GST were bound to glutathione Sepharose while ZNF216 WT and Znf\_A20 were covalently coupled to CNBr Seph 4B. All were bound/coupled to Sepharose at approximately equimolar concentrations. 100% of bound protein was loaded. Anti-ubiquitin immunoblotting revealed that no ubiquitinated proteins bound GST alone, but did bind to all other Sepharose. (K48)=0.25 $\mu$ g K48-linked polyubiquitin, (K63)=0.25 $\mu$ g K63-linked polyubiquitin, (L)=Load 1/400<sup>th</sup> lysate loaded onto beads.

deubiquitination. This seems likely as evidenced from the co-precipitation of *in vivo* deubiquitinating enzymes (activities) in the absence of NEM. Consistent with this proposal we noted that K48-Ub<sub>2</sub> from a commercial polyubiquitin chain mixture was not spared from processing by USP2 when bound to the Znf\_A20 domain on beads (Fig 4.6). Additionally, we found it is possible to co-precipitate the p62 ubiquitin-receptor with ubiquitinated proteins from cultured cells using immobilised wild type rZNF216 protein, but not with the C30/33A mutant (Fig 5.14) i.e. simultaneous binding of multiple ubiquitin receptors to the same ubiquitin or polyubiquitin chain(s) is possible [217]. Equally, it is possible that binding of one ubiquitin receptor to a polyubiquitin chain sterically blocks another ubiquitin binding protein. Some ubiquitin receptors exhibit linkage specificity, as noted in Chapter 4, that may bind non-K48 linked polyubiquitin. Thus it is possible that other linkage ubiquitin dimers exist, but are bound by *in vivo* ubiquitin receptors that inhibit that Znf\_A20 domain from binding at the D58 surface, thus preventing capture of other linkage polyubiquitin chains *via* our purification strategy.

#### **5.6.7. The Znf\_UBP domain of isopeptidase T binds the free C-terminus of unanchored polyubiquitin**

Identification of K48-Ub<sub>2</sub> in our Znf\_A20 domain-purified fractions and evidence of longer chains present after limited USP2 treatment drew our attention to the existence of unanchored polyubiquitin in tissue samples; however, the Znf\_A20 domain binds both unanchored and anchored polyubiquitin, which led us to consider an alternative method for selective purification of free chains. To determine the complement of unanchored polyubiquitin chains which exist *in vivo*, including ubiquitin dimers, we reasoned that a common property of

**Figure 5.14**

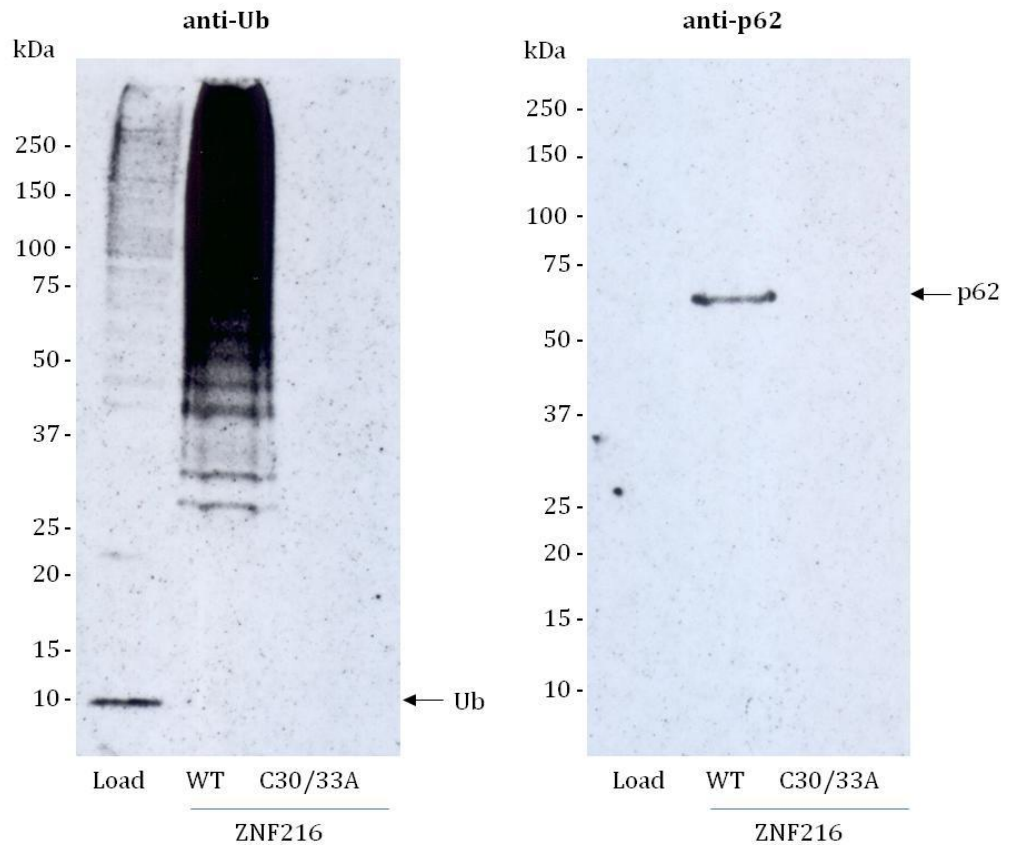


**Figure 5.14** Endogenous p62 co-purifies with ubiquitinated proteins purified from U2OS cells captured on rZNF216 WT Sepharose, but not on the double cysteine C30/33A rZNF216 mutant which does not bind polyubiquitin. U2OS cells (~6mg protein) were homogenised (in 8ml of 50mM Tris, 150mM NaCl, 0.5% NP-40, 5mM N-ethylmaleimide, 20µM MG132, 0.1% mammalian protease inhibitor cocktail (Sigma), pH 7.5) and centrifuged. DTT added to the supernatant to a final concentration of 10mM, and mixed at 4°C for 15 minutes. Supernatant split between 50µl of WT or mutant Sepharose and incubated overnight at 4°C. Beads were washed three times in wash buffer (50mM Tris, 150mM NaCl, 0.5% NP-40, 1mM DTT, pH 7.5), and 50% probed with anti-ubiquitin or anti-p62. Load= 1/80<sup>th</sup> protein loaded onto beads.

unanchored ubiquitin chains is a free C-terminus. As an alternative route to purifying diubiquitin and possibly longer unanchored polyubiquitin chains, we cloned a ubiquitin-binding domain (Znf\_UBP or BUZ domain) of isoT. IsoT is the human homologue of *S. cerevisiae* deubiquitinating enzyme UBP14, that disassembles the majority of unanchored polyubiquitin [134] and the Znf\_UBP domain is responsible for binding the free C-terminus of ubiquitin but contains no intrinsic catalytic activity [141]. Purification and immobilisation of the Znf\_UBP domain provides a route to the capture of unanchored polyubiquitin regardless of its chain linkage, and binding of the previously characterised K48-Ub<sub>2</sub> would further confirm the existence and integrity of this protein. This UBD was recently utilised as part of a protein standard absolute quantification (PSAQ) method, used to selectively capture and quantify unanchored polyubiquitin [176]. We cloned the Znf\_UBP domain of human isoT from U20S cDNA (Fig 5.15a), and inserted it into the pGEX-4T-1 plasmid. GST-tagged protein was purified using glutathione-Sepharose and the GST-tag was cleaved with thrombin, as previously described for purification of FL rZNF216, the C30/33A mutant and the Znf\_A20 domain (Fig 5.15b).

#### **5.6.8. Specificity of the Znf\_UBP domain for unanchored polyubiquitin**

Purified Znf\_UBP domain was coupled to CNBr Seph 4B (at 10mg/ml) and found to bind to commercial unanchored K48 or K63-linked polyubiquitin chains, whereas control Sepharose did not (Fig 5.16a). Ub<sub>5</sub><sup>+1</sup> is a ubiquitin polymer which contains K48-linked Ub<sub>4</sub> with a proximal Ub<sup>+1</sup> moiety. This Ub<sup>+1</sup> lacks a free C-terminus, with Gly76 replaced with 20 residues of nonsense sequence, and was originally identified as a frame shift ubiquitin mutant associated with Alzheimer's disease [70]. The Znf\_A20 domain binds polyubiquitin *via* the D58

**Figure 5.15**

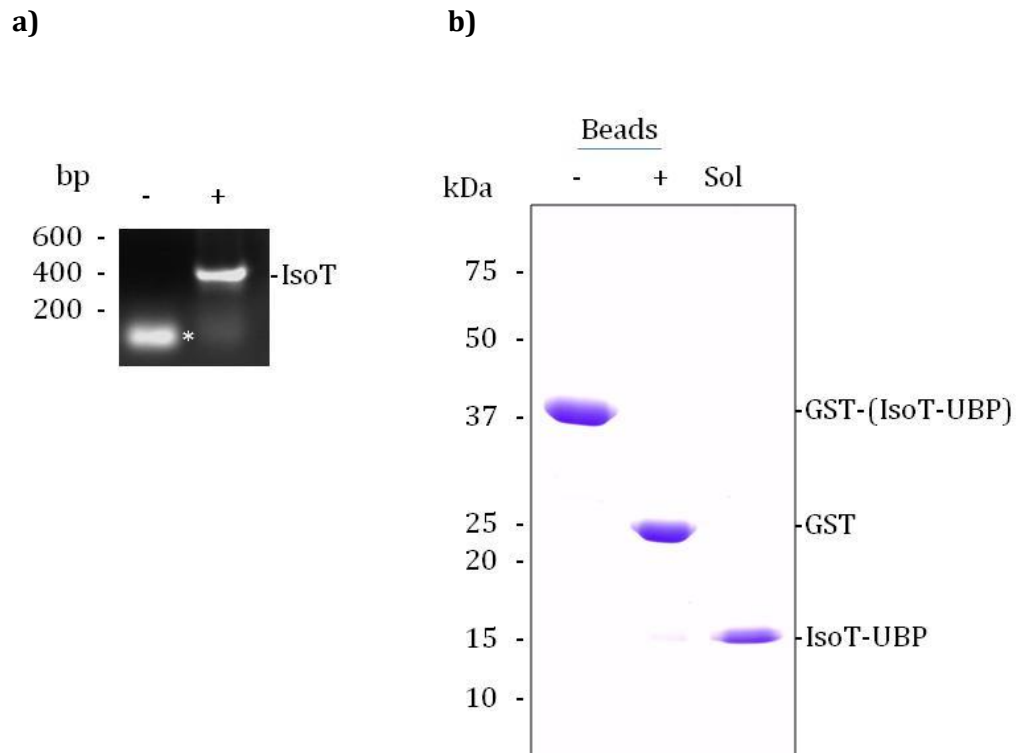


**Figure 5.15** Cloning and expression of the Znf\_UBP domain of isopeptidase T. **a)** PCR reactions were set up using primers targeted to bases 487-873 of the full length isopeptidase T mRNA sequence, +/- U20S cDNA. Samples were resolved by 1% agarose gel electrophoresis and stained with ethidium bromide. A band of the correct size (386 bp) was detected in the + cDNA sample only. \* Represents non-specific primer dimers. **b)** Capture and purification of recombinant GST-Znf\_UBP expressed in IPTG-induced *E. coli*, captured on glutathione Sepharose beads and thrombin cleaved overnight (Beads +), as described in Figure 4.5. The Znf\_UBP domain was eluted into solution (Sol), and the GST-tag remained attached to glutathione Sepharose beads.

**Figure 5.16**

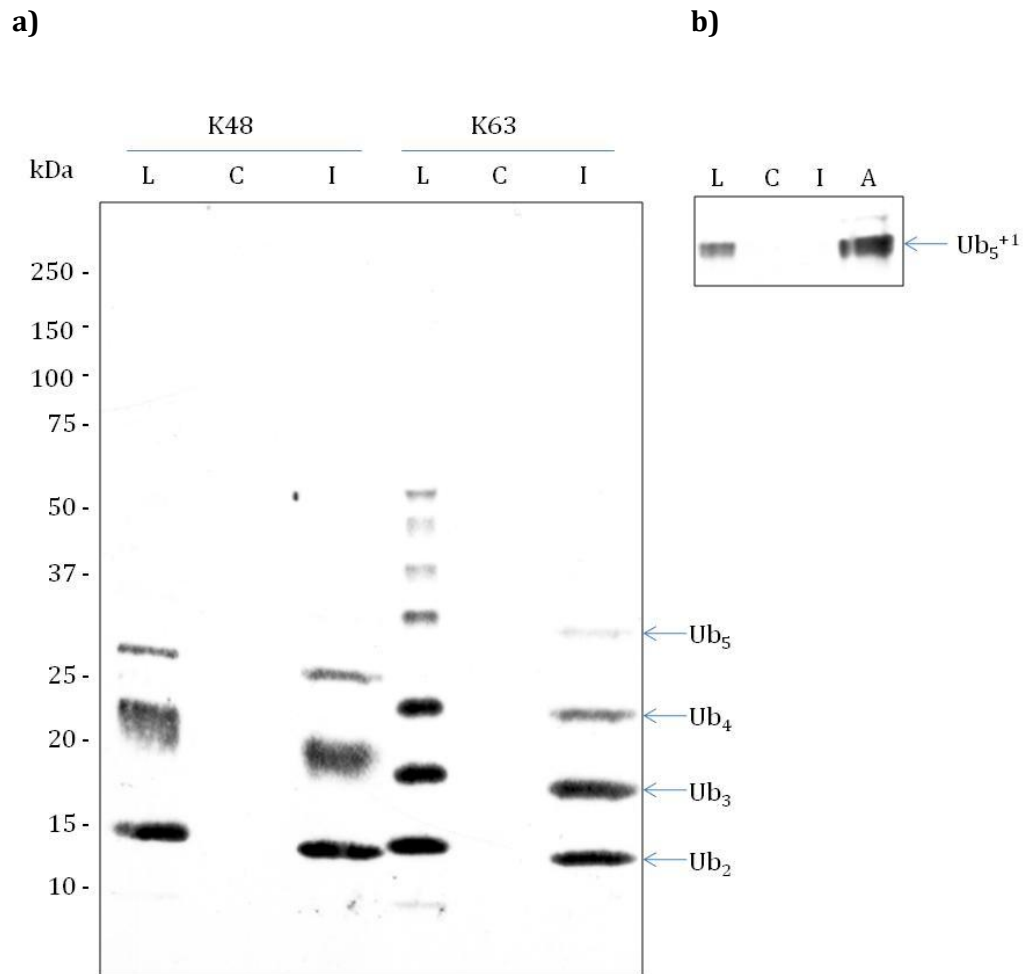


**Figure 5.16** The Znf\_UBP domain binds specifically to unanchored polyubiquitin. **a)** Znf\_UBP-Sepharose (I) or control-Sepharose (C) was incubated with 0.25 $\mu$ g of K48-linked or K63-linked polyubiquitin chains. **b)** Znf\_UBP-Sepharose (I), Znf\_A20-Sepharose (A) or control-Sepharose (C) was incubated with 0.125 $\mu$ g of Ub<sub>5</sub><sup>+1</sup>. Binding of a) and b) was in binding buffer (50mM Tris, 150mM NaCl, 0.5% NP-40, 0.1% bovine serum albumin (BSA) (Sigma) 1mM DTT, pH 7.5) for 30 minutes at 4°C. Beads were washed twice in binding buffer, bound proteins were eluted with gel application buffer, resolved by SDS PAGE and immunoblotted with anti-ubiquitin. Control Sepharose failed to bind any ubiquitin, but isoT's Znf\_UBP bound only unanchored polyubiquitin and not the Ub<sub>5</sub><sup>+1</sup> mutant, unlike ZNF216's Znf\_A20 domain. K48/K63 Load (L) represents 100% of the load. Ub<sub>5</sub><sup>+1</sup> Load (L) represents 50% of the polyubiquitin load.

interaction surface and does not require a free C-terminus for binding, thus is capable of binding to Ub<sub>5</sub><sup>+1</sup> (Fig 5.16b). However, the Znf\_UBP domain failed to bind Ub<sub>5</sub><sup>+1</sup>, consistent with its strong preference for a ubiquitin chain with a free C-terminus.

#### **5.6.9. Skeletal muscle diubiquitin binds to the Znf\_UBP domain**

To further characterise the diubiquitin species previously purified from skeletal muscle, which (based on its intact mass) should have a free C-terminus on the proximal ubiquitin, we used immobilised Znf\_UBP domain to purify proteins from rat skeletal muscle. In parallel, proteins were also purified using the Znf\_A20 domain, at an equimolar concentration. Beads with captured ubiquitinated muscle proteins were treated +/-USP2 for 2 hours, as previously, and a sample was tested by ubiquitin immunoblotting (Fig 5.17).

Monoubiquitin is present as high concentrations in the cell and has a free C-terminus. Unlike binding with immobilised Znf\_A20 domain, in which multiple Znf\_A20 proteins interact with multiple ubiquitins within a polyubiquitin chain, the Znf\_UBP domain binds only at the C-terminus of ubiquitin. Thus not only are free (unanchored) dimers and longer polyubiquitin chains captured using the Znf\_UBP domain, but monoubiquitin is also purified and due to the high concentration of the latter, it is omitted from the blot in Figure 5.17. An immunoreactive band comigrating with commercial K48- and K63-linked diubiquitin was, again, purified from skeletal muscle using the Znf\_UBP domain and notably this species was again spared from deubiquitination by USP2 (Fig 5.17).

**Figure 5.17**

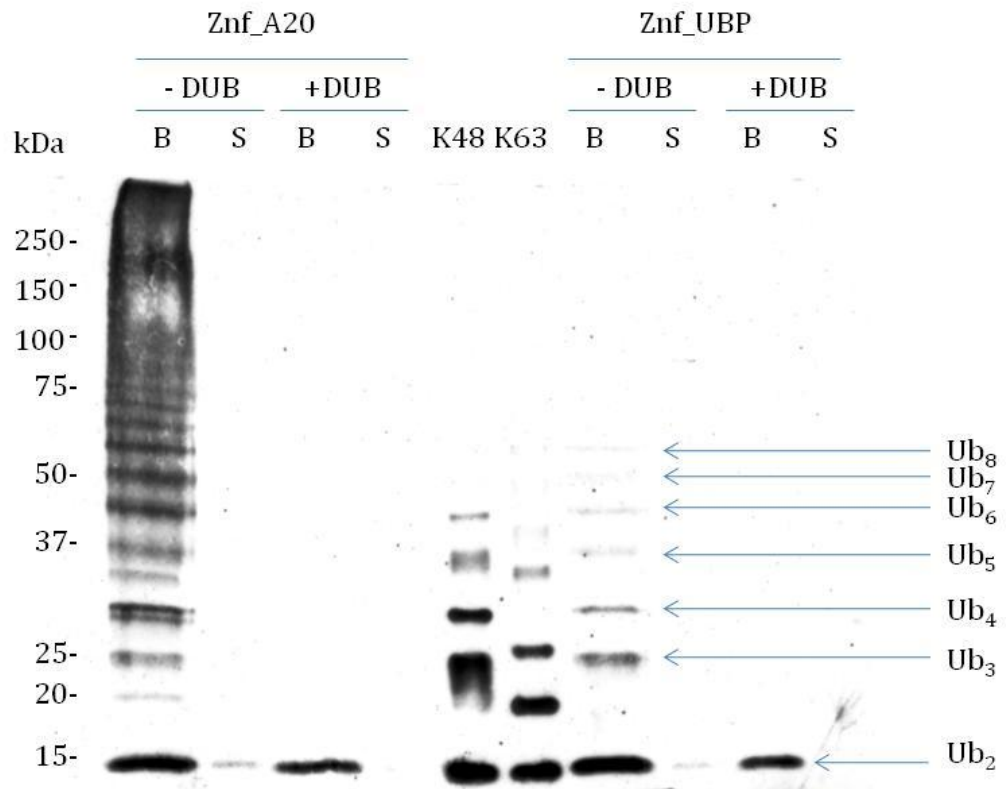


**Figure 5.17** Znf\_UBP-Sepharose bound ubiquitinated proteins co-migrated with commercial K48-linked polyubiquitin chains. Znf\_UBP- and Znf\_A20-Sepharose were incubated with rat muscle (~15g), under conditions as described in Figure 4.14, but incubated +/- 10µg USP2 core overnight at 37°C. Again, 1/40<sup>th</sup> of proteins bound to beads (B) in the absence (-DUB) and presence (+DUB) of USP2 core, and their respective solutions (S) were resolved by SDS PAGE and immunoblotted with anti-ubiquitin. Monoubiquitin avidly bound to the Znf\_UBP domain, so were omitted from the blot for clarity. Both the Znf\_A20 and Znf\_UBP bound ubiquitin dimer was spared from deubiquitination, and unanchored polyubiquitin chains as long as Ub<sub>8</sub> were detected binding to the Znf\_UBP domain. (K48)=0.25µg K48-linked polyubiquitin, (K63)=0.25µg K63-linked polyubiquitin.

#### **5.6.10. Existence of longer chains of unanchored polyubiquitin in the Znf\_UBP domain-purified fractions**

Previously, in Section 5.6.3.1, we probed partially USP2-deubiquitinated Znf\_A20 Sepharose with antibodies that detect ubiquitin and the K48-linkage. We noted the presence of a ladder containing discrete bands that remained bound to Znf\_A20 after limited deubiquitination, longer than Ub<sub>2</sub>, providing evidence that polyubiquitin chains up to 13 ubiquitin moieties in length may have been captured. Their prominent presence after partial deubiquitination implies that they may be protected, possibly by co-purifying ubiquitin receptors (such as p62, see Section 5.6.6), or that polyubiquitinated substrates are deubiquitinated by USP2 core preferentially. Znf\_UBP captured proteins in Figure 5.17 appeared to include also the unanchored ubiquitin dimer, captured previously on Znf\_A20 Sepharose, but strikingly also contained polyubiquitin chains of up to eight ubiquitin moieties in length (detected with anti-ubiquitin). In contrast to binding to the Znf\_A20 domain, ubiquitin positive binding proteins in the Znf\_UBP fraction form a discrete ladder rather than a smear (Fig 5.17). Interestingly, the *in vivo* purified unanchored polyubiquitin chain mixture migrates in what appears to be an identical pattern to commercial K48-as opposed to K63-linked polyubiquitin chains, which migrate differently for reasons discussed in Section 5.6.1. We probed the same Znf\_UBP-purified fractions with the anti-K48 ubiquitin specific antibody, which preferentially bound to epitopes in longer chains, revealing for the first time purified endogenous K48-linked unanchored polyubiquitin chains containing as many as 15 ubiquitin moieties (Fig 5.18).

**Figure 5.18**

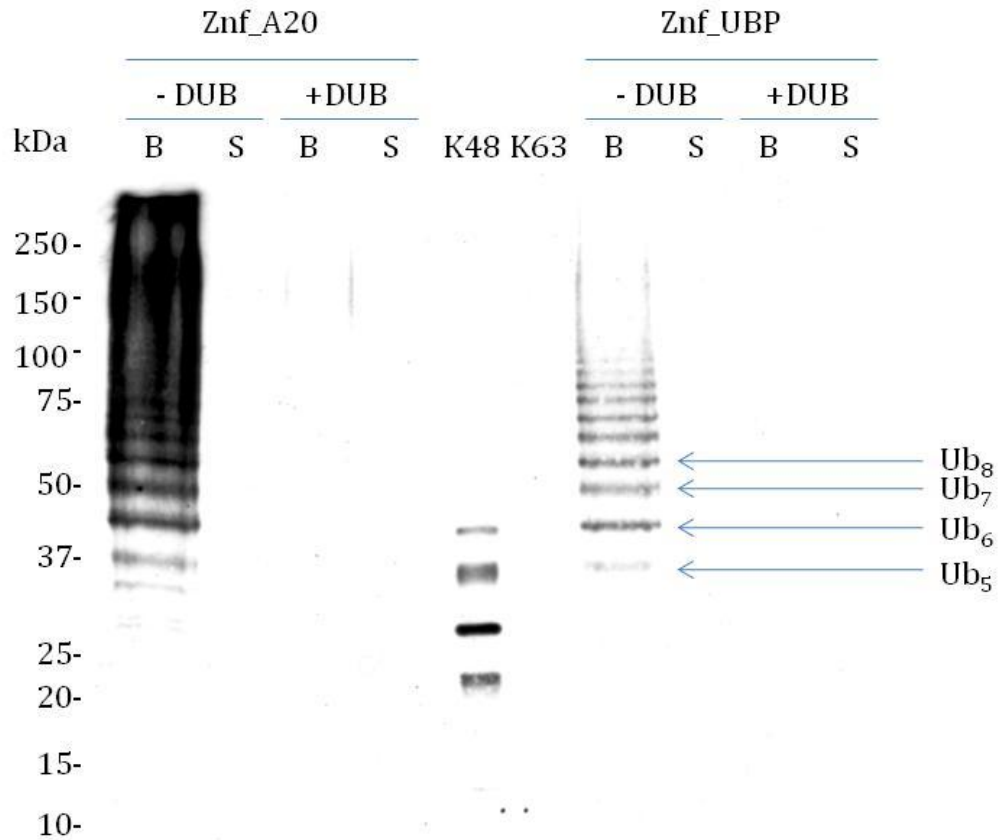


**Figure 5.18** Znf\_UBP-Sepharose bound K48-linked ubiquitinated proteins that co-migrated with commercial K48-linked Ub<sub>5</sub> and Ub<sub>6</sub>, and chains as long as Ub<sub>15</sub> were detected. The same volume of samples that were probed for ubiquitin from Figure 5.17 was immunoblotted with anti-K48. (K48)=0.25μg K48-linked polyubiquitin, (K63)=0.25μg K63-linked polyubiquitin.

#### **5.6.11. Increase in unanchored polyubiquitin chains following MG132 treatment of cultured cells**

Previously, we captured polyubiquitinated proteins from cultured cells using Znf\_A20 Sepharose, and noted an enrichment of polyubiquitinated substrates upon proteasomal inhibition relative to untreated cells (Figure 5.1b). The polyubiquitinated material presumably also included unanchored polyubiquitin, as the Ub<sub>2</sub> species was captured, and this and a number of other lower molecular weight ubiquitin species were noted to increase after proteasomal inhibition. To confirm the existence of unanchored polyubiquitin chains in cultured cells and to ascertain whether unanchored polyubiquitin levels changed under conditions where the total polyubiquitin pool is known to alter, human U2OS cells were treated +/- 1µM MG132 overnight to inhibit proteasomes. Cells were homogenised and incubated with Znf\_UBP Sepharose, in an identical protocol to the MG132 treatment of cells used for Znf\_A20 Sepharose binding, and captured proteins probed with anti-ubiquitin and anti-K48 (Fig 5.19). Affinity capture with the Znf\_UBP domain revealed that longer unanchored polyubiquitin chains could also be captured from human cells and that levels of Ub<sub>2</sub> and longer unanchored polyubiquitin chains increased following MG132 treatment, that appeared to include the K48-linkage.

#### **5.6.12. Optimisation for purification of unanchored polyubiquitin chains**

Ubiquitin is a small globular protein which has been found to be highly stable even when heated. Zeng *et al.* 2010 were interested in the role of unanchored polyubiquitin chains during innate immunity [181]. They found that the unanchored chains could not be deubiquitinated by isoT, while protected by retinoid-inducible gene 1 (RIG-I) protein. Thus they heated samples for 5 minutes

**Figure 5.19**

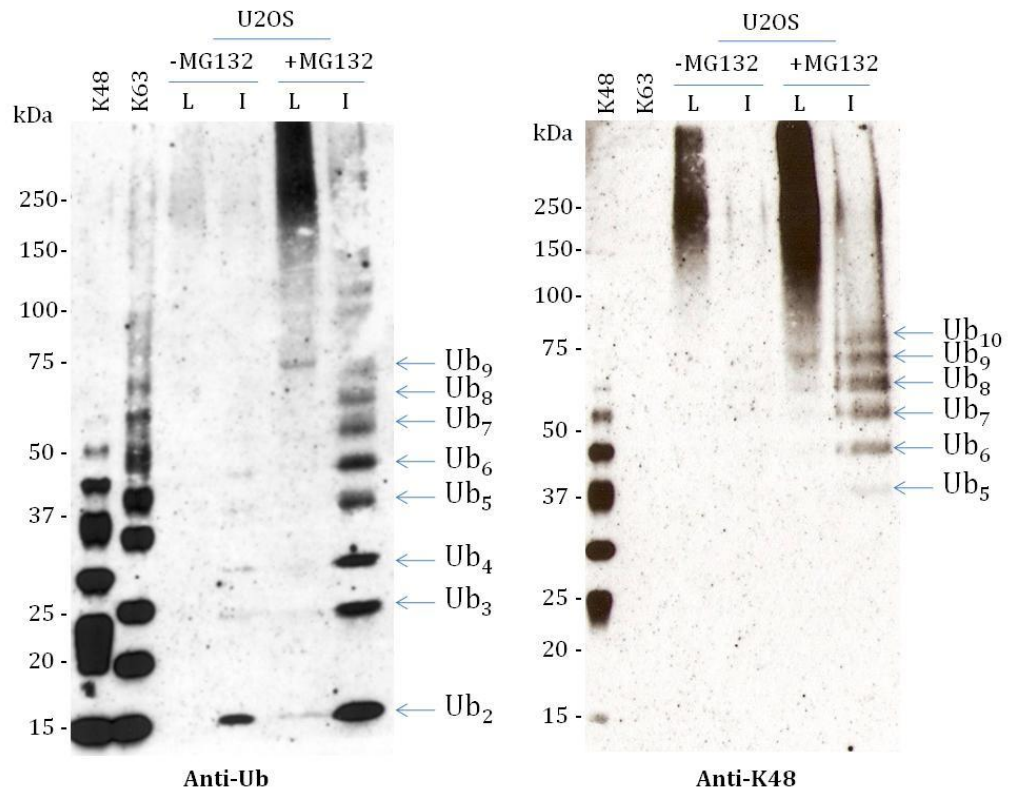


**Figure 5.19** +/- MG132 treated U2OS cell proteins (cells treated with 1 $\mu$ M MG132 for 16 hours) bound to Znf\_UBP beads. Samples (containing ~4mg protein) were homogenised in 4ml homogenising buffer (50mM Tris, 150mM NaCl, 0.5% NP-40, 5mM N-ethylmaleimide, pH 7.5), centrifuged, and the supernatant collected. DTT was added to the lysate to a final concentration of 10mM and mixed at 4 $^{\circ}$ C for 15 minutes. 50% of the lysate was passed twice through 80 $\mu$ l Znf\_UBP-Sepharose at 4 $^{\circ}$ C. Beads were washed three times in wash buffer (50mM Tris, 150mM NaCl, 0.5% NP-40, 1mM DTT, pH 7.5). Bound proteins were eluted in gel application buffer; 50% probed with anti-ubiquitin and 50% with anti-K48. (K48)=0.25 $\mu$ g K48-linked polyubiquitin, (K63)=0.25 $\mu$ g K63-linked polyubiquitin, (L)= 1/80<sup>th</sup> lysate loaded onto beads, (I)=Znf\_UBP bound proteins. Arrows denote an increase in ubiquitin species presumed to be unanchored chains after MG132 treatment, from Ub<sub>2</sub> and above. Monoubiquitin is omitted from the blot for clarity.

at 70°C -80°C, reasoning this would denature RIG-I without affecting the more stable unanchored polyubiquitin. We adopted this method and heated muscle to denature and precipitate non-ubiquitinated proteins prior to affinity purification, reasoning that unanchored polyubiquitin would be heat stable. This not only prevents non-specific interactors from binding to the Znf\_UBP domain but may have an additional advantage; we previously established how *in vivo* deubiquitinating enzymes and other ubiquitin receptors such as p62 can co-purify along with ubiquitinated proteins. Such proteins may also bind to unanchored ubiquitin *via* the C-terminus and sterically hinder binding to the Znf\_UBP domain. Thus, we heated muscle protein extracts at 75°C for 20 minutes prior to purification and compared heated to non-heated muscle for binding to the Znf\_UBP domain. Not only can fewer bands (presumed to be non-specific interactors and/or ubiquitin receptors) be visualised in purified fractions derived from the heat-treated samples by Coomassie staining (Figure 5.20), but immunoblotting revealed an intensification of the ladder of unanchored chains containing the K48 linkage (Figures 5.21 and 5.22) as long as 15 ubiquitin moieties. It is interesting that despite all of the recent literature regarding unanchored polyubiquitin chains recognising the involvement of K63-linked polyubiquitin chains [179-181], to date we have failed to detect K63-linked unanchored polyubiquitin, by MS of the ubiquitin dimer bound to Znf\_A20 or by immunoblotting of Znf\_UBP captured polyubiquitin species with K63-linkage specific antibodies (not shown). This offers a highly useful protocol for the future purification, and determination in molecular detail, of unanchored polyubiquitin from an *in vivo* source under different physiological and pathological conditions.

**Figure 5.20**

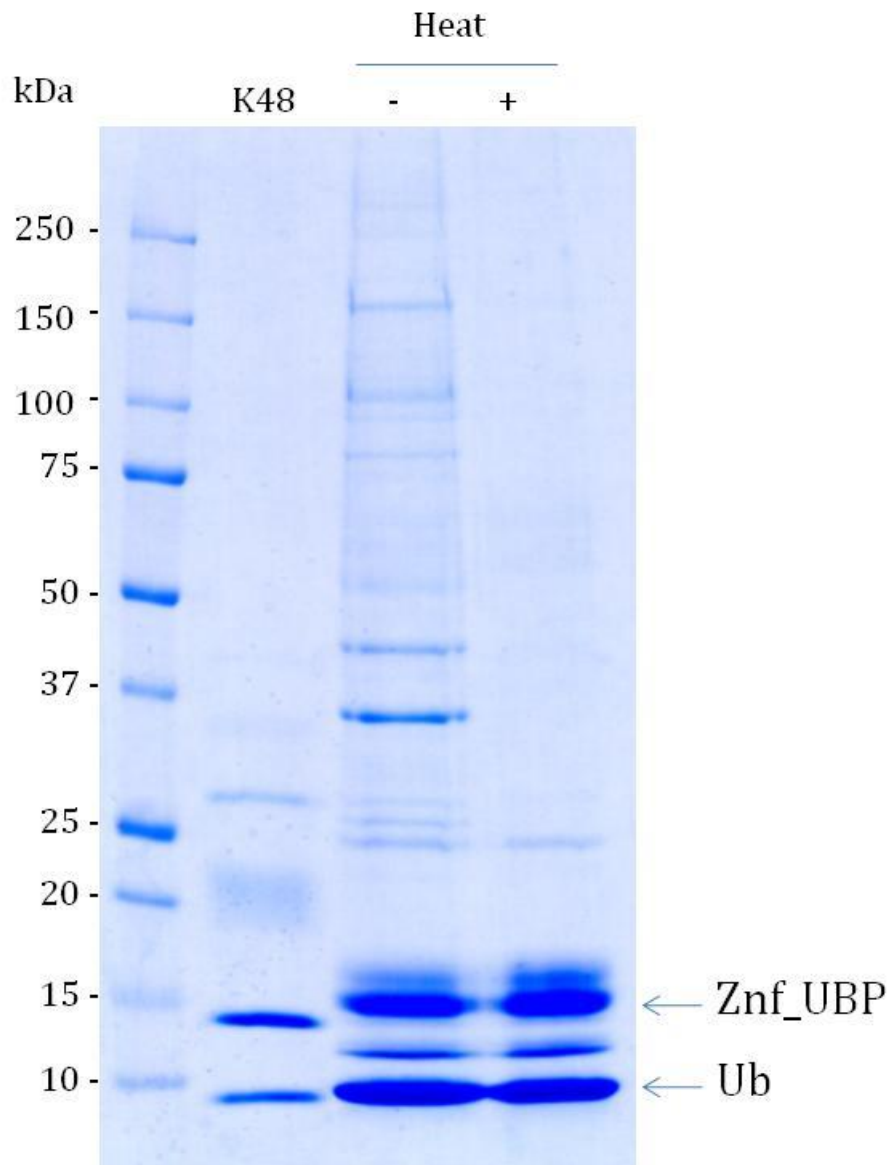


**Figure 5.20** Rat muscle (~20g) was homogenised in 100ml homogenising buffer (50mM Tris, 150mM NaCl, 0.5% NP-40, 5mM N-ethylmaleimide, pH 7.5), centrifuged, and the supernatant collected. DTT was added to the lysate to a final concentration of 10mM and mixed at 4°C for 15 minutes. 50% of the lysate was heated at 75°C for 20 minutes and centrifuged. +/- Heated rat muscle supernatant was then passed twice through 400µl Znf\_UBP-Sepharose at 4°C. Beads were washed three times in wash buffer (50mM Tris, 150mM NaCl, 0.5% NP-40, 1mM DTT, pH 7.5). Bound proteins were eluted in gel application buffer, and ¼ of beads loaded. (K48)=3µg K48-linked polyubiquitin. Monoubiquitin (Ub) and the isoT “bait” proteins (Znf\_UBP) are denoted by arrows.

**Figure 5.21**

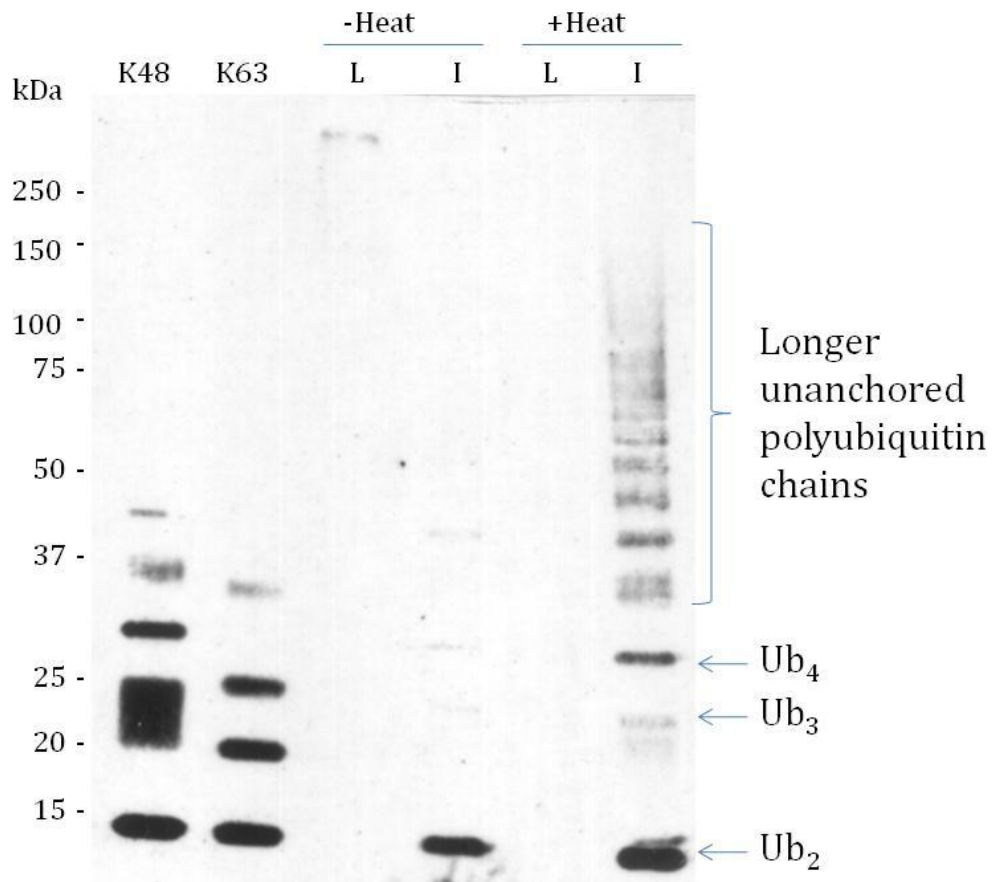


**Figure 5.21** Anti-ubiquitin Western blot of +/- heated muscle bound to Znf\_UBP, under conditions described in Figure 5.20. Bound proteins were eluted in gel application buffer, and 1/40<sup>th</sup> loaded. (L) = 1/150<sup>th</sup> lysate loaded onto beads, (I)=Znf\_UBP bound proteins, (K48)=0.25 $\mu$ g K48-linked polyubiquitin, (K63)=0.25 $\mu$ g K63-linked polyubiquitin.

**Figure 5.22**

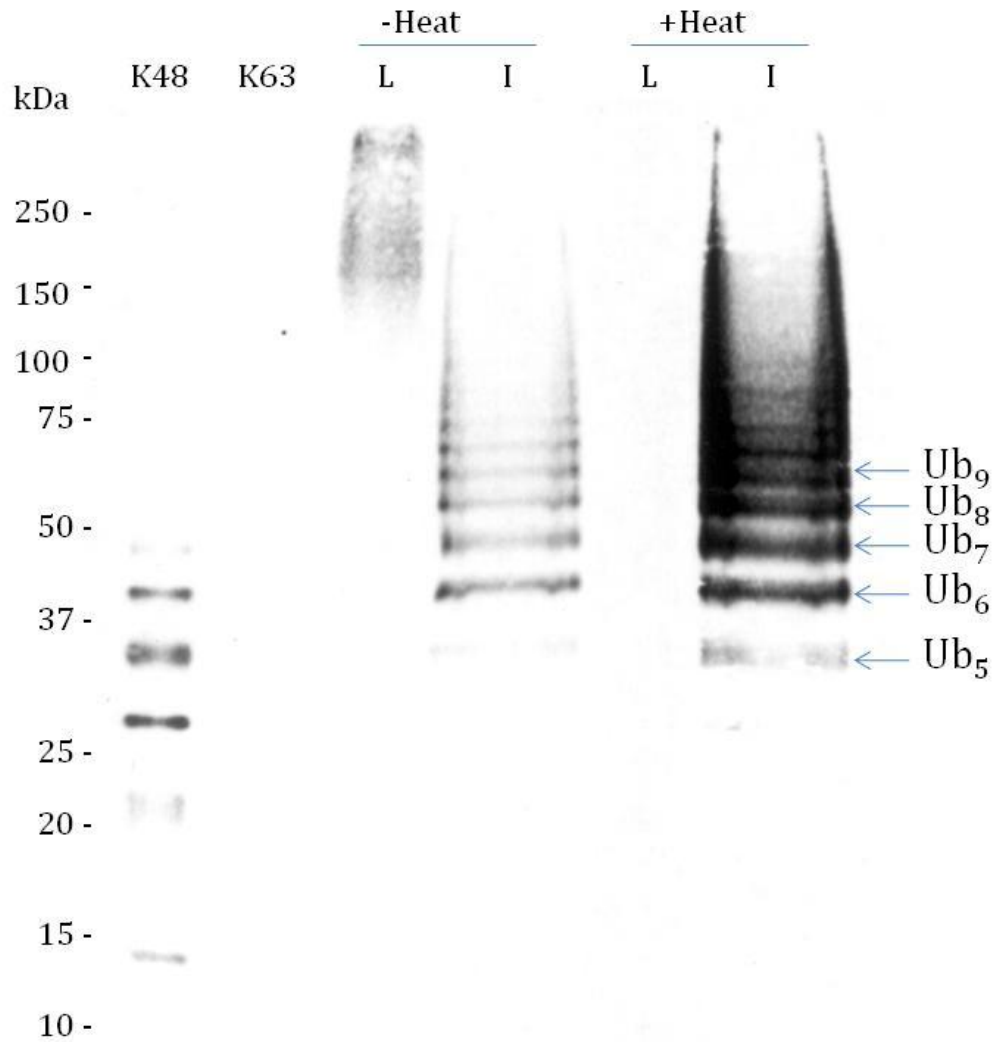


**Figure 5.22** Anti-K48 ubiquitin linkage Western blot of +/- heated muscle bound to ZnF\_UBP, under conditions described in Figure 5.20. Bound proteins were eluted in gel application buffer and 1/20<sup>th</sup> loaded. (L) = 1/150<sup>th</sup> lysate loaded onto beads, (I)=ZnF\_UBP bound proteins, (K48)=0.25 $\mu$ g K48-linked polyubiquitin, (K63)=0.25 $\mu$ g K63-linked polyubiquitin.

## 5.7 Discussion

### 5.7.1. Evidence that the skeletal muscle ubiquitin dimer is an endogenous species

Diubiquitin has been detected in rat muscle, human U20S cells and mouse brain, after enrichment of polyubiquitinated proteins using our purification strategy with the Znf\_A20 domain. Samples were treated with NEM to irreversibly inhibit *in vivo* DUBs, but rat muscle and mouse brain samples cannot be removed and frozen for subsequent analysis instantly. Thus the ubiquitin dimer may conceivably be produced *via* endogenous processing post-mortem. However, we further purified ubiquitinated proteins from human muscle biopsies from five healthy volunteers using the Znf\_A20 domain. These samples were snap-frozen in liquid nitrogen immediately after removal, and subsequently rapidly homogenised in the presence of NEM and protease/proteasome inhibitors (Figure 5.23). Despite the relatively small mass of muscle used (10mg of human muscle compared to several grams of rat muscle), rapid freezing after sample removal and immediate treatment with a number of inhibitors of cellular processing, the ubiquitin dimer is still present in human muscle. Human derived U20S cells are also instantly lysed into homogenising buffer and, again, the ubiquitin dimer is detected. This strongly supports the notion of an endogenous diubiquitin species existing *in vivo*, as opposed to artifactually arising from proteolysis during sample preparation and importantly suggests the dimer is relevant in a human context. In addition, we noted that upon USP2 treatment there is no apparent increase in the dimer, simply it is spared, further supporting it to be endogenous rather than a transient intermediate of DUB-catalysed polyubiquitin processing. Thus we can assume that conjugated polyubiquitin was

**Figure 5.23**

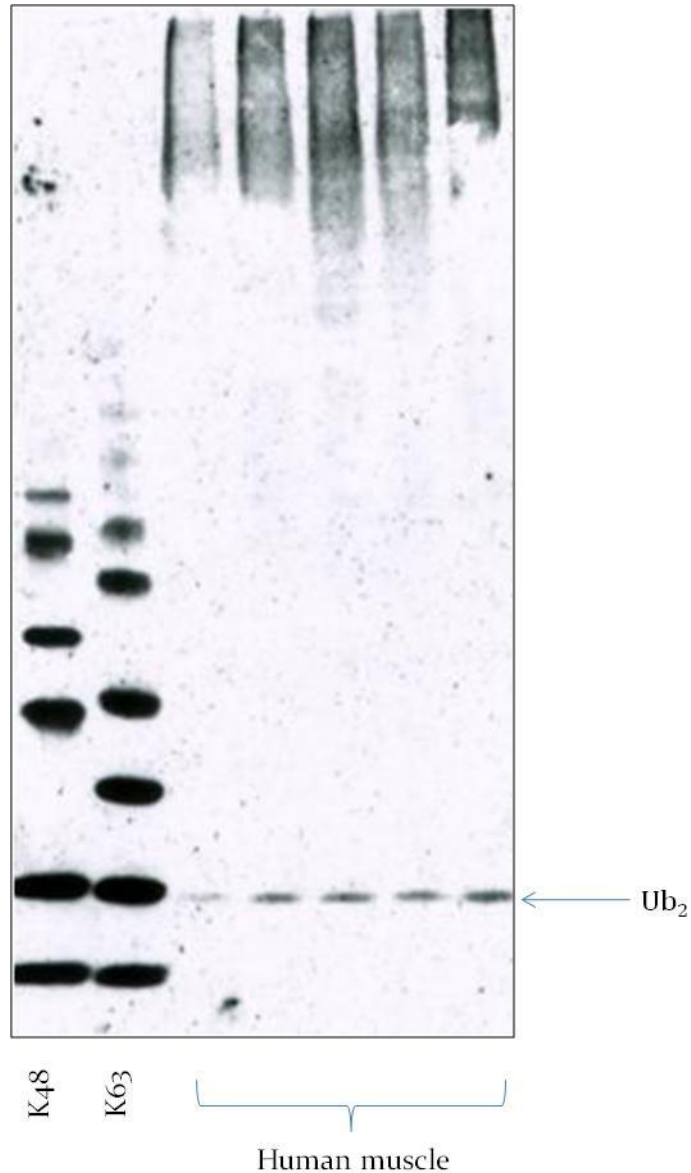


**Figure 5.23** Ubiquitin dimer can be detected in human muscle, captured on Znf\_A20 Sepharose. Human muscle biopsy samples (~10mg each), taken from 5 healthy volunteers, were homogenised in 1ml homogenising buffer (50mM Tris, 150mM NaCl, 0.5% NP-40, 5mM N-ethylmaleimide, 20 $\mu$ M MG132, 0.1% mammalian protease inhibitor cocktail (Sigma), pH 7.5). Homogenate was centrifuged and DTT added to the supernatant to a final concentration of 10mM, and mixed at 4 $^{\circ}$ C for 15 minutes. Supernatant was incubated with 50 $\mu$ l Znf\_A20-Sepharose for 1 hour at 4 $^{\circ}$ C. Beads were washed three times in wash buffer (50mM Tris, 150mM NaCl, 0.5% NP-40, 1mM DTT, pH 7.5) and 100% bound proteins eluted with gel application buffer and immunoblotted with anti-ubiquitin. (K48)=0.25 $\mu$ g K48-linked polyubiquitin, (K63)=0.25 $\mu$ g K63-linked polyubiquitin.

processed straight to free monoubiquitin by USP2. Importantly, Ub<sub>2</sub> has not only been detected in rat EDL muscle, but also increases after 24 hours of LPS infusion relative to saline control rats, connecting diubiquitin to a disease state and further validating it as an *in vivo* species.

### **5.7.2. Proposed biological roles of unanchored polyubiquitin**

Ubiquitin has traditionally been considered for its role in modifying other proteins post-translationally. However, previous *in vitro* experiments as far back as 1997 supported a potential role for unanchored polyubiquitin chains as a regulator of proteolysis, in which free K48-linked chains synthesised *in vitro* were found to compete with polyubiquitinated substrates for binding to the proteasome [68]. Proteasomal binding affinity of unanchored polyubiquitin chains of eight ubiquitins in length was 90-fold higher than that of diubiquitin, indicative that longer chains may compete more effectively with polyubiquitinated substrates for binding to the proteasome and may reduce protein degradation rates. Interestingly, recent studies have identified the presence of an unstructured region within proteasome targeted substrates that serves as an “initiation region” for proteasomal degradation [126]. Should this region be too close to or far from the proteasomal tag (i.e. polyubiquitin chain), the substrates degradation is inhibited. Therefore proteasomal regulation and degradation is more complex than originally considered and competition between unanchored and conjugated species may not be straight forward. However, accumulated unanchored polyubiquitin chains, produced in a cellular context upon isoT suppression in mammalian cells [177], have been shown to act as competitive inhibitors of degradation of ubiquitinated p53 by the 26S proteasome. This mammalian model validates earlier studies in yeast, where

deletion of the UBP14 gene, a functional homolog of isoT, results in accumulation of unanchored polyubiquitin that inhibits ubiquitin dependent proteolysis [134]. Additionally free chains have been demonstrated to have other biological roles *in vivo*, activating ubiquitin-dependent kinases I- $\kappa$ B kinase (IKK) and transforming growth factor  $\beta$ -activated kinase 1 (TAK1) (the latter *via* unanchored polyubiquitin binding to the accessory protein TAB2) [179]. Interestingly, TNF-receptor associated factor 6 (TRAF6), an E3 ubiquitin ligase essential for NF- $\kappa$ B activation, produced unanchored K63-linked polyubiquitin chains in an *in vitro* reconstituted system that subsequently activated TAK1. Additionally, alternative linkages to K48- and K63-isopeptide linked unanchored polyubiquitin chains were implicated in activating the IKK complex. More recently the same group noted a further role for unanchored K63-linked polyubiquitin in signalling during innate immunity *via* binding to RIG-I at its caspase activation and recruitment domains (CARD) domains and resulting activation of the IRF3 signalling cascade [181]. These studies identified unanchored polyubiquitin indirectly, the former by the use of deubiquitinating enzymes, that specifically disassemble free chains (isoT) [179] and the latter by the ability of co-precipitated ubiquitin chains to form thiolester intermediates with the E1 ubiquitin-activating enzyme [181]. Zeng *et al.* 2010 provided evidence that CYLD could deubiquitinate RIG-I-activating polyubiquitin chains (a DUB that specifically cleaves K63-linked polyubiquitin chains). In combination with data that these polyubiquitin chains could be detected by K63-specific antibodies, this confirmed that RIG-I-activating polyubiquitin chains were K63-linked. This paper approximated that as many as 6000 molecules of K63-linked free Ub<sub>6</sub> chains may exist in human cells under non-stimulated conditions, and yet reported that RIG-I signalling may be activated with a EC<sub>50</sub> of as little as 50pM (equivalent to only 15 chains per cell), implicating them as potent regulators of RIG-I. Studies into a tripartite motif

containing 5 (TRIM5)-mediated innate immunity signalling pathway has recently provided further evidence supporting the role of unanchored K63-linked chains in TAK1 activation [180]. *In vitro* polyubiquitin conjugation mediated by E3 ubiquitin ligase TRIM5 produced unanchored chains that were detected by K63-linkage specific immunoblotting. MS/MS analysis of tryptic peptides detected the K63-linkage and the absence of alternative linkage signature peptides or peptides corresponding to TRIM5. These free chains activated TAK1 and downstream AP-1 and NF- $\kappa$ B signalling pathways. Notably, we have failed to detect K63-linked unanchored polyubiquitin by immunoblotting or MS of the Znf\_A20 ubiquitin dimer from skeletal muscle. However, it is unclear whether this is a MS sensitivity issue, and it is possible that under “stimulated” conditions, such as innate immunity signalling or IL-1 $\beta$  stimulation, there may be an increase in K63-linked unanchored polyubiquitin chains within a detectable range.

The importance of a free C-terminal di-glycine of ubiquitin was revealed by the identification of a frameshift ubiquitin mutant in Alzheimer’s disease, which caps polyubiquitin chains and results in proteasomal inhibition [69]. The severe consequences of ubiquitin gene knockout studies have highlighted that maintaining sufficient levels of free ubiquitin is essential; Ubb knockout inhibits meiotic progression, inducing infertility [244] as well as neurodegeneration [244], while Ubc deletion results in embryonic lethality [245]. Levels of free unanchored chains are reduced under heat stress conditions in *S. cerevisiae*, mediated in part by deubiquitinating enzyme Doa4 and its inhibitor Rfu1 [178]. Free chains were proposed to act as a source of monoubiquitin, which is depleted by increased polyubiquitination under heat stress conditions. Short unanchored chains accumulated when Rfu1 was overexpressed, which presumably spared

free chains from Doa4 mediated deubiquitination, whereas Rfu1 deletion prevented Doa4 inhibition, simultaneously increasing monoubiquitin levels and depleting unanchored chains. The authors noted that this correlated with a potential role of unanchored chains as a ubiquitin reservoir, perhaps parallel to the intracellular system that permits storage of glucose as glycogen [178]. Our optimised strategy for capturing specifically free chains was to exploit the Znf\_UBP domain of isoT, which contains no intrinsic catalytic activity, but binds with high affinity to the C-terminal di-glycine of unanchored polyubiquitin [141]. The existence of enzymes such as isoT and Rfu1 that regulate existing unanchored polyubiquitin species, together with evidence of the ubiquitin conjugating enzyme E2<sub>25K</sub> regulating synthesis of unanchored polyubiquitin chains [246] supports the notion that free chains have a biological role and require regulation. Observations of unanchored chains regulating kinase activation, innate immunity signalling, proteasomal inhibition and monoubiquitin levels provides convincing evidence of free polyubiquitin regulating a wide variety of processes.

### **5.7.3. Biological role of shorter unanchored polyubiquitin**

Our MS analysis of the Znf\_A20 captured Ub<sub>2</sub> has exclusively detected K48-linked diubiquitin. Studies into the biological relevance of shorter diubiquitin chains is somewhat more limited, as *in vitro* observations note that K48-linked Ub<sub>2</sub> was a considerably weaker inhibitor of the proteasome, relative to longer chains (see previous Section 5.7.2). However, Ub<sub>2</sub> has been detected in other studies in mammalian cells [241] and wheat germ; the latter was confirmed to contain the K48-linkage by Edman degradation [247]. It is interesting to note that our data corresponds with previous observations of an endogenous K48-linked ubiquitin

dimer [247], which was suggested to provide a pre-formed short ubiquitin chain, that was observed to successfully conjugate to other target proteins *in vitro*. A K48-linked ubiquitin dimer was also specifically reported to reduce the hydrolase activity of the deubiquitinating enzyme UCH-L3 *in vitro* [241]. Although it is improbable that the purified ubiquitin dimer resulted from processing during sample preparation, this does not exclude the possibility of its formation during endogenous deubiquitination of longer free chains in a physiologically relevant context, as Ub<sub>2</sub> is detected during deubiquitination with a wide variety of DUBs [187].

#### **5.7.4. Characterisation of unanchored polyubiquitin chains purified *via* the Znf\_UBP domain**

Results of anti-ubiquitin immunoblotting of longer chains from skeletal muscle and U2OS cells bound to Znf\_UBP hint that these may be K48-linked, as evidenced by their co-migration with the commercially produced K48-linked polyubiquitin chains, and further supported by detection with anti-K48 antibody. As discussed previously, K48- and K63-linked ubiquitin dimers co-migrate, unlike longer chains, thus migration of the Znf\_UBP bound dimer provides no information on possible linkage. Interestingly, the anti-K48 antibody does not even weakly detect this dimer. However, currently we lack detailed MS analysis of the Znf\_UBP captured Ub<sub>2</sub> and longer chains, which is required to identify the linkage of purified dimers bound to Znf\_UBP and validate anti-K48 immunoblotting evidence of longer K48-linked chains. MS can be used to investigate whether alternative linkages, other than K48, of longer free chains can be detected *via* MS techniques, including K63-linked unanchored chains, of which there is mounting evidence of a role during innate immunity signalling. It is notable that

unanchored chain levels increase during the innate immunity response [180, 181] and upon  $\text{I}\text{I}1\beta$  treatment [179]. Future Znf\_UBP purification of free chains from stimulated cells may provide a previously undetectable source of unanchored K63-linked polyubiquitin and other linkages. A similar Znf\_UBP domain affinity capture approach has been recently applied to different biological samples and captured unanchored polyubiquitin, but was not optimised for bulk capture and only detected low levels of free polyubiquitin chains [176]. However, unanchored polyubiquitin chains are yet to be comprehensively characterised by linkage types and chain lengths.

#### **5.7.5. Stability of unanchored polyubiquitin chains**

Although we have yet to purify ubiquitin proteins from signalling-stimulated cells, we have captured polyubiquitinated proteins from MG132-mediated proteasome-inhibited cells. We observed increased polyubiquitinated proteins binding to both the Znf\_A20 (Figure 5.1b) and Znf\_UBP domain (Figure 5.19). The increased ubiquitin smear of proteins bound to the Znf\_A20 domain are unprocessed polyubiquitinated proteins that have accumulated as a result of proteasome inhibition. Interestingly, proteasomal inhibition also resulted in accumulation of unanchored polyubiquitin, revealed by binding to the Znf\_UBP domain. Recent studies has identified two distinct deubiquitinating activities associated with the proteasome, acting to either amputate chains whole (RPN11) or to progressively cleave polyubiquitin from the distal end (UCH37 and USP14) [122, 248]. Studies have previously detected coupling of proteasomal degradation with deubiquitination [249], and correspondingly Zhang *et al.* 2011 noted that inhibition of the proteasome not only blocks degradation, but also deubiquitination [122]. Since DUB activities are still active during proteasomal

inhibition, and given that these processes are not independent of each other, it is possible that MG132 treatment forces irregular deubiquitination. The accumulation of free chains implicates possible blocking of the ubiquitin chain trimming activities, which are believed to remove lingering unanchored chains bound to the proteasome, that may otherwise compete with polyubiquitinated substrates for binding.

#### **5.7.6. Predominance of K48-linked unanchored polyubiquitin**

Whilst there are no studies to date that have exclusively analysed the abundance of different linkage ubiquitin dimers, studies have looked into the abundance of different linkage polyubiquitin chains [176]. Kaiser *et al.* 2011 assessed the composition of various cell and tissue samples for K48, K63 and K11-linkages, but excluded other linkages from their analysis which altogether comprised less than 1% of their samples. However, other studies have detected the less “conventional” linkages in samples including the yeast proteome [155] and mouse brains [174]. Therefore it is interesting to consider the presence of what appears to be exclusively K48-linked polyubiquitin using our purification strategy, considering the apparent abundance of other linkages. Observations of increased unanchored K63-linked polyubiquitin have been made under rapid signalling events. This may account for not observing free chains co-migrating with K63-linked commercial chains, as our primary source of tissue is from muscle under basal conditions. Whilst unanchored K63 chains are associated with a rapid/acute physiological events, K48-linked chains (whether considered anchored/unanchored) are mostly associated with chronic events, such as proteasomal degradation. Multiple roles have been suggested for unanchored K48-linked chains, the longer chains associated with competition for proteasomal

binding, as rapid sources of free ubiquitin, or as pre-emptive “building blocks” for rapid polyubiquitination of targets. What is of particular interest, is that we have captured polyubiquitin up to 15 monomers in length, according to immunoblotting with anti-K48. To date, the function of polyubiquitin chains in binding to the proteasome has been observed to increase with chain length. However, no increased binding is detected for polyubiquitin chains of longer than 8 monomers, which raises the question of why free chains of 15 monomers in length are detected in rat muscle. Even if unanchored polyubiquitin chains prove to be cellular “garbage”, produced as a by-product of proteasomal degradation, purification and analysis of unanchored polyubiquitin may give us an insight into the topology, composition and length of chains that were previously conjugated, and improve our understanding of the regulators of the unanchored polyubiquitin pool. Analysis of free chains may even provide information on previously unknown biological roles of unanchored polyubiquitin, which is supported by mounting evidence of functions from regulating deubiquitinating activity to signalling during the innate immune response.

## **CHAPTER 6**

### **General discussion**

## 6.1. Summary

Our initial interest in zinc finger protein 216 (ZNF216) was attributable to its involvement in the skeletal muscle atrophy programme [56]. In Chapter 3 we measured increased ZNF216 mRNA expression under septic conditions in rats (continuous lipopolysaccharide (LPS) infusion), which mirrored muscle atrophy F-box protein (MAFbx) and muscle RING-finger 1 (MuRF1) responses in the same model and was consistent with ZNF216 expression changes observed in other models of muscle atrophy (induced *via* denervation and starvation [56]). A low dose of dexamethasone (Dex) infused simultaneously with LPS spared muscle from the LPS-induced atrophy response. However, LPS-induced elevated ZNF216 mRNA levels were not blunted by Dex, mirroring another groups observations that MAFbx and MuRF1 expression also remained elevated in the same Dex+LPS model, relative to LPS alone [208]. A statin model of myopathy, in which severe muscle damage and atrophy occurs, also significantly elevated ZNF216 mRNA levels further, mimicking MAFbx and MuRF1 increased responses relative to less severe models [209]. In Chapter 4, we verified that recombinant ZNF216 protein was functional in its ability to bind polyubiquitin chains. Subsequently, using an affinity capture method, we purified polyubiquitinated proteins from rat skeletal muscle using recombinant ZNF216 or its N-terminal ubiquitin-binding Znf\_A20 domain and committed purified material to proteomic analysis, in an attempt to identify ZNF216's substrates. However, due to limitations of the liquid chromatography tandem mass spectrometry (LC-MS/MS) approach, which only calculated ion scores below the significance threshold, combined with a lack of validation *via* immunoblotting, prompted us to apply affinity capture to looking more generally at global changes in ubiquitination, detailed in Chapter 5. The role of unanchored polyubiquitin is a question increasing in interest in the scientific community with the revelation that unanchored K63-linked polyubiquitin has a

role in activating protein kinases transforming growth factor  $\beta$ -activated kinase 1 (TAK1) and I- $\kappa$ B kinase (IKK) [179] and may have a role in signalling during innate immunity [180, 181]. Unexpectedly, we detected a ubiquitin dimer from skeletal muscle, mouse brain and human U20S cells, consistently binding immobilised ZNF216 and/or the Znf\_A20 domain. Ubiquitin dimers have not previously been characterised as biologically active species *in vivo*. However, our observations that levels of this presumed ubiquitin dimer are elevated in skeletal muscle after 24 hours of LPS infusion (Figure 5.2) suggest it may have a physiological relevance. In Section 6.4, we speculate about possible novel roles for ZNF216 and unanchored polyubiquitin during muscle atrophy.

## **6.2. The Znf\_A20 domain does not bind monoubiquitin in pulldowns and shows no linkage specificity**

Preferential binding of the Znf\_A20 domain to polyubiquitin over monoubiquitin has been previously attributed (in the previous chapter) to avidity effects (Figures 4.2c and 4.11). Some ubiquitin binding proteins bind polyubiquitin but not monoubiquitin for alternative reasons, which may confer polyubiquitin linkage specificity. For example, proteins that bind to specific ubiquitin linkages preferentially to monoubiquitin/other linkages may be because the ubiquitin binding domain is incomplete; for example TAB2/TAB3 specifically binds to K63-linked ubiquitin, but does not bind to the K63-isopeptide linkage directly. Instead, there is simultaneous binding to the proximal and distal ubiquitin within a K63-linked chain, but the affinity of a single binding domain within TAB2/TAB3 is not high enough alone to bind to monoubiquitin [237]. Our Znf\_A20 captured ubiquitin dimer has been shown to be exclusively K48-linked, which may implicate linkage specific binding. However, our structural studies do not support

a model where a single Znf\_A20 can form any additional contacts with polymeric ubiquitin to provide linkage specificity (see Figure 5.11), and MS analyses in the gas phase did not detect preferential binding to the ubiquitin dimer over the monomer, nor between K48- and K63 ubiquitin dimers (Chapter 5.8.3). Together, these observations strongly indicate that the purification of the K48-linked dimer is reflective of its predominance *in vivo* as opposed to Znf\_A20 specificity and binding is likely achieved by two separate domains each interacting independently with a single ubiquitin moiety in the dimer, producing a higher affinity interaction than that of the Znf\_A20 to monoubiquitin (~8uM), which is presumably below the limits of what can be detected in the pull-down. Notably, ZNF216 is reported to be dimeric [196] suggesting a mechanism by which Ub<sub>2</sub> binding could potentially be achieved *in vivo*, although related studies from our own group found no evidence for ZNF216 dimerisation (Tom Garner; personal communication).

### **6.3. Sparring of diubiquitin during USP2 deubiquitination**

Our observation that diubiquitin is spared from ubiquitin carboxyl-terminal hydrolase 2 (USP2)-mediated deubiquitination (of which only the catalytic core is used to remove USP2-specificity) occurred regardless of whether it bound to the Znf\_A20 or the Znf\_UBP domain, which bind at the D58 surface and C-terminal diglycine, respectively. We have previously established that the Znf\_A20 domain was unable to spare commercial diubiquitin from USP2 treatment (Figure 4.6), implicating it is spared through an alternative mechanism than steric hindrance. The ability to co-precipitate p62 upon purification of polyubiquitin (Figure 5.14) supports a hypothesis in which an unidentified binding protein(s) is/are co-purified during capture on both the Znf\_A20 domain and the Znf\_UBP domain

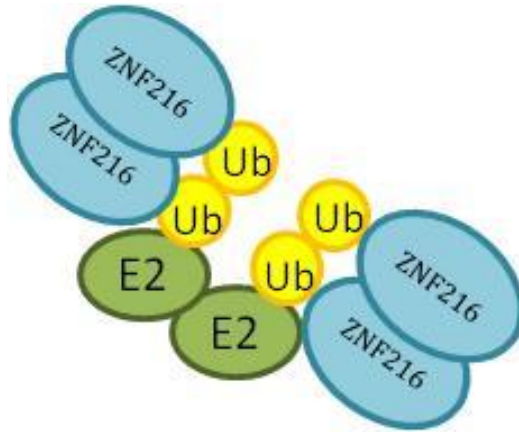
that blocks USP2 core access, although the lack of protection of longer polyubiquitin species implies that it is the simultaneously binding of the Znf\_A20/Znf\_UBP with this unidentified co-precipitating protein that confers protection.

#### **6.4. Possible novel roles of ZNF216 and unanchored polyubiquitin chains during skeletal muscle atrophy**

Polyubiquitination is generally assumed to occur by the addition of a single ubiquitin at a time to a substrate by an E3 ubiquitin ligase. However, there is evidence that polyubiquitin chains may be preformed and the chain attached *en bloc* to a target protein. This is demonstrated by mouse E2 enzyme Ube2g2 which can form K48-linked polyubiquitin in the absence of a substrate [146]. This may provide a rapid method of polyubiquitination, in which the benefit of diubiquitin may be that it is short enough to not inhibit the proteasome but is longer than monoubiquitin to accelerate polyubiquitination of substrates. A K48-linked ubiquitin dimer was purified on immobilised ZNF216 or its Znf\_A20 domain, which was spared from USP2 core mediated ubiquitination. In our LPS-induced atrophy model, in which there is notable upregulation of the UPS and hence increased polyubiquitination, we observed both an increase in a Znf\_A20 captured ubiquitin dimer after 24 hours (Figure 5.2) and upregulated ZNF216 mRNA levels (Figure 3.4). We speculate that dimeric ZNF216 (as evidenced by Huang *et al.* 2004 [196]) may bind to diubiquitin *in vivo*, that is simultaneously bound to E2 enzymes (that according to Li *et al.* 2007 are likely to be dimers to facilitate ubiquitin transfer [146]) and sterically hinders deubiquitination of the preformed polyubiquitin chains to aid polyubiquitination without having a direct role in the process (Figure 6.1). ZNF216 may remain associated with

**Figure 6.1**

a)



b)

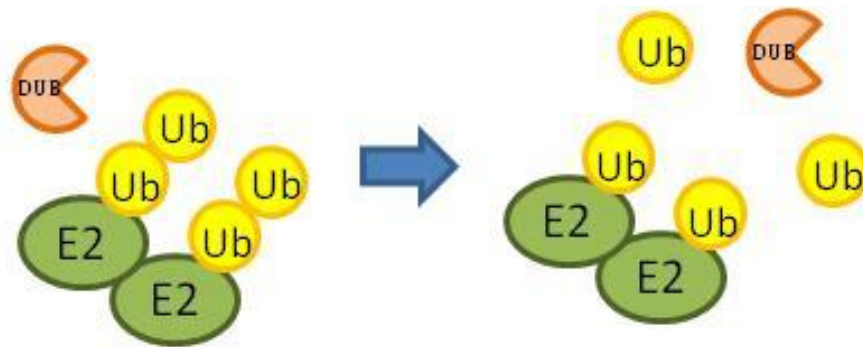


**Figure 6.1** Model of ZNF216 binding to E2 enzyme-associated diubiquitin, in which **a)** ZNF216 may dimerise and bind diubiquitin, sterically hindering access of deubiquitinating enzymes (DUBs) that may otherwise cleave polyubiquitin chains, as demonstrated in **b)**. Note that E2 enzymes are modelled as a dimer, which has been suggested to assist the formation of preformed polyubiquitin chains for *en bloc* polyubiquitination of substrates; ZNF216 binding would promote this model of substrate polyubiquitination.

polyubiquitin after the formation of longer chains, and then shuttle polyubiquitinated proteins to the proteasome, perhaps having a role in preventing deubiquitination of substrate-attached polyubiquitin chains. It is interesting to consider studies of the deubiquitinating enzyme ubiquitin carboxyl-terminal hydrolase isozyme L3 (UCH-L3) in light of our connection of diubiquitin to LPS-induced atrophy. Setsuie *et al.* 2009 observed that UCH-L3's deubiquitinating activity was impaired in the presence of K48-linked diubiquitin [241]. The same group published evidence that UCH-L3 had a role indirectly phosphorylating the transcription factor forkhead box, class O 1 (FOXO1) [250]. Phosphorylation of FOXO1 retains it within the cytosol, and prevents FOXO1 dependent transcription. This is particularly interesting, in light of various studies that have observed LPS-induced upregulation of FOXO1, and its subsequent transcriptional activation of key proteins required for muscle atrophy. Our observation that diubiquitin is increased after 24 hours of LPS infusion suggests a potential mechanism of positive feedback during muscle wasting, demonstrated in Figure 6.2.

## **6.5. Final conclusions and future work**

ZNF216 expression increased after 24 hours of LPS-infusion in a sepsis model of atrophy in rats, supporting previous evidence that denervation- and fasting-induced atrophy upregulated ZNF216 expression [56]. Although ZNF216's ability to bind polyubiquitinated proteins did not permit identification of elusive atrophy substrates, affinity capture has highlighted the presence of a K48-linked ubiquitin dimer, increased expression in extensor digitorum longus (EDL) muscle under LPS-induced atrophy conditions in rats at the 24 hour time point. These results, together with mounting evidence of the importance and abundance of

Figure 6.2

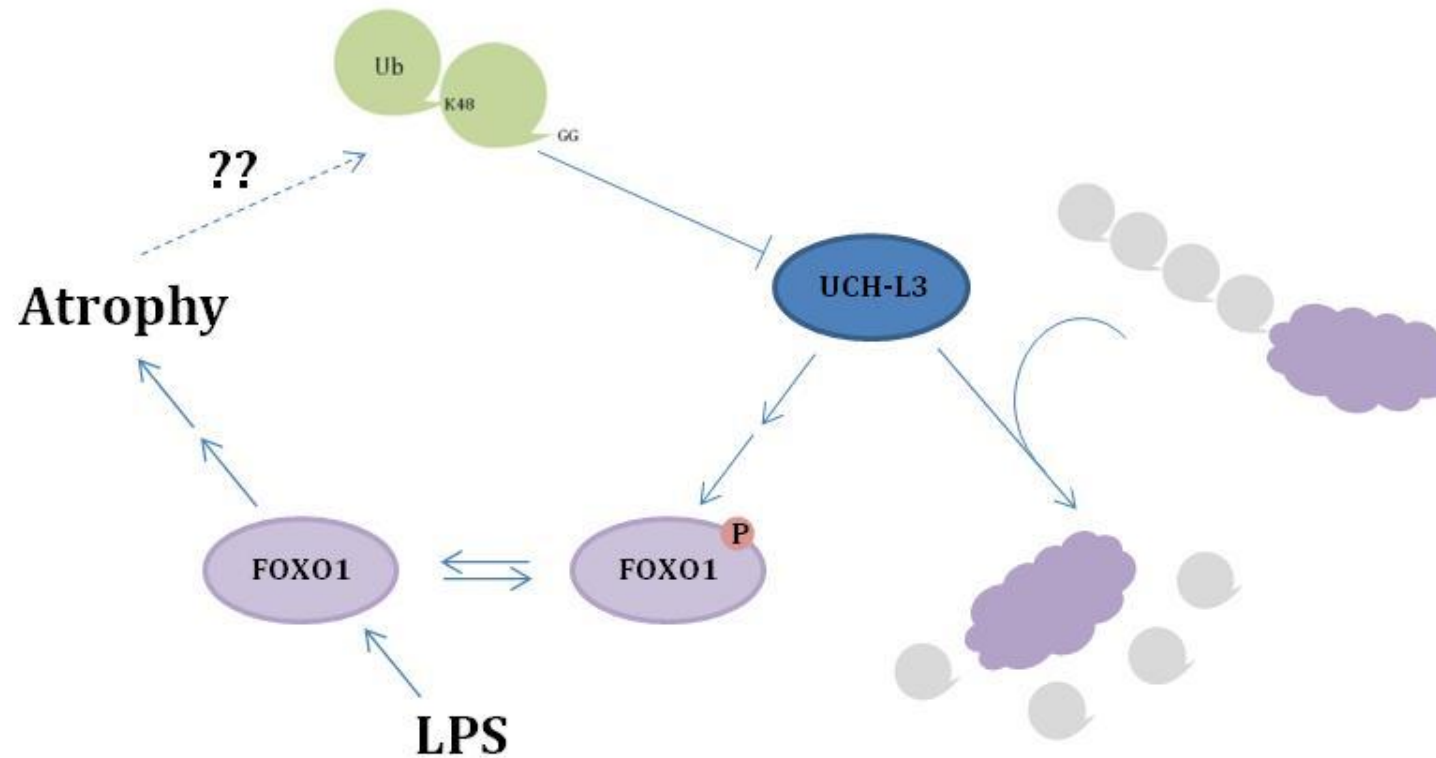


**Figure 6.2** Model of positive feedback during LPS-induced atrophy. Deubiquitinating enzyme UCH-L3 deconjugates polyubiquitinated proteins. It also indirectly leads to phosphorylation, and thus cellular retention, of transcription factor FOXO1. LPS induces FOXO1 dephosphorylation and subsequent activation, resulting in atrogene transcription and onset of atrophy. A K48-linked ubiquitin dimer has been shown to inhibit the deubiquitinating activity of UCH-L3 *in vitro*, and thus may impair FOXO1 inactivation. K48-linked ubiquitin dimer levels appear to increase after 24 hours of LPS infusion, that may induce positive feedback by reducing UCH-L3 mediated FOXO1 inhibition, and inducing further atrophy symptoms and further ubiquitin dimers.

unanchored polyubiquitin chains in recent literature, advocates the need for further research into the role of unanchored polyubiquitin. Our optimised affinity capture method affords the opportunity to enrich unanchored polyubiquitin and characterise it using MS techniques. Unanchored polyubiquitin affinity capture can be applied to different physiological conditions to identify changes in the unanchored polyubiquitin pool. ZNF216 knockout (KO) mice has been previously associated with accumulation of polyubiquitinated proteins under denervation-induced atrophy relative to wild type [56]. Future experiments of interest include generating a ZNF216 KO model and comparing unanchored polyubiquitin levels between atrophying wild type and ZNF216 KO samples, or inducing unanchored polyubiquitin *via* interleukin-1 beta (IL-1 $\beta$ ) stimulation of cells, as indirectly noted by Xia *et al.* 2009 [179], for purification and subsequent MS analysis.

Our method for purifying unanchored polyubiquitin is timely, considering growing interest in this field, and provides an opportunity to investigate this novel area and discover previously unidentified physiological conditions and diseases associated with free polyubiquitin chains.

## References

1. Dewys, W.D., et al., *Prognostic effect of weight loss prior to chemotherapy in cancer patients. Eastern Cooperative Oncology Group.* Am J Med, 1980. **69**(4): p. 491-7.
2. Coats, A.J., *Origin of symptoms in patients with cachexia with special reference to weakness and shortness of breath.* Int J Cardiol, 2002. **85**(1): p. 133-9.
3. Pajak, B., et al., *Crossroads of cytokine signaling--the chase to stop muscle cachexia.* J Physiol Pharmacol, 2008. **59 Suppl 9**: p. 251-64.
4. Zamir, O., et al., *Muscle protein breakdown during endotoxemia in rats and after treatment with interleukin-1 receptor antagonist (IL-1ra).* Ann Surg, 1992. **216**(3): p. 381-5; discussion 386-7.
5. Tiao, G., et al., *Energy-ubiquitin-dependent muscle proteolysis during sepsis in rats is regulated by glucocorticoids.* J Clin Invest, 1996. **97**(2): p. 339-48.
6. Tiao, G., et al., *Sepsis stimulates nonlysosomal, energy-dependent proteolysis and increases ubiquitin mRNA levels in rat skeletal muscle.* J Clin Invest, 1994. **94**(6): p. 2255-64.
7. Furuno, K., M.N. Goodman, and A.L. Goldberg, *Role of different proteolytic systems in the degradation of muscle proteins during denervation atrophy.* J Biol Chem, 1990. **265**(15): p. 8550-7.
8. Finol, H.J., D.M. Lewis, and R. Owens, *The effects of denervation on contractile properties of rat skeletal muscle.* J Physiol, 1981. **319**: p. 81-92.
9. Huey, K.A. and S.C. Bodine, *Changes in myosin mRNA and protein expression in denervated rat soleus and tibialis anterior.* Eur J Biochem, 1998. **256**(1): p. 45-50.
10. Patterson, M.F., G.M. Stephenson, and D.G. Stephenson, *Denervation produces different single fiber phenotypes in fast- and slow-twitch hindlimb muscles of the rat.* Am J Physiol Cell Physiol, 2006. **291**(3): p. C518-28.
11. Veldhuizen, J.W., et al., *Functional and morphological adaptations following four weeks of knee immobilization.* Int J Sports Med, 1993. **14**(5): p. 283-7.
12. Booth, F.W. and P.D. Gollnick, *Effects of disuse on the structure and function of skeletal muscle.* Med Sci Sports Exerc, 1983. **15**(5): p. 415-20.
13. Frimel, T.N., et al., *A model of muscle atrophy using cast immobilization in mice.* Muscle Nerve, 2005. **32**(5): p. 672-4.
14. Hasselgren, P.O., et al., *Novel aspects on the regulation of muscle wasting in sepsis.* Int J Biochem Cell Biol, 2005. **37**(10): p. 2156-68.
15. Rennie, M.J., S.M. Phillips, and E.A. Richter, *Newton's force as countermeasure for disuse atrophy.* J Appl Physiol, 2009. **107**(1): p. 6-7.
16. Thompson, L.V., *Age-related muscle dysfunction.* Exp Gerontol, 2009. **44**(1-2): p. 106-11.
17. Marzetti, E., et al., *Multiple pathways to the same end: mechanisms of myonuclear apoptosis in sarcopenia of aging.* ScientificWorldJournal, 2010. **10**: p. 340-9.
18. Murton, A.J. and P.L. Greenhaff, *Physiological control of muscle mass in humans during resistance exercise, disuse and rehabilitation.* Curr Opin Clin Nutr Metab Care, 2010. **13**(3): p. 249-54.
19. Constantin, D., et al., *Novel events in the molecular regulation of muscle mass in critically-ill patients.* J Physiol, 2011. **589** (Pt 15): p3883-95.
20. van Halteren, H.K., et al., *Recombinant human erythropoietin attenuates weight loss in a murine cancer cachexia model.* J Cancer Res Clin Oncol, 2004. **130**(4): p. 211-6.

21. Toledo, M., et al., *Cancer cachexia: physical activity and muscle force in tumour-bearing rats*. *Oncol Rep*, 2011. **25**(1): p. 189-93.
22. Doyle, A., et al., *Toll-like receptor 4 mediates lipopolysaccharide-induced muscle catabolism via coordinate activation of ubiquitin-proteasome and autophagy-lysosome pathways*. *FASEB J*, 2011. **25**(1): p. 99-110.
23. Triantafilou, M. and K. Triantafilou, *The dynamics of LPS recognition: complex orchestration of multiple receptors*. *J Endotoxin Res*, 2005. **11**(1): p. 5-11.
24. Fisher, A.L., *Of worms and women: sarcopenia and its role in disability and mortality*. *J Am Geriatr Soc*, 2004. **52**(7): p. 1185-90.
25. Chow, D.K., et al., *Sarcopenia in the *Caenorhabditis elegans* pharynx correlates with muscle contraction rate over lifespan*. *Exp Gerontol*, 2006. **41**(3): p. 252-60.
26. Kashyap, L., S. Perera, and A.L. Fisher, *Identification of Novel Genes Involved in Sarcopenia Through RNAi Screening in *Caenorhabditis elegans**. *J Gerontol A Biol Sci Med Sci*, 2012. **67**(1):56-65
27. Colman, R.J., et al., *Muscle mass loss in Rhesus monkeys: age of onset*. *Exp Gerontol*, 2005. **40**(7): p. 573-81.
28. McKiernan, S.H., et al., *Caloric restriction delays aging-induced cellular phenotypes in rhesus monkey skeletal muscle*. *Exp Gerontol*, 2011. **46**(1): p. 23-9.
29. Zierath, J.R. and J.A. Hawley, *Skeletal muscle fiber type: influence on contractile and metabolic properties*. *PLoS Biol*, 2004. **2**(10): p. e348.
30. Gamrin, L., et al., *A descriptive study of skeletal muscle metabolism in critically ill patients: free amino acids, energy-rich phosphates, protein, nucleic acids, fat, water, and electrolytes*. *Crit Care Med*, 1996. **24**(4): p. 575-83.
31. Murton, A.J., et al., *Effects of endotoxaemia on protein metabolism in rat fast-twitch skeletal muscle and myocardium*. *PLoS One*, 2009. **4**(9): p. e6945.
32. Crossland, H., et al., *A potential role for Akt/FOXO signalling in both protein loss and the impairment of muscle carbohydrate oxidation during sepsis in rodent skeletal muscle*. *J Physiol*, 2008. **586**(Pt 22): p. 5589-600.
33. Ogata, T., et al., *Fasting-related autophagic response in slow- and fast-twitch skeletal muscle*. *Biochem Biophys Res Commun*, 2010. **394**(1): p. 136-40.
34. Beehler, B.C., et al., *Reduction of skeletal muscle atrophy by a proteasome inhibitor in a rat model of denervation*. *Exp Biol Med (Maywood)*, 2006. **231**(3): p. 335-41.
35. Vermaelen, M., et al., *Ubiquitin targeting of rat muscle proteins during short periods of unloading*. *Acta Physiol Scand*, 2005. **185**(1): p. 33-40.
36. Wing, S.S., A.L. Haas, and A.L. Goldberg, *Increase in ubiquitin-protein conjugates concomitant with the increase in proteolysis in rat skeletal muscle during starvation and atrophy denervation*. *Biochem J*, 1995. **307** (Pt 3): p. 639-45.
37. Murton, A.J., D. Constantin, and P.L. Greenhaff, *The involvement of the ubiquitin proteasome system in human skeletal muscle remodelling and atrophy*. *Biochim Biophys Acta*, 2008. **1782**(12): p. 730-43.
38. Li, W., et al., *Interleukin-1 stimulates catabolism in C2C12 myotubes*. *Am J Physiol Cell Physiol*, 2009. **297**(3): p. C706-14.
39. Sandri, M., *Signaling in muscle atrophy and hypertrophy*. *Physiology (Bethesda)*, 2008. **23**: p. 160-70.

40. Sacheck, J.M., et al., *IGF-I stimulates muscle growth by suppressing protein breakdown and expression of atrophy-related ubiquitin ligases, atrogin-1 and MuRF1*. *Am J Physiol Endocrinol Metab*, 2004. **287**(4): p. E591-601.
41. Stitt, T.N., et al., *The IGF-1/PI3K/Akt pathway prevents expression of muscle atrophy-induced ubiquitin ligases by inhibiting FOXO transcription factors*. *Mol Cell*, 2004. **14**(3): p. 395-403.
42. Fan, J., et al., *Differential tissue regulation of insulin-like growth factor-I content and binding proteins after endotoxin*. *Endocrinology*, 1994. **134**(4): p. 1685-92.
43. Attard-Montalto, S.P., et al., *Changes in protein turnover, IGF-I and IGF binding proteins in children with cancer*. *Acta Paediatr*, 1998. **87**(1): p. 54-60.
44. Penna, F., et al., *Muscle atrophy in experimental cancer cachexia: is the IGF-1 signaling pathway involved?* *Int J Cancer*, 2010. **127**(7): p. 1706-17.
45. Costelli, P., et al., *IGF-1 is downregulated in experimental cancer cachexia*. *Am J Physiol Regul Integr Comp Physiol*, 2006. **291**(3): p. R674-83.
46. Emery, P.W., et al., *Protein synthesis in muscle measured in vivo in cachectic patients with cancer*. *Br Med J (Clin Res Ed)*, 1984. **289**(6445): p. 584-6.
47. Tisdale, M.J., *Cancer cachexia*. *Langenbecks Arch Surg*, 2004. **389**(4): p. 299-305.
48. Svanberg, E., et al., *IGF-I/IGFBP-3 binary complex modulates sepsis-induced inhibition of protein synthesis in skeletal muscle*. *Am J Physiol Endocrinol Metab*, 2000. **279**(5): p. E1145-58.
49. Latres, E., et al., *Insulin-like growth factor-1 (IGF-1) inversely regulates atrophy-induced genes via the phosphatidylinositol 3-kinase/Akt/mammalian target of rapamycin (PI3K/Akt/mTOR) pathway*. *J Biol Chem*, 2005. **280**(4): p. 2737-44.
50. Wray, C.J., et al., *Sepsis upregulates the gene expression of multiple ubiquitin ligases in skeletal muscle*. *Int J Biochem Cell Biol*, 2003. **35**(5): p. 698-705.
51. Tiao, G., et al., *Sepsis is associated with increased mRNAs of the ubiquitin-proteasome proteolytic pathway in human skeletal muscle*. *J Clin Invest*, 1997. **99**(2): p. 163-8.
52. Hobler, S.C., et al., *Sepsis-induced increase in muscle proteolysis is blocked by specific proteasome inhibitors*. *Am J Physiol*, 1998. **274**(1 Pt 2): p. R30-7.
53. Bodine, S.C., et al., *Identification of ubiquitin ligases required for skeletal muscle atrophy*. *Science*, 2001. **294**(5547): p. 1704-8.
54. Cong, H., et al., *Inhibition of atrogin-1/MAFbx expression by adenovirus-delivered small hairpin RNAs attenuates muscle atrophy in fasting mice*. *Hum Gene Ther*, 2010. **22**(3): p. 313-24.
55. Lecker, S.H., et al., *Multiple types of skeletal muscle atrophy involve a common program of changes in gene expression*. *FASEB J*, 2004. **18**(1): p. 39-51.
56. Hishiya, A., et al., *A novel ubiquitin-binding protein ZNF216 functioning in muscle atrophy*. *EMBO J*, 2006. **25**(3): p. 554-64.
57. Paul, P.K., et al., *Targeted ablation of TRAF6 inhibits skeletal muscle wasting in mice*. *J Cell Biol*, 2010. **191**(7): p. 1395-411.
58. Bialek, P., et al., *Distinct Protein Degradation Profiles are Induced by Different Disuse Models of Skeletal Muscle Atrophy*. *Physiol Genomics*, 2011. **43**(19): 1075-86.
59. Sandri, M., *Autophagy in skeletal muscle*. *FEBS Lett*, 2010. **584**(7): p. 1411-6.

60. Raben, N., et al., *Suppression of autophagy in skeletal muscle uncovers the accumulation of ubiquitinated proteins and their potential role in muscle damage in Pompe disease*. Hum Mol Genet, 2008. **17**(24): p. 3897-908.
61. Masiero, E., et al., *Autophagy is required to maintain muscle mass*. Cell Metab, 2009. **10**(6): p. 507-15.
62. Maiuri, M.C., et al., *Self-eating and self-killing: crosstalk between autophagy and apoptosis*. Nat Rev Mol Cell Biol, 2007. **8**(9): p. 741-52.
63. Yousefi, S., et al., *Calpain-mediated cleavage of Atg5 switches autophagy to apoptosis*. Nat Cell Biol, 2006. **8**(10): p. 1124-32.
64. Smith, I.J., S.H. Lecker, and P.O. Hasselgren, *Calpain activity and muscle wasting in sepsis*. Am J Physiol Endocrinol Metab, 2008. **295**(4): p. E762-71.
65. Smuder, A.J., et al., *Oxidation enhances myofibrillar protein degradation via calpain and caspase-3*. Free Radic Biol Med, 2010. **49**(7): p. 1152-60.
66. Jagoe, R.T. and A.L. Goldberg, *What do we really know about the ubiquitin-proteasome pathway in muscle atrophy?* Curr Opin Clin Nutr Metab Care, 2001. **4**(3): p. 183-90.
67. Donohoe, C.L., A.M. Ryan, and J.V. Reynolds, *Cancer cachexia: mechanisms and clinical implications*. Gastroenterol Res Pract, 2011. **2011**: p. 601434.
68. Piotrowski, J., et al., *Inhibition of the 26 S proteasome by polyubiquitin chains synthesized to have defined lengths*. J Biol Chem, 1997. **272**(38): p. 23712-21.
69. Lam, Y.A., et al., *Inhibition of the ubiquitin-proteasome system in Alzheimer's disease*. Proc Natl Acad Sci U S A, 2000. **97**(18): p. 9902-6.
70. van Leeuwen, F.W., et al., *Molecular misreading: a new type of transcript mutation expressed during aging*. Neurobiol Aging, 2000. **21**(6): p. 879-91.
71. Layfield, R., *Does an inhibition of the ubiquitin/26S proteasome pathway of protein degradation underlie the pathogenesis of non-familial Alzheimer's disease?* Med Hypotheses, 2001. **56**(3): p. 395-9.
72. Imai, J., et al., *Proteasomes and molecular chaperones: cellular machinery responsible for folding and destruction of unfolded proteins*. Cell Cycle, 2003. **2**(6): p. 585-90.
73. Ross, C.A. and M.A. Poirier, *Protein aggregation and neurodegenerative disease*. Nat Med, 2004. **10** Suppl: p. S10-7.
74. Claeys, K.G., et al., *DNAJB2 Expression in Normal and Diseased Human and Mouse Skeletal Muscle*. Am J Pathol, 2010. **176**(6):2901-10
75. Johnston, J.A., C.L. Ward, and R.R. Kopito, *Aggresomes: a cellular response to misfolded proteins*. J Cell Biol, 1998. **143**(7): p. 1883-98.
76. Taylor, J.P., et al., *Aggresomes protect cells by enhancing the degradation of toxic polyglutamine-containing protein*. Hum Mol Genet, 2003. **12**(7): p. 749-57.
77. Olzmann, J.A. and L.S. Chin, *Parkin-mediated K63-linked polyubiquitination: a signal for targeting misfolded proteins to the aggresome-autophagy pathway*. Autophagy, 2008. **4**(1): p. 85-7.
78. Kraft, C., M. Peter, and K. Hofmann, *Selective autophagy: ubiquitin-mediated recognition and beyond*. Nat Cell Biol, 2010. **12**(9): p. 836-41.
79. Pankiv, S., et al., *p62/SQSTM1 binds directly to Atg8/LC3 to facilitate degradation of ubiquitinated protein aggregates by autophagy*. J Biol Chem, 2007. **282**(33): p. 24131-45.
80. Ravid, T. and M. Hochstrasser, *Diversity of degradation signals in the ubiquitin-proteasome system*. Nat Rev Mol Cell Biol, 2008. **9**(9): p. 679-90.
81. Varshavsky, A., *The N-end rule pathway and regulation by proteolysis*. Protein Sci, 2011. doi: 10.1002/pro.666

82. Mogk, A., R. Schmidt, and B. Bukau, *The N-end rule pathway for regulated proteolysis: prokaryotic and eukaryotic strategies*. Trends Cell Biol, 2007. **17**(4): p. 165-72.
83. Hershko, A. and A. Ciechanover, *The ubiquitin system*. Annu Rev Biochem, 1998. **67**: p. 425-79.
84. Ciechanover, A., *N-terminal ubiquitination*. Methods Mol Biol, 2005. **301**: p. 255-70.
85. Nagy, V. and I. Dikic, *Ubiquitin ligase complexes: from substrate selectivity to conjugational specificity*. Biol Chem, 2010. **391**(2-3): p. 163-9.
86. Rotin, D. and S. Kumar, *Physiological functions of the HECT family of ubiquitin ligases*. Nat Rev Mol Cell Biol, 2009. **10**(6): p. 398-409.
87. Cardozo, T. and M. Pagano, *The SCF ubiquitin ligase: insights into a molecular machine*. Nat Rev Mol Cell Biol, 2004. **5**(9): p. 739-51.
88. Ohi, M.D., et al., *Structural insights into the U-box, a domain associated with multi-ubiquitination*. Nat Struct Biol, 2003. **10**(4): p. 250-5.
89. Hatakeyama, S. and K.I. Nakayama, *U-box proteins as a new family of ubiquitin ligases*. Biochem Biophys Res Commun, 2003. **302**(4): p. 635-45.
90. Marin, I., *Ancient origin of animal U-box ubiquitin ligases*. BMC Evol Biol, 2010. **10**: p. 331.
91. Zeng, L.R., et al., *Classification, expression pattern, and E3 ligase activity assay of rice U-box-containing proteins*. Mol Plant, 2008. **1**(5): p. 800-15.
92. Chen, L. and K. Madura, *Rad23 promotes the targeting of proteolytic substrates to the proteasome*. Mol Cell Biol, 2002. **22**(13): p. 4902-13.
93. Funakoshi, M., et al., *Budding yeast Dsk2p is a polyubiquitin-binding protein that can interact with the proteasome*. Proc Natl Acad Sci U S A, 2002. **99**(2): p. 745-50.
94. Sasaki, T., et al., *Budding yeast Dsk2 protein forms a homodimer via its C-terminal UBA domain*. Biochem Biophys Res Commun, 2005. **336**(2): p. 530-5.
95. Todi, S.V., et al., *Cellular turnover of the polyglutamine disease protein ataxin-3 is regulated by its catalytic activity*. J Biol Chem, 2007. **282**(40): p. 29348-58.
96. Zhang, D., et al., *Together, Rpn10 and Dsk2 can serve as a polyubiquitin chain-length sensor*. Mol Cell, 2009. **36**(6): p. 1018-33.
97. Gomes, M.D., et al., *Atrogin-1, a muscle-specific F-box protein highly expressed during muscle atrophy*. Proc Natl Acad Sci U S A, 2001. **98**(25): p. 14440-5.
98. Bai, C., R. Richman, and S.J. Elledge, *Human cyclin F*. EMBO J, 1994. **13**(24): p. 6087-98.
99. Bai, C., et al., *SKP1 connects cell cycle regulators to the ubiquitin proteolysis machinery through a novel motif, the F-box*. Cell, 1996. **86**(2): p. 263-74.
100. Cenciarelli, C., et al., *Identification of a family of human F-box proteins*. Curr Biol, 1999. **9**(20): p. 1177-9.
101. Kipreos, E.T. and M. Pagano, *The F-box protein family*. Genome Biol, 2000. **1**(5): p. REVIEWS3002.
102. Winston, J.T., et al., *A family of mammalian F-box proteins*. Curr Biol, 1999. **9**(20): p. 1180-2.
103. Maragno, A.L., M.M. Baqui, and M.D. Gomes, *FBXO25, an F-box protein homologue of atrogin-1, is not induced in atrophying muscle*. Biochim Biophys Acta, 2006. **1760**(6): p. 966-72.
104. Jang, J.W., et al., *A novel Fbxo25 acts as an E3 ligase for destructing cardiac specific transcription factors*. Biochem Biophys Res Commun, 2011. **410**(2): p. 183-8.

105. Tintignac, L.A., et al., *Degradation of MyoD mediated by the SCF (MAFbx) ubiquitin ligase*. J Biol Chem, 2005. **280**(4): p. 2847-56.
106. Lagirand-Cantaloube, J., et al., *The initiation factor eIF3-f is a major target for Atrogin1/MAFbx function in skeletal muscle atrophy*. EMBO J, 2008. **27**(8): p. 1266-76
107. Centner, T., et al., *Identification of muscle specific ring finger proteins as potential regulators of the titin kinase domain*. J Mol Biol, 2001. **306**(4): p. 717-26.
108. Fielitz, J., et al., *Myosin accumulation and striated muscle myopathy result from the loss of muscle RING finger 1 and 3*. J Clin Invest, 2007. **117**(9): p. 2486-95.
109. Witt, S.H., et al., *MURF-1 and MURF-2 target a specific subset of myofibrillar proteins redundantly: towards understanding MURF-dependent muscle ubiquitination*. J Mol Biol, 2005. **350**(4): p. 713-22.
110. Lange, S., et al., *The kinase domain of titin controls muscle gene expression and protein turnover*. Science, 2005. **308**(5728): p. 1599-603.
111. Clarke, B.A., et al., *The E3 Ligase MuRF1 degrades myosin heavy chain protein in dexamethasone-treated skeletal muscle*. Cell Metab, 2007. **6**(5): p. 376-85.
112. Cohen, S., et al., *During muscle atrophy, thick, but not thin, filament components are degraded by MuRF1-dependent ubiquitylation*. J Cell Biol, 2009. **185**(6): p. 1083-95
113. Kedar, V., et al., *Muscle-specific RING finger 1 is a bona fide ubiquitin ligase that degrades cardiac troponin I*. Proc Natl Acad Sci U S A, 2004. **101**(52): p. 18135-40.
114. Polge, C., et al., *Muscle actin is polyubiquitinated in vitro and in vivo and targeted for breakdown by the E3 ligase MuRF1*. FASEB J, 2011. **25**(11): p. 3790-802.
115. Arendt, C.S. and M. Hochstrasser, *Identification of the yeast 20S proteasome catalytic centers and subunit interactions required for active-site formation*. Proc Natl Acad Sci U S A, 1997. **94**(14): p. 7156-61.
116. Heinemeyer, W., et al., *The active sites of the eukaryotic 20 S proteasome and their involvement in subunit precursor processing*. J Biol Chem, 1997. **272**(40): p. 25200-9.
117. Husnjak, K., et al., *Proteasome subunit Rpn13 is a novel ubiquitin receptor*. Nature, 2008. **453**(7194): p. 481-8.
118. Schreiner, P., et al., *Ubiquitin docking at the proteasome through a novel pleckstrin-homology domain interaction*. Nature, 2008. **453**(7194): p. 548-52.
119. Bar-Nun, S. and M.H. Glickman, *Proteasomal AAA-ATPases: Structure and function*. Biochim Biophys Acta, 2012. **1823**(1): p. 67-82
120. Yao, T. and R.E. Cohen, *A cryptic protease couples deubiquitination and degradation by the proteasome*. Nature, 2002. **419**(6905): p. 403-7.
121. Reyes-Turcu, F.E., K.H. Ventii, and K.D. Wilkinson, *Regulation and cellular roles of ubiquitin-specific deubiquitinating enzymes*. Annu Rev Biochem, 2009. **78**: p. 363-97.
122. Zhang, N.Y., et al., *Ubiquitin chain trimming recycles the substrate binding sites of the 26 S proteasome and promotes degradation of lysine 48-linked polyubiquitin conjugates*. J Biol Chem, 2011. **286**(29): p. 25540-6
123. Prakash, S., et al., *An unstructured initiation site is required for efficient proteasome-mediated degradation*. Nat Struct Mol Biol, 2004. **11**(9): p. 830-7.
124. Schrader, E.K., K.G. Harstad, and A. Matouschek, *Targeting proteins for degradation*. Nat Chem Biol, 2009. **5**(11): p. 815-22.

125. Takeuchi, J., H. Chen, and P. Coffino, *Proteasome substrate degradation requires association plus extended peptide*. EMBO J, 2007. **26**(1): p. 123-31.
126. Inobe, T., et al., *Defining the geometry of the two-component proteasome degron*. Nat Chem Biol, 2011. **7**(3): p. 161-7
127. Kimura, Y. and K. Tanaka, *Regulatory mechanisms involved in the control of ubiquitin homeostasis*. J Biochem, 2010. **147**(6): p. 793-8.
128. Li, M., et al., *Deubiquitination of p53 by HAUSP is an important pathway for p53 stabilization*. Nature, 2002. **416**(6881): p. 648-53.
129. Kruse, J.P. and W. Gu, *Modes of p53 regulation*. Cell, 2009. **137**(4): p. 609-22.
130. Li, M., et al., *A dynamic role of HAUSP in the p53-Mdm2 pathway*. Mol Cell, 2004. **13**(6): p. 879-86.
131. Cummins, J.M. and B. Vogelstein, *HAUSP is required for p53 destabilization*. Cell Cycle, 2004. **3**(6): p. 689-92.
132. Sun, S.C., *CYLD: a tumor suppressor deubiquitinase regulating NF-kappaB activation and diverse biological processes*. Cell Death Differ, 2010. **17**(1): p. 25-34.
133. Wang, T., et al., *Evidence for bidentate substrate binding as the basis for the K48 linkage specificity of otubain 1*. J Mol Biol, 2009. **386**(4): p. 1011-23.
134. Amerik, A., et al., *In vivo disassembly of free polyubiquitin chains by yeast Ubp14 modulates rates of protein degradation by the proteasome*. EMBO J, 1997. **16**(16): p. 4826-38.
135. Wiborg, O., et al., *The human ubiquitin multigene family: some genes contain multiple directly repeated ubiquitin coding sequences*. EMBO J, 1985. **4**(3): p. 755-9.
136. Baker, R.T. and P.G. Board, *The human ubiquitin gene family: structure of a gene and pseudogenes from the Ub B subfamily*. Nucleic Acids Res, 1987. **15**(2): p. 443-63.
137. Ozkaynak, E., et al., *The yeast ubiquitin genes: a family of natural gene fusions*. EMBO J, 1987. **6**(5): p. 1429-39.
138. Redman, K.L. and M. Rechsteiner, *Identification of the long ubiquitin extension as ribosomal protein S27a*. Nature, 1989. **338**(6214): p. 438-40.
139. Bosanac, I., et al., *Ubiquitin binding to A20 ZnF4 is required for modulation of NF-kappaB signaling*. Mol Cell, 2010. **40**(4): p. 548-57.
140. Bomar, M.G., et al., *Structure of the ubiquitin-binding zinc finger domain of human DNA Y-polymerase eta*. EMBO Rep, 2007. **8**(3): p. 247-51.
141. Reyes-Turcu, F.E., et al., *The ubiquitin binding domain ZnF UBP recognizes the C-terminal diglycine motif of unanchored ubiquitin*. Cell, 2006. **124**(6): p. 1197-208.
142. Hayden, M.S. and S. Ghosh, *Signaling to NF-kappaB*. Genes Dev, 2004. **18**(18): p. 2195-224.
143. Hayden, M.S. and S. Ghosh, *Shared principles in NF-kappaB signaling*. Cell, 2008. **132**(3): p. 344-62.
144. Liu, S. and Z.J. Chen, *Expanding role of ubiquitination in NF-kappaB signaling*. Cell Res, 2011. **21**(1): p. 6-21.
145. Perkins, N.D., *Integrating cell-signalling pathways with NF-kappaB and IKK function*. Nat Rev Mol Cell Biol, 2007. **8**(1): p. 49-62.
146. Li, W., et al., *A ubiquitin ligase transfers preformed polyubiquitin chains from a conjugating enzyme to a substrate*. Nature, 2007. **446**(7133): p. 333-7.
147. Goldknopf, I.L., et al., *Isolation and characterization of protein A24, a "histone-like" non-histone chromosomal protein*. J Biol Chem, 1975. **250**(18): p. 7182-7.

148. Zhou, W., X. Wang, and M.G. Rosenfeld, *Histone H2A ubiquitination in transcriptional regulation and DNA damage repair*. Int J Biochem Cell Biol, 2009. **41**(1): p. 12-5.
149. Carter, R.S., et al., *Persistent activation of NF-kappa B by the tax transforming protein involves chronic phosphorylation of IkappaB kinase subunits IKKbeta and IKKgamma*. J Biol Chem, 2001. **276**(27): p. 24445-8.
150. Carter, R.S., et al., *Site-specific monoubiquitination of IkappaB kinase IKKbeta regulates its phosphorylation and persistent activation*. J Biol Chem, 2005. **280**(52): p. 43272-9.
151. Carter, R.S., et al., *Signal-induced ubiquitination of IkappaB Kinase-beta*. J Biol Chem, 2003. **278**(49): p. 48903-6.
152. Niida, M., M. Tanaka, and T. Kamitani, *Downregulation of active IKK beta by Ro52-mediated autophagy*. Mol Immunol, 2010. **47**(14): p. 2378-87.
153. Mosesson, Y. and Y. Yarden, *Monoubiquitylation: a recurrent theme in membrane protein transport*. Isr Med Assoc J, 2006. **8**(4): p. 233-7.
154. Hicke, L. and R. Dunn, *Regulation of membrane protein transport by ubiquitin and ubiquitin-binding proteins*. Annu Rev Cell Dev Biol, 2003. **19**: p. 141-72.
155. Xu, P., et al., *Quantitative proteomics reveals the function of unconventional ubiquitin chains in proteasomal degradation*. Cell, 2009. **137**(1): p. 133-45.
156. Kirkpatrick, D.S., et al., *Quantitative analysis of in vitro ubiquitinated cyclin B1 reveals complex chain topology*. Nat Cell Biol, 2006. **8**(7): p. 700-10.
157. Thrower, J.S., et al., *Recognition of the polyubiquitin proteolytic signal*. EMBO J, 2000. **19**(1): p. 94-102.
158. Ishida, T., et al., *Identification of TRAF6, a novel tumor necrosis factor receptor-associated factor protein that mediates signaling from an amino-terminal domain of the CD40 cytoplasmic region*. J Biol Chem, 1996. **271**(46): p. 28745-8.
159. Cao, Z., et al., *TRAF6 is a signal transducer for interleukin-1*. Nature, 1996. **383**(6599): p. 443-6.
160. Deng, L., et al., *Activation of the IkappaB kinase complex by TRAF6 requires a dimeric ubiquitin-conjugating enzyme complex and a unique polyubiquitin chain*. Cell, 2000. **103**(2): p. 351-61.
161. Iwai, K., *Functions of Linear Ubiquitin Chains in the NF-kappaB Pathway : Linear Polyubiquitin in NF-kappaB Signaling*. Subcell Biochem, 2010. **54**: p. 100-6.
162. Iwai, K., *Linear polyubiquitin chains: A new modifier involved in NF-kappaB activation and chronic inflammation including dermatitis*. Cell Cycle, 2010. **10**(18): p. 3095-104
163. Iwai, K. and F. Tokunaga, *Linear polyubiquitination: a new regulator of NF-kappaB activation*. EMBO Rep, 2009. **10**(7): p. 706-13.
164. Niu, J., et al., *LUBAC regulates NF-kappaB activation upon genotoxic stress by promoting linear ubiquitination of NEMO*. EMBO J, 2011. **30**(18): p. 3741-53.
165. Rahighi, S., et al., *Specific recognition of linear ubiquitin chains by NEMO is important for NF-kappaB activation*. Cell, 2009. **136**(6): p. 1098-109.
166. Tokunaga, F. and K. Iwai, *[Involvement of LUBAC-mediated linear polyubiquitination of NEMO in NF-kappaB activation]*. Tanpakushitsu Kakusan Koso, 2009. **54**(5): p. 635-42.
167. Arimoto, K., et al., *Polyubiquitin conjugation to NEMO by tripartite motif protein 23 (TRIM23) is critical in antiviral defense*. Proc Natl Acad Sci U S A, 2010. **107**(36): p. 15856-61.

168. Nishikawa, H., et al., *Mass spectrometric and mutational analyses reveal Lys-6-linked polyubiquitin chains catalyzed by BRCA1-BARD1 ubiquitin ligase*. J Biol Chem, 2004. **279**(6): p. 3916-24.
169. Bremm, A. and D. Komander, *Emerging roles for Lys11-linked polyubiquitin in cellular regulation*. Trends Biochem Sci, 2011. **36**(7): p. 355-63.
170. Hoege, C., et al., *RAD6-dependent DNA repair is linked to modification of PCNA by ubiquitin and SUMO*. Nature, 2002. **419**(6903): p. 135-41.
171. Zhao, S. and H.D. Ulrich, *Distinct consequences of posttranslational modification by linear versus K63-linked polyubiquitin chains*. Proc Natl Acad Sci U S A, 2010. **107**(17): p. 7704-9.
172. Ben-Saadon, R., et al., *The polycomb protein Ring1B generates self atypical mixed ubiquitin chains required for its in vitro histone H2A ligase activity*. Mol Cell, 2006. **24**(5): p. 701-11.
173. Kim, H.T., et al., *S5a promotes protein degradation by blocking synthesis of nondegradable forked ubiquitin chains*. EMBO J, 2009. **28**(13): p. 1867-77.
174. Bedford, L., et al., *Diverse polyubiquitin chains accumulate following 26S proteasomal dysfunction in mammalian neurones*. Neurosci Lett, 2010. doi: 10.1016/j.neulet.2010.12.064
175. Dammer, E.B., et al., *Polyubiquitin linkage profiles in three models of proteolytic stress suggest the etiology of Alzheimer disease*. J Biol Chem, 2010. **286**(12): p. 10457-65.
176. Kaiser, S.E., et al., *Protein standard absolute quantification (PSAQ) method for the measurement of cellular ubiquitin pools*. Nat Methods, 2011. **8**(8): p. 691-6.
177. Dayal, S., et al., *Suppression of the deubiquitinating enzyme USP5 causes the accumulation of unanchored polyubiquitin and the activation of p53*. J Biol Chem, 2009. **284**(8): p. 5030-41.
178. Kimura, Y., et al., *An inhibitor of a deubiquitinating enzyme regulates ubiquitin homeostasis*. Cell, 2009. **137**(3): p. 549-59.
179. Xia, Z.P., et al., *Direct activation of protein kinases by unanchored polyubiquitin chains*. Nature, 2009. **461**(7260): p. 114-9.
180. Pertel, T., et al., *TRIM5 is an innate immune sensor for the retrovirus capsid lattice*. Nature, 2011. **472**(7343): p. 361-5.
181. Zeng, W., et al., *Reconstitution of the RIG-I pathway reveals a signaling role of unanchored polyubiquitin chains in innate immunity*. Cell, 2010. **141**(2): p. 315-30.
182. Dikic, I., S. Wakatsuki, and K.J. Walters, *Ubiquitin-binding domains - from structures to functions*. Nat Rev Mol Cell Biol, 2009. **10**(10): p. 659-71.
183. Brzovic, P.S., et al., *A UbcH5/ubiquitin noncovalent complex is required for processive BRCA1-directed ubiquitination*. Mol Cell, 2006. **21**(6): p. 873-80.
184. Cavey, J.R., et al., *Loss of ubiquitin-binding associated with Paget's disease of bone p62 (SQSTM1) mutations*. J Bone Miner Res, 2005. **20**(4): p. 619-24.
185. Lee, S., et al., *Structural basis for ubiquitin recognition and autoubiquitination by Rabex-5*. Nat Struct Mol Biol, 2006. **13**(3): p. 264-71.
186. Raasi, S., et al., *Diverse polyubiquitin interaction properties of ubiquitin-associated domains*. Nat Struct Mol Biol, 2005. **12**(8): p. 708-14.
187. Komander, D., et al., *Molecular discrimination of structurally equivalent Lys 63-linked and linear polyubiquitin chains*. EMBO Rep, 2009. **10**(5): p. 466-73.
188. Peng, J., et al., *A proteomics approach to understanding protein ubiquitination*. Nat Biotechnol, 2003. **21**(8): p. 921-6.

189. Kirkpatrick, D.S., et al., *Proteomic identification of ubiquitinated proteins from human cells expressing His-tagged ubiquitin*. *Proteomics*, 2005. **5**(8): p. 2104-11.
190. Jeon, H.B., et al., *A proteomics approach to identify the ubiquitinated proteins in mouse heart*. *Biochem Biophys Res Commun*, 2007. **357**(3): p. 731-6.
191. Layfield, R., et al., *Purification of poly-ubiquitinated proteins by S5a-affinity chromatography*. *Proteomics*, 2001. **1**(6): p. 773-7.
192. Matsumoto, M., et al., *Large-scale analysis of the human ubiquitin-related proteome*. *Proteomics*, 2005. **5**(16): p. 4145-51.
193. Hjerpe, R., et al., *Efficient protection and isolation of ubiquitylated proteins using tandem ubiquitin-binding entities*. *EMBO Rep*, 2009. **10**(11): p. 1250-8.
194. Ventadour, S., et al., *A new method of purification of proteasome substrates reveals polyubiquitination of 20 S proteasome subunits*. *J Biol Chem*, 2007. **282**(8): p. 5302-9.
195. Kim, W., et al., *Systematic and Quantitative Assessment of the Ubiquitin-Modified Proteome*. *Mol Cell*, 2011. **44**(2): p. 325-40
196. Huang, J., et al., *ZNF216 Is an A20-like and IkappaB kinase gamma-interacting inhibitor of NFkappaB activation*. *J Biol Chem*, 2004. **279**(16): p. 16847-53.
197. Scott, D.A., et al., *Identification and mutation analysis of a cochlear-expressed, zinc finger protein gene at the DFNB7/11 and dn hearing-loss loci on human chromosome 9q and mouse chromosome 19*. *Gene*, 1998. **215**(2): p. 461-9.
198. Hishiya, A., K. Ikeda, and K. Watanabe, *A RANKL-inducible gene Znf216 in osteoclast differentiation*. *J Recept Signal Transduct Res*, 2005. **25**(3): p. 199-216.
199. Fenner, B.J., M. Scannell, and J.H. Prehn, *Identification of polyubiquitin binding proteins involved in NF-kappaB signaling using protein arrays*. *Biochim Biophys Acta*, 2009. **1794**(7): p. 1010-6.
200. Forsberg, A.M., et al., *Muscle composition in relation to age and sex*. *Clin Sci (Lond)*, 1991. **81**(2): p. 249-56.
201. Mitch, W.E., et al., *Metabolic acidosis stimulates muscle protein degradation by activating the adenosine triphosphate-dependent pathway involving ubiquitin and proteasomes*. *J Clin Invest*, 1994. **93**(5): p. 2127-33.
202. Bailey, J.L., et al., *The acidosis of chronic renal failure activates muscle proteolysis in rats by augmenting transcription of genes encoding proteins of the ATP-dependent ubiquitin-proteasome pathway*. *J Clin Invest*, 1996. **97**(6): p. 1447-53.
203. Hanai, J., et al., *The muscle-specific ubiquitin ligase atrogin-1/MAFbx mediates statin-induced muscle toxicity*. *J Clin Invest*, 2007. **117**(12): p. 3940-51.
204. Sugita, H., et al., *Burn injury impairs insulin-stimulated Akt/PKB activation in skeletal muscle*. *Am J Physiol Endocrinol Metab*, 2005. **288**(3): p. E585-91.
205. Lundholm, K., et al., *Skeletal muscle metabolism in patients with malignant tumor*. *Eur J Cancer*, 1976. **12**(6): p. 465-73.
206. Pruznak, A.M., et al., *Skeletal and cardiac myopathy in HIV-1 transgenic rats*. *Am J Physiol Endocrinol Metab*, 2008. **295**(4): p. E964-73.
207. Sacheck, J.M., et al., *Rapid disuse and denervation atrophy involve transcriptional changes similar to those of muscle wasting during systemic diseases*. *FASEB J*, 2007. **21**(1): p. 140-55.

208. Crossland, H., et al., *Low-dose dexamethasone prevents endotoxaemia-induced muscle protein loss and impairment of carbohydrate oxidation in rat skeletal muscle*. J Physiol, 2010. **588**(Pt 8): p. 1333-47.
209. Mallinson, J.E., et al., *Blunted Akt/FOXO signalling and activation of genes controlling atrophy and fuel use in statin myopathy*. J Physiol, 2009. **587**(Pt 1): p. 219-30.
210. Tiao, G., et al., *Intracellular regulation of protein degradation during sepsis is different in fast- and slow-twitch muscle*. Am J Physiol, 1997. **272**(3 Pt 2): p. R849-56.
211. Thompson, P.D., P. Clarkson, and R.H. Karas, *Statin-associated myopathy*. JAMA, 2003. **289**(13): p. 1681-90.
212. Frost, R.A., et al., *Hormone, cytokine, and nutritional regulation of sepsis-induced increases in atrogin-1 and MuRF1 in skeletal muscle*. Am J Physiol Endocrinol Metab, 2007. **292**(2): p. E501-12.
213. Manfiolli, A.O., et al., *FBXO25-associated nuclear domains: a novel subnuclear structure*. Mol Biol Cell, 2008. **19**(5): p. 1848-61.
214. Moylan, J.S., et al., *TNF induction of atrogin-1/MAFbx mRNA depends on Foxo4 expression but not AKT-Foxo1/3 signaling*. Am J Physiol Cell Physiol, 2008. **295**(4): p. C986-93.
215. Constantin, D., et al., *PPARdelta agonism induces a change in fuel metabolism and activation of an atrophy programme, but does not impair mitochondrial function in rat skeletal muscle*. J Physiol, 2007. **583**(Pt 1): p. 381-90.
216. Vary, T.C., R.A. Frost, and C.H. Lang, *Acute alcohol intoxication increases atrogin-1 and MuRF1 mRNA without increasing proteolysis in skeletal muscle*. Am J Physiol Regul Integr Comp Physiol, 2008. **294**(6): p. R1777-89.
217. Garner, T.P., et al., *Independent interactions of ubiquitin-binding domains in a ubiquitin-mediated ternary complex*. Biochemistry, 2011. **50**(42): 9076-87
218. McTigue, M.A., D.R. Williams, and J.A. Tainer, *Crystal structures of a schistosomal drug and vaccine target: glutathione S-transferase from Schistosoma japonica and its complex with the leading antischistosomal drug praziquantel*. J Mol Biol, 1995. **246**(1): p. 21-7.
219. Chau, V., et al., *A multiubiquitin chain is confined to specific lysine in a targeted short-lived protein*. Science, 1989. **243**(4898): p. 1576-83.
220. Labeit, S., et al., *Modulation of muscle atrophy, fatigue and MLC phosphorylation by MuRF1 as indicated by hindlimb suspension studies on MuRF1-KO mice*. J Biomed Biotechnol, 2010. **2010**: p. 693741.
221. Schwartz, A.L. and A. Ciechanover, *Targeting Proteins for Destruction by the Ubiquitin System: Implications for Human Pathobiology*. Annu Rev Pharmacol Toxicol, 2009. **49**: p. 73-96
222. Tung, C.W. and S.Y. Ho, *Computational identification of ubiquitylation sites from protein sequences*. BMC Bioinformatics, 2008. **9**: p. 310.
223. Raasi, S. and C.M. Pickart, *Rad23 ubiquitin-associated domains (UBA) inhibit 26 S proteasome-catalyzed proteolysis by sequestering lysine 48-linked polyubiquitin chains*. J Biol Chem, 2003. **278**(11): p. 8951-9.
224. Li, W. and Y. Ye, *Polyubiquitin chains: functions, structures, and mechanisms*. Cell Mol Life Sci, 2008. **65**(15): 2397-406
225. Seibenhener, M.L., et al., *Sequestosome 1/p62 is a polyubiquitin chain binding protein involved in ubiquitin proteasome degradation*. Mol Cell Biol, 2004. **24**(18): p. 8055-68.

226. Raue, U., et al., *Proteolytic gene expression differs at rest and after resistance exercise between young and old women*. J Gerontol A Biol Sci Med Sci, 2007. **62**(12): p. 1407-12.
227. Nakahara, T., et al., *Acute and chronic effects of alcohol exposure on skeletal muscle c-myc, p53, and Bcl-2 mRNA expression*. Am J Physiol Endocrinol Metab, 2003. **285**(6): p. E1273-81.
228. Salehian, B., et al., *The effect of glutamine on prevention of glucocorticoid-induced skeletal muscle atrophy is associated with myostatin suppression*. Metabolism, 2006. **55**(9): p. 1239-47.
229. Hara, M.R., et al., *S-nitrosylated GAPDH initiates apoptotic cell death by nuclear translocation following Siah1 binding*. Nat Cell Biol, 2005. **7**(7): p. 665-74.
230. Tian, F., et al., *[Experimental study on losartan decreasing denervated skeletal muscle atrophy through reducing cell apoptosis]*. Zhongguo Xiu Fu Chong Jian Wai Ke Za Zhi, 2008. **22**(5): p. 602-5.
231. Nagano, K., et al., *The activation of apoptosis factor in hindlimb unloading-induced muscle atrophy under normal and low-temperature environmental conditions*. Acta Histochem, 2008. **110**(6): p. 505-18.
232. Guller, I. and A.P. Russell, *MicroRNAs in skeletal muscle: their role and regulation in development, disease and function*. J Physiol, 2010. **588**(Pt 21): p. 4075-87.
233. Prins, K.W., et al., *Quadriceps myopathy caused by skeletal muscle-specific ablation of beta(cyto)-actin*. J Cell Sci, 2011. **124**(Pt 6): p. 951-7.
234. Newton, K., et al., *Ubiquitin chain editing revealed by polyubiquitin linkage-specific antibodies*. Cell, 2008. **134**(4): p. 668-78.
235. Bocik, W.E., et al., *Mechanism of polyubiquitin chain recognition by the human ubiquitin conjugating enzyme ube2g2*. J Biol Chem, 2011. **286**(5): p. 3981-91.
236. Bremm, A., S.M. Freund, and D. Komander, *Lys11-linked ubiquitin chains adopt compact conformations and are preferentially hydrolyzed by the deubiquitinase Cezanne*. Nat Struct Mol Biol, 2010. **17**(8): p. 939-47.
237. Sato, Y., et al., *Structural basis for specific recognition of Lys 63-linked polyubiquitin chains by NZF domains of TAB2 and TAB3*. EMBO J, 2009. **28**(24): p. 3903-9.
238. Lange, A., et al., *NMR Reveals a Different Mode of Binding of the Stam2 VHS Domain to Ubiquitin and Diubiquitin*. Biochemistry, 2010. **50**(1): p. 48-62.
239. Virdee, S., et al., *Engineered diubiquitin synthesis reveals Lys29-isopeptide specificity of an OTU deubiquitinase*. Nat Chem Biol, 2010. **6**(10): p. 750-7.
240. Ryabov, Y. and D. Fushman, *Structural assembly of multidomain proteins and protein complexes guided by the overall rotational diffusion tensor*. J Am Chem Soc, 2007. **129**(25): p. 7894-902.
241. Setsuie, R., et al., *Ubiquitin dimers control the hydrolase activity of UCH-L3*. Neurochem Int, 2009. **54**(5-6): p. 314-21.
242. Penengo, L., et al., *Crystal structure of the ubiquitin binding domains of rabex-5 reveals two modes of interaction with ubiquitin*. Cell, 2006. **124**(6): p. 1183-95.
243. Baker, R.T., et al., *Using deubiquitylating enzymes as research tools*. Methods Enzymol, 2005. **398**: p. 540-54.
244. Ryu, K.Y., et al., *The mouse polyubiquitin gene Ubb is essential for meiotic progression*. Mol Cell Biol, 2008. **28**(3): p. 1136-46.
245. Ryu, K.Y., et al., *The mouse polyubiquitin gene Ubc is essential for fetal liver development, cell-cycle progression and stress tolerance*. EMBO J, 2007. **26**(11): p. 2693-706.

246. Chen, Z. and C.M. Pickart, *A 25-kilodalton ubiquitin carrier protein (E2) catalyzes multi-ubiquitin chain synthesis via lysine 48 of ubiquitin*. J Biol Chem, 1990. **265**(35): p. 21835-42.
247. van Nocker, S. and R.D. Vierstra, *Multiubiquitin chains linked through lysine 48 are abundant in vivo and are competent intermediates in the ubiquitin proteolytic pathway*. J Biol Chem, 1993. **268**(33): p. 24766-73.
248. Lee, M.J., et al., *Trimming of ubiquitin chains by proteasome-associated deubiquitinating enzymes*. Mol Cell Proteomics, 2011. **10**(5): p. R110 003871.
249. Wojcik, C., *Two blades of a sword: degradation coupled to deubiquitination*. Trends Cell Biol, 2002. **12**(12): p. 549.
250. Suzuki, M., R. Setsuie, and K. Wada, *Ubiquitin carboxyl-terminal hydrolase 13 promotes insulin signaling and adipogenesis*. Endocrinology, 2009. **150**(12): p. 5230-9.

## Appendix I

| Category                                 | Primer name                              | 5'-3' Sequence  |
|--|--|---|
| <b>Taqman® primers and probe</b>         | <i>AWP1 forward primer</i>               | AAGACCTGCAAGGACCCAGA                                      |
|  | <i>AWP1 reverse primer</i>               | GAGACTTGCTTTGCTCTCAGATG                                   |
|  | <i>AWP1 mRNA MGB probe</i>               | CCTTGTTCCCTTTGAATGTGATCCTCCATCT                           |
| <b>Site-directed mutagenesis primers</b> | <i>ZNF216 C30A_C33A sense</i>            | GGAATCCTAGGACAAATGGAATGGCTTCTGTTGCCTACAAAGAACATCTTCAGAGAC |
|  | <i>ZNF216 C30A_C33A antisense</i>        | GTCTCTGAAGATGTTCTTTGTAGGCAACAGAAGCCATTCCATTTGTCCTAGGATTCC |
|  | <i>ZNF216 (1-60) sense (Znf_A20)</i>     | GTTCCAACAGTCCTACCTAAGACTCTGCGTCTGTA                       |
|  | <i>ZNF216 (1-60) antisense (Znf_A20)</i> | TACAGACGCAGAGTCTTAGGTAGGACTGTTGGAAC                       |
| <b>Znf_UBP primers</b>                   | <i>Znf_UBP forward primer</i>            | ACAGGATCCAAGCAGGAGGTGCAGGCATG                             |
|  | <i>Znf_UBP reverse primer</i>            | GCTCGAGTTACTTGTCTGTCTTCTGCATCTTCAGC                       |

## Appendix II

| Antibody  | Wash buffer        | Blocking buffer/conditions              | Antibody conditions                                       | 2° Antibody conditions <sup>1</sup> |
|---|--------------------|---|---|-------------------------------------|
| <b>Ubiquitin<sup>2</sup></b><br><i>(in house)</i> | TBS <sup>3</sup>   | 4% Marvel, TBS<br>RT <sup>4</sup> , 1hr | 1° anti-ubiquitin<br>1/1000, RT, 1 hr                     | 2° anti-rabbit<br>1/2000, RT, 1 hr  |
| <b>Lys48 (K48)</b><br><i>(Millipore)</i>          | TBS-0.05%<br>Tween | 5% Marvel, TBS-0.05% Tween<br>RT, 1hr   | 1° anti-K48<br>1/1000, 4°C, overnight                     | 2° anti-rabbit<br>1/2000, RT, 1 hr  |
| <b>GST</b><br><i>(Bethyl)</i>                     | TBS-0.05%<br>Tween | 5% Marvel, TBS-0.05% Tween<br>RT, 1hr   | HRP <sup>5</sup> -conjugated anti-GST<br>1/1000, RT, 1 hr | N/A                                 |
| <b>p62<br/>Ick ligand (BD<br/>Biosciences)</b>    | TBS                | 5% Marvel, TBS<br>RT, 1hr               | 1° anti-p62<br>1/5000, RT, 1 hr                           | 2° anti-mouse<br>1/2000, RT, 1 hr   |
| <b>Adenylate Kinase 1</b><br><i>(Genetex)</i>     | TBS                | 5% Marvel, RT, 1hr                      | 1° anti-adenylate kinase I<br>1/1000, RT, 1 hr            | 2° anti-mouse<br>1/2000, RT, 1 hr   |

Note: All blots are blocked, incubated with antibody (1° or HRP-conjugated), washed 3 x 5 min in wash buffer, incubated with 2° antibody where relevant, washed 3 x 5 min in wash buffer and then developed.

<sup>1</sup> 2° Antibodies sourced from Dako

<sup>2</sup> Blots probed with anti-ubiquitin are first autoclaved prior to blocking, to enhance the immunoreactivity of ubiquitin

<sup>3</sup> Tris buffered saline

<sup>4</sup> Room temperature

<sup>5</sup> Horseradish peroxidase